CRANFIELD INSTITUTE OF TECHNOLOGY

I.P.S.Craig

Fluid Driven Rotary Atomiser for Controlled Droplet Application of Herbicides

ENGINEERING FOR AGRICULTURE

SILSOE COLLEGE

Supervisor : Dr. C. S. Parkin

Ph.D. Thesis

April, 1991

FLUID DRIVEN ROTARY ATOMISER FOR CONTROLLED DROPLET APPLICATION OF HERBICIDES.

CONTENTS

4. CONSIDERATIONS INVOLVED IN THE DESIGN OF A FLUID DRIVEN ROTARY ATOMISER

4.1 Nozzle design

- 4.1.1 Flowrate and filtration requirements, and implications for nozzle orifice number and size
- 4.1.2 Orifice shape and discharge efficiency
- 4.1.3 Calculation of nozzle performance
- 4.1.4 Position in relation to inner wall

4.2 Bearing design

- 4.2.1 Choice of bearing
- 4.2.2 Development of bearing design
- 4.2.3 Isolation of bearing from spray fluid
- 4.2.4 Relationship between frictional torque and bearing size
- 4.2.5 Shaft design

4.3 Cup design

- 4.3.1 Cup shape
- 4.3.2 Motion of liquid ascending inner wall
- 4.3.3 Peripheral fluid distribution and weirs
- 4.3.4 Cup size
- 4.3.5 Inertial effects
- 4.3.6 Size limitation due to gyroscopic effects
- 4.3.7 Required cup diameter to sustain moderate changes in bearing friction

4.4 Disc design

- 4.4.1 Behavior of fluid layers on rotating surfaces
- 4.4.2 Grooves and teeth
- 4.4.3 Calculation of the effect of viscosity on fluid acceleration upon three types of surface
- 4.4.4 Design implications for an energy efficient spinning disc

5.0 ATOMISER TESTING METHODS

- 5.1 Objectives
- 5.2 Test Methodology
- 5.3 The PMS laser droplet sizing system
- 5.4 Tests on a single groove/issuing point system
- 5.5 Tests on the Micron Herbi, a standard CDA rotary atomiser for herbicide application

ABSTRACT

Handheld electrically driven spinning disc atomisers are capable of applying pesticides more efficiently than with hydraulic nozzles, because the narrower droplet spectra they produce leads to reduced drift and wastage of chemical. Despite these savings however, farmers are frequently reluctant to use such methods because of poor reliability, and high maintenance costs of the electrical drive systems.

This research has therefore examined an alternative drive system using a jet of the pesticide fluid to power the atomiser. Experiments have been carried out to increase understanding of the processes involved, with the aim of producing an optimum design suitable for mounting to a knapsack sprayer.

The fluid drive mechanism is comparable to that of a Pelton Wheel; driving torque arises from a change in momentum of a fluid jet as it strikes the inside of a cup causing it to rotate. The fluid is emitted from grooves and teeth to form ligaments which produce uniform droplets. Peripheral distribution of fluid is made uniform by a series of slotted weirs on the inside wall of the cup.

Form and size of various components including the nozzle, bearing, cup and atomising disc have been investigated. The requirement for low flowrate necessitates the use of a small nozzle with filter. Supply pressure available from hand-pressurised knapsack sprayers is also restricted. Available input energy is therefore limited, requiring that all the processes leading up to atomisation are as efficient as possible.

Rotational speed is a function of jet velocity, mass flowrate, inner and outer cup radius, and bearing frictional torque. A simple computer model has been developed to predict the effects of changing these parameters. Radial exit velocity of the fluid has been derived from a consideration of the viscous forces to which thin fluid layers are subject during centrifugal acceleration upon rotating surfaces. This has enabled undisturbed ligament radius to be calculated, and has therefore provided a satisfactory method for the prediction of dropsize.

Spectral and deposit characteristics are satisfactory for CDA herbicide application with water based formulations, although antifoam agent is required for formulations containing surfactant. Typical average droplet size for an operating pressure of 3 bar is 250µm, and optimum swath width is 1.2m for an intended application rate of 30 to 40 litres per hectare.

ACKNOWLEDGEMENTS

To the following I express my thanks and appreciation:

Dr Steve Parkin, and Professor John Spillman for their supervision of the project, and helpful advice and encouragement throughout

Mr. Derik Giles for his excellent craftsmanship

Mr. John Wyatt, for advice upon computing matters and data handling

Mr. John Dyson for useful discussions

All my collegues at ICAP for their support

and to my fiancee Gillian

NOTATION

Waterwheel Performance

N	rotation rate (revolutions per minute)
w	angular rotation rate (radians s^{-1})
Q	flowrate (ml/min)
q	flowrate per issuing point (m^3s^{-1})
p	fluid density (kgm^{-3})
μ	fluid viscosity ($kg\ m^{-1}s^{-1}$)
v	fluid kinematic viscosity (m^2s^{-1})
n	number of grooves or teeth
D	disc diameter (m)
R_i	radius to inner wall (mm)
R_o	radius to tip of tooth on disc (mm)
P	fluid supply pressure relative to atmospheric (Bar, 10^5 Pascal)
V_J	jet velocity (ms^{-1})
V_I	inner wall velocity (ms^{-1})
d_n	nozzle orifice diameter (mm)
d_c	nozzle clearance from inner wall (mm)
t	thickness of fluid along inner wall (mm)
V_A	liquid ascension velocity (ms^{-1})
h	inner wall height (mm)
V_{ann}	inviscid radial velocity for an annulus (ms^{-1})
V_{disc}	inviscid radial velocity for a disc (ms^{-1})
c	V_{ann}/V_{disc}
T	total non-useful torque (Nm)
F	torque due to bearing friction (Nm)
D	drag due to fluid drag on nozzle (Nm)
A,B,C	polynomial regression coefficients for F
f, g	polynomial regression coefficients for D

Ligament instability theory

r	ligament radius (m)
z	axial distance (m)
Θ	azimuthal angle (radians)
k	axial wave number
m	azimuthal wave number
a_o	wave equation parameter
$c_{m,k}$	wave pertubation amplitude (m)

Droplet sizing

μm	micrometer or micron (10^{-6}m)
NMD	Number Median Diameter (μm)
NAD	Number Average Diameter (μm)
SAD	Sauter Average Diameter (μm)
VAD	Volume Average Diameter (μm)
VMD	Volume Median Diameter (μm)
R	NMD/VMD ratio
d	droplet diameter (μm)
j	bin number
n	total number of droplets in sample
D_{tj}	upper size limit of bin j (μm)
D_{tj-1}	upper size limit of bin j-1 (μm)
Db	lower bin diameter (μm)
Dm	mid bin diameter (μm)
$d_{(DROP)}$	theoretical droplet diameter (μm)
$d_{(LIG)}$	undisturbed ligament diameter (μm)
f_B	breakup factor, $d_{(DROP)}/d_{(LIG)}$

Fluid mechanics.

R	degree of reaction of turbine
m	mass flowrate (kgs^{-1})
r_1	radius at inlet (m)
r_2	radius at outlet (m)
Vt_1	initial tangential velocity (ms^{-1})
Vt_2	final tangential velocity (ms-1)
P	power (Watts, W)
η	efficiency
E_h	Euler's head (m)
$E_{h,max}$	Euler's head, maximum efficiency (m)
T	torque (Nm)
V_1	velocity of jet (ms-1)
U	peripheral vane velocity (ms-1)
V_{R1}	initial relative velocity (ms-1)
V_{R2}	final relative velocity (ms-1)
V_T	whirl velocity (ms-1)
V_F	flow velocity (ms-1)
α	angle between V_{R2} and U (degrees)
k	velocity reduction due to friction (ms-1)
Θ	angle between jet and inner wall of cup (degrees)
Θ_{min}	minimum jet angle (degrees)
ø	angle of jet in vertical plane (degrees)
C_d	coefficient of discharge
C_v	coefficient of velocity
C_c	coefficient for vena contraction
A_o	area of opening (m^2)
l	length of nozzle (m)
d_n	diameter of nozzle (m)

Vmax	maximum velocity
Vr	velocity at r (ms^{-1})
τ	shear force at wall (Nm^{-2})
H	head (m)
N_s	specific speed (ms^{-1})
ϕ	speed factor

Bearing Friction

δ	small element
N	normal force (Newtons, N)
A	contact area (m^2)
F	friction force (N)
M	friction moment (Nm)
W	weight (kg)
μ_k	dry friction coefficient
r	shaft radius (m)
R_1	inner collar radius (m)
R_2	outer collar radius (m)
V	velocity (ms^{-1})
h	lubricant film thickness (m)
u	shaft velocity (ms^{-1})
l	bush length (m)
c	bush shaft clearance (m)
P_P	power loss for plain bearing (W)
P_T	power loss for thrust bearing (W)
t	lubricant film thickness (m)
M_v	running torque (kg-mm)
f_o,	lubrication factor
p	vapourisation factor
d_m	pitch diameter (mm)
M_L	load torque (kg-mm)
f_1	load factor
g_1	direction factor
P_o	load (kg)
α_{nom}	nominal stress (Nm^{-2})

Viscous flow

τ_o	shear stress at surface (Nm^{-2})
A	wetted area per unit length (m)
k	factor dependant upon velocity profile
δ	local fluid thickness (m)
r	distance from centre of rotation (m)
a	$2w^2$
b	$g_s.kv/Q$
g_s	number depending on groove shape

Miscellaneous

m	meter
kg	kilogram
s	second
N	Newton
J	Joule
W	Watt
g	acceleration due to gravity (ms^{-1})
π	pi = 3.412
h	release height (m)
u^*	eddy velocity (ms^{-1})
u	mean windspeed (ms^{-1})
v_s	sedimentation velocity (ms^{-1})
K.E	kinetic energy (Joules, J)
C.F	centrifugal force (N)
SP	supply pressure (Nm^{-2})
CDA	Controlled Droplet Application
RPM	revolutions per minute
WW	Waterwheel
Mk.	prototype number
I	moment of inertia (kg m^2)
Φ	precession angle (radians)
α	proportional to
^	raised to power

LIST OF FIGURES

Appendix I (Design Drawings)

LIST OF TABLES

LIST OF PLATES

Chapter One

INTRODUCTION

1.1 Background

The term "Waterwheel" describes well the kind of spraying device with which this study is concerned. The name was adopted because motive power is derived from an off-centre jet of the spray liquid, in similar fashion to a Pelton Wheel. Intended use is primarily as an attachment to existing hand pressurised knapsack sprayers, for the application of herbicides.

Conventional ground spraying techniques using knapsacks generally utilise hydraulic nozzles to atomise and disperse the spray liquid. This entails the formation of droplets via sheet breakup, producing an undesirably wide dropsize distribution particularly in the size range required for herbicide application. The Waterwheel however, operates on a rotary atomisation principle, producing ligaments which break up in a controlled manner. The resultant dropsize distribution is therefore narrow, and suits low volume applications with reduced drift.

Controlled Drop Application (CDA) by rotary means is already well established (Matthews, 1977). Devices used usually consist of an electrically driven spinning disc upon which the spray fluid is fed via gravity. However, problems are associated with their extended use in Third World countries due to the fact that batteries and electric motors wear out and are expensive to replace.

For these reasons, many farmers whom adopted CDA have subsequently abandoned the technique in favour of the more reliable hydraulic nozzle, despite higher overall costs in terms of chemical applied to crops, and increased environmental hazard.

Reliance on high volume spraying is however, not advisable in areas prone to draught. In some instances, where the farmer has been unable to obtain sufficient water to fill his knapsack, chemical weed control has been foregone completely in favour of hand weeding or hoeing. The result is generally a dramatic reduction in yield.

The Waterwheel therefore represents an additional option for the farmer in that it offers the advantages of low volume CDA, without the expense and inconvenience caused by an electrical drive system.

1.2 Growing environmental concern about the application of pesticides

In recent years there has been increased criticism expressed by scientific institutions, governmental and non-governmental organisations, and the general public, concerning the application of pesticides. Soil and crop residues have been reduced by improving the degradation of chemicals, and also by general moves towards reduced volumes of chemical applied. However, spray drift leading to off-target damage to crops, and also human detection of chemical during crop spraying are still causes for concern.

Leglislation against crop spraying is therefore set to increase in the future. Operators and land owners urgently require new methods of applying agrochemicals inorder to continue to grow crops economically, whilst conforming to increased restrictions on pesticide use.

Off target damage caused by spray drift is a particular problem with conventional herbicide application. Much can be done to minimise problems of drift, by careful application under correct meteorological conditions for example. However, it is difficult to enforce this strategy, especially when farmers and operators are under economic pressures to spray.

One potential solution to the problem would be to use an intergrated programme of non-chemical methods for controlling weeds; biological control using fungi is an example of one new method. However extensive research is required to make sure that methods such as these are both safe and effective.

Increased values put on the environment may eventually provide the funds for such research, and so make non-chemical methods a reality for the future. At the present however, the only effective and economic way of controlling weeds on a large scale is through the use of chemicals.

Pesticides are still very much required for the production of cheap food for a starving world population. It is hoped that the Waterwheel may in some small way contribute to this cause, whilst reducing chemical pollution of the environment to a minimum.

1.3 General aims and objectives

The overall aim of the project was to develop a fluid driven rotary atomiser suitable for Controlled Droplet Application of herbicides. Inorder to achieve this it was necessary to perform experiments to gain a theoretical understanding of the various processes involved, which would enable a successful fluid driven design to be produced.

The main objectives of the study were as follows:

1) To establish an optimum design for the fluid drive system, inorder to obtain a working prototype. Initial theory for the fluid drive mechanism would be provided by comparison with a standard Pelton Wheel. Experimentation with various designs would the lead on to a design particularly suited for driving a spinning disc.

2) To carry out theoretical and experimental investigations inorder to optimise the design of the various components; ie the nozzle, bearing, cup and disc. Further tests would be introduced at an appropriate stage to deal with any problems which arose; for example, avoiding fluid contamination of the bearing, obtaining an even fluid distribution etc.

3) To study the behavior of fluid over rotating surfaces and to carry out a theoretical calculation of the acceleration of liquid due to centrifugal force, taking into account the effect of surface friction due to viscosity. The theory would be supported with tests on single groove and emitting point system with the aim of deducing implications for an energy efficient spinning disc.

4) To obtain performance data for various prototype designs of fluid driven atomiser, and show that the droplet spectra produced would be suitable for controlled application of herbicides. A swath pattern produced by a moving atomiser would be measured to obtain the optimum swath width for spray operation.

5) To develop a simple model to predict performance, and the effect changing the various design parameters. To assess how this study may have contributed to the field of pesticides application and outline requirements for further research.

Chapter Two

LITERATURE REVIEW

2.1 Introduction to herbicides

Herbicides are be defined as chemicals used to control weeds. Weeds, defined simply as unwanted plants, occur in all crops throughout the world. The term "control" may mean a number processes ranging from total or partial eradication, to inhibited develoment of the weed.

As a pest problem weeds are unique in that they frequently cause major losses in yeild without any visable symptions of damage to the crop. Farmers are therefore often unaware of the scale of the problem

With the large surplus of cheap labour in Third World countries, chemical weed control is frequently disregarded in favour of mechanical removal or hand weeding during later stages of growth. However, the physiological effects of weeds are frequently at their greatest during the early stages. Hoeing in particular can cause root injury and increased likelyhood of infection of the crop plant, and may encourage rather than discourage the production of new weed plants. Also, weed resistant hybrids generally have a lower yield than varieties which could be grown in conjunction with chemical weed control.

The case for herbicides is therefore strong in many instances. However, as the sophistication of chemical manufacture increases, acceptable chemicals are becoming increasingly more expensive. Effective and efficient application of herbicides is therefore of crucial importance if economic weed control is to be achieved.

Herbicides may be classified in a number of ways, and a large body of literature is devoted to this purpose. Classifications according to the following criteria are the most common :

1) Chemical composition.
   Herbicides may be simply referred to according to what major group of chemicals they belong, eg phenoxys, ureas, amides, carbamates, triazines. Note may also be made of toxicity to humans and animals and of their degree of persistance in the environment.

2) Mode of action.
   Herbicides may also be described according to their site of entry, (eg foliar or root absorbed), their retention, subsequent degree of movement throughout the plant (eg. contact, translocated, systemic), the type

of plant upon which they are active (eg broadleaved or grass weeds) and their degree of selectivity. The biochemical reactions which are believed to take place inside the plant may also be used (eg interference with cell growth, biosynthesis, respiration, photosynthesis).

3) Application
Timing of application in relation to the crop or weed (eg pre-sowing, pre emergence, post emergence) or with respect to environmental conditions. The nature of the spraying is also relevent (eg broadcast or spot treatments)

It is useful for the application engineer to have at least an elementary knowledge of all of the above since all three aspects are relevant in the design of spraying apparatus. A knowledge of composition and toxicity of chemicals intended to be used is important for safety aspects as well as possible effects on materials used in the design of the sprayer. Biological mode of action and intended target for the spray droplets is also important in the design of an appropiate herbicide application system

2.2 Review of ground herbicide application techniques

A comprehensive review of ground application of herbicides has been undertaken by Combellack (1984). He categorises the various techniques as follows:

i) application directly to, or injection into, the plant
ii) injection into the soil
iii) release into irrigation water
iv) release or propulsion through the air to the target in the solid state
v) release or propulsion through the air to the target in the liquid state

Application directly to the plant is the oldest method of herbicide application known: common salt was applied in this way by the Arabs after the conquest of Rome in AD 460 (Smith and Secoy, 1976). Today, a smear may be deposited on the plant by means of the ropewick applicator (Dale, 1978), consisting of a short length of rope with the ends immersed in a reservoir of herbicide. Similar applicators include the roller herbicide applicator (Wyse and Habstritt, 1977) which has a saturated nylon carpet that slowly rotates in a direction opposite to that of travel.

Injection or incorporation into the soil can sometimes improve the performance of herbicides by reducing

photochemical degredation, volatility and wind losses. Instruments such as blade applicators (Wooton and McWhorter,1961) and injection planters (Barrentine and Wooten,1967) have therefore been developed for such a purpose.

Equipment has also been developed for applying herbicides through irrigation (Ashton, 1961) and granular application (Haywood, 1980). For various reasons they may provide the best solution to a particular weed problem, although frequently it is to avoid the problem of spray drift, a common problem associated with the final category listed.

The category with which this study is primarily concerned is release or propulsion through the air to the target in the liquid state, and may be more simply referred to as "spraying". The spraying operation may be characterised into five distinct phases:

i) addition of herbicide to a diluent to make a spray solution or suspension
ii) droplet production and droplet distribution over the target area
iii) movement of droplets on the target
iv) impingement and retention of the droplets and their resultant effectiveness on the target
v) achievement of a biological result

The subject area to which this study is primarily addressed, is the second phase, droplet production and droplet distribution over the target area.

By far the most common method by which herbicides are applied in this category, is by using pressure to force liquid through an orifice to produce a sheet, by changing the direction of flow of liquid. This is done by means of the pressure or hydraulic nozzle. Three mechanisms of sheet breakup can be identified: these are perforated sheet, wavy sheet and rim disintegration (Dombrowski and Fraser,1954), all of which produce heterogeneous droplet spectra.

Two main types of hydraulic nozzle exist, according to the shape of the sheet which they produce. The first is the fan nozzle. Three basic types of fan nozzle exist, impinging jet, solid surface impact and single orifice. The second type is the cone nozzle, so called because the nozzle has a swirl plate and an orifice separated by a swirl chamber. This gives the fluid a rotational velocity forming an air core (Tate and Marshall, 1953).

An increase in pressure reduces droplet size, an increase in viscocity reduces fan or cone angle and increases sheet length, while a decrease in surface tension generally produces a decrease in droplet size. Combellack and Matthews

(1981a) reported changes in droplet spectra with flowrate, orifice size, and solvent used in the formulation, and concluded that dynamic surface tension was likely to be of importance.

2.3 The problem of herbicide drift

Herbicide application using hydraulic nozzles is not satisfactory under certain circumstances, because due to the nature of the atomisation processes involved, some small droplets are produced which are prone to drift which causes damage to off target crops.

Common examples of such damage include injury to horticultural crops resulting from hormone herbicides applied to cereals. Glass house crops such as tomatoes and cucumber lettuce have a reputation for being the most commonly damaged crop, and their susceptability to small doses (0.1 to 0.01% of the usually applied dose) of herbicides such as TBA, MCPA, and 2,4-D has frequently been demonstrated (Davidson, 1961, Kingham and Fletcher, 1963, Martin and Fletcher (1972). Vegetable crops are also frequently sublethally effected, and an assessment of losses in yeild and marketability has been carried out by Hemphill and Montgomery (1981), Svensson (1975) and Schweitzer (1978). Fruit, vineyards, and oilseed rape are also notable examples. An extensive review of literature concerning the drift of herbicides has been carried out by Elliott and Wilson, (1983).

Whether droplets are large enough to be classed as non driftable, depends to a large extent upon windspeed and the degree of turbulence in the atmosphere. A suitable parameter for turbulence is the friction velocity u^*, which can be regarded as the tangential velocity of the eddies relative to the mean air flow. The magnitude of u^* depends on atmospheric stability and surface roughness of the terrain, although with a neutrally stable atmosphere over typical agricultural surfaces (soil, grass, crops) it is usually about 10% of the mean wind speed, u.

Droplets are said to be "large" if sedimentation dominates their movement. This has been shown to be the case by Cramer and Boyle (1973) if the ratio of the sedimentation velocity of the droplet (v_s) to turbulent eddy velocity (u^*) is greater than 3. If it is less than 0.3 then turbulence is said to predominate. This argument has been extended for the range of drop sizes and wind speeds typically encountered in spray application, and the results are shown in Figure 2.3 (from Cramer and Boyle, 1973).

For herbicide application from the ground there should ideally be no droplets which drift. All droplets produced

must therefore be above the minimum line for large droplets in Figure 2.3. For a windspeed of 1 ms^{-1}, and $u^*/u = 0.1$, the spraying device should be capable of producing a droplet spectra with drops no less than 100um in size. For a windspeed of 2 ms^{-1}, the minimum size which constitutes a "large" droplet rises to around 150um. This is a useful target to aim for in the design of a driftless herbicide sprayer. For hydraulic nozzles producing droplet spectra with VMDs around 300um, typically up to 5 or 10% of the spray volume may consist of droplets less than 150 um.

Large drops move a distance downwind x, from the point of release given by hu/v_s. With $v_s/u^* = 3$ or $v_s/u = 3/10$, the furthest distance which a "large" droplet can move downwind is 10/3 h. If in typical ground spraying the release height is 1m for example, acceptable downwind movement of droplets, ignoring droplet exit velocity from the sprayer is therefore 3.3m, .

For small droplets, dispersal can be regarded schematically as a spreading cone. The angle of the cone is dependant upon u^*/u, and the axis is inclined below the horizontal at an angle depending upon mean v_s. The simplest assumption is that the distribution of drops about the cone centre line is Gaussian, and models based upon these assumptions have been given by Bache and Sayer (1975) and Dumbauld et al. (1976).

Intersection of the cone with the ground leads to an assymmetrical ground deposit with a peak at hu/u^*, or about 10 h with $u^*/u = 0.1$. Notable is that the position of this peak is independant of both wind speed and dropsize. Further downwind, the ground deposit from small drops decreases in inverse proportion to the square of the downwind distance. For ground based hydraulic sprayers, this relationship occurs at distances greater than about 100m, and can be seen in the experimental results of, for example, Yates et al. (1978) and Goering and Butler (1975).

The importance of herbicide sprays with no driftable droplets is probably more crucial in the tropics, where atmospheric conditions are frequently very stable or inversions occur encouraging drift of droplets over large distances. Since the angle of dispersion is small, when the spray cone does reach the ground, the deposit density is much higher than would occur in neutral conditions.

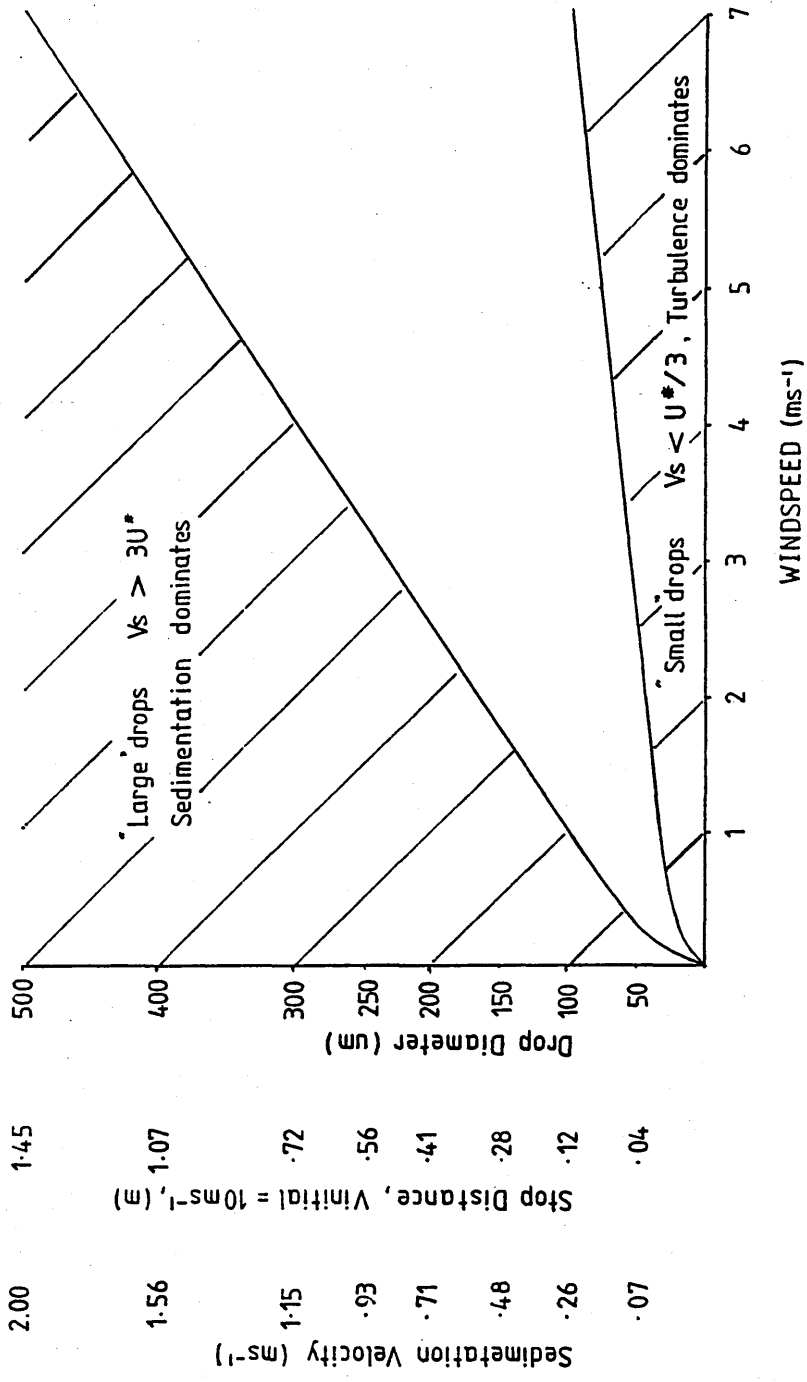

Figure 2.3 Classification of large and small droplets (adapted from Cramer and Boyle, 1973)

2.4 Existing methods of reducing spray drift

Methods currently used for reducing drift may be categorised into three broad approaches:

1) choice of correct meteorological conditions in which to spray
2) modification of the local airflow between sprayer and target
3) use of specialised formulations
4) use of specialised nozzles

The principle behind approach number one has been explained in the previous section, and essentially relies on no spraying taking place with windspeed and turbulence conditions which would categorise droplets released as anything other than large. With herbicide sprays with an average droplet size small enough to provide adequate coverage and to be effective, spraying is basically restricted to neutral conditions with windspeeds less than 1 or 2 metres per second. This has the major drawback that it may seriously reduce the number of spraying days available for a particular weed control programme.

The use of shielded booms to modify the local airflow between sprayer and target has been an approach adopted by a number of workers, notably Rogers et al,(1984) who claimed no increase in off-target deposits in windspeeds up to 27km/hr. Smith, Harris and Butler (1982) however, carried out tests which showed that downwind spray deposits could either be reduced or increased when comparing shielded verses unshielded spray booms. Other possible disadvantages envisaged with the technique are contact of the spray with the shield, contact of the shield with the crop, and of the airflow across the shield resulting in turbulent eddies.

A promising and relatively new technique is the use of an air curtain in combination with a standard hydraulic nozzle spray boom. The rapidly downward moving air entrains the spray so that velocity and therefore collection efficiency of crop surfaces is increased, therefore reducing drift of small droplets. There are already a number of commercial units in use, and the further research into the technique is taking place at Cranfield Institute of Technology.

The third approach is to use specialised formulations in an attempt to reduce drift. A common method of achieving this is to use an additives such as adjuvants to increase viscosity and therefore VMD (Butler, Akesson and Yates, 1976). Such liquids exhibit non-Newtonian pseudo-plastic behavior during the high shear rates involved with atomisation. This means that highly viscous formulation is

required in the spray tank, to produce liquid emitting from the nozzle only a few times more viscous than water (Butler, Akesson and Yates, 1969). This may cause inconvenience in handling and other problems including increased phytotoxity. Also, although small droplets are eliminated, there is little evidence to suggest that increasing viscosity narrows the size distribution of a spray from a hydraulic nozzle. Generally, a spectral shift towards the coarse end occurs, which may result in poorer coverage and reduced efficacy.

The use of specialised nozzles to narrow droplet spectra is probably the most direct and effective way of reducing herbicide drift. Various forms of hydraulic nozzle come under this category. By lowering spray pressure, it is possible to reduce droplet breakup. Specialised forms of hydraulic nozzle which utilise this principle are termed low pressure nozzles, and consist of large orifice nozzles with straight flow internal design to reduce shear forces. However, pressure must be reduced as much as four times to double the average droplet size produced.

Some hydraulic nozzles utilise air incorporation at a late stage during the passage of the liquid, for example, the Spraying Systems Foamjet^{tm}. This produces a foam if sufficient surfactant is added to the formulation which can expand the spray volume up to ten times its original. However, studies strongly suggest that drift reducing benefits claimed for foam sprays are due to the coarse nature of the nozzles used rather than the foam itself (Akesson et al 1972, Bouse and Leerskov 1973). Infact addition of the foaming agent reduces the surface tension of the spray and may form drift susceptable clusters of air bubbles. Improved sticking and spreading due to the surfactant properties of the foam adjuvants may however compensate for reduced plant coverage caused by the coarse spray. This possible effect is the only justification for using foam sprays.

The fundamental mechanism of atomisation involved with all hydraulic nozzles is a very random and chaotic process of sheet disintergration (Dombrowski, 1967). A more controlled and predictable process which produces droplets of more even size is that of ligament or jet disintergration. (Lord Rayleigh 1890, and section 2.7). Spraying via such a process is known as Controlled Droplet Application or CDA.

Jets may be simply produced by a row of needles, for example, the helicopter mounted Microfoil Boom^{tm} system (Kirch, 1969) used for band spraying in forests. However, since droplets produced are approximately twice the diameter of the needle, very small needles are required, and fine filter systems are required to prevent clogging. The smallest droplets obtainable are about 800µm. Needless to

say, high viscosity sprays and wettable powders cannot be used.

Disturbance of the jet may be controlled by a pulse, for example in transducer nozzles which use the vibration of a piezoelectric crystal (Wilce et al 1974, Young, 1986.). Alternatively, electrostatic charging may be used (Stent, 1981). Such devices are useful for producing small quantities of droplets of very constant size for laboratory purposes. So far however, they have not proved successful for the application of herbicides, due to the unrealistically low flowrates obtainable.

Realistic flowrates can be obtainable however if centrifugal force is used to thin the fluid which then issues from emitting points to form ligaments. This is referred to as rotary CDA and is the subject with which the rest of this work will be primarily concerned.

2.5 Controlled Droplet Application

The "Father" of Rotary CDA is undoubtedly Edward Bals. Bals was one of the earliest workers in the field of pesticides application to realise the potential of rotary methods of atomisation in drastically increasing the efficiency with which pesticides are applied. In his paper given at the 1969 BCPC conference at Brighton he stated that the efficiency of a spraying machine is inversly proportional to the range of droplet sizes it emits. He has been the predominant inventor of most rotary application equipment, and still continues to manufacture and carry out further research into the field.

Probably the most fundamental concept behind what Bals referred to as efficiency, arises from the fact that there is cubic relationship between the diameter of a droplet and its volume. This means that if the average diameter of droplets in a spray is halved, then coverage, or droplet density per unit area can be increased by a factor of eight. Alternatively, volume of chemical applied can be reduced by a factor of eight for the same coverage.

This principle works very well if small droplets are acceptable, and application can take place via drift spraying. This is the case with many insecticide application programmes, where minute quantities of liquid can be used to cover vast areas.

However, with herbicide application, drift is predominantly what the operator is trying to avoid. This therefore places a lower limit of 100 to 150 µm on acceptable droplet size as discussed in section 2.3.

There may also be lower limits on droplet size due to other factors. For example, the droplet has to be of sufficient size to impact onto the target for which it is intended. Also there are commonly lower limits due to biological phenomena, For example, the herbicide deposit must be of sufficient size to penetrate leaf cuticle. This may be of varying difficulty according to the degree of hairyness or waxyness of the weed species concerned.

Droplets which are too large generally result in poor coverage and wastage of chemical. It is generally agreed that droplets over 300 µm will run or bounce off foliage, if indeed they suceed in striking a leaf before hitting the ground. These droplets contain most of the spray volume, thus contributing to soil pollution rather than crop protection.

Dropsize may also be too large for biological reasons. For example, particularly with herbides with contact rather than systemic action, good even coverage is required. Oversize drops may cause localised scorching and death of leaf material, with no penetration of active ingredient further into the plant

Doubtless there is a truly biologically optimum droplet size for any particular pesticide application, which must of necessity also be linked to chemical formulation and concentration as the other major factor. To quote again from Edward Bals " if it doesn't work - use less ". This has been the theme of many efficacy trials investigating CDA which have generally tended to show improved biological effect of CDA over conventional spraying, although for various reasons this has not been universally the case. For full reviews the reader is referred to Buehring et al (1973), Akesson (1978), Merritt (1980), Prasad (1987), and Bailey et al (1982).

For the purposes of this project, which is primarilily concerned with the design of hand-held rotary CDA sprayers for herbicide application, a mean droplet size of between 200 and 250µm will be considered as the target to aim for.

2.6 Review of hand-held rotary CDA equipment.

Arnold (1983), carried out a useful summary of fourteen hand-held battery operated spinning disc sprayers including the Berthoud H2, Geno, Jucos, Blitz, Tecnoma T5, Turbair Weeder, Leizer, Pulver, Ramey for herbicide application. All of these devices are broadly similar consisting of gravity fed electrically driven spinning disc, but have good points and bad points which are elucidated in the paper.

To this list the following can be added, which are presently commercially available in the United Kingdon :

Microfit Herbi *Microfit Herbi Twin* *Microfit Herbaflex*	Micron Sprayers Ltd Three Mills, Bromyard Herefordshire

(Also distributed by CDA Ltd, Lockinge, Wantage, Oxon)

Lynx CDA System	Rigby Taylor Garside Street, Bolton Lancashire
Attilla SBC	Microcide Ltd Sheperds Grove, Stanton Bury St. Edmunds
Lancelot	Horstine Farmery Ltd (Rhone-Poulenc Group) North Newbald, York
Nimbus 2	ICI Agrochemicals Professional Products Farnham, Surry
CDA 250	Agri-technics International Ltd Muston Gorse, Redmile, Nottingham
Superpro Compact	Nomix Manufacturing Company Ltd (distributed by Chipman Ltd. Horsham, West Sussex)

Some comments will now be made about the above sprayers as follows:

Micron were certainly among the early pioneers to launch a spinning disc sprayer for herbicide application. The Micron Herbi is still considered as the standard CDA applicator, and so a set of droplet size test results have been included (Chapter Five).

The Herbi head consists of a disc, or more correctly a shallow cup with walls inclined at 45^0. The inside of the walls are finely grooved, each groove leading to 360 teeth. The tip to tip diameter is 77mm. Power supply consists of 4 R20S batteries (6v DC) to drive a mechanically governed motor at 2000 RPM under load, with a power consumption of 0.6 Watts. Recommended feed rate is 60ml/min giving an application rate of 10 to 30 l/ha, with a swath width of 1.2 m. The manufacturers give 250µm as a typical spray droplet size. This is supported by the VMD value of 254µm obtained experimentally by the PMS laser droplet sizing technique (refer to spectra file 2, record 35/36, Appendix II).

At 60 ml/min, flowrate per tooth of the atomiser is 0.16 ml/min/groove, which is well below the value of 0.2 ml/min/groove stipulated for the transition between direct droplet production and ligament disintergration for water at 2000 RPM (Chapter Five). Assuming that the feed to each tooth is constant, direct droplet production will therefore predominate at this flowrate leading to a narrow droplet spectra.

Tangential velocity at the periphery of the disc is 8.17 ms^{-1} at 2000 RPM. The velocity of a direct droplet leaving a tooth will have a small radial component, so it is probable that the total velocity of the droplet relative to air is about 10 ms^{-1}. The stop distance of a 250µm droplet initially travelling at 10 ms^{-1} is 0.56m.

If the spray head is held with the disc horizontal, and at sufficient height so that the droplets will achieve their full stop distance before striking the ground, a circular pattern will be produced with diameter 1.12m. The pattern will actually be annulus with a thickness according to the range of droplet sizes produced. The swath width of 1.2m quoted in the Herbi specifications was probably derived by moving an annulus, the maximum diameter of which coinciding with the largest droplets produced.

The Herbi Microfit series offers great flexibility in swath width obtainable. For example, the Herbi twin offers increased swath width of between 1.8m and 2.4m. This is achieved by mounting two Herbi heads on an adjustable frame which fits into an existing Herbi lance. The Herbi twin is useful in the situation where it is convenient to cover a lot of ground quickly, for example, turf spraying. It is also widely used in orchards and plantations where the areas between rows need to be kept weed free.

Alternatively, swath width may be reduced by using an adjustable shroud, as with the Herbaflex system. This is particularly useful if a narrow strip of weeds needs to be controlled, as would be the case with inter-row crop spraying, or spraying along buildings or fencelines for example. Swath width can be selected between 10 and 50cm with the standard shroud, or a wider opening shroud is available to allow swath widths between 15 and 75cm. Angle of the spray head to the ground can also be adjusted to achieve further swath width control. Additionally, a spray shield option is available for situations where it is necessary to spray right up to sensitive plants.

The shroud mechanism consists of an adjustable window to control the internal angle of the segment of spray emitted. That proportion of the spray which is not emitted hits the side and falls to the bottom of a chamber enclosing the disc. The base of the disc is conical, so picks up liquid

from this reservoir to feed the disc periphery once again. The liquid therefore, which is initially fed into the base of the chamber, undergoes circulation until it is emitted through the window. Liquid feedrate is quoted as being adjustable between 15 and 60 ml/min for the herbaflex, by means of interchangable colour coded nozzles with different sized orifices.

Besides control of swath width, shrouding and shielding enable downward projection of the spray, and therefore greater control of drift prone droplets. According to published specifications, the mechanically governed disc speed for the herbaflex is therefore 2800 RPM, giving a spray droplet size of the 200, rather than 2000 RPM and 250µm for the herbi. This therefore means that droplet production is predominantly in ligament disintergration mode, especially if flowrates per tooth exceed 0.2 ml/min/groove

Comparing Herbi droplet spectra (Chapter Five), decreasing VMD from 250µm to 200µm can increase the percentage of droplets less than 145µm to anything between 6 and 20% , according to what flowrate per tooth is chosen. Decreasing droplet size will result in improved coverage, although more operator vigilance will be required to ensure that no off target damage results from the increased numbers of driftable droplets that will be present in the spray.

The Herbi and the Herbaflex are also marketed by Rigby Taylor as the Lynx CDA system. Differences offered include an improved carrying handle, and a backpack rather than a plastic screw in bottle for containing chemical. Backpacks offer the advantage in that the chemical container is less likely to crack upon dropping compared to the screw in type. However, they may be less comfortable to use for the operator, and care has to be taken to ensure that the flexible tube linking the container to the lance is not snagged or punctured.

The Microcide Attila SBC is a somewhat more sophisticated shrouded spinning disc sprayer, and so the head is correspondingly larger and therefore heavier. Recirculation of the liquid takes place via a centrifugal pump which returns fluid to a constant flow reservoir and float chamber. The atomiser is also has two stacked discs to halve flowrate per tooth to enable higher application rates of up to 60 l/ha. Two speeds are also available, which enables insecticides and fungicides to be applied as smaller droplets than herbicides. A disadvantage of the Attila however, is that due to the weight of the spray head, the operator invariably has to hold the lance with two hands which may prove inconvenient and awkward.

The Horstine Farmery Lancelot offers a similar spray head with pumped recirculation, although the disc is not stacked and only has one speed. Balance is achieved by an ergonomically designed lance whereby the carrying handle is inbetween the head and the battery compartment.

Other companies on the other hand have opted for increased simplicity in design, mainly for reasons of reliability and robustness. The spinning discs on the ICI Nimbus 2 and Agritechnics 250 for example, are of small radius (less than 50mm) and have plain emitting surfaces with no grooves or teeth. This approach has several points in its favor, including cheapness of manufacture and low power consumption enabling batteries to last longer. A problem with spinning discs with fine teeth is that they are easily prone to damage, and also fine grooves become clogged if highly viscous or particulate formulations are used. The simpler discs may therefore be said to cope with a wider range of formulations. However, atomisation from a plain edge, even if sharp has been shown to be markedly inferior with water (Chapter Five) compared to one with grooves and teeth, which positively encourages the formation of ligaments. Atomisation is ragged, and is akin to sheet breakup rather than controlled ligament disintergration.

The Agritechnics CDA 250 has a number of attachments including a standard disc, a large disc for larger swath width (up to 1.5m), a double disc with top and bottom atomising edges for the application of higher flowrates, and also a non-adjustable shroud for sectoral spraying. Supplied as standard are rechargeable NiCd batteries (each lance battery consists two 1.2 volt, 4Ah cells welded together). Optional extras include an in lance charger requiring a standard 240 ac supply. Alternatively, a multiple charger is available to charge a bank of 5 lance batteries from a 12 volt vehicle battery, or an ATI Solar Panel. Clearly some attention has been paid to solving the problem of unavailability of batteries in some Third World Countries where CDA operations take place.

A slightly different approach, probably more with the U.K. market in mind is that taken by the Chipmans and Nomix. With the Superpro for example disc speed is fully controllable, enabling the operator some degree of choice of swath width and to a certain extent droplet size. Additional features include a audio-pacing device, and a closed system calibration bottle, with which a variable orofice at the end of the lance may be calibrated to control flowrate. The Compact sprayer is similar except it has only 3 disc speeds, and a small snap in chemical bottle at the top of the lance rather than a backpack.

Both Superpro and Compact are supplied with a short lance with 10mm square disc producing a narrow swath as little as

/ contradiction

20cm. The square disc can be operated at low speeds to ensure absolutely no drift; the penalty however is that since the spray liquid is emitted from four corners only, droplets are large and few in number. However this may be quite suitable for spot treatments or spraying in narrow lines where dropsize is not important.

Alternatively a longer lance is available to be used with a 40mm diameter toothed or "serrated" disc to produce a wider swath. Quality of atomisation is superior with the toothed disc which has 40 well defined teeth, although no grooves are present. This disc would be selected if dropsize was important, as is the case if selective herbicides are used, or if a wide swath was required for broadcast treatments.

The design of the sprayer as a whole is asthetically pleasing, and ergonomically advanced. Counter balance weights slot into the back of the handle; two are available, one for each length of lance.

A rotary CDA sprayer worthy of special mention is the Ciba Geigy Berki. The Berki is similar to the others in that it consists of a gravity fed spinning disc. However, it is unique in that it is pneumatically rather than electrically driven. One half of the backpack, which is moulded in a similar fashion to a conventional knapsack, contains the chemical, the other half is an air reservoir with lever operated pump to generate air pressure to drive the air turbine. The spray head which contains the turbine and a large disc (100mm in diameter) is mounted on a rigid telesopic tube which is inturn attached to an adjustable arm on the knapsack, so that it can be held in a forward or rearward position relative to the operator.

A rattle lets the operator choose the correct pumping rhythm. A whistle warns that the disc speed is too high, clicking indicates indicates that it is too low. This is intended to ensure an optimum disc speed of 1200 to 1600 RPM to produce droplets within the range 250 to 300µm. Swath width is quoted at 1.6m, and two flowrate restrictors are available to provide 20 and 30 l/ha application rates.

The Berki is probably the most complex CDA sprayer on the market with 82 components making up a complete sprayer. This together with cost of production is really is its main drawback. The subject of this thesis may be seen as a simplication of the Berki concept, whereby a hydraulic turbine using the spray fluid itself is used to power the disc rather the pneumatic system. The immediate advantage of not requiring an air pump is that any existing knapsack sprayer may be used, offering a low cost alternative for the user.

2.7 Theories on rotary atomisation.

It has long been recognised that rotating discs or cups are effective atomisers, and many detailed studies have been undertaken: Walton and Prewett (1949), Hinze and Milborn, (1949), Dombrowski and Lloyd (1974), Frost (1981).

These rotating devices operate by imparting velocity to the liquid, which is fed at some point onto the rotating disc, usually at its centre. Under the action of centrifugal force, the liquid spreads out towards the periphery of the disc until it reaches the edge and is ejected.

Most workers agree that three distinct mechanisms of atomisation occur at the edge of the disc, of which flowrate is the predominant control. These are as follows:

i) direct drop formation
ii) ligament formation
iii) sheet formation

In the first mode at very low flowrates, fluid builds up at the edge of the rotating disc. In the case of a smooth edged disc, a continuous ring is formed. As liquid continues to flow into the ring its inertia increases. Disturbances appear on the outer edge and grow in size until centripetal force provided by surface tension is overcome, and liquid breaks off as direct drops. The droplets produced by this method, as shown later, can be very uniform in size.

The second mode occurs at higher flowrates. As flowrate is increased, droplets are produced at an increasing rate. Eventually the stage is reached where a new droplet is forming before the previous one has escaped, giving a merged column of fluid which will tend to minimise its surface energy by forming a cylinder or ligament. This mode of atomisation is described by Hinze and Milborn as disintegration by ligament formation.

These jets are themselves unstable and eventually breakup into droplets by capillary instability as described by Rayleigh (1878). This mode of atomisation can also result in a fairly uniform droplet size, and since higher flowrates can be obtained than with direct drop formation, it is the predominant mode utilised by spinning discs for CDA.

With a further increase in feed rate the jets are unable to remove all the liquid, the ring of liquid is forced away from the periphery and a thin sheet extends around the disc. The sheet will eventually break down by a random process producing irregular sized drops. A significant amount of work has been carried out on the disintegration of sheets produced by spinning cups, predominantly for purpose of oil burning. For further information the reader is referred to

Hinze and Milborn (1949), Fraser, Dombrowski and Routley (1963) and Dombrowski and Lloyd, (1974).

Size for direct droplets

Walton and Prewett (1949) developed the following relationship for the size of drops produced by direct droplet formation. Firstly, the accelerating force may be said to be proportional to the retaining forces due to surface tension

$$\pi d^3 p/6 \times w^2 D/2 \quad \alpha \quad \sigma d$$

Thus for direct drop formation we have

$$d = \frac{C}{w} \left[\frac{\sigma}{D\ p} \right]^{\frac{1}{2}} \qquad (1)$$

where :

d	=	droplet diameter, m
w	=	angular speed, rad/s
σ	=	surface tension, N/m
D	=	disc diameter, m
p	=	liquid density, kg/m^3

The constant C has been experimentally determined to have an average value of around 3.8. It is thought to vary slightly with edge profile of the disc, and degree of slippage due to failure of the liquid to reach full cup speed at high flowrates.

Transition from direct droplet to ligament mode

The transition from one mode to the next is a complex process. However, it can be summarised that transition from direct droplet to ligament, or from ligament to sheet is promoted by increased flowrate Q, w, p, and fluid viscosity μ, and by decreased D and σ. Hinze and Milborn (1949), semi-empirically derived an expression for the transition from ligaments to sheets, based upon maximum ligament number and thickness as follows:

$$\left[\frac{\rho Q^2}{\sigma D^3}\right]\left[\frac{\rho w^2 D^3}{\sigma}\right]^{0.6}\left[\frac{\mu^2}{\rho\sigma D}\right]^{0.167} = 1.77 \qquad (2)$$

A number of other workers have also obtained empirical criteria including Matsumoto et al.(1974), Kamiya and Kayano (1979). However, Frost (1981) has noted that the change over from mode to mode is not sudden. This is probably due to the effects of surface tension and small irregularities on the disc, ensuring that the feedrate to each issuing point is not absolutely constant. Frost has therefore provided empirical criteria for transition between intermediate regions, based on experiment and dimensional analysis as follows :

Direct drop formation

$$\left[\frac{Q\ \rho}{\mu\ D}\right]\left[\frac{w\rho D^2}{\mu}\right]^{0.95}\left[\frac{\sigma D\rho}{\mu^2}\right]^{-1.00} < 1.52 \qquad (3)$$

Fully developed ligament formation

$$\left[\frac{Q\ \rho}{\mu\ D}\right]\left[\frac{w\rho D^2}{\mu}\right]^{0.63}\left[\frac{\sigma D\rho}{\mu^2}\right]^{-0.90} > 0.46 \qquad (4)$$

First appearance of sheet formation

$$\left[\frac{Q\ \rho}{\mu\ D}\right]\left[\frac{w\rho D^2}{\mu}\right]^{0.84}\left[\frac{\sigma D\rho}{\mu^2}\right]^{-0.90} > 19.8 \qquad (5)$$

Dropsize for ligaments

Ligaments or jets, or cylinders of fluid break up into droplets because they are unstable, ie. if they have small initial disturbance, it will grow with time. Disturbances may be axi-symmetric (longitudinal), asymmetric (transverse) or asymmetric (non-transverse). The corresponding azimuthal wave number, m, describing each mode is 0, 1, 2 respectively.

Scarlett and Parkin (1976) have suggested that the following expression represents the surface of the jet for all possible modes of disturbance:

$$r = a_0 + c_{m,k}\, e^{\{i(kz + m\theta)\}} \qquad (6)$$

where :
- r = jet radius
- a_0 = wave equation parameter
- $c_{m,k}$ = wave perturbation amplitude, dependant upon m and k
- z = axial distance
- θ = azimuthal angle

Stroboscopic observation of ligaments disintegrating after leaving a single issuing point (Chapter 5) confirmed that the primary mode was axi-symmetric, at least when the sideways velocity of the ligament in air was below 20 m/s. The jet surface in this case, when m = 0, is defined by :

$$a_0 = a\left[1 - \frac{1}{4}\frac{(c_{0,k})^2}{a^2}\right] \qquad (7)$$

where a is the radius of the undisturbed jet, and the value k is the axial wave number defined as 2π/wavelength of breakup.

According to Rayleigh (1879), the wavelength of breakup which determines the size of the drops formed, depends to some extent on the nature of the external disturbances, although the shortest sections into which the cylinder will break have a length of 2πa, where a is the radius of the undisturbed cylinder. The drop diameter produced can therefore be calculated by equating the volume of fluid under one wavelength of disturbance, to that of the spherical droplet that it will eventually produce :

for shortest wavelength, 2πa,

$$\pi a^2 . 2\pi a = \pi d^3/6$$

$$\begin{aligned} d &= (12\pi)^{1/3} a_0 \\ &= 3.35a \\ &= 1.68\, d_{(LIG)} \end{aligned} \qquad (8)$$

where $d_{(LIG)}$ = undisturbed ligament diameter, 2a

The wavelength for maximum rate of growth is 9.0a,

therefore

$$\begin{aligned} d &= (54)^{1/3} a \\ &= 3.78a \\ &= 1.89\, d_{(LIG)} \end{aligned} \qquad (9)$$

Other workers eg Merrington and Richardson (1947) have reported ratios of drop diameter to ligament diameter exceeding 2. A useful rule of thumb is that under most conditions, drops produced by a ligament breaking up have roughly twice the diameter of the ligament.

The breakup of liquid jets is too complex to permit the development of theoretical relationships expressing the dropsize distribution from spinning discs, and is outside the scope of this study. Several expressions to predict dropsize have however been developed on the basis of experiment and dimensional analysis.

Freidman et al. (1952) found that :

$$d_{32} = 0.4 \left[\frac{Q}{\pi n r^2} \right]^{0.6} \left[\frac{\mu}{Q} \right]^{0.2} \left[\frac{\sigma \rho L}{Q^2} \right]^{0.1} \qquad (10)$$

and deduced the following

$$d_{32} \approx \frac{\sigma^{0.1}}{w^{0.6}\, D^{0.2}\, \rho^{0.5}} \qquad (11)$$

Dombrowski and Lloyd (1974) obtained the following correlation

$$d_{32} = 0.25 \frac{Q^{0.334}}{n^{1.32}\, D^{1.22}\, \mu^{0.1}} \qquad (12)$$

and Kamiya and Kayano (1979)

$$d \approx \frac{Q^{1/3}}{w^{1}\, D^{0.5}} \qquad (13)$$

Frost (1981) has obtained an emperical relationship for the drop size as follows :

$$d = 1.87 \frac{Q^{0.44}\, \sigma^{0.15}\, \mu^{0.017}}{D^{0.8}\, w^{0.75}\, \rho^{0.16}} \qquad (14)$$

where :

d	=	droplet diameter, m
Q	=	liquid feedrate, m^3/s
σ	=	surface tension, N/m
D	=	disc diameter, m
w	=	angular speed, rad/s
ρ	=	liquid density, kg/m^3

A summary of the power indices obtained by a number of workers, for the relationship between dropsize and various physical quantities is given in Table 2.7.

SOURCE	PHYSICAL QUANTITY w	R	Q	σ	μ	p
Walton and Prewitt (1949)	-1.00	-.50	-	.50	-	-.50
Friedman et al (1952)	-.60	-.20	.20	.10	.20	-.50
Oyama et al (1953)	-1.00	-.30	.20	-	-	-
Ryley (1959)	-1.41	-.47	.19	1.35	-1.48	-.06
Dombrowski and Lloyd (1974)	-1.32	-1.22	.33	-	-.10	-
Kamiya and Kayano (1979)	-1.00	-.50	.33	-	-	-
Frost (1981)	-.75	-.80	.44	.15	.02	-.16
Sanderson (1982)	-.58	-.15	.18	-	-	-
Kinnersley (1987)	-.72	-.73	.16	-	-	-
Parkin and Siddiqui (1990)	-.49	-.68	.17	-	-	-
Present study	.60	-	.20	-	-	-

Table 2.7 Summary of power indices obtained by different workers for the relationship between dropsize and various physical quantities.

Chapter 3

PRINCIPLES BEHIND A HYDRAULIC DRIVE MECHANISM FOR ROTARY ATOMISERS

3.1 Introduction to turbines

A turbine may be defined as a machine which transforms hydraulic energy into mechanical energy. Hydraulic energy is energy which may be possessed by a fluid, and may take several forms including kinetic, pressure, potential, strain or thermal. Mechanical energy is that which is associated with moving or rotating parts of machines, usually transmitting power. The counterpart of a turbine ie. a machine which converts mechanical energy into hydraulic energy is known as a pump.

Both turbines and pumps are referred to as rotodynamic machines, since there is a net passage of fluid through the machine. Thus they may be distinguished from other forms of hydraulic machinery known as positive displacement machines, within which the fluid is sealed.

Turbines may be further categorised according to the nature of the flow through the machine in relation to the part which is moving, usually referred to as the runner, impeller or rotor. These categories are as follows:

i) Axial Flow (Kaplan)
ii) Mixed Flow (Francis)
iii) Radial Flow (Banki or early Francis)

With axial flow turbines, flow is perpendicular to the impeller, and hence along its axis of rotation. In radial machines, although the fluid approaches the impeller axially, it exits in the plane of rotation. The Waterwheel may therefore be categorised as a radial flow turbine.

In considering the flow through a typical radial flow turbine, we can derive a general expression for the energy transfer between the fluid and the impeller, based on simple one dimensional theory.

The impeller of a turbine experiences a driving torque, T, due to a change in angular momentum of the fluid passing through it. According to Newton's second law applied to angular momentum

$$T = m (v_{t2}r_2 - v_{t1}r_1) \quad (15)$$

where :
- m = mass flow of fluid per second
- r_1 = radius at inlet
- r_2 = radius at exit
- v_{t1} = tangential component of initial fluid velocity at r_1
- v_{t2} = tangential component of final fluid velocity at r_2

now, Work Done per second, or power,

$$Tw = m (v_{t2}r_2 - v_{t1}r_1) w \quad (16)$$

but since $wr_2 = u_2$, and $wr_1 = u_1$,

$$P = Tw = m (u_2v_{t2} - u_1v_{t1}) \quad (17)$$

where
- P = energy transferred per second
- u_1 = impeller velocity at r_1
- u_2 = impeller velocity at r_2

dividing through by the weight of fluid flowing per second, mg, gives rise to Eulers Head, E_h,

$$E_h = (1/g) (u_2v_{t2} - u_1v_{t1}) \quad (18)$$

This equation is known as Euler's turbine equation, and will be referred to in the next section when dealing with a special form of turbine termed a Pelton Wheel.

3.2 The Pelton Wheel.

Turbines may also be classified according to whether they are impulse or reaction machines. With reaction turbines, only part of the available total head is converted into kinetic energy. Therefore the fluid entering the runner has pressure energy as well as kinetic energy. Relative velocity increases during passage, producing a pressure difference across the impeller.

With impulse turbines however, the total head available is first converted into kinetic energy. This is achieved by means of one or more nozzles which produce jets which strike the periphery of a rotating wheel. Such a turbine is termed a Pelton Wheel.

A parameter which describes the reaction of turbines is the degree of reaction. It is derived by the application of Bernoulli's equation to the inlet and outlet of a turbine, assuming ideal flow (no losses). Thus if the conditions at inlet are denoted by the use of suffix 1, and those at outlet by use of suffix 2, then,

$$P_1/pg + v_1^2/2g = E_h + P_2/pg + v_2^2/2g \qquad (19)$$

where E_h is the energy transferred by the fluid to the turbine per unit weight of the fluid. Thus,

$$E_h = (P_1 - P_2)/pg + (v_1^2 - v_2^2)/2g \qquad (20)$$

In this equation, the first term on the right hand side represents the drop in static pressure in the fluid across the turbine, whereas the second term represents the drop in the velocity head. The two extreme solutions are obtained by making either of these terms equal to zero. If $v_1 = v_2$, then $E_h = (P_1 - P_2)/pg$, and this represents pure reaction. If on the other hand the pressure is constant, so that $P_1 = P_2$, then $E_h = (v_1^2 - v_2^2)/2g$, and such a turbine is purely impulsive. Referring to Douglas, Gasiorek and Swaffield (1985) for full derivation, the intermediate possibilities are described by the degree of reaction (R), defined as

$$R = \frac{\text{Static pressure drop}}{\text{Total energy transfer}} \quad (21)$$

$$= 1 - (v_1^2 - v_2^2)/2gE_h \quad (22)$$

from Euler's equation

$$R = 1 - (v_1^2 - v_2^2)/2v_{T1}u_1 \quad (23)$$

With the Waterwheel, there is no static pressure drop, since the static pressure of the fluid when in the form of a jet prior to striking the turbine, and at all subsequent stages, is approximately atmospheric. Thus,the Waterwheel is entirely impulsive. It may therefore be defined as a radial impulse turbine, or Pelton Wheel.

Conventional Pelton wheels, however, usually have vanes, sometimes called "buckets". These generally have an elliptical shape and are attached to the periphery of a rotating wheel, as shown in Figure 3.1. The jet strikes each vane in turn, spreading out into a thin layer which then discharges in the manner depicted. In doing so there is a momentum change in the liquid and energy is transferred to the wheel.

The following analysis assumes that the fluid layer on the surface of the bucket is thin. For a more detailed examination of steady, three dimensional flow, including a consideration of pressure changes based on thickness of flow, one is referred to Nakase (1985).

Let us now define all of the terms in figure 3.1. They are as follows :

V_1 is the velocity of the jet before it strikes the bucket.

U is the peripheral vane velocity

V_{R1} is the initial velocity of the fluid upon striking the vane, relative to the vane

V_{R2} is the final velocity of the fluid upon exiting the vane, relative to the vane, at angle 0 to the direction of U.

V_2 is the resultant final velocity of the fluid upon leaving the vane

V_T is the tangential component of V_2, resolved parallel to the direction of U. Alternatively it is known as the whirl velocity

V_F is the radial component of V_2, resolved perpendicular to the direction of U. Alternatively it is known as the flow velocity.

The total energy transferred to the wheel is given by Euler's equation :

$$E_h = (u_1V_{T1} - u_2V_{T2}) /g \qquad (24)$$

However, with a Pelton wheel, if the vanes are small compared to the overall radius of the wheel, peripheral vane velocity at outlet is the same as that at inlet,

$$u_1 = u_2 = U \qquad (25)$$

so that

$$E_h = U/g \ (V_{T1} - V_{T2}) \qquad (26)$$

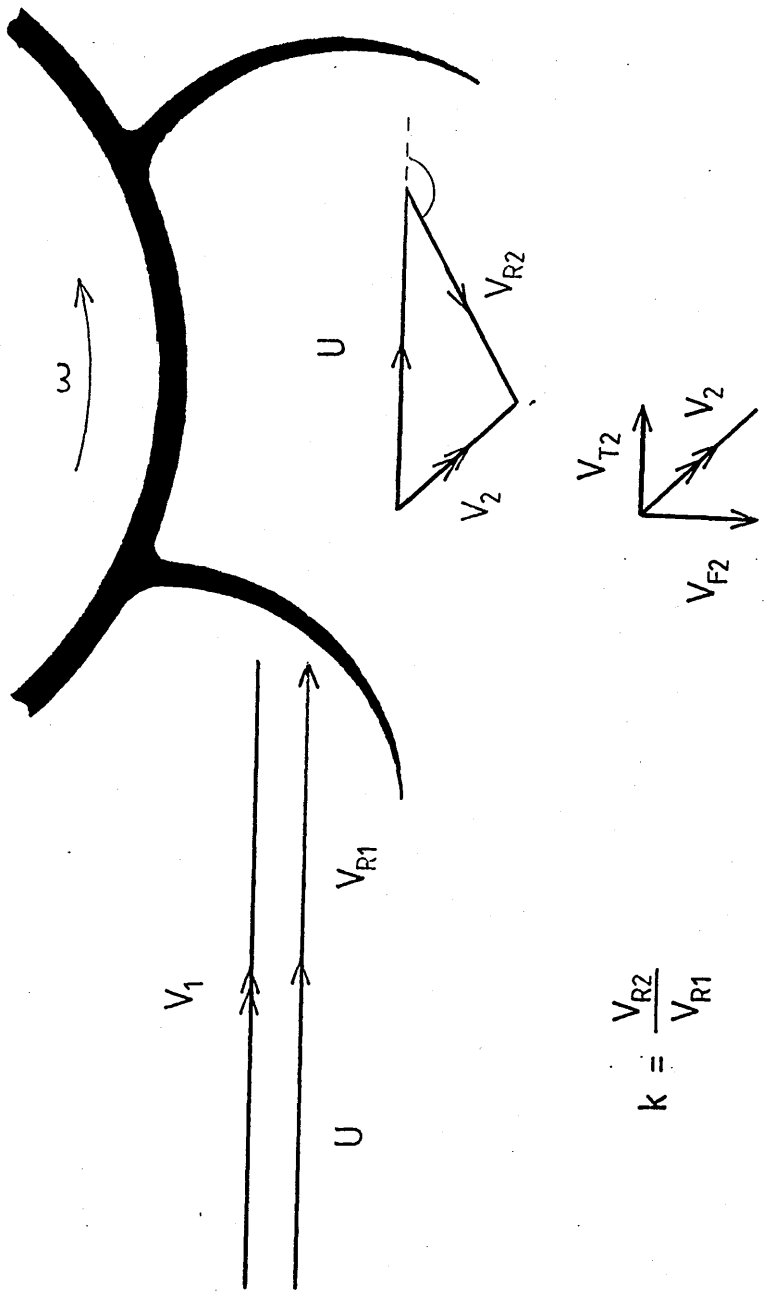

Figure 3.2 Vector diagram showing passage of fluid through a conventional Pelton Wheel (from Douglas, Gasiorek and Swaffield, 1985)

However, it would be useful to obtain everything in terms of V_1 and U, since these are quantities which can be directly measured.

$$V_{T2} = U - V_{R2} \cos (180^0 - \alpha)$$

$$= U + V_{R2} \cos \alpha \qquad (27)$$

where α = angle between velocity relative to the vane V_{R2}, and U.ie. the vane angle.

and $$V_{R2} = kV_{R1} = k(V_1 - U) \qquad (28)$$

where k represents the reduction of the relative velocity due to friction. Thus

$$V_{T2} = U + k(V_1 - U) \cos \alpha \qquad (29)$$

For a Pelton wheel, the initial tangential velocity of the fluid, V_{T1} is equal to the velocity of the jet, V_1, assuming that the jet strikes the wheel tangentially.

i.e. $$V_{T1} = V_1 \qquad (30)$$

so that $$E_h = (U/g) \{ V_1 - [U + k(V_1 - U) \cos \alpha] \}$$

$$= (U/g) \{ V_1 - U - k(V_1 - U) \cos \alpha \}$$

$$= (U/g)(V_1 - U)(1 - k \cos \alpha) \qquad (31)$$

3.3 Equations for drive efficiency

Equation (31) shows that there is no energy transfer when the vane velocity is either zero or equal to the jet velocity. It is reasonable to expect, therefore, that the maximum energy transfer will occur at some intermediate value of the vane velocity. This may be obtained by differentiation as follows :

$$E_h = (U/g)(V_1 - U)(1 - k \cos \alpha)$$

$$= \{(1 - k \cos \alpha)/g\} (V_1U - U^2) \quad (32)$$

$$\frac{dE_h}{dU} = \{(1 - k \cos \alpha)/g\} (V_1 - 2U) = 0 \quad (33)$$

hence, $$V_1 - 2U = 0 \quad (34)$$

and $$U = \tfrac{1}{2} V_1 \quad (35)$$

also $$\frac{d^2E_h}{dU^2} = -2 \quad \text{(maxima)} \quad (36)$$

The second derivative is a negative value, therefore we can say that energy transfer is a maximum when the ratio of the peripheral vane velocity to the jet velocity is a half.

Substituting $U = 1/2v_1$ back into equation (31), the expression for the maximum energy transfer is obtained :

$$E_{h,max} = (V_1/2g)(V1 - \tfrac{1}{2}V_1)(1 - k \cos \alpha)$$

$$= (V_1{}^2/4g)(1 - k \cos \alpha) \quad (37)$$

Now the energy input from the nozzle is the kinetic energy, which per unit weight of fluid flowing is

$$\text{K.E./unit weight per second} = V_1{}^2/2g \quad (38)$$

The units are in metres, as is E_h. Thus the maximum theoretical efficiency becomes

$$\eta_{max} = \frac{E_{hmax}}{\text{Kinetic energy of the jet}}$$

$$= \frac{(V_1^2/4g)(1 - k \cos \alpha)}{V_1^2/2g}$$

$$= (1 - k \cos \alpha)/2 \qquad (39)$$

In the ideal case assuming no friction, there is no reduction of the relative velocity over the vane, and therefore $k = 1$. Also, if $\alpha = 180°$, $k \cos \alpha = -1$ and therefore $\eta_{max} = 1$, ie. the maximum efficiency becomes 100%. In practice, however, friction exists and the value of k is in the region of 0.8 to 0.85. Also the vane angle is usually 165°, to avoid interference between oncoming and outgoing jets. Thus the ratio of the wheel velocity to the jet velocity for maximum drive efficiency becomes, in practice, somewhat smaller than the theoretical ie. about 0.46

3.4 Concept of a smooth, internally driven Pelton wheel for driving a spinning disc atomiser.

A conventional Pelton wheel arrangement has been attempted for driving a conventional spinning disc atomiser, suitable for mounting to a ground vehicle boom (Bals, personal communication) and has been mentioned in an earlier section. The turbine utilised here depends on the use of liquid circulation inorder to produce sufficient power to drive the disc. This arrangement however, leads to undesirable complications the design of the sprayer which are outside the brief of the present study.

Fluid driven rotary atomisers which have been developed at Cranfield, with the aim of producing a simple, low flowrate device suitable for handheld or knapsack application, have been primarily designed without a circulatory mechanism in mind.

Preliminary investigations into the possibity of utilising a non-circulating fluid propulsion system, included driving a ribbed, toothed, wheel using an external jet, as is done with the conventional Pelton wheel system. However, it was observed that since the fluid adhered to the periphery of the wheel for only a very short length of time, this resulted in the fluid bouncing directly off the wheel in a thick sheet, resulting in very poor atomisation characteristics.

It was therefore decided at an early stage that the wheel had to be driven in a manner which enabled the fluid, once exhausted from the jet, to be retained within the wheel system long enough to be distributed and atomised satisfactorily. This lead to the concept of driving a cup, with the jet striking the inner rather than the outerwall.

It was also decided that the surface of the inner wall should be smooth i.e. it should have no vanes or buckets. The reasoning behind this is expanded upon in the next chapter, but briefly it is because the nozzle orifice housing ideally has to be placed as close to the periphery of the cup as possible, inorder to exert maximum torque to overcome bearing friction. Also, the exhausted fluid in rotating with the cup, has to spread out evenly into a thin layer inorder to ascend the inner wall of the cup and be expelled, being atomised as it does so. The presence of vanes or buckets, as well as causing energy wasting interference between incoming and outgoing jets, and would also disrupt the spreading process.

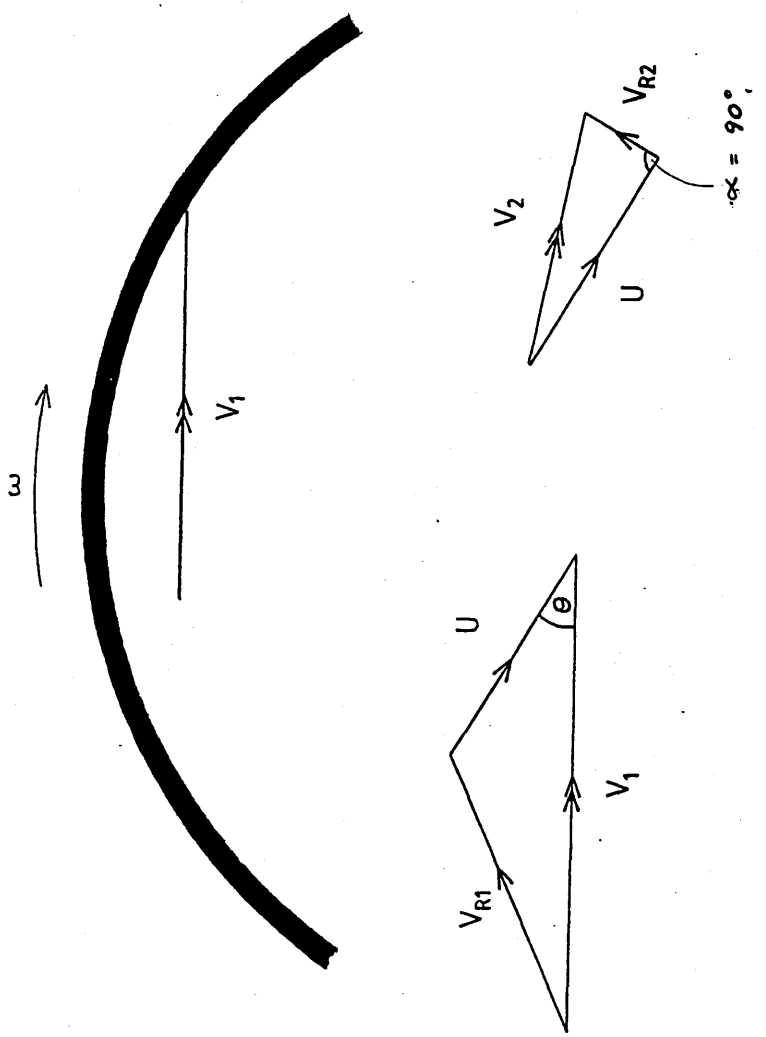

Figure 3.4 Vector diagram showing passage of fluid through the Waterwheel

3.5 Basic equations governing the fluid drive system

With reference to figure 3.2, the Pelton wheel equations of section 3.3 will now be applied to the case of a smooth internally driven cup. From equation (26)

$$E_h = U/g\ (V_{T1} - V_{T2})$$

now $$V_{T1} = V_1 \cos \theta \qquad (40)$$

where θ = angle with which jet approaches inner wall of cup

and $$V_{T2} = U - V_{R2} \cos (180 - \alpha)$$

$$= U + V_{R2} \cos \alpha \qquad (41)$$

from (28) $$V_{R2} = k\ V_{R1} = k(V_1 \cos \theta - U) \qquad (42)$$

thus $$V_{T2} = U + k(V_1 \cos \theta - U) \cos \alpha \qquad (43)$$

and

$$E_h = U/g \{ V_1 \cos \theta - (U + k(V_1 \cos \theta - U)\cos \alpha) \} \qquad (44)$$

Equation (26) can be simplified by making angle $\alpha = 90^0$, ie fluid exits in a direction perpendicular to U.

So $$V_{T2} = U \qquad (45)$$

and $$E_h = U/g\ (V_1 \cos \theta - U) \qquad (46)$$

This is indeed the case with the waterwheel, since the atomising disc has radial grooves in it, which forces the fluid to exit the system perpendicularly to U. In other words, if the final tangential velocity of the fluid relative to the cup is zero, ie. the fluid has attained the same tangential velocity as the cup, equation (46) holds true. This is a reasonable assumption, so long as the fluid layers are thin, and therefore behave viscously (Chapter 5).

In summary then, the energy per unit weight flow per second, (= E_h)

$$E/mg = U/g\ (V_1 \cos\theta - U) \quad [m] \qquad (47)$$

or, energy per unit mass flow per second,

$$E/m = U(V_1 \cos\theta - U) \quad [m^2\ s^{-1}]$$

or, energy per unit volume flow per second,

$$E/vol = \rho U(V_1 \cos\theta - U) \quad [kg\ m^{-1}\ s^{-1}]$$

Alternatively, the Input Energy per second, or Input Power.

$$\text{Input Power} = mU(V_1 \cos\theta - U) \quad [kg\ m^2\ s{-}^3] \qquad (48)$$

If U is the velocity of the inner wall of the cup, V_I, and V_1 is the jet velocity, V_J, then

$$\text{Input Power} = mV_I(V_J \cos\theta - V_I) \quad [kg\ m^2\ s{-}^3] \qquad (49)$$

In Chapter 7, an expression for input energy in the form of equation (49) above, has been used to equate the energy going in with the energy going out of the Waterwheel. This has provided the basis for a model to predict the performance of the Waterwheel, against which experimentally obtained data (Chapter 6) has been compared.

Chapter Four

CONSIDERATIONS INVOLVED IN THE DESIGN OF A FLUID DRIVEN ATOMISER

4.1 Nozzle design

4.1.1 Flowrate and filtration requirements and implications for nozzle orifice number and size

It was decided in the early stages of this project that for design purposes, a suitable typical flowrate, ie. throughput of fluid through the machine per unit time, should be established. A flowrate of 0.25 litres per minute was chosen, as this is typical for handheld CDA herbicide application.

If a flowrate of several litres per minute was the design aim, then a free floating atomiser would be possible. For example, Vann Won (1986) describes such a device, with the rotor supported and propelled, by means of fluid discharging through numerous parallel slits. With bearing friction almost eliminated, rotational speeds of the order of 20 000 RPM may be obtained.

However, the requirement for ground CDA is reduced volumes. Energy is therefore not available for this type of atomiser, at the pressures readily obtainable by knapsack sprayers. A free floating multi-nozzle atomiser may however, have applications for aerial herbicide application.

Figure 4.1.1 shows calculated flowrates through single different sized orifices (assuming constant coefficient of discharge) under a typical supply pressure of say 3 bar. It can be seen that the required orifice diameter for a flowrate of 0.25 litres per minute, assuming only one nozzle is used, is approximately 0.5 mm.

Holes smaller than 0.5 mm are of some concern when discharging liquids containing suspensions of particulate matter, as are many herbicides, especially wettable powders. To avoid blockage, adequate filtration without large pressure losses is required.

Assuming particles to be reasonably spherical (ie. they have shapes where maximum diameter never exceeds twice the minimum diameter), a filter with a pore size of half the nozzle orifice diameter, ie. 250um, would theoretically prevent nozzle blockage.

A commercially popular filter with an inter-element distance of slightly less than 200 µm (Spraying Systems 100 mesh,

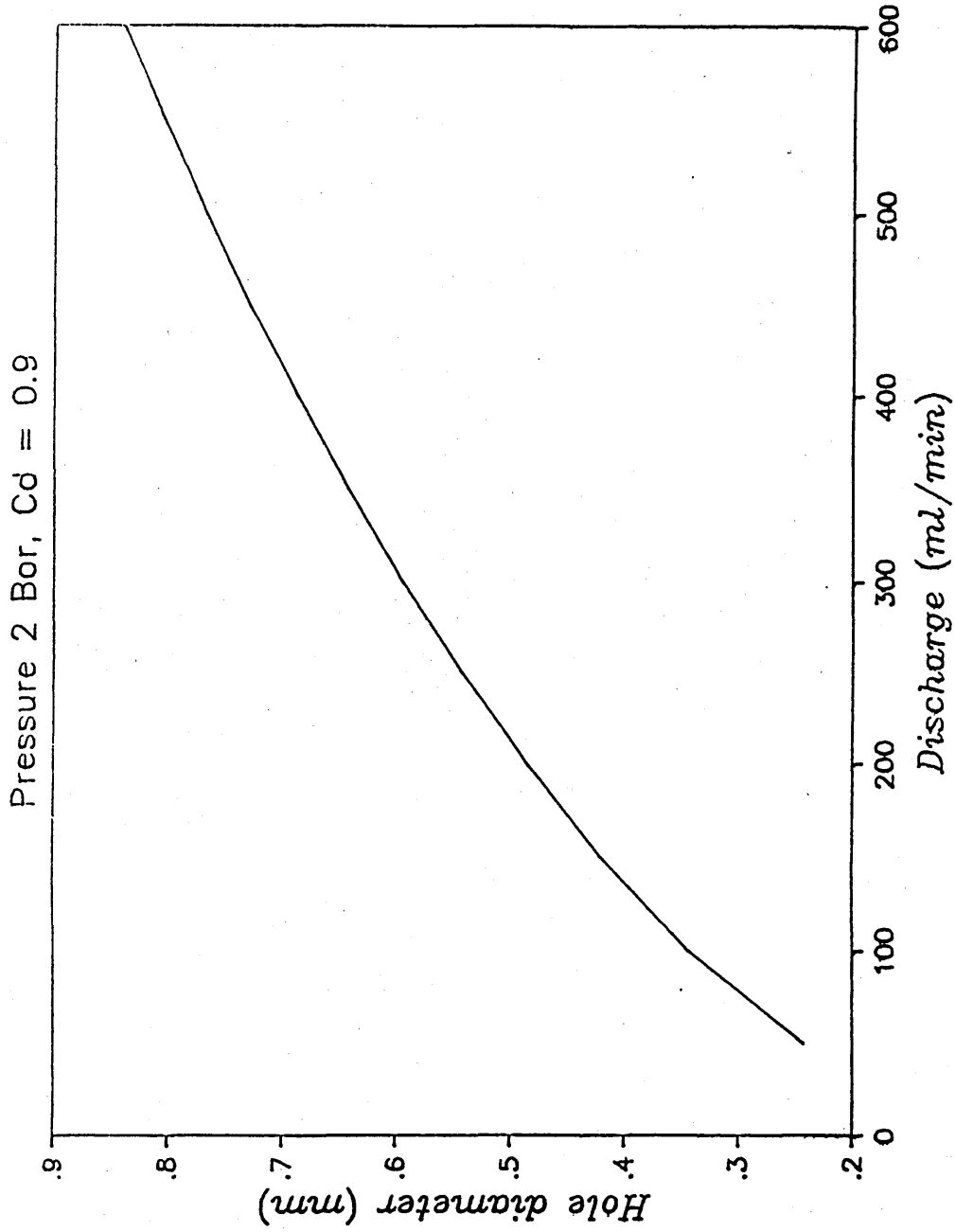

Figure 4.1.1 Variation in flowrate with nozzle orifice diameter

surface area 4cm^2) has been used throughout all tests. Flowrates were measured with clean tap water, both with and without the filter in place. Pressure losses were found to be negligable.

If smaller nozzle orifices were used, in attempt to lower the flowrate, or increase the number of nozzles used whilst maintaining the same overall flowrate, finer filters would be required avoid blockage. Filters with increased surface area would have to be incorporated into the design of the sprayer to avoid significant pressure loss. A foreseable problem with this is filter blockage with suspension formulations. The filter would probably have to be changed or cleaned far more regularly than would be operationally convenient.

For the purposes of this study, therefore, a lower limit for nozzle orifice size of 0.5mm has been accepted for any commercial version of the handheld waterwheel. This has therefore necessitated a design which features a single nozzle only.

The most likely material for the nozzle is Kematal^{tm}, or another hard wearing plastic. It is important that the nozzle is made from a material resistant to both corrosion and wear, since changes in orifice shape with time would be highly undesirable.

In case of the advent of a blockage, it is desirable that the nozzle be easily replacable by the operator, or alternatively that the whole nozzle/holder assembly be interchangable. This is deemed necessary since any attempt to unblock the orifice by insertion of pins, wire or any other sharp object would more than likely result in enlargement of the hole and an increase in throughput of liquid, resulting in a deterioration of performance of the sprayer.

4.1.2 Orifice shape and discharge efficiency

The terms *orifice*, *pipe*, *tube* and *nozzle* are often misinterpreted, and so a brief definition of each is given as follows:

An *orifice* may be defined as an opening in a wall or plate (usually circular) whereby the thickness of the wall or plate is small relative to the size of the opening.

A *pipe* is defined as having the wall or plate thickness, or more commonly the length of the pipe, many times greater than the size of the opening.

A *tube* is a short pipe whose length is not more than two or three diameters.

A *nozzle* is a tube whose diameter is not constant along its length ie it may be converging or diverging, or the inlet may be rounded, for example.

In determining the optimum shape of "opening" to use for the Waterwheel, a number of factors have to be considered. These are as follows:

i) energy losses associated with viscous flow through the nozzle
ii) susceptability to blockage
iii) cost and ease of manufacture
iv) wear

To understand the first process, it is useful to define a term known as discharge coefficient, C_d. C_d may be expressed in terms of two other coefficients described as follows:

Imagining that there were no viscous losses through an opening, volume flowrate, Q_{Ideal}, can be expressed as the product of the area of the opening A_0, and a "theoretical" velocity, V_{Ideal}

$$Q_{Ideal} = A_0 \cdot V_{Ideal} \qquad (51)$$

However, due to a phenomena known as Vena Contracta, the minimum area of the issuing jet, A, is commonly less than A_0 by a ratio C_c known as the coefficient of contraction, so that $A = C_c A_0$.

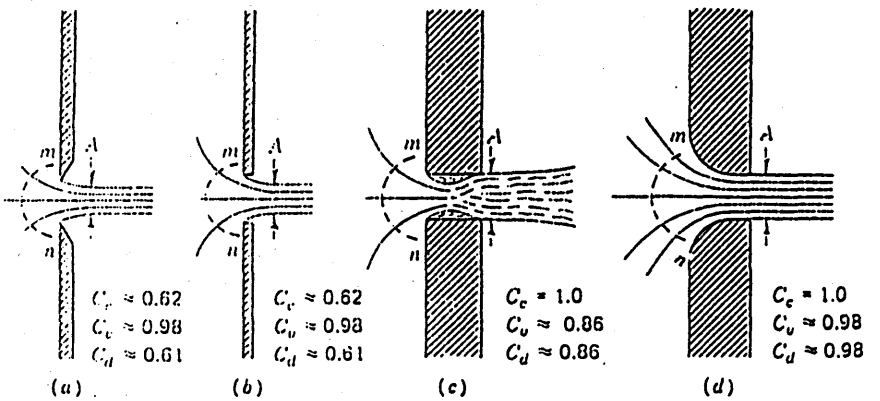

Figure 12.11 Orifices. (*a*) Sharp-edge. (*b*) Square shoulder. (*c*) Thick-plate, square edge. (*d*) Rounded.

[1] Pelton water wheel is the common name for an impulse turbine (Sec. 15.2).

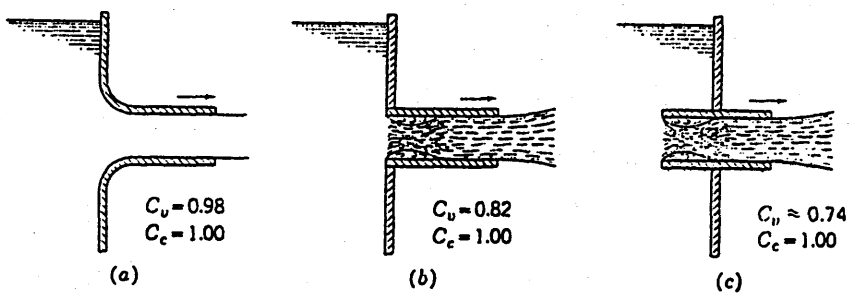

Figure 12.15 Coefficients for tubes.

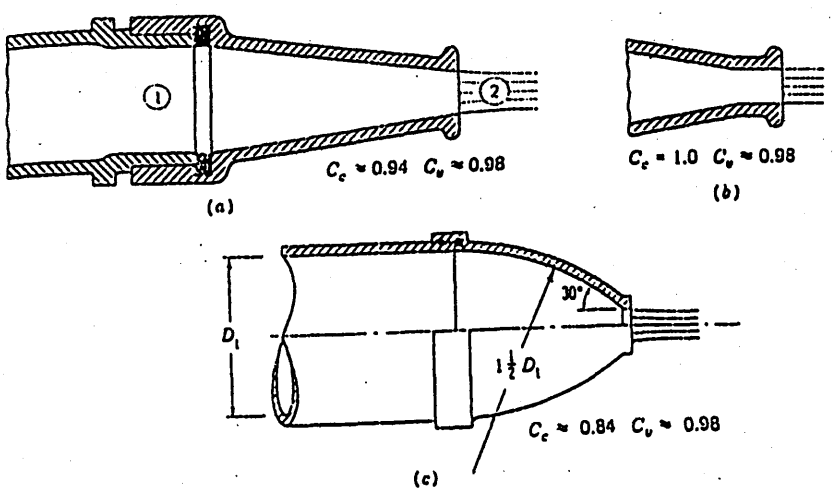

Figure 12.12 Nozzles. (*a*) Conical. (*b*) Straight-tip. (*c*) Fire.

Figure 4.1.2 Effect of orifice shape on discharge efficiency (after Daugherty et al, 1989)

Also, the presence of viscous forces mean that the average velocity of the jet V_J, is less than V_{Ideal}, defined by the coefficient of velocity C_v, so that $V_J = C_v V_{Ideal}$. Therefore:

$$\begin{aligned} Q &= C_c A_0 \cdot C_v V_{Ideal} \\ &= C_c C_v \cdot A_0 V_{Ideal} \\ &= C_d \, A_0 \, \{2\delta P/\rho\} \end{aligned} \qquad (52)$$

It may be noted that $C_d = C_c C_v$ (53)

Orifices which have sharp edges as depicted in Figure 4.1.2a are characterised by low C_c. A well rounded inlet is therefore recommended if large vena contracta losses are to be avoided.

Rounding the entrance to a tube also increases the coefficient of velocity, since flow separation may be avoided. Tubes which are long enough usually create $C_c \approx 1$. However, although length increases the size of the jet from the given area, it also tends to produce more friction.

Gently converging nozzles appear to have the highest coefficients, and are the best choice if energy efficiency is the first priority. However, if considerations ii) and iii) are of significance, perhaps a converging nozzle is not the optimum design. For example, a particulates of a greater range of sizes are capable of lodging themselves at some point along a converging tube, increasing the statistical likelyhood of blockage.

If filtration is poor, and surplus δP is available to do work overcoming viscous losses at a sharp edged orifice, which of course may be larger than a nozzle for the same Q, then this may be a better strategy to adopt.

However, sharp edged orifices are difficult to manufacture in that orifices with constant and correct diameter are difficult to reproduce cheaply. Additionally, sharp edges are prone to wear.

A short tube with mildly rounded entrance therefore probably represents the best nozzle design for the Waterwheel.

4.1.3 Calculation of nozzle performance

(after Spillman, personal communication, 1990).

The relationship between discharge coefficient and supply pressure of the liquid has been measured experimentally, and an a simple emperical relationship was determined (Chapter 6 and 7). However, if a relationship derived from first principles is required, the following provides an expression for Coefficient of Velocity for a smooth long nozzle.

Definitions :

Length of nozzle, l
Diameter of nozzle, d
Maximum velocity at centre of flow, V_m
Velocity, V, at a particular point, r.

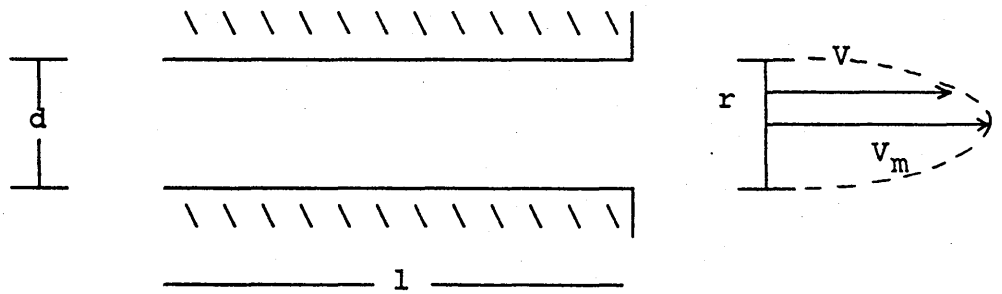

Assuming that the velocity profile across the nozzle flow is parabolic, which will be true for laminar flow when l >> d, and assuming that the inlet is smooth

$$V = V_m (1 - 4r^2/d^2) \quad (54)$$

when

$$r = 0, \quad V = V_m \text{ and } (dV/dr)_{r=0} = 0 \quad (55)$$

and when

$$r = d/2, \quad V = 0 \text{ and } (dV/dr)_{wall} = 8V_m r/d^2 = 4V_m/d \quad (56)$$

The frictional force, or fluid drag at the wall may therefore be defined as follows:

$$\begin{aligned} \text{Drag} &= \pi d l \, \tau_w \\ &= \pi d l \, \mu (dV/dr)_{wall} \\ &= 4\pi l \mu V_m \end{aligned} \tag{57}$$

Now, the mass flow through the hole

$$m = \int_0^{d/2} p \, 2\pi r . \delta r \, V$$

$$= \int_0^{d/2} p \, 2\pi r . \left[V_m (1 - 4r^2/d^2) \right] dr$$

$$= \int_0^{d/2} p \, 2\pi P \, V_m \left(r - 4r^3/d^2 \right) dr$$

$$= \left[2\pi p V_m \left(r^2/2 - r^4/d^2 \right) \right]_0^{d/2}$$

$$= \pi p V_m \left[d^2/4 - d^2/8 \right]$$

$$= \pi/8 \; p \; V_m \; d^2 \tag{58}$$

And, momentum per unit time, mv

$$mv = \int_0^{d/2} p\ 2\pi r.\delta r\ V^2 \qquad (59)$$

$$= 2\pi p \int_0^{d/2} r.\delta r\ V_m^2\ (1-4r^2/d^2)$$

$$= 2\pi p\ V_m^2 \int_0^{d/2} r\ (1-4r^2/d^2)^2\ dr$$

$$= 2\pi p\ V_m^2 \int_0^{d/2} r\ (1 - 8r^2/d^2 + 16r^4/d^4)\ dr$$

$$= 2\pi p\ V_m^2 \int_0^{d/2} (\ r - 8r^3/d^2 + 16r^5/d^4\ )\ dr$$

$$= 2\pi p\ V_m^2 \left[\ r^2/2 - 2r^4/d^2 + 16r^6/d^4\ \right]_0^{d/2}$$

$$= 2\pi p\ V_m^2 \left[\ d^2/8 - d^2/8 + d^2/24\ \right]_0^{d/2}$$

$$= \pi/12\ p\ V_m^2\ d^2 \qquad (60)$$

If the differential supply pressure (pressure minus atmospheric) upstream of the nozzle is P, and the initial flow velocity is negligable, assuming no entry losses

$$\pi/4\ d^2\ P = \pi/12\ \rho\ V_m^2\ d^2 + 4\pi.1\ \mu\ V_m$$

$$3\ d^2\ P = \rho\ d^2\ V_m^2 + 48.1\ \mu\ V_m$$

$$V_m^2 + 481\mu/\rho d^2\ V_m - 3P/\rho = 0 \qquad (61)$$

Therefore,

$$Vm = \frac{-\ 481\mu/\rho d^2 \pm \sqrt{(481\mu/\rho d^2)^2 + 12P/\rho}}{2} \qquad (62)$$

and for a parabolic profile, $u = \frac{1}{2}V_m$, therefore,

$$u = \frac{-\ 481\mu/\rho d^2 \pm \sqrt{(481\mu/\rho d^2)^2 + 12P/\rho}}{4} \qquad (63)$$

Ideal velocity without friction is defined as

$$V_{Ideal} = \sqrt{2P/\rho} \qquad (64)$$

Therefore, Coefficient of Velocity, C_v, may be expressed as

$$C_v = u/V_{Ideal} \qquad (65)$$

or

$$C_v = \frac{-\ 481\mu/\rho d^2 \pm \{(481\mu/\rho d^2)^2 + 12P/\rho\}^{\frac{1}{2}}}{4\{2P/\rho\}^{\frac{1}{2}}} \qquad (66)$$

4.1.4 Nozzle position in relation to inner wall

Earlier versions of the waterwheel, notably Mk. 1 and 2 were tested with the nozzle in different positions with respect to the inner wall of the cup. The following parameters were varied:

i) distance from inner wall
ii) orientation of jet
iii) height relative to inner wall

It was found that maximum cup velocity was obtained when the distance between nozzle orifice and inner wall was as small as could be possible, without the nearest edge of the nozzle body actually impinging into the thin fluid layer ascending the wall. This partly due to the torque supplied by the jet being a maximum. It is also due to the angle of impingement of the jet being a minimum.

Figure 4.1.4 shows a nozzle discharging a horizontal jet onto the inner wall of the cup. It can be seen that the angle with which the jet approaches the wall, Θ, is a minimum when the jet is perpendicular to the radius upon which the nozzle body lies. The value of Θ_{min} is dependant on distance of orifice from innerwall, d, and inner cup radius, R_i, as follows:

$$\cos \Theta_{min} = \frac{R_i - d}{R_i} \qquad (67)$$

A typical value for Θ_{min}, for a cup with inner radius 60mm and a nozzle orifice clearance of 3mm is therefore 18^0.

If the orientation of the jet is anything other than perpendicular then the length of the jet is either increased or decreased, but the impingement angle is increased from its minimum value Θ_{min}.

The position and orientation of the jet has also been varied in the vertical plane. As one would expect, maximum cup velocities were obtained with the jet horizontal. With the jet inclined at an angle ϕ either upwards or downwards, the velocity V is reduced to $V\cos\phi$. For small values of ϕ, therefore, the reduction in velocity is small.

It was discovered that there was an advantage in having a small downward component in the orientation of the jet in that it resulted in improved fluid distribution around the cup, probably due to longer fluid residence time. Also, positioning of the nozzle slightly below the centre-line had similar effect. This will be discussed more fully in Section 4.3.

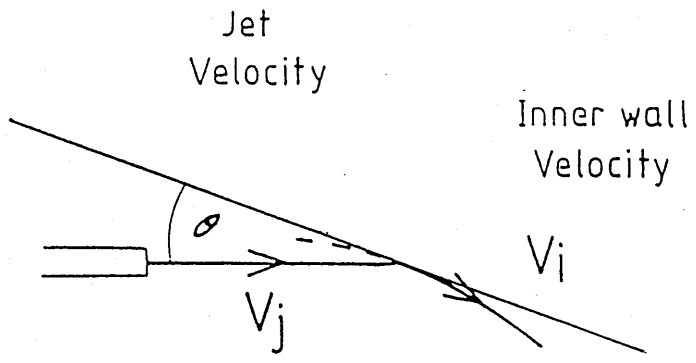

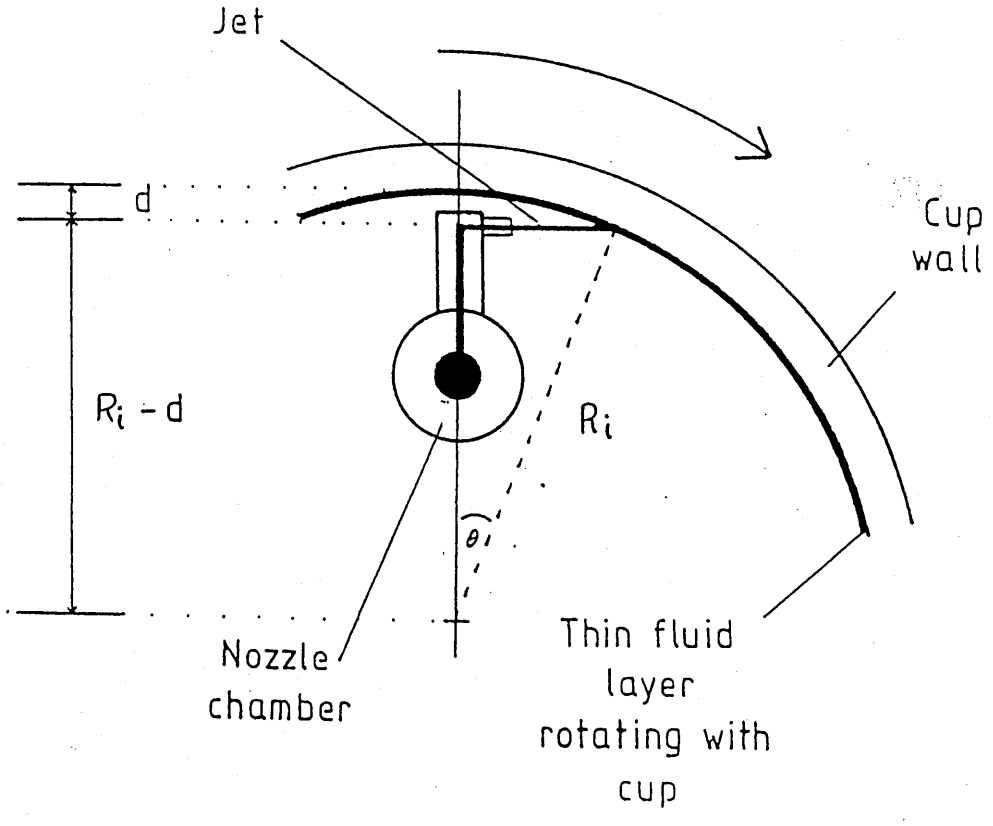

$$\theta \text{ min} = \cos^{-1}\left(\frac{R_i - d}{R_i}\right)$$

Figure 4.1.4 Effect of nozzle position on minimum angle of impingement, θ_{min}

4.2 Bearing design

4.2.1 Choice of bearing

There are several factors to be considered in choosing a suitable bearing for the waterwheel. These include :

i) frictional properties
ii) robustness (shaft diameter)
iii) resistance to fluid contamination and intrusion of foreign particles
iv) resistance to wear
v) production cost

The first primary requirement for the bearing system is low frictional torque inorder that torque provided by the jet can overcome it effectively so sufficient cup speeds are obtained. The high relative friction of sealed bearing arrangements makes their use unlikely. Particular care is therefore required in the design of the bearing housing inorder to avoid contamination.

Bearings with low frictional properties however, tend to be delicate in nature, and accept only small shaft diameters which are prone to bending. As well as possessing low friction, therefore, the bearing must be robust, or have a sufficient shaft diameter of sufficient strength, so as to withstand normal operator handling of the sprayer.

Another very important requirement arises from the fact that the operating environment associated with the application of pesticides is generally wet and frequently corrosive. Every attempt has been made in the design of the bearing housing to try and keep entry of the pesticide fluid to a minimum (section 4.2.2). However, the bearing material must be resistant to corrosion from any chemical likely to be used.

The environment in which agrochemicals are applied is also inherently dirty. The entry of dirt has been considered an important factor in the design of the later prototypes, with the advent of a dust cap to avoid external entry (refer to drawing, Appendix 1). However, internal entry of small quantities of dirt, and particulates from the spray fluid itself is unlikely to be entirely avoided, especially with an unsealed bearing system. The bearing therefore must be reasonably resistant to intrusion of foreign particles.

There are two main types of bearing which have been considered as practical for the purpose of this project; i) ball, and ii) plain.

Ball bearings have two main disadvantages. Firstly, they are expensive to produce, especially the minature versions. This

would increase the unit cost of each unit by a significant amount threatening commercial viability. Secondly, although when clean and well lubricated, frictional torque is very low, friction can increase dramatically with fluid or particulate contamination. This may result in varying speeds and therefore varying droplet size during operations. Also, in severe cases of contamination, complete seizure may be likely.

The attractive feature of plain bearings is that they are cheaper to produce than ball bearings, and that under certain conditions they may have greater resistance to particulate contamination. Disadvantages are that plain bearings have higher friction compared to ball bearings with similar internal diameter. Also, their rate of wear is higher, although this is dependant on the materials used.

As for suitable materials for a plain bearing, a number of substances could be used eg. graphite, molybdenum disulphide, nylon. One material, however, stands out as being exceptional ie. polytetrafluoroethylene (PTFE or Teflon^{tm}). PTFE is noted for its extremely low coefficient of friction (as low as 0.01 in some circumstances) and also for its chemical inertness. Although PTFE has low structural strength and expands rapidly with heat, with the loads and operational speeds expected with the waterwheel this is not seen to be a problem. For corrosion resistance and strength, polished stainless steel is the most likely shaft material.

If cost is not so important, and quality of atomisation is the main object, then minature ball bearings are probably the best choice of bearing to use. Certainly, their greatly reduced friction especially when well lubricated and kept contamination free, enables higher speeds to be achieved, and cup designs with smaller diameter to be used (refer to section 4.3.8 and Chapter 6).

4.2.2 Development of bearing design

The first two prototypes with separate nozzle units, Mk.1 and Mk.2, utilised a light duty an air grinder bearing situated beneath the cup. The bearing consisted of two widely separated, minature ball races. This arrangement was of low friction when lubricated, and worked satisfactorily.

However, the air grinder, after being left in a contaminated condition for several months prior to the commencement of this project, had suffered a marked increase in friction despite repeated efforts at cleaning and lubricating the ball bearings.

In succeeding experiments, an attempt was made to use a single large ball bearing (external diameter 20mm) attached

to the base of the cup. Tests with this bearing proved disappointing. The ball bearing used was of too higher friction for the cup to reach sufficient speeds for satisfactory atomisation, and was prone to fluid contamination

The original Mk.2 prototype was then mounted upon the plain shaft of an electric motor (Mabuchi 540) and redesignated Mk.3. The motor bearing had a polished steel shaft of 3mm diameter. With sufficient lubricant provided, (Fospro general purpose) enough speed was obtained for a number of tests to take place, although rotation speeds were below that required for optimum atomisation.

With subsequent prototypes (Mk.5 to Mk.8), two minature ball races (external diameter 10mm) were used for the bearing (refer to plans in Appendix 1). This enabled the internal diameters of these cups to be reduced from 70mm to 44mm. The races were separated by 1cm for stability, and located near to the centre of gravity of the cup. With the races kept clean and well lubricated, as is possible under laboratory conditions, they served well for all experimental tests, having exceptionally low and constant frictional characteristics.

The possibility of using a plain bearing of with polished steel shaft and carbon impregnated PTFE housing was investigated with the later Mk.9 prototype. Internal diameter was increased to 60mm. Satisfactory rotation speeds were obtained with lubrication, although at higher supply pressures and flowrates than were deemed ideal (Chapter 6). A marked improvement was obtained by reducing the area of contact of the shaft with the PTFE housing by skimming the central portion of the shaft. However this resulted in a marked increase in the rate of wear of the PTFE material, resulting in 1mm of play and cup vibration after approximately 10 hours of use.

4.2.3 Isolation of the bearing from spray fluid

Isolation of the bearing from the spray fluid is probably one of the largest obstacles which the engineer has to overcome when designing rotary atomisers. With electrically driven spinning discs of the hand- held type (Arnold, 1983), the problem is usually overcome by housing the motor (usually a steel shaft with two self-aligning plain bearings) in a well sealed chamber. Because the disc is powered electrically, there is sufficient power availiable to overcome friction encountered at the seal. Additional wetting of the area by splashing is frequently avoided by making the route the liquid would have to take to the bearing as tortious as possible. This is usually achieved by

a series of interleaving vertical walls on both the rotating disc and stationary part of the atomiser (Figure 4.2.3).

Due to the limited surplus power availiable with the fluid driven system, a good seal on the shaft is unlikely. Other means are therefore employed, to make fluid entry of the bearing as difficult as possible. This is achieved by housing the bearing in a central column within the cup, with the entry area located as high as possible (Appendix 1). With the cup in the vertical or near vertical position, the fluid has to rise to the height of the column before entering the bearing. The only occasion when the fluid is likely to do this, is when the cup is flooded. This can be done by artificially stopping the cup, or may occur upon startup with an unusually stiff bearing. With a reasonably free bearing however, full operating speed is reached before the liquid has any contact with the the central bearing housing.

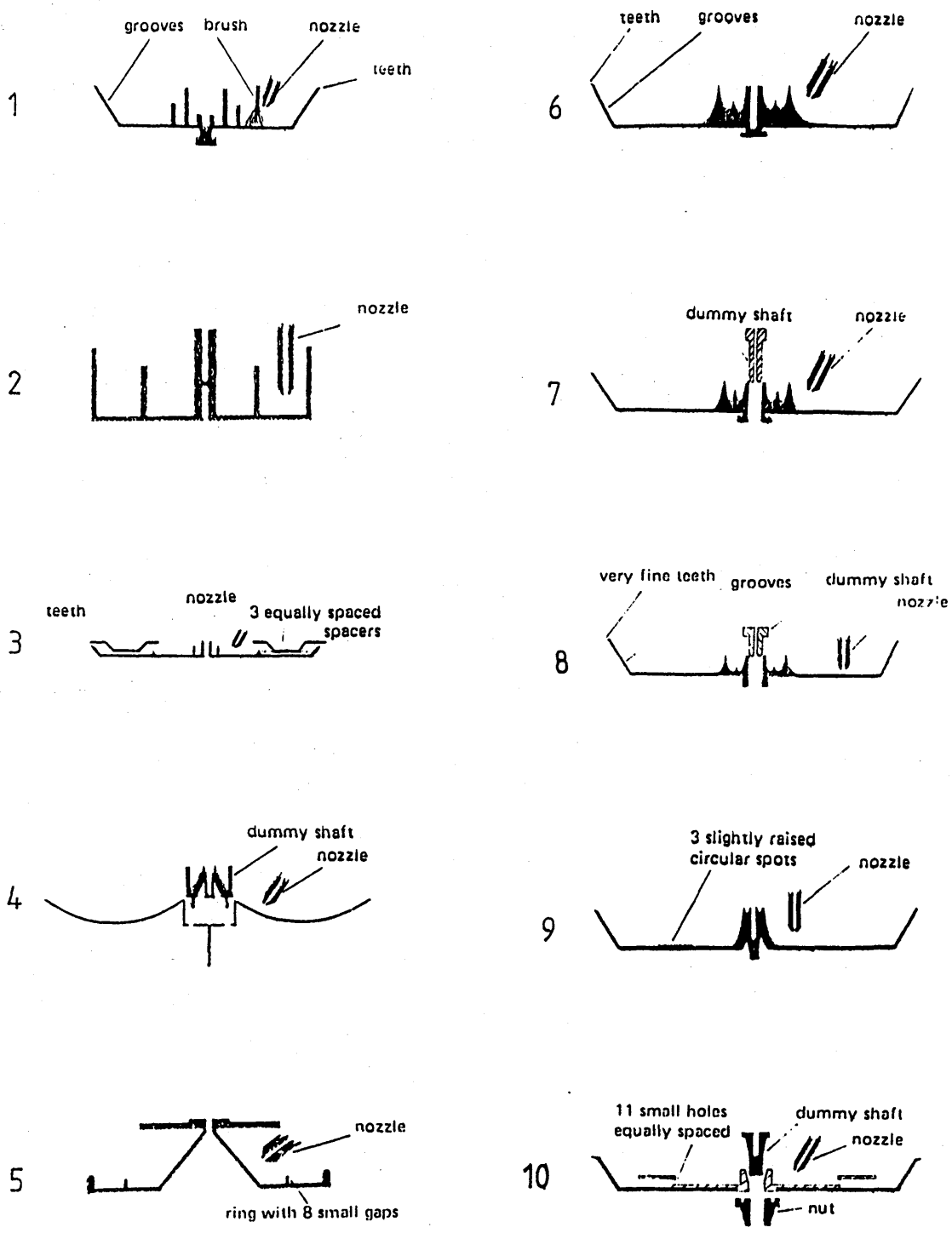

Figure 4.2.3 Schematic drawings of typical fluid isolation systems for hand-held spinning disc sprayers (after Arnold, 1983)

4.2.4 Relationship between frictional torque and bearing size

Dry friction at collar

A polished steel shaft with retaining collar has for reasons given in 4.2.1, has been considered as possible type of bearing to use for the waterwheel, and is shown in the drawing for Mk.9, Appendix 1. In the first test carried out with this bearing, no lubrication was used. Not surprisingly, the atomiser failed to rotate at a speed sufficient to achieve fluid atomisation. The reason for this may be explained by calculating the dry friction generated at the bearing as follows:

A first approximation of the dry friction generated at the bearing can be made by assuming that the waterwheel is operated in an upright position so that no component of the weight of the wheel acts upon the shaft. Ignoring this as well any gyroscopic forces (section 4.3.7) or out of balance forces due to eccentricity, normal forces and therefore friction on the vertical walls of the shaft itself can be discounted.

Friction between the shaft and the bearing therefore only takes place over the ring shaped area of the collar, with inner radius R_1 and outer radius R_2. The weight of the cup, W, gives rise to pressure between the two surfaces. Assuming that this pressure is uniform, the magnitude of the normal force δN exerted on an element of area δA is

$$\delta N = W\,\delta A/A \qquad (68)$$

where $A = \pi(R_2^2-R_1^2)$, and the magnitude of the friction force δF acting on δA is

$$\delta F = \mu_k\,\delta N \qquad (69)$$

Denoting by r the distance of the axis of the shaft to the element of the area δA, the moment δM of δF about the axis of the shaft is

$$\delta M = r\delta F = \frac{r\,\mu_k\,W\,\delta A}{\pi(R_2^2-R_1^2)} \qquad (70)$$

The total moment M of the couple applied to the shaft is equal in magnitude to the sum of the moments of the friction forces δF. Replacing δA by the infinitesimal element $dA = rd\theta\,dr$, and intergrating over the area of contact, we thus obtain the following expression for the moment M of

the couple required to overcome the dry frictional resistance of the collar:

[from Boothroyd and Poli, (1980)]

$$M = \frac{\mu_k W}{\pi(R_2^2-R_1^2)} \int_0^{2\pi} \int_{R_1}^{R_2} r^2 \, dr \, d\theta$$

$$= \frac{\mu_k W}{\pi(R_2^2-R_1^2)} \int_0^{2\pi} 1/3(R_2^3 - R_1^3) \, d\theta$$

$$= 2/3 \, \mu_k W \frac{(R_2^3 - R_1^3)}{(R_2^2 - R_1^2)} \qquad (71)$$

For acceptable shaft strength (section 2.4.5), shaft radius and therefore R_1 was 1.5 mm for Mk.9 (Chapter 6). With a value of 2mm for R_2, a cup weight of 1 Newton, and μ_k = 0.01 for PTFE against polished steel:

$$M \approx 0.017 \text{ Nm}$$

This greatly exceeds the total amount of torque provided by a 0.5mm jet at the highest supply pressure available (5 bar) which is of the order of .0005 Nm or 0.5 mNm. (Chapter 3 and 7). Infact, nozzle orifice size had to be increased to the undesirably high value of 0.75mm, before there was sufficient rotation speed for atomisation, although due to the excessively high flowrate this was predictably very poor.

Lubricated plain bearing

In all the successful tests with the Waterwheel using plain bearings, some form of lubrication of the bearing was found to be necessary for satisfactory rotation speeds to be obtained.

Bearings which depend for their successful operaton upon load-carrying oil-film pressures may be referred to as acting hydrodynamically. The hydrodynamic behavior of bearings is almost completely dependant on the viscous behavior of the lubricant. Viscosity may be defined as the resistance of a fluid to motion ie. its internal friction.

The force, F, required to move a surface of area A at velocity V, over a stationary surface is as follows:

$$F = \mu \frac{A\ V}{h} \tag{72}$$

where h is the separation between the two surfaces, or the layer thickness of the lubricant.

Applying this law of viscous behavior to plain or "journal" bearings, a very useful result on the power loss may be obtained. Assumptions are that the journal bearing is lightly loaded and that the shaft is centered, and that viscosity of the lubricant is constant. The viscous force on the shaft is as follows:

$$F = \frac{2\pi\mu url}{c} \tag{73}$$

where, referring to Figure 4.2.4,

μ = mean dynamic viscosity of lubricant, kg m^{-1} s^{-1}
u = shaft velocity at shaft/lubricant interface, m s^{-1}
r = shaft radius
l = bush length, m
c = bush/shaft clearance, or lubricant layer thickness, m.

This equation was first published by the Russian scientist Petroff in 1833, and is known as Petroff's equation. The power loss, P_P is simply FU, or since u = rw,

$$P_P = 2\pi\mu w^2 r^3 l/c \tag{74}$$

Similarly, the law of viscous flow may be applied to simple thrust bearings of constant lubrication film thickness, t. The power loss, P_T, is :

$$P_T = \mu w^2/t(r_2^4 - r_1^4) \tag{75}$$

These equations for simple journal and thrust bearings have important similarities. Power loss is directly proportional to the viscosity of the lubricant. It increases as the square of the speed. It decreases as lubricant thickness is increased.

PLANE OR JOURNAL

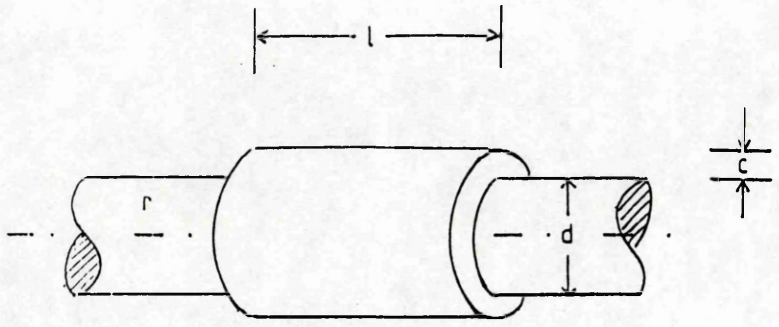

THRUST AND ROLLER

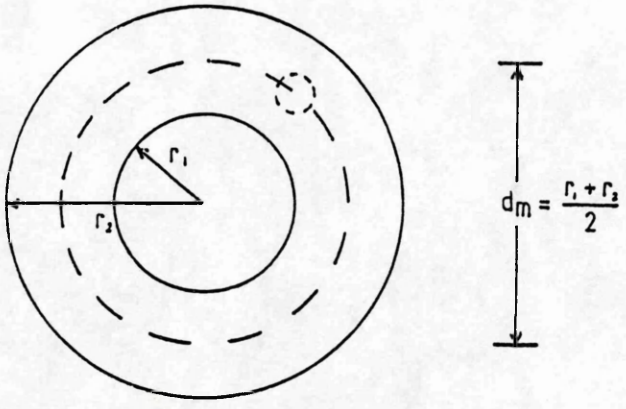

Figure 4.2.4 Explanation of bearing nomenclature

In journal bearings, the loss increases directly with length, and in proportion to the cube of the diameter. In thrust bearings, the loss increases as the fourth power of the diameter. The advantages of keeping bearing diameters as small as possible are obvious.

Friction of ball bearings

However, the shaft for the Waterwheel bearing has to be reasonably thick to withstand shock loads upon dropping. Ball bearings with their lower overall friction at higher shaft diameters are for this reason preferable to journal bearings.

The reason why ball bearings have intrinsically lower friction than plain or journal bearings is that rolling friction is less than sliding friction. However, a mixture of rolling and sliding phenomena occur at the various contact surfaces of ball bearings. Analysis of their friction is therefore very complicated and behond the scope of this work. However, the equations of Palmgren will be included for the sake of completion.

$$M_V = f_0 p d_m^3 (\mu w/p)^{2/3} \qquad (76)$$

where :-

M_V = "torque of running resistance" expressed in kg-mm due to viscosity of the lubricant
f_0 = factor depending on bearing design and lubrication method
p = difference between atmospheric and vaporisation pressure of lubricant
d_m = pitch diameter of set of rolling elements
μ = dynamic viscosity of lubricant, kg-sec/mm^2
w = angular velocity of the bearing rings in relation to each other

This formula is valid for $\mu w/p \geq 2 \times 10^{-6}$. Below this limit the film thickness goes down below approximately 1 µm and resistance is almost constant. The hydrodynamic theory ceases to be valid in this range due to the roughness of the surfaces. Resistance caused by bearing load becomes dominant. An expression for this is as follows:

$$M_L = f_1 g_1 P_0 d_m \qquad (77)$$

where :-

M_L = "load torque" expressed in kg-mm, due to sliding and hysteresis resistance
f_1 = factor depending on bearing design and relative bearing load
g_1 = factor depending on direction of load
P_0 = static equivalent bearing load, kg
d_m = pitch circle diameter, mm

Bearings for Waterwheel prototypes Mk.5 to 8 consist of relatively slow running well lubricated ballraces, which are lightly loaded. This is helped by the fact that two are utilised, separated by several shaft diameters to keep play and radial loads to a minimum (refer to Appendix 1). The first equation is therefore the most applicable.

Frictional torque for ballraces, in similar fashion to plain bearings, varies according to the third power of diameter. Although the reduced friction of ball bearings allows a larger shaft diameter to be used, it is therefore still important to keep the overall size of the bearings down. It was for this reason that minature ball races were used .

4.2.5 Shaft design

The main problem involved with the design of the shaft, is that it has to have a diameter sufficient to withstand bending loads, foreseen to arise primarily from dropping of the atomiser on the ground. However, from the point of view of bearing friction, the diameter of the shaft has to be as small as possible. A design is therefore required giving maximum strength for minimum shaft diameter.

A protective ring could be used to protect the cup from direct impact with the ground and reduce maximum momentary stress to a minimum. However, it is still required that the shaft be fairly robust to withstand general handling.

Full strength analysis is complicated, especially for shock loading, and has not been attempted here. However, an idea of how strength (ie. resistance to deformation) might vary with shaft diameter, may be derived from the following simple expression, for the nominal stress of a cylindrical uniform shaft:

$$\alpha_{nom} = 32\ M/\pi d^3 \qquad (78)$$

where

α_{nom} = nominal stress
M = applied bending moment
$d^3/32$ = section modulus.

From the above, it may be deduced that stresses within such a shaft, as well as bearing friction, are inversely proportional to diameter cubed.

Shaft diameter may be reduced with decreased risk of damage by bending, if a shoulder fillet is included where the shaft base meets the fluid chamber body (Appendix 1) and Figure 4.2.5a. This is due to a reduction of the stress concentration $\sigma_{max}/\sigma_{nom}$ at sharp corners (Peterson, 1974).

Stress concentration factors based on photoelastic tests are illustrated for a stepped round bar with circular shoulder fillet in Figure 4.2.5b. The circular shoulder fillet however does not correspond to the minimum stress concentration; alternative shapes ie. compound, parabolic, elliptic, or derived from fluid flow theories, may provide lower stress concentrations, and may well be worth incorporating into the design of the shaft. The profile in Figure 4.2.5a was derived from a simple graphical method (Grodinski, 1941). A review of optimum transition shapes, many found in nature, has been provided by Haywood (1969).

Alternatively, if manufacture of such a shaft proves too expensive, the cylindrical shaft could be inserted into a hard rubber housing which would absorb impact energy and reduce shock loads. Such a housing however would have to be chemically resistant to the herbicide used, or be capable of being replaced regularly.

FIG. 78

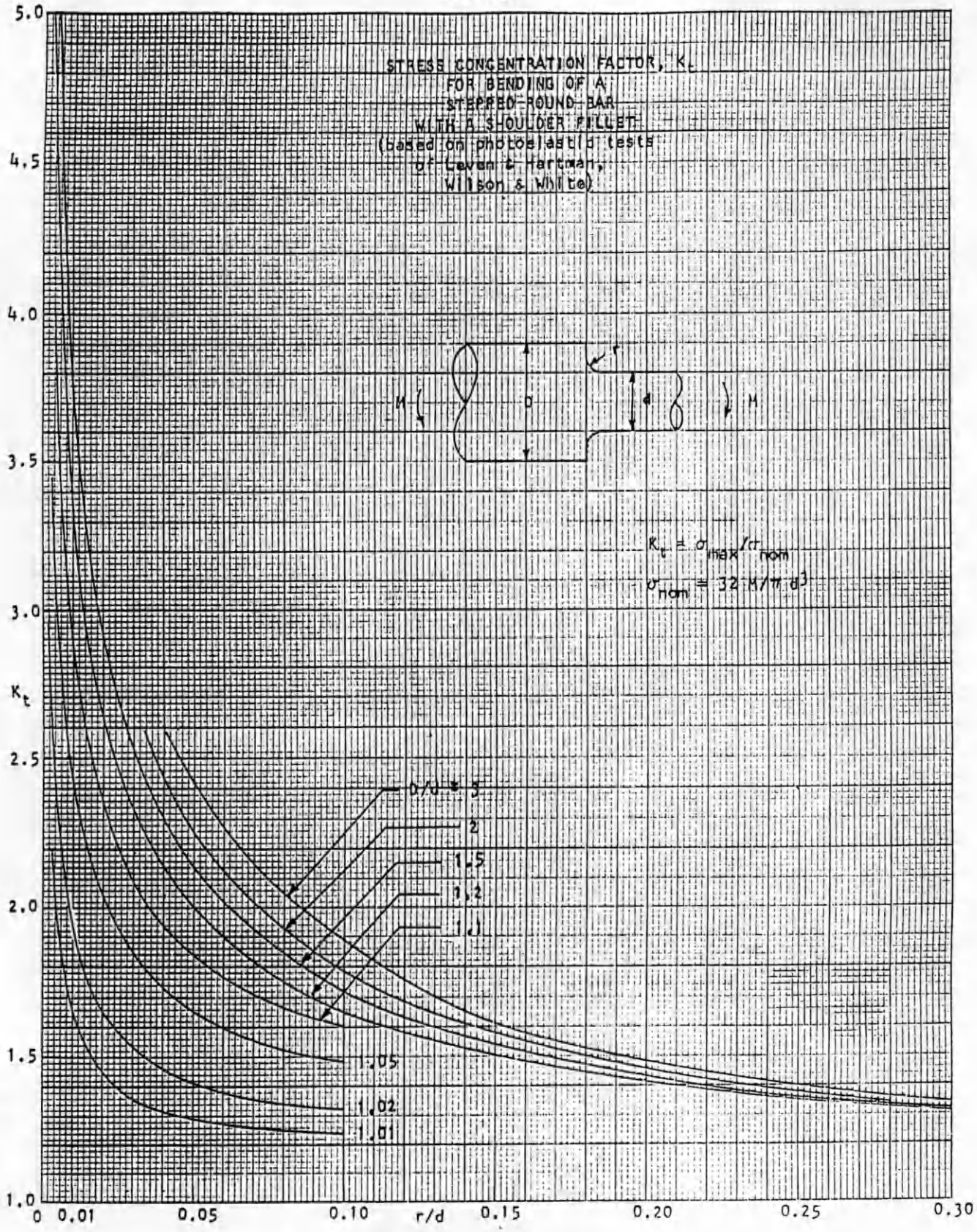

Figure 4.2.5 Stress concentration factors for bending of a shaft with circular shoulder fillet (from Peterson, 1974)

4.3 Cup Design

4.3.1 Cup Shape

Cup shape has gone through an evolutionary process since studies first commenced on fluid driven spinning discs at Cranfield in 1982, initiated by Professor John Spillman. Experiments were carried out by Print (1983), on various shapes of disc including flat discs with central wells, cones with 10^0, 15^0,30^0,and 45^0 concavity, and a bell shaped version. Moderate rotation speeds were obtained, but liquid emmision velocities were low resulting in poor atomisation characteristics.

Tests by Kinnersley (1987) however, showed that a grooved, toothed annulus mounted upon a cup with thin, smooth, vertical walls, enabling the jet to be situated as near to the periphery of the atomiser as possible, combined high rotation speeds with improved fluid emmision. The cup was approximately 8cm in diameter and 2cm deep (refer to Chapter 6).

These early studies provided a useful starting point from which to continue development in design. Essentially, they established that a flat, grooved and toothed disc with a large central well is desirable. The basic reason for this is that distance of the jet from the centre of rotation is as large as possible, providing the maximum amount of torque inorder to overcome bearing friction.

The rest of this section discusses development of this basic form inorder to improve atomisational performance, and also provides experimental data to suggest optimum dimensions.

4.3.2 Motion of liquid ascending inner wall

The jet in striking the inner wall of the cup, spreads and experiences a change in momemtum which provides the driving torque for the cup. Energy transferred is used to overcome bearing friction and also in providing kinetic energy to the liquid.

Once liquid has been released onto the inner wall, which is rotating at speed w, it experiences centrifugal forces which spread the liquid out into a thin layer. This layer experiences a pressure due to centrifugal effects which may be defined as follows:

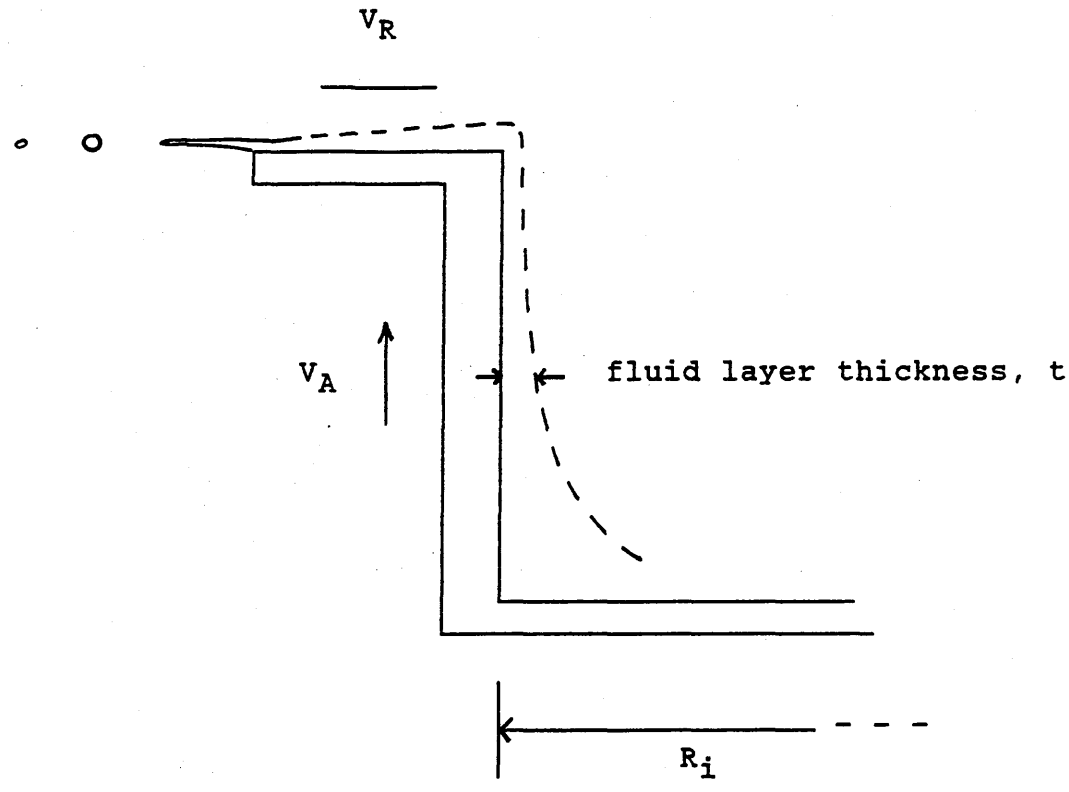

The pressure per unit length, P, on the fluid, or force per unit volume is as follows

$$P = \rho w^2 r \tag{79}$$

Intergrating across the depth of the fluid, we obtain energy per unit volume

$$E = \int_{R_i - t}^{R_i} \rho w^2 r \quad \delta r$$

$$= \rho w^2 \left[r^2/2 \right]_{R_i - t}^{R_i}$$

$$= \rho w^2 \left[R_i t - t^2/2 \right] \tag{80}$$

where E = total energy per unit volume
p = liquid density
w = rotational speed of cup
R_i = inner wall radius
t = fluid layer thickness

Assuming the fluid layer thickness to be thin compared to the cup radius

$$\text{thus } t \ll R_i, \quad \text{so } t^2/2 \ll R_i t$$

$$\text{and} \quad E \approx pw^2 R_i t \tag{81}$$

It is worthy to note at this stage, that energy responsable for spreading the fluid varies with angular speed squared. This therefore implies that for good fluid distribution, small cups are favorable since, ignoring frictional torque effects, they rotate at greater angular velocity than larger cups for a given jet speed.

Centrifugal effects therefore cause the fluid to have energy, defined by the above equation. This energy is initially in the form of static pressure. Upon reaching the disc at the top of the cup, the liquid is free to exit radially, and static pressure here is equal to atmospheric pressure. This therefore gives rise to a small pressure gradient which in turn causes a net flow of liquid up the walls an enables the fluid to exit the cup.

In flowing up the walls, static pressure energy is converted into kinetic energy.

$$pw^2 R_i t = \tfrac{1}{2} p V_A^2 \tag{82}$$

If the walls of the cup are vertical and equal to height h, energy is also required to raise the liquid against gravity,

$$pw^2 R_i t = \tfrac{1}{2} p V_A^2 + pgh \tag{83}$$

The final velocity of the liquid ascending the wall may therefore be obtained, for a typical case outlined below:

$$\begin{aligned} w &= 2000 \text{ revs per min} \\ R_i &= 50 \text{ mm} \\ t &= 1 \text{ mm} \\ h &= 25 \text{ mm} \end{aligned}$$

$$V_A = \left[2w^2 R_i t - 2gh \right]^{\frac{1}{2}} \qquad (84)$$

$$= \left[\{2(2000/60.2\pi)^2.(.05).(.001)\} - \{2(9.81)(.025)\} \right]^{\frac{1}{2}}$$

$$= \left[\{ 4.39 \} - \{ 0.49 \} \right]^{\frac{1}{2}}$$

$$= 1.97 \quad \text{or} \quad 2 \text{ m/s}$$

As can be seen, energy required to overcome gravity, is a small proportion of the total for shallow cups. However, for larger values of h, the gravity term becomes increasingly more important.

4.3.3 Perpheral fluid distribution and weirs

The calculation in the above section assumes that the fluid layer immediately assumes uniform thickness around the cup. Unfortunately in practice, this is not the case. Stroboscopic observation of the fluid on the inner wall surface has enabled its general behavior to be established, and is depicted in Figure 4.3.3.

Upon impact with the inner wall, the jet appears to divide into two main streams which diverge from the original direction of motion of the jet. The angle at which the streams diverge from one another is to a small degree dependant on the angle of incidence of the jet on the wall. However, it is generally between 15^0 and 30^0 for most jet angles.

One stream descends to the base of the cup, and under certain conditions has actually been observed to rebound from the bottom corner of the cup and start rising again. However, with distance around the wall, the streams become weaker as centrifugal forces act to spread the fluid into a layer of uniform thickness.

The other stream immediately starts to ascend the inner wall after jet impact, forming a spiral upwards. The spiral would typically take about one revolution to travel from the base to the top of the cup. Rotation rate was noted to time for one revolution, thus ascension velocity could be determined. Results agreed reasonably well to values predicted from equation (84), despite the fact that constant fluid layer thickness is assumed.

The upper stream is the source of a problem which manifests itself in the atomisation characteristics of the sprayer (Chapter 6). At the point where the stream approaches the atomising disc, there is a segment where flowrate is higher than that of surrounding areas on the disc, giving rise to a sector where the droplet size is greater. This variation in droplet size with position relative to the nozzle is fully illustrated in section 6.

A modification to the shape of the inner wall has therefore been developed, which to a large extent overcomes the irregularity in peripheral fluid distribution (Section 6). This feature was the main design change between prototypes Mk.1 and Mk.2. (refer to Appendix 1). The modification took the form of a series of four, vertically stacked L shaped rings inset into the upper portion of the wall. These rings or weirs contain gaps, increasing in number upwards, which allow the fluid to travel from one channel to the next, and finally to the atomising disc. This arrangement appears to delay the exit of the liquid sufficiently, so that fluid distribution is much improved.

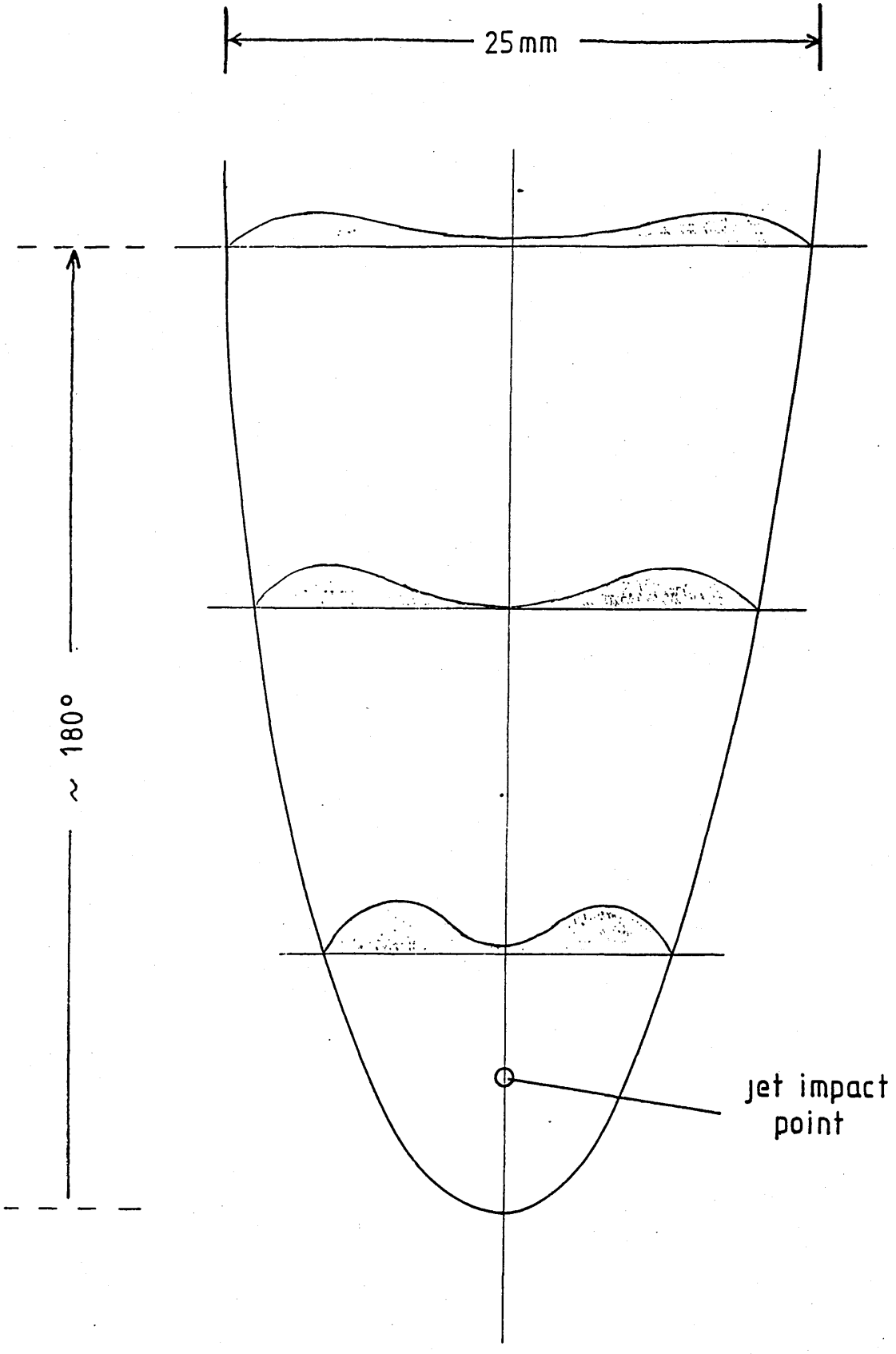

Figure 4.3.3 Behavior of fluid along inner wall of cup, based upon stroboscopic observation

4.3.4 Cup diameter

One of the most important questions to be answered in this chapter is undoubtedly "what size should the atomiser be ?". The most obvious dimensional parameter to use is that of diameter of cup. The rest of this section therefore investigates the factors which are effected by cup diameter, and presents an arguments for the optimum.

Relationship between nozzle orifice size and cup diameter for optimum hydraulic efficiency

(Pelton wheel calculations based on Round and Garg, 1986)

eg. Waterwheel Mk.6

pressure, P	2.5 bar
rotation rate, N	2500 rpm
flowrate, Q	250 ml/min
	or 4 ml/sec
	or 4×10^{-6} m^3/sec

Pressure = 2.5 bar

$$H = \frac{\text{Pressure}}{\rho g} \qquad (84)$$

where ρ = fluid density
g = acc^n due to gravity

$$= \frac{250\ 000}{1000 \times 9.81}$$

$$= 25.48 \approx 25\text{m}$$

now, $$\text{Power} = \rho g H Q \eta \qquad (85)$$

where $\rho g H$ = pressure
η = efficiency

for a wheel with 100% efficiency,

$$P = 1000 \times 9.81 \times 25 \times 4 \times 10^{-6}$$

$$= 250\ 000 \times 4 \times 10^{-6}$$

$$= 1 \text{ Watt}$$

taking a trial value for specific speed, N_s, say 1

$$N = \frac{N_s H^{5/4}}{P^{1/2}} \tag{86}$$

$$= \frac{1 \times (25)^{5/4}}{\sqrt{.001}}$$

$$= \frac{55.9t}{.0316}$$

$$= 1769 \text{ rpm}$$

using $N = 2500$ rpm

$$N_s = \frac{2500 \times \sqrt{.001}}{(25)^{5/4}} \tag{87}$$

$$= \frac{79.06}{55.90}$$

$$= 1.414$$

from Round and Garg (1986), fig. 10.4, page 326

Speed Factor $\phi = 0.48$

$$U = \phi (2gH)^{\frac{1}{2}}$$

$$= .48 \sqrt{2 \times 9.81 \times 25}$$

$$= 10.63 \text{ m s}^{-1}$$

$$w = \frac{2500}{60} = 262 \text{ rads / sec.}$$

$$= 1646 \text{ RPM}$$

now, $V = rw$

$$r = \frac{V}{w} = \frac{10.63}{262} = 0.041$$

therefore $D = 0.082$ m

$\approx$ 8 cm

Jet Velocity

$$V_j = C_v (2gH)^{1/2} \quad (89)$$

$$= .9 \times 22.15$$

$$\approx 20 \text{ m s}^{-1}$$

$$Q = A V$$

Area of nozzle required $= \frac{Q}{V}$ (90)

$$= \frac{4 \times 10^{-6}}{20}$$

$$= 2 \times 10^{-7} \text{ m}^2$$

$$r = (2 \times 10^{-7}/\pi)^{1/2}$$

$$= 252 \times 10^{-6} \text{ m}$$

therefore $d \approx 500$ um

theoretically, $D = 0.082$
$d = 500 \times 10^{-6}$

therefore $\frac{D}{d} = 164$ (91)

Accepted D/d for best efficiency is

$$\frac{206}{N_s} = \frac{206}{1.414} = 146 \quad (92)$$

Therefore, with a single nozzle and the wheel operating at 2500 rpm, a wheel diameter of 82mm gives a value of efficiency close to the optimum as regards hydraulic efficiency. However, as will be discussed later, this may not be the optimum diameter overall, since the Waterwheel has to perform as an atomiser and a Pelton Wheel turbine.

4.3.5 Inertial effects

The rate at which the Waterwheel cup initially accelerates, under a given applied torque, provided by the fluid jet for example, is described by the following:

$$dw/dt = T/I \qquad (93)$$

where

T	=	applied torque
dw/dt	=	rate of change of rotation rate with time
I	=	moment of inertia, or second moment of mass, $\Sigma\, mr^2$

Moment of inertia for a plane cup may be derived from the following :

$$I_{cup} = I_{disc} + I_{cylinder}$$

$$= p\pi R^2 t.[R^2/2] + p\pi(R^2-r^2)h.[(R^2+r^2)/2]$$

$$= p\pi/2.\{\, R^4 t + (R^4-r^4)h \,\} \qquad (94)$$

where

R	=	outer cup radius
r	=	inner cup radius
h	=	inner cup depth
t	=	thickness of base
p	=	density of material (2750 kg m^{-3} for the aluminium alloy used)

Splitting the design drawing (Appendix 1) into 8 component parts (either a disc or a cylinder, refer to Figure 4.3.5) and summing I for each has provided an estimation for the total moment of inertia for Waterwheel Mk.5 to 8 as follows

$$I_{(WW\ Mk.6)} = 3.92 \times 10^{-5}\ kg\ m^2 \qquad (95)$$

It can be seen therefore that that inertia is dependant on R^4. Large cups with high moments of inertia are advantageous since speed would be more constant if supply pressure was unregulated. However this is offset by the fact that the atomiser would take a long time to reach operational speed. A cup with a intermediate moment of inertia ie around 10^{-5} to 10^{-4} kg m^2 therefore represents the optimum.

Moment of Inertia, I_c, of Cylinder $= \dfrac{p\pi L(R^4-r^4)}{2}$

where p = density (Aluminium = 2750 kg m^{-3})
L = length of cylinder
R = outer radius of cylinder
r = inner radius of cylinder

Part	L (mm)	R (mm)	r (mm)	I_c x 10^{-6} (kg m^2)
1	3	22	0	3.0
2	25	25	22	16.9
3	22	16	8	5.8
4	2.5	28	22	4.1
5	2	25	18	2.5
6	1.5	31	18	5.3
7	6	22	20.5	1.5
8	2	9.5	0	0.1

Total Moment of Inertia of Waterwheel Mk.6 = 3.92×10^{-5}

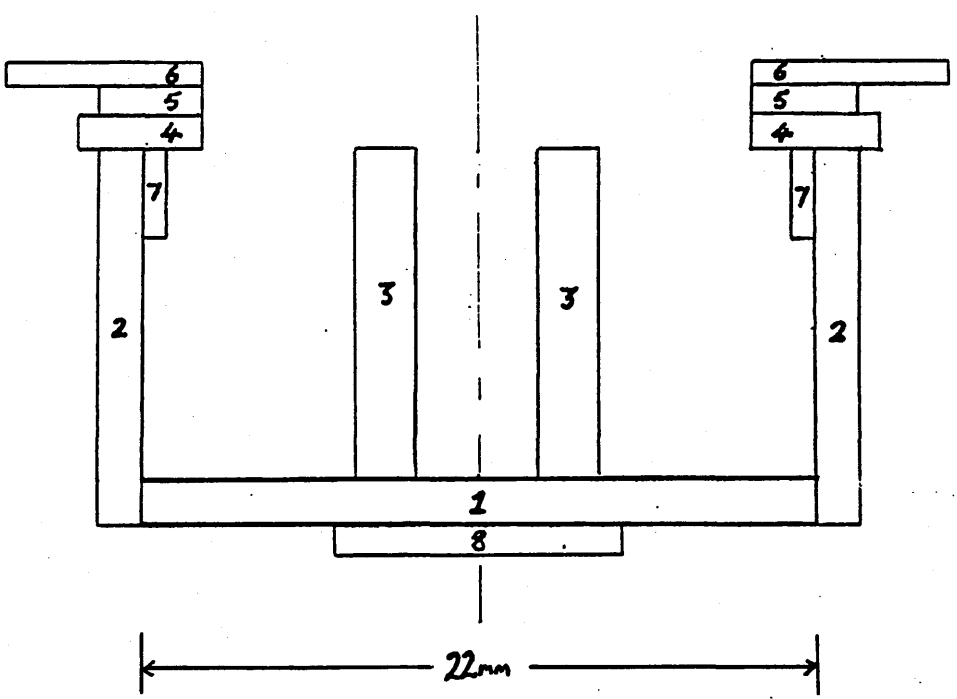

Figure 4.3.5 Calculation of moment of inertia, I, of Waterwheel Mk.6

Moment of inertia is a direct function of mass, and can therefore be reduced by making the cup out of lightweight plastic with thin walls. This would also have the advantage of reducing bending moments on the shaft, especially during impact if the atomiser was dropped on the ground.

4.3.6 Gyroscopic effects

If the axis of rotation of a spinning body is itself rotated, the axis is subject to a moment due to a phenomena known as gyroscopic precession. This is of some concern in the design of a rotary atomiser because gyroscopic moments should not be so great that they become an inconvenience to the operator. This moment is given as follows:

$$M = Iw\, d\Phi/dt \qquad (96)$$

where $d\Phi/dt$ = rate of precession or rate of rotation of spin axis (rads/sec).

For a typical situation with the waterwheel rotating at say 2500 RPM, the operator may want to move the lance at angular velocity of say 1 radian per second.

Therefore

$$M = 3.92 \times 10^{-5} \times (2500 \times 2\pi/60) \times 1$$

$$= 0.01 \text{ Nm} \qquad (97)$$

A handling force required to oppose this moment may therefore be deduced

$$= 0.1 \text{ N} \quad \text{over a grip length of 10cm}$$

This is considered as an insignificant force which the operator would hardly feel. If the diameter of the cup is doubled, raising its moment of inertia by a factor of 16, the force felt in the handle would be 1.6 N, which may be detectable by the operator but is unlikely to cause him any inconvenience. Gyroscopic forces are therefore not foreseen as a major problem to be considered in the design of the waterwheel.

4.3.7 Effect of cup diameter on performance with small increases in bearing torque.

One of the main problems encountered during testing, and one which is envisaged to some extent for commercial operation of the waterwheel, is the variability in performance ie rotation speed, and droplet size produced due to small, uncontrollable variations in bearing torque. Unfortunately, quite small variations in bearing torque, produce large variations in rotational speed, not only because extra energy is expended in overcoming the extra torque, but because hydraulic efficiency of the pelton turbine (energy transferred by the jet) is reduced if cup speed departs significantly from the optimum ½ Vj (section 3.3).

It was noticed at an early stage that this intolerance to variable bearing torque was more pronounced with the smaller cup diameters Mk.3 - 8 (44mm internal diameter) as compared to the earlier larger versions Mk. 1 and 2 (70 mm internal diameter). Possible reasons to explain this observation are as follows:

i) for a given rate of change of momentum of the jet, the torque which it able to provide varies directly with distance from centre of rotation. The larger the radius of the cup, therefore, the greater the torque which can be provided inorder to overcome increased bearing friction.

ii) since the area of inner wall over which fluid can spread also varies directly with radius, fluid layer thickness is less likely to build up causing additional slowing (mechanisms explained later)

iii) the hydraulic optimum wheel size, according to Round and Garg (1986), for a jet diameter of 0.5mm is around 80mm (section 4.3.5)

To assess the effect of diameter on rotation speed, four plain cups with internal diameters of 40mm, 60mm, 80mm, and 100mm respectfully were manufactured and their rotation speeds measured. The cups were driven using a nozzle with orifice drilled to 0.4mm, since this was considered as a likely minimum orifice diameter, and would be a "worst case" situation to provide a useful margin of error for design purposes.

Bearing torque was artificially varied using a dynamo brake system. The cups were mounted upon a small electric motor with a variable 50 Ω resistor connected across its

terminals. Resistance across the terminals could be reduced to make the motor do work by producing a current, and therefore provide controlled and consistant opposing torque.

The dynamo brake system was crudely, although satisfactorily calibrated by recording the rate of slowing of the 60mm cup, for each of 10 resistor settings. It was decided that this was more convenient than calculating the electrical power produced by the dynamo, since this was only a proportion of the total torque provided by the whole system. Knowing the moment of inertia of the cup (section 4.3.6), actual torque values could be assigned to each resistor setting, since:

$$F_w = I(dw/dt) \qquad (98)$$

where F_w = total frictional torque at speed w
I = moment of inertia of cup
(dw/dt) = rate of slowing of cup at a speed w

Figure 4.3.7a is a summary of the slowing rates of the 60mm cup. The cup was initially driven up to 8000 RPM using a jet of air, the jet quickly taken away and times recorded to pass through 1000 RPM intervals recorded to the nearest half second (although for graphical purposes they are presented in Figure 4.3.7a to the nearest second). Since 2000 RPM is considered to be the most likely operating speed for the Waterwheel, we are most interested in torques produced at this speed. Tangents were therefore carefully drawn at 2000 RPM to determine the slowing rates. These were then multiplied by the moment of inertia of the cup to give torque values. This calibration is provided in Figure 4.3.7b.

Figure 4.3.7c shows rotation speeds with the resistor disconnected. As can be seen from Figure 4.3.7b, the bearing torque value provided by the motor alone is 0.75 mNm. It interesting to note that at the highest supply pressures, the 40mm cup rotates at maximum w, whereas at lower pressure its speed falls off dramatically compared to the larger diameter cups.

Probably of more significance in determining what droplet size the sprayer produces is cup tangential velocity, rather than rotation rate, and graphs of inner wall velocity verses jet velocity for the four cup diameters are drawn in Figure 4.3.7d. As can be seen the velocities of the larger cups are very near to half Vj, the condition for optimum energy transfer (Chapter 3). At a typical supply pressure of 3 bar, the jet velocity is approximately 22 ms^{-1} The velocities for the 60mm cup are a little reduced, but for the 40mm cup, inner wall velocity is reduced to just over 1/4 Vj.

Rotation rates were then measured at 3 bar for the different resistor settings, and these are depicted in Figure 4.3.7e. The 0.75 mNm line with the 40mm and 60mm rotation speeds of around 2800 RPM has been omitted for clarity. For the next five friction values up to 1.2 mNm, it may be noted that the 60mm cup produces the fastest rotation rates. However, as bearing friction is further increased, the 80mm cup, and eventually the 100mm cup perform the best. It is worthy to note that increasing bearing friction by just over 100% has only caused a reduction in speed of less than 50% with the largest cup diameter. However, with the smallest cup, the change is over 80%.

Unfortunately, the cups were not manufactured with finely milled grooves and teeth, and so they did not atomise the liquid sufficiently well to warrant extensive optical droplet sizing, although a few brief tests were carried out to check the expected trends.

A parameter likely to be a reasonable indicator of dropsize is $1/(wr)^{0.5}$ (refer to Chapter 5). From Figure 4.3.7f, one can see the effect on this parameter of increasing bearing friction, for each of the four cup diameters. The spread of droplet sizes produced by the 40mm cup at the different friction levels is large, although this is greatly reduced with the 60mm cup. Data for the two larger cups show that there are diminishing returns for cup sizes above 60mm.

This exercise proved particularly useful, in that it provided a reliable empirical guide for cup diameter, for various values of bearing friction. For example, it led to the choice of 60mm (internal diameter) for the Mk.9 Waterwheel, to be mounted upon a plain bearing with an expected torque value of around 1 mNm at 2000 RPM.

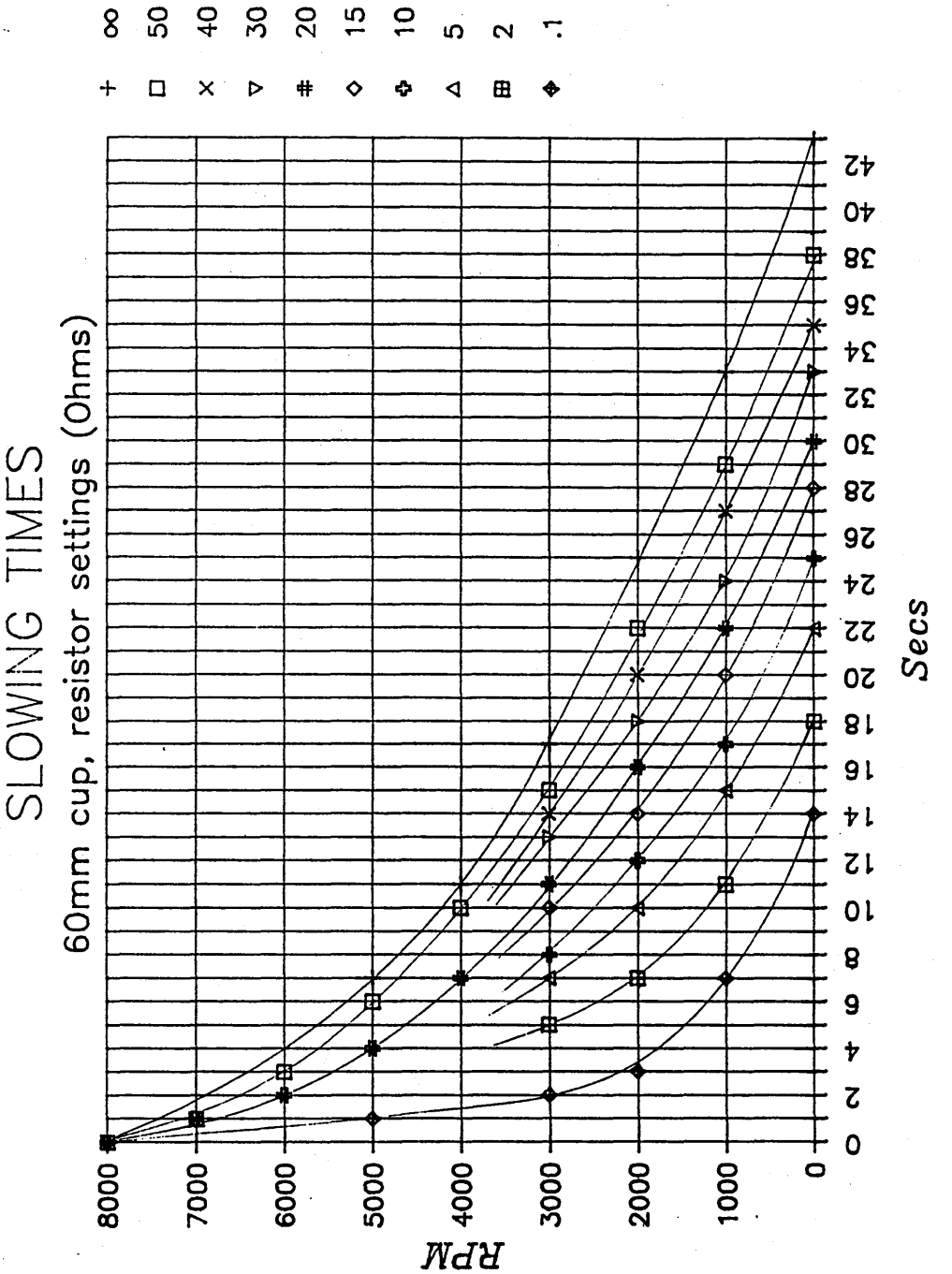

Figure 4.3.7a Summary of slowing rates of 60mm cup

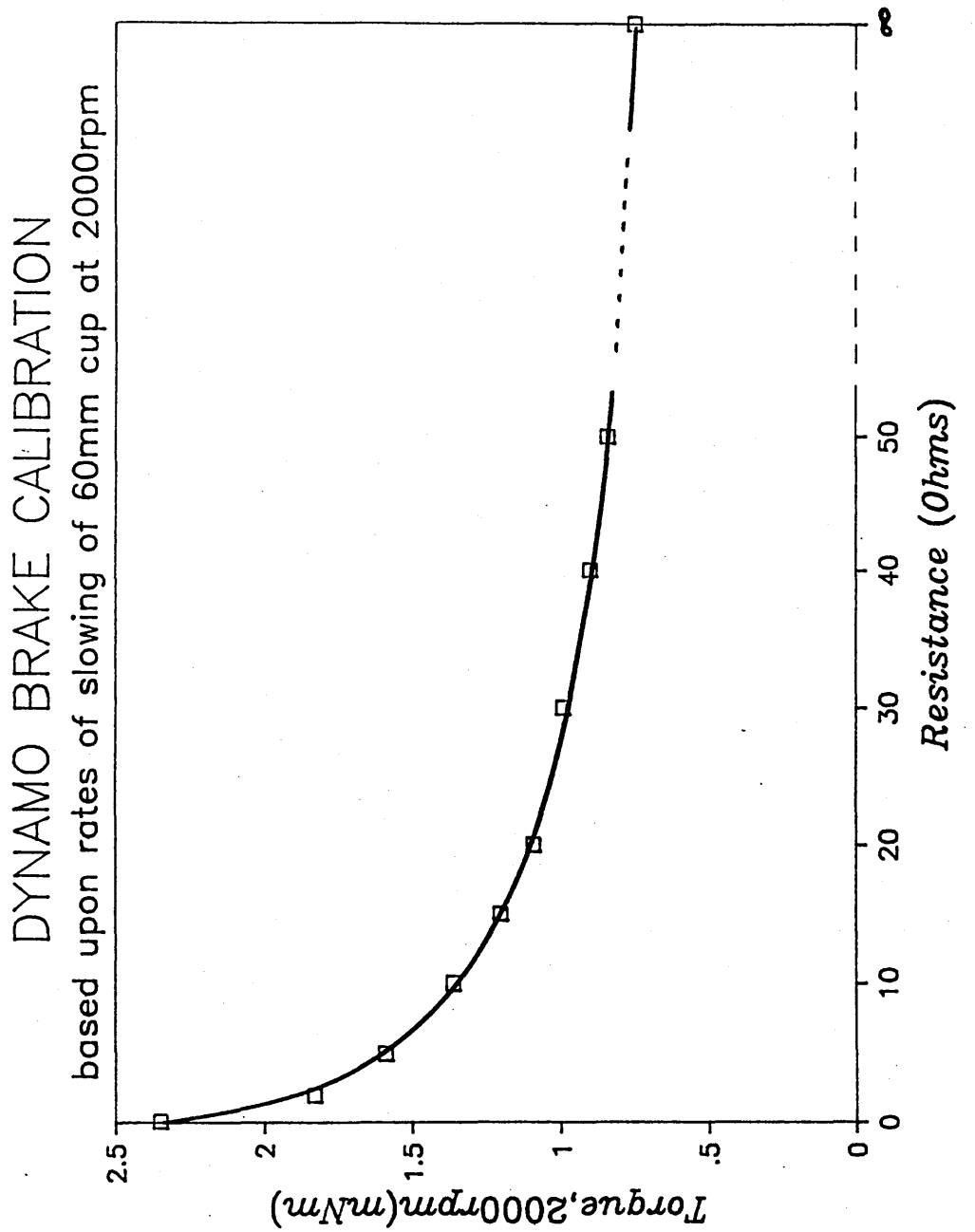

Figure 4.3.7b Dynamo brake calibration

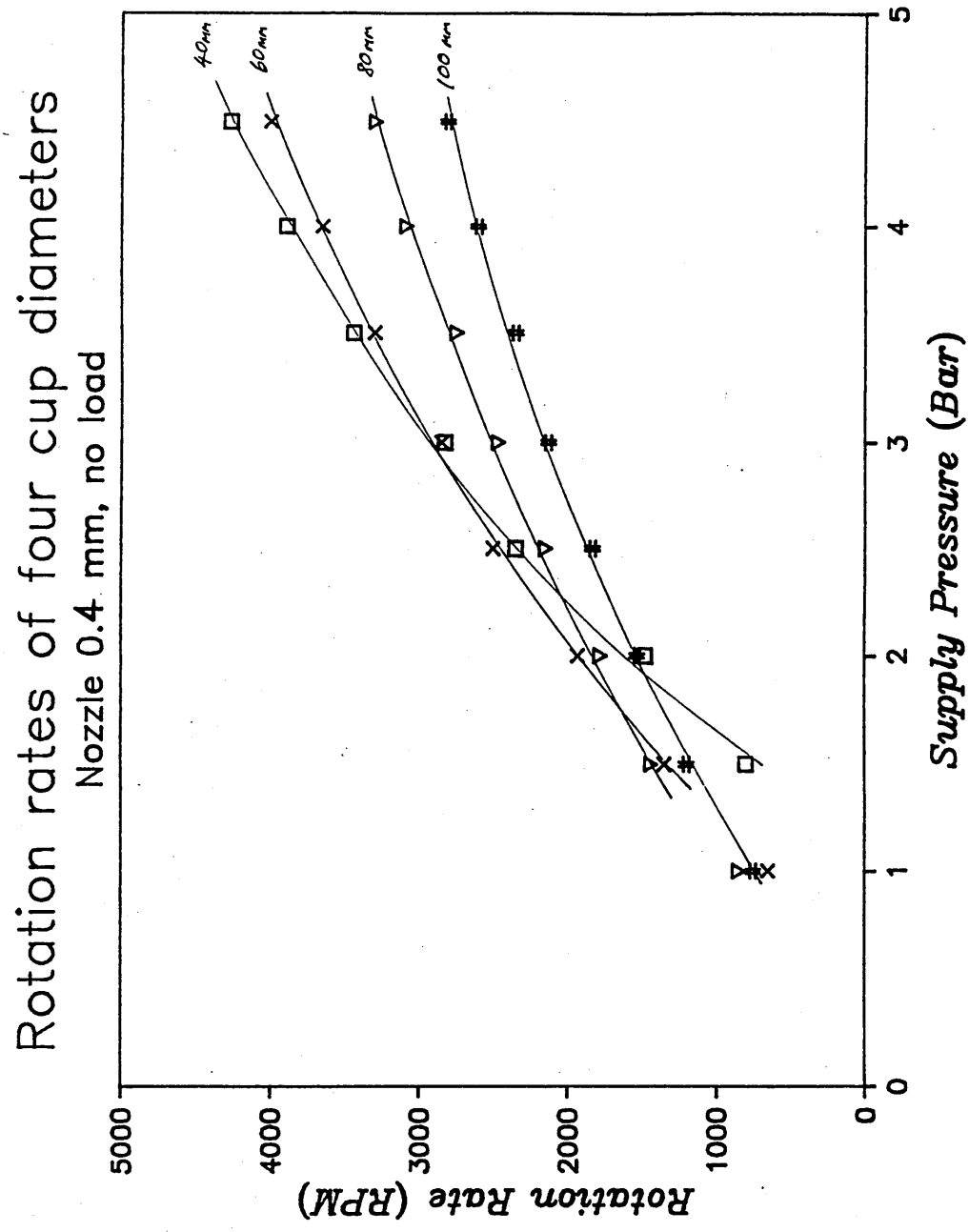

Figure 4.3.7c Cup rotation speeds with brake off

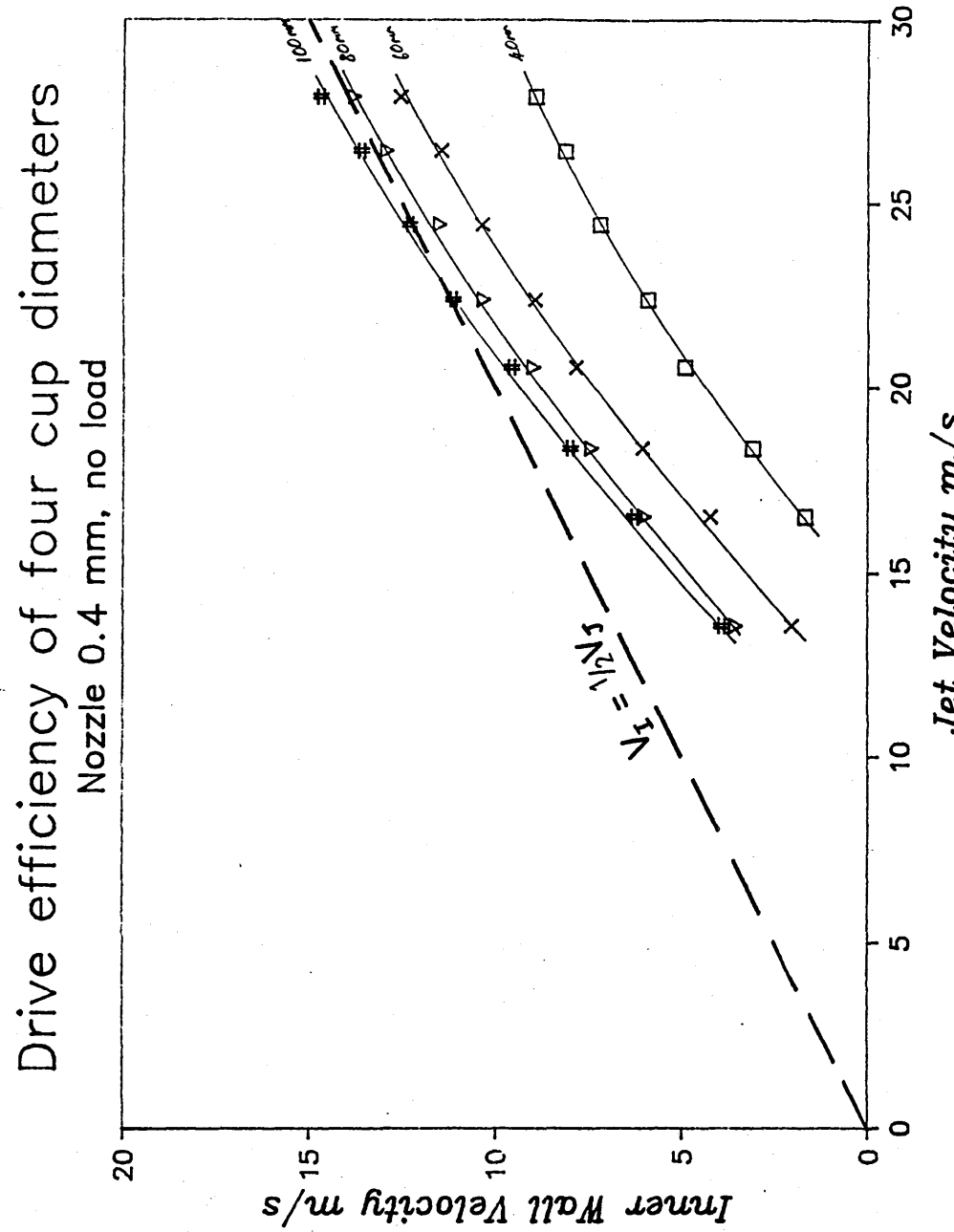

Figure 4.3.7d Inner wall velocity V_I, vs jet velocity V_J, with brake off

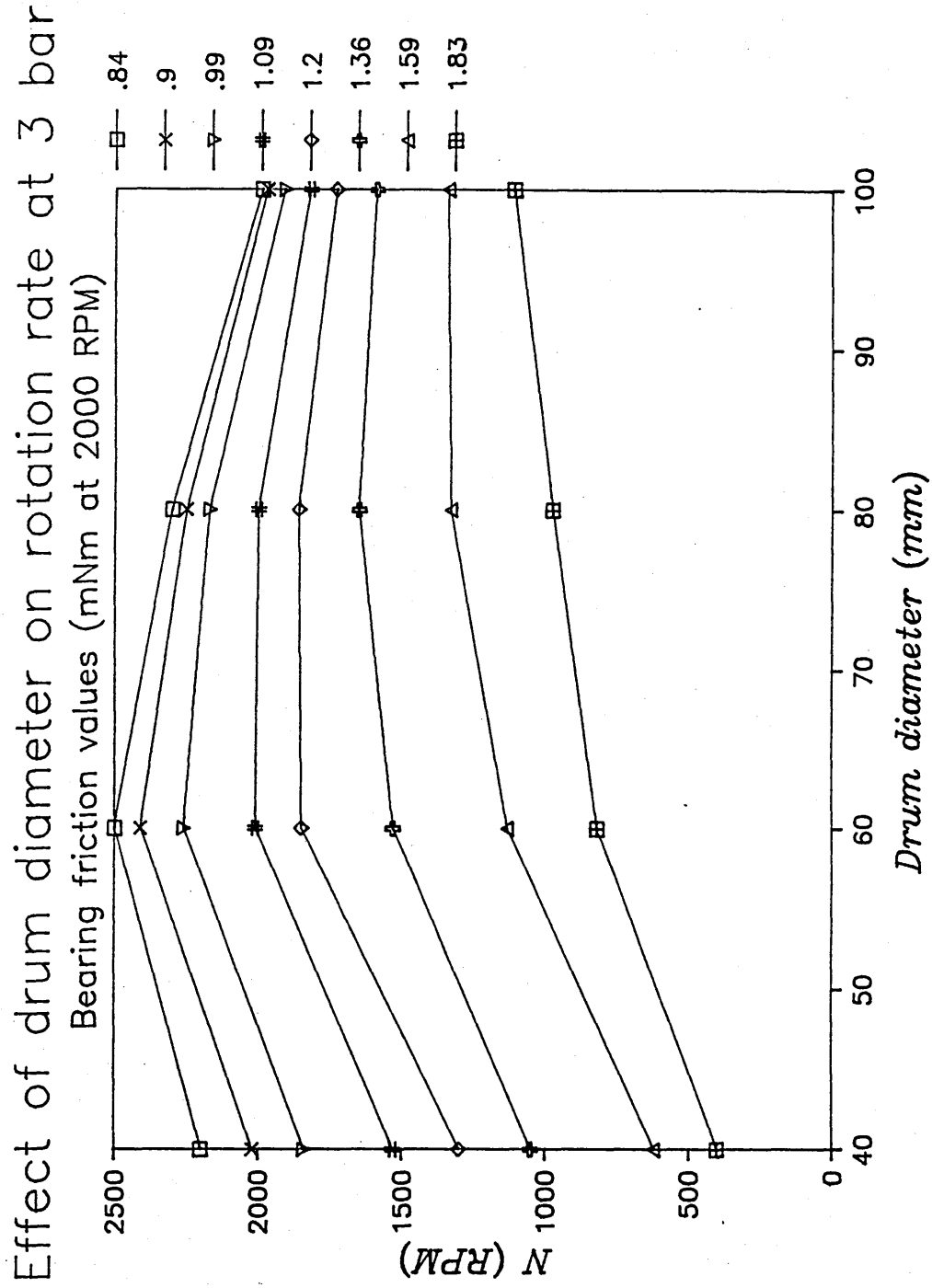

Figure 4.3.7e Rotation rates for 4 cup diameters at 3 bar, for varying total non-useful torque values

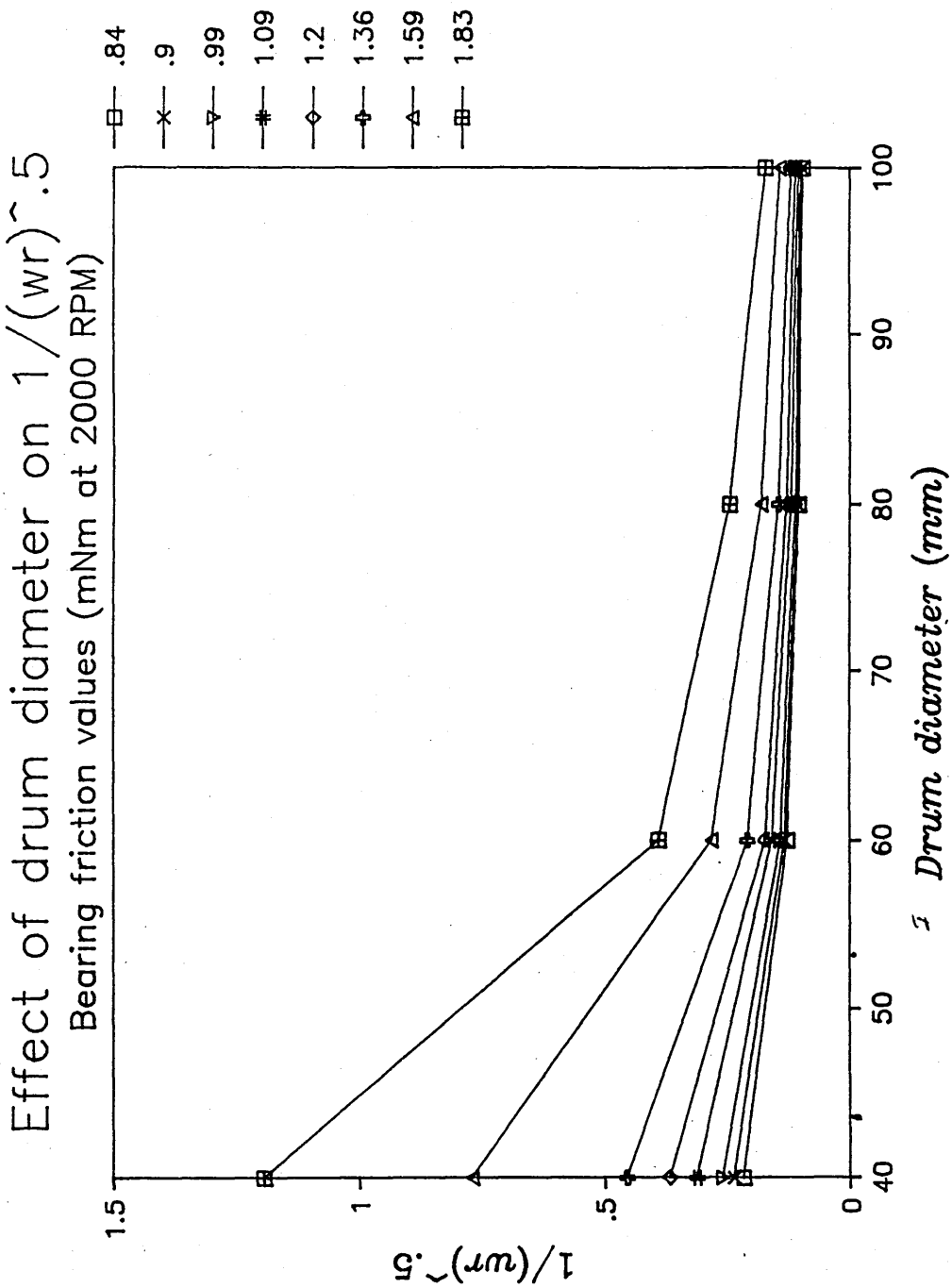

Figure 4.3.7f Effect of cup size and non-useful torque on dropsize parameter

4.4 Disc Design

4.4.1 Behavior of fluid layers on rotating surfaces

A thin fluid layer upon a plain rotating surface moves around with that surface, because viscosity within the fluid tends to "adhere" the fluid to it. Assuming no flow separation, tangential velocity of the fluid at the surface $V_{T,0}$, is equal to the velocity of the surface, and may be defined as the product of the rate of rotation w, times distance from centre of rotation, r.

With distance away from the surface, tangential velocity relative to a stationary observer decreases resulting in a velocity profile leading to $V_{T,1} = 0$ at the air interface. The fluid is said to have a boundary layer, which in this instance will be defined as the layer in which tangential velocity is greater than 99% of the maximum value of $V_T,0$.

A thick fluid layer does not "adhere" to the surface but will lag behind with a mean tangential velocity less than that of the surface. This phenomena is known as slippage. Slippage is an undesirable feature in rotary atomisation since maximum energy is not being imparted to the fluid.

Due to the action of centrifugal force, the fluid also moves radially, which eventually leads to atomisation. The resultant path of the fluid as seen by a stationary observer is therefore a spiral leading outwards away from the centre of rotation. This may be revealed by trace of paint introduced into the flow with a syringe.

Slippage may also be effected by rotation speed. However, this is not a simple effect since although increased speed will lead to an increased shear-rate encouraging slippage initially, the fluid layer will itself be thinner as it progresses radially. Properties of the fluid are also important; a low viscosity low surface tension oil may be more prone to slippage than water for example. In fluids which are very viscous and non-Newtonian in character, the development of shear layers within the fluid may also cause slippage.

4.4.2 Grooves and teeth

The primary purpose of grooves and ribs are to delay the onset of slippage and enable higher rotation rates and flowrates to be achieved. This is probably due to surface tension effects and the affinity of fluids for edges and corners. The exact mechanism is complex and outside the scope of this thesis.

However, some observational experimentation was undertaken which involved varying the orientation of a single groove milled along a 50mm long aluminium bar (Figure 4.4.2 and section 5.4 for description of apparatus). Effectiveness in retaining an accelerating layer of fluid, in this case water, was noted under varying conditions of rotation speed, flowrate, and surface tension.

Stroboscopic illumination enabled observation of the fluid as it progressed along the bottom of the "V" shaped groove. The approximate speed of the liquid trail was revealed by the presence of an occasional air bubble on its upper surface. When the tip of the groove was reached, the liquid was flung off in the form of droplets or a ligament depending on the flowrate/rotation speed condition.

The first groove tested was orientated in conventional manner as in the upper diagram of Figure 4.4.2 a. ie. sideways mounted with respect to the direction of travel with a windward and leeward facing wall. Above certain flowrates the liquid trail was observed to suddenly exit the base of the groove, sometimes after having initially travelled a short distance along it. The fluid would ascend the windward wall until the intersection of the wall with the upper surface was reached. The fluid would then typically remain attached to this edge until the corner of the groove was reached, and then be atomised.

The exact point of fluid exit was unpredictable, but did not move once established. Increasing the rotation speed and flowrate generally lead to earlier exit of the groove. Care had to be taken to ensure that the base of the groove was free from dust particles or tiny irregularities since these could also trigger fluid exit. The presence of a dust particle was seen to cause early exitting and then prompt return of the fluid trail to the base of the groove.

Rotating the groove through 90° along its long axis had a profound effect in eliminating slippage. Instead of the groove having its plane of symmetry perpendicular to the plane of rotation (ie "open" or "v" shaped), it was parallel to it so that both walls faced direction of travel at an angle of 45° ("closed" or ">" shaped). Now with the base of the groove behind both walls, any slippage would tend to return the fluid back to the base of the groove. Thus the groove would have to flood inorder for any slippage to occur.

The optimum choice of groove shape therefore appears to be one orientated such that both walls face the direction of travel. However, problems would be encountered with the manufacture of such a disc, since it would be difficult to mould in one piece.

Figure 4.4.2 b. shows three disc types which have been tested with the Waterwheel (Chapter Six). The upper diagram shows the first disc produced for the Waterwheel with conventional "open" grooves.

A modification of the standard open groove is illustrated in the middle diagram. The internal angle of the groove has been reduced to 45° and orientated such that one face ie the windward face is perpendicular to the direction of travel. Although slippage is now possible at high flowrates, it is delayed significantly compared to slippage with the sideways facing groove described earlier. A disc with 80 such grooves (Appendix 1), each ending with a sharp tip or tooth, produced narrower dropsize spectra compared to the earlier "open" groove disc (section 6.2). The "reduced slip" disc has therefore been used as standard with tests on the Waterwheel from Mk.5 onwards.

Tooth shape was also investigated, qualitatively using the the experimental groove, and quantitatively using different disc designs for the Waterwheel dropsizing tests (Chapter Six).

Firstly, the end of the experimental groove was fashioned into various different shapes to the study the effect of tooth shape on quality of ligament formation and subsequent atomisation. The basic conclusion found was that the sharper the tooth, the cleaner the detachment of fluid and the more stable the ligaments produced. The effect of increased sharpness was also that smaller direct droplets could be produced.

In addition, a special "no slip" disc with 80 drilled cylidrical channels (lower diagram of Figure 4.4.2 b and Appendix 1) was manufactured so that the Waterwheel could be tested at higher flowrates. The disc was tested at various stages of its manufacture. Stroboscopic observation revealed atomisation to be very poor with channels ending in a plain face. A marginal improvement was found with the chamfering of upper and lower corners to form a sharp rim. Vertical "V" cuts in between the openings resulted in each channel ending in a sharp tip. This led to a great improvement in the quality of ligaments produced.

In both cases it was important that the tip of the groove had accutely angled chamfers on at least four faces. Infact the ideal tooth shape would probably be a cone with a small internal angle. However, ease of manufacture probably dictates a pyramidal shape. The tooth also has to be fairly resistant to damage, so therefore should not have an internal angle of less than about 30°.

A number of factors led to the choice of 80 for the number of grooves and teeth. Firstly it is important that the number of issuing points are as high as possible, so that flowrate per tooth is low leading to narrow droplet spectra (section 5.4). However, the grooves need to be of such size and depth so that flooding is avoided. 80 was finally decided upon because it provides a simple progression from the fluid distribution slots which number 5,10,20 and 40 (section 4.3.3).

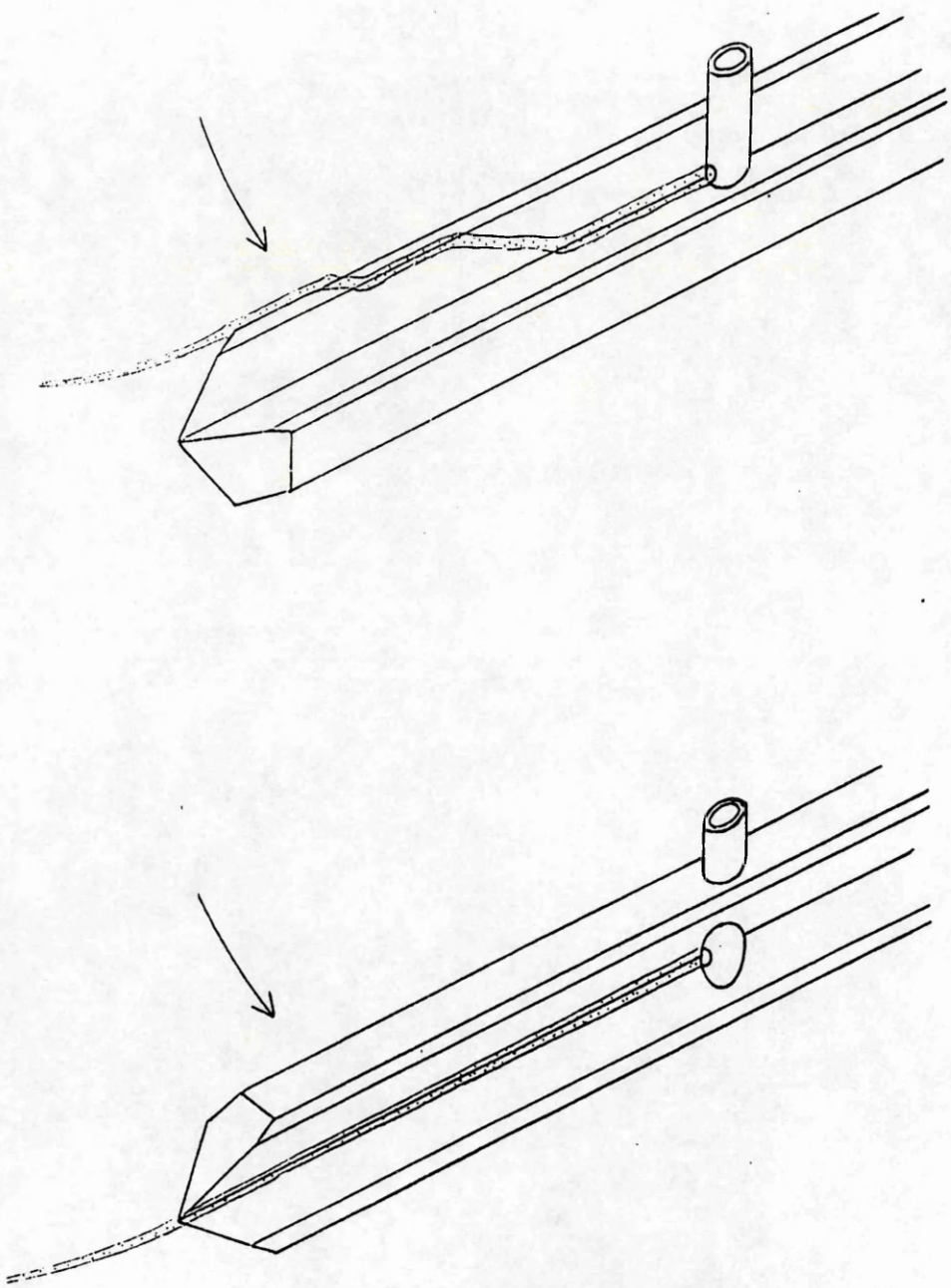

Figure 4.4.2a Groove shape and the problem of fluid slippage

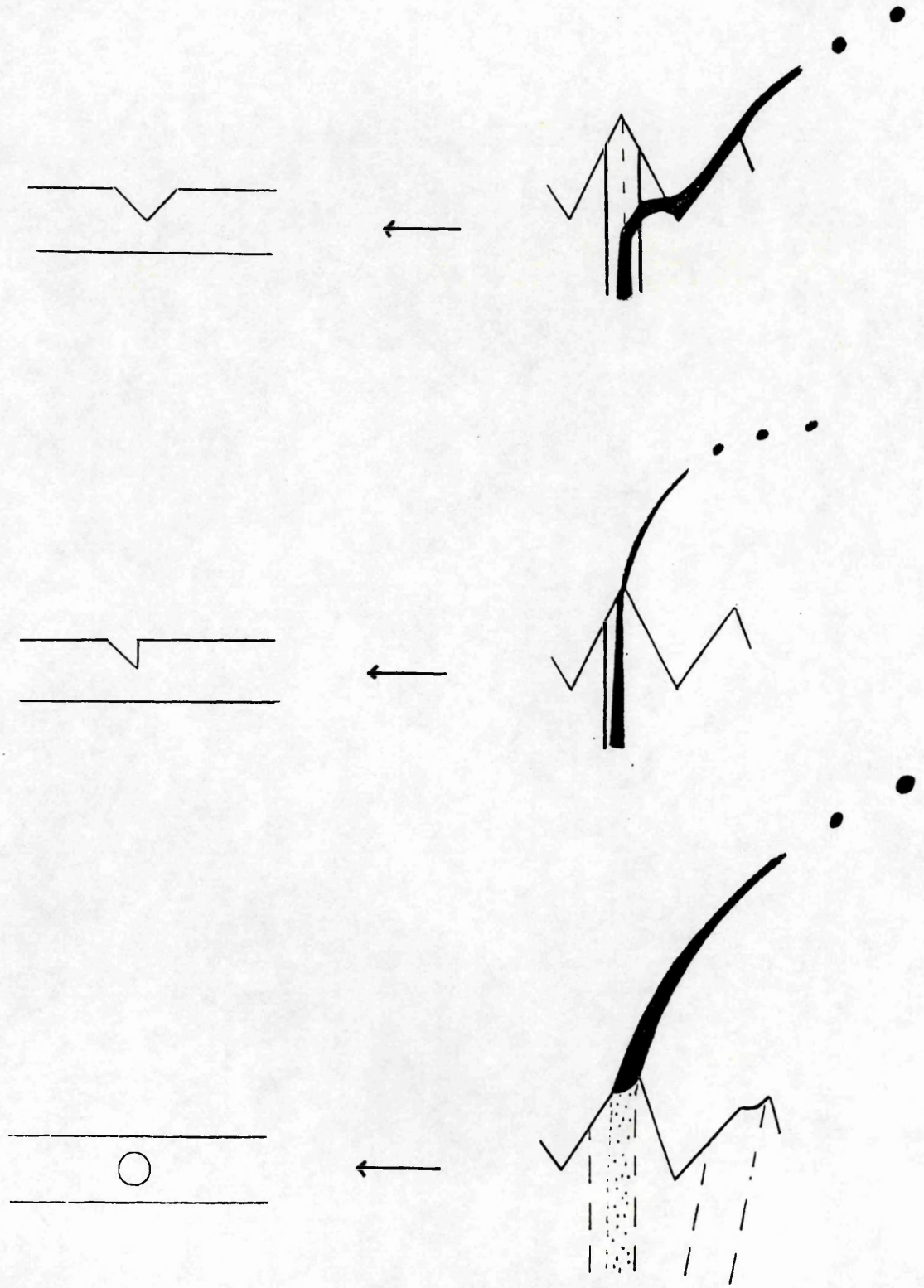

Figure 4.4.2b Three designs of tooth tested with Waterwheel Mk.6

4.4.3 Calculation of the effect of viscous drag on fluid acceleration along three types of surface.

(after Spillman, personal communication, 1988)

Design of an energy efficient spinning disc is of utmost importance for the Waterwheel, since the energy available from the jet is limited. It is therefore important to have a design where losses due to viscous drag within the accelerating fluid layer are minimised.

Fluid upon a rotating surface is subject to "centrifugal force" which also moves the fluid radially. Although viscosity is required so that the fluid achieves tangential velocity, viscosity is now providing centripetal force acting to impede the radial movement of the fluid. As a result, the radial velocity of the fluid is less less than its tangential velocity.

As from now, slippage will be assumed to be minimal, and velocity of the fluid shall be considered relative to the surface.

Firstly, we can make the following statement:-

Mass per unit length	x	Acceleration	=	Centrifugal Force per unit length	-	Viscous Drag per unit length

$$m(dV/dt) = mw^2r - \tau_o A \qquad (100)$$

where:-

m	=	mass per unit length, kg m^{-1}
V	=	mean velocity, m s-1
t	=	time, s
w	=	angular velocity of surface, s^{-1}
r	=	radius from centre of rotation, m
τ_o	=	shear stress at surface due to viscous drag, Nm^{-2}
A	=	wetted area of surface per unit length, m^2

The above equation can be written as:

$$dV/dt = w^2r - \tau_o A/m \qquad (101)$$

or

$$d(V^2)/dr = 2w^2r - 2\tau_o A/m \qquad (102)$$

Now the fluid will have a velocity gradient from zero at the surface to a maximum value at the free surface. The shear stress at the surface

$$\tau_o = \mu (du/dy)_o = \mu k (V/\delta) \qquad (103)$$

where k is a factor depending upon the velocity profile, for a parabolic profile $k = 3$

δ is the local thickness of the fluid

Thus $$d(V^2)/dr = 2w^2r - 2k\mu(V/\delta)A/m \qquad (104)$$

Now the value A/m depends upon the type of surface on which the fluid is being rotated. A/m will be high if the surface has no grooves ; the presence of grooves or channels, depending on their shape will act to lower A/m and therefore viscous loss.

Four types of surface will now be considered, and are illustrated in Figure 4.4.3.

PLAN SECTION

a) Smooth circular disc

b) Radial parallel channel

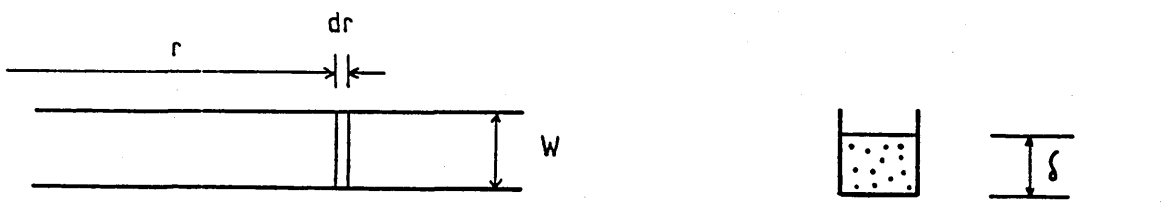

c) 90° radial groove

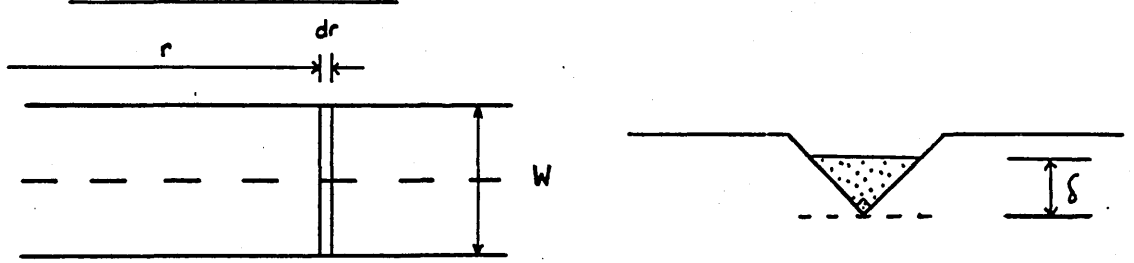

d) 45° radial groove

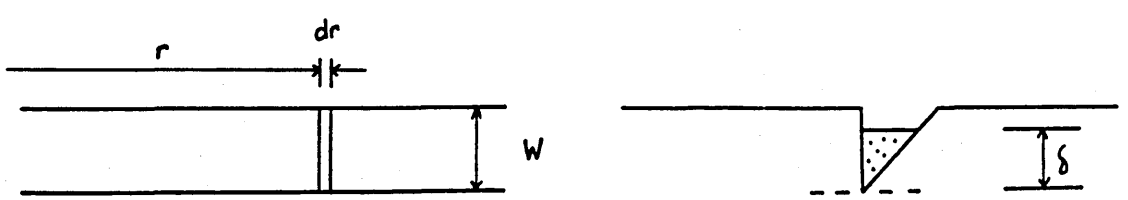

Figure 4.4.3 Four types of surface with nomenclature

a) Smooth circular disc - assuming no slip of fluid

In this case $A = r\theta dr$

and $m = p r\theta\delta dr$

where p = density of fluid kg m^{-3}

And the local velocity, for a flowrate Q_a m^3/s onto the disc

$$V = \frac{Q_a}{2\pi r\delta}$$

Thus for this case the last term of the equation becomes

$$2k\mu(V/\delta)A/m = 2k\mu(V/\delta).1/p\delta = 2k(\mu/p)V(2\pi rV/Q_a)^2$$

$$= 8\pi^2 k\nu.\ r^2/Q_a{}^2.\ V^3 \qquad (105)$$

where ν = kinematic viscosity = $\mu/p = 1.0 \times 10^{-6}$ m^2s^{-1}

and equation (104) becomes

$$d(V^2)/dr = 2w^2 r - 8\pi^2 k\nu.\ r^2/Q_a{}^2.\ V^3$$

$$= 2w^2 r\left[1 - \frac{4\pi^2 k\nu\ r\ V^3}{w^2 Q_a{}^2}\right] \qquad (106)$$

This has no simple analytical solution. It is evident that as r increases V will increase initially, but as r and V increase the term in the bracket will eventually become zero. If this happens the speed will be constant as r increases. But then the negative term in the bracket will become more negative and the flow will decelerate as r increases. Thus for high values of w and Q for a given disc, the radial flow velocity may reach a maximum and decrease. The maximum value is reached when the bracket value is zero, that is when

$$\frac{rV^3}{w^2 Q_a{}^2} = \frac{1}{4\pi^2 k\nu} \approx 8443, \text{ for water} \qquad (107)$$

b) Radial parallel channel

In this case $A = W.dr$

and $m = p\delta W.dr$

and $V = Q/W\delta$

where Q is the flowrate, m^3s^{-1}, along channel
W is width of channel

Thus the last term of equation (2) becomes

$$2k\mu(V/\delta)A/m = 2k(\mu/p)(V/\delta^2) = 2k\nu V(WV/Q)^2 \quad (108)$$

If Q_b = flowrate per unit width of channel, $m^3/s.m$, $= Q/W$

$$2k\mu(V/\delta)A/m = 2k\nu.\ V^3/Q_b^2 \quad (109)$$

and equation (104) becomes

$$d(V^2)/dr = 2w^2r - 2k\nu.\ V^3/Q_b^2$$

$$= 2w^2r\left[1 - \frac{k\nu}{w^2Q_b^2}\frac{V^3}{r}\right] \quad (110)$$

Again this has no simple analytical solution. Initially when $V \approx 0$, $d(V^2)/dr \approx 2w^2r$, and $V = wr$. However as V and r increase, the negative term in the bracket will increase and the acceleration decrease. It is unlikely that acceleration will fall to zero because in that case an increase in r would give the same velocity, but the bracketed term would become more positive because of the r^{-1} term. The limiting case might be :

$$\frac{V^3}{wQ_b^2r} = \frac{1}{k\nu} \approx 3.3 \times 10^5 \text{ for water,} \quad (111)$$

c) Flow down a 90° internally angled radial groove

In this case $A = 2\sqrt{2}.\ \delta\ dr$

$m = p\ \delta^2\ dr$

and $V = Q_c/\delta^2$

where Q_c = flowrate per groove, m^3/s

Thus the last term of equation (104) becomes

$$2k\mu(V/\delta)A/m = 2k\mu(V/\delta)\ 2\sqrt{2}/p\delta = 4\sqrt{2}.\ k\ (\mu/p)\ V/\delta^2$$

$$= 5.657\ k\ \nu\ V^2/Q_c \qquad (112c)$$

and equation (104) becomes

$$d(V^2)/dr = 2w^2r - 5.657k\nu\ V^2/Q_c \qquad (113c)$$

writing $a = 2w^2$ (114)

$b = 5.657k\nu/Q_c$ (115c)

$$d(V^2)/dr = ar - bV^2 \qquad (116)$$

$$d(V^2)/dr + bV^2 = ar$$

$$e^{br}.d(V^2)/dr + e^{br}.bV^2 = e^{br}.ar \qquad (117)$$

$$d/dr.[V^2\ e^{br}] = ar\ e^{br} \qquad (118)$$

$$V^2\ e^{br} = \int ar\ e^{br}.dr$$

$$= a\left[\frac{re^{br}}{b} - \frac{e^{br}}{b^2}\right] + C \qquad (119)$$

$$V^2 = a\ [\ r/b - 1/b^2\ ] + C\ e^{-br} \qquad (120)$$

If initially, $V = V_1$ when $r = r_1$,

$$V_1^2 = a\,[\, r_1/b - 1/b^2 \,] + C\, e^{-br_1} \qquad (121)$$

so $$C = \{\, V_1^2 - a[r_1/b - 1/b^2] \,\}\, e^{br_1} \qquad (122)$$

substituting (122) into (120)

$$V^2 = a[r/b-1/b^2] + \{V_1 - a[r_1/b-1/b^2]\}\, e^{br_1}.e^{-br}$$

or

$$V^2 = (a/b^2).[br-1] + \{V_1^2 - (a/b^2).[br_1-1]\}\, e^{b(r_1-r)} \qquad (123)$$

Assuming that the fluid starts from rest at the centre of rotation ie. $V_1 = r_1 = 0$,

$$V^2 = (a/b^2).[br-1] + (a/b^2).e^{-br}$$

$$= (a/b^2).[br - 1 + e^{-br}] \qquad (124)$$

So $$V^2.b^2/a = [br - 1 + e^{-br}] \qquad (125)$$

since $a = 2w^2$

$$\frac{V\,b}{w} = \left[\, 2\,(br - 1 + e^{-br}) \right]^{\frac{1}{2}} \qquad (126)$$

A sketch of this relationship is shown in Figure 4.4.3(b) for br values 0 to 5.

Above br = 5, since $e^{-br} < .0067$

$$\frac{V\,b}{w} = \left[\, 2\,(br - 1) \,\right]^{\frac{1}{2}} \qquad (127)$$

squaring and dividing through by $(br)^2$ we obtain

$$\frac{V^2}{w^2r^2} = 2/br - 2/(br)^2 \qquad (128)$$

and $$V/wr = \left[\, 2/br(1 - 1/br) \,\right]^{\frac{1}{2}} \qquad (129)$$

A sketch of this relationship is shown in Figure 4.4.3(c).

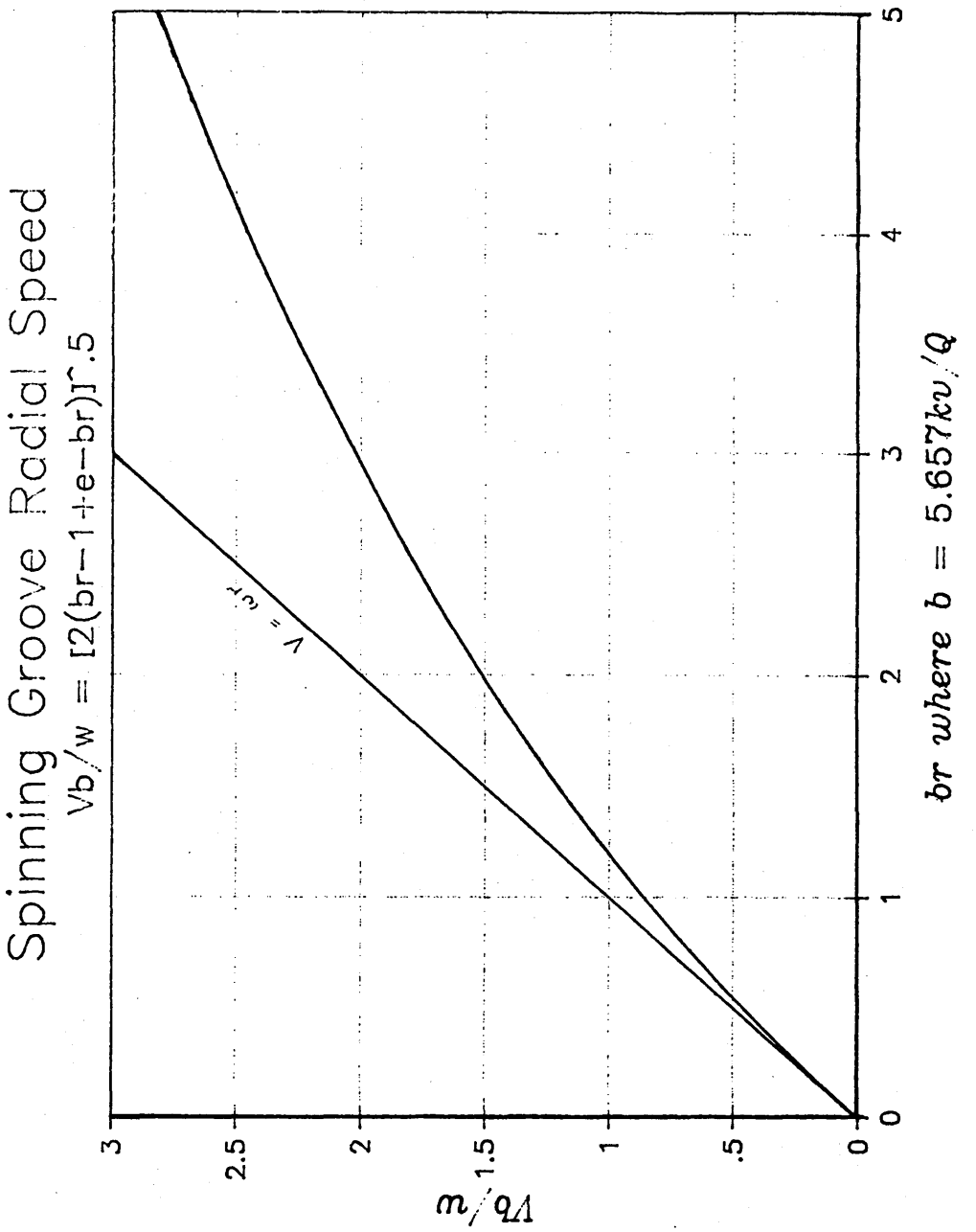

Figure 4.4.3b Radial velocity prediction for viscous fluid progressing along a "V" shaped groove, for low values of br (low r, high Q)

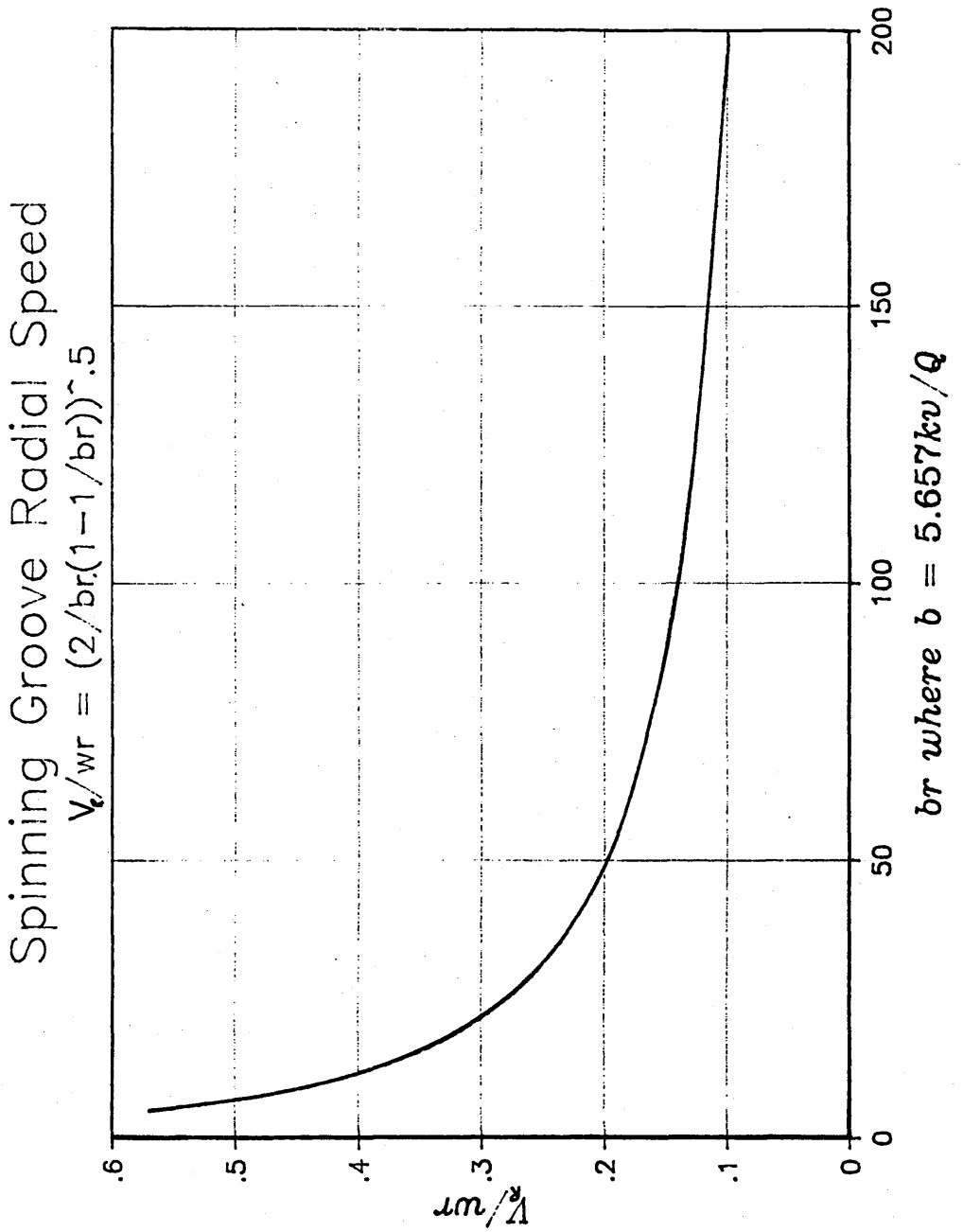

Figure 4.4.3c Radial velocity prediction for viscous fluid progressing along a "V" shaped groove, for high values of br (high r, low Q) (after Spillman, personal communication)

d) Flow down a 45° internally angled radial groove

The disc used on Waterwheel prototypes Mk.5 to 12 has grooves as illustrated in the bottom diagram of Figure 4.4.3

In this case $A = \sqrt{2} + \delta\ dr$

$= 2.4142\ \delta\ dr$

$m = p\ \delta^2/2\ dr$

Thus $A/m = 4.828/\delta p$

where Q_d = flowrate per groove, m^3/s

$Q_d = V.\delta^2/2$

so $V = 2\ Q_d/\delta^2$

and $\delta^2 = 2\ Q_d/V$

Thus the last term of equation (104) becomes

$$2k\mu(V/\delta)A/m = 2k\mu(V/\delta)\ 4.828/p\delta = 2x4.828\ k\nu(V/\delta^2)$$

$$= 4.828\ k\nu\ V^2/Q_d \qquad (112d)$$

c.f $5.657\ k\nu\ V^2/Q_c$ for "v" shaped groove (112c)

and equation (104) becomes

$$d(V^2)/dr = 2w^2r - 4.828k\nu\ V^2/Q_d \qquad (113d)$$

Equations 116 to 129 still apply, except b is now

$$b = 4.828k\nu/Q_d \qquad (115d)$$

4.4.4 Design implications for an energy efficient spinning disc

V/wr is in effect the ratio of the mean velocity, V, of the fluid divided by the maximum theoretical velocity wr, which the fluid would have if invicid. Since V/wr decreases rapidly with increasing radius for a given value of b ($= 4.828kv/Q_c$ for a 45° groove), it is obvious that to minimise losses due to viscosity and to get velocities as close to the inviscid value of $V = wr$ as possible, the product should be obtained by high w and low r, that is high rotational speed and low overall radius.

However, as demonstrated in section 4.3.3, a large cup radius is preferable to to overcome high bearing friction, and for optimum hydraulic efficiency, thus leading to high viscous loss on the disc.

To provide an indication of the losses due to viscosity with the Waterwheel, the following values will be used in calculating V/wr:

$$k = 3$$
$$v = 1 \times 10^{-6} \ m^2s\text{-}1$$

With a typical flowrate of 240 ml/min for the Waterwheel at 3 bar:

$$= 4 \text{ ml/sec}$$
$$= 4 \times 10^{-6} \ m^3/sec$$
$$= .05 \times 10^{-6} \ m^3/sec/groove \ (80 \text{ grooves})$$

Therefore

$$b = 4.828 \ kv/Q_c$$
$$= 4.828 \times 3 \times 10^{-6} / 0.05 \times 10^{-6}$$
$$= 289.7$$

With a disc radius of 28mm (ie that for Waterwheel Mk.5-8)

$$br = 8.1$$

Since br > 1,

$$V_R/wr = \{2/8.1(1-1/8.1)\}^{½}$$
$$= 0.46 \qquad (130)$$

The effect of viscous drag on fluid accelerating from the centre of rotation along a 28mm long "7" shaped groove is therefore to reduce the mean radial velocity of the fluid by more than half.

Case for an annulus

The distance along which the fluid has to travel may be shortened thus reducing viscous losses markedly, by not accelerating the fluid from the centre of rotation. Infact the shape for the spinning disc can be an annulus rather than a disc.

A hole in the centre of the disc is actually preferable, since the nozzle feed necessarily occupies an off-centre position. Also the central portion of the disc can be usefully occupied by the filtration chamber saving weight and space (Appendix 1.)

Fluid accelerating upon an annulus rather than a disc will start from rest at the inner radius and will therefore have a lower final velocity than if it had started its acceleration at the centre of rotation.

If the annulus has inner radius r_i at which initial fluid velocity V_1 is 0, fluid velocity $\bar{V}$ at any point r along the annulus groove may be calculated as follows:

(from equation (123), where $a = 2w^2$, and $b = 4.828kv/q$)

$$V^2 = a/b^2(br-1) - a/b^2(br_1-1).e^{b(r_1-r)} \qquad (131)$$

If the annulus has a maximum outer radius r_o, final radial velocity of the fluid V_R is as follows:

$$V_R = \left[a/b^2 \{(br_o - 1) - (br_1 - 1).e^{b(r_1-r_o)}\} \right]^{\frac{1}{2}} \qquad (132)$$

Calculations of V_R based upon equation (132), have been used successfully to simulate dropsize produced by the various Waterwheel annuli discs (refer to Chapter 7).

Chapter Five

ATOMISER TESTING METHODS

5.1 Objectives

In addition to experimentation with fluid driven prototypes, which is the subject of Chapter Six, rotary atomisation tests were carried out with conventional electrically driven atomisers so that a standard set of data was available for purposes of comparison.

The objectives of the testing may be grouped into three main areas as follows:

1) To determine the physical characteristics of the sprayer with respect to:-

   i) mechanical performance ie rotation speed, flowrate etc.
   ii) spray characteristics ie droplet size, spectral width etc.
   iii) spray deposit analysis ie swath width, evenness of radial distribution

2) To provide additional data to augment, evaluate or criticise existing theories on rotary atomisation. The main area of interest is the effect of i) on ii), ie the factors controlling droplet size.

3) To obtain background data to support model a which will predict the effects of changing various design features on sprayer performance, with the aim of optimising sprayer design.

5.2 Test Methodology

The two basic physical parameters which were measured with every test were speed of rotation and flowrate of liquid through the sprayer. Additionally, applied voltage and current was noted if the atomiser was driven electrically, or liquid supply pressure if driven hydraulically. Recording this data would enable later calculation of the input energy supplied to the atomiser. A diagramatic summary of the equipment used is presented in Figure 5.2.

Visual examination of the atomisation process was made possible using stroboscopic light. Satisfactory operation of the sprayer was checked visually prior to each dropsizing test as a matter of routine.

Disc rotation rate was measured using an digital infrared tachometer, receiving light from an infrared reflective sticker, attached to some rotating part of the atomiser. The tachometer was usually mounted 10 to 15 cm above the reflective sticker to give continuous readings.
A direct reading was provided every few seconds in Revolution Per Minute or RPM.

Flowrate was measured using an inline flowmeter tube (Rotameter GEC Process Instruments Ltd.) calibrated for water, and a higher viscosity liquid Butyldigol (Figure 5.2). The flowtube enabled flowrate to be recorded rapidly with each test, and gave consistant readings accurate to within 1 or 2 ml/min.

Electrical power for driving the disc was provided by a Kingshill 10 amp constant current power unit. Liquid was either fed onto the disc gravitationally, or delivered using a medical syringe pump with a range of flowrates between 13.3 ml/min to 0.0065 ml/hour (Sage Instruments, Orion Research Inc.)

Liquid supply pressure with fluid driven systems was measured using a standard Bourdon pressure guage. The guage was checked regularly against a second, and was found to provide accurate and consistant readings to within 0.1 bar. The guage was inserted into the fluid supply line as near as possible to the atomiser to reduce possible inaccuracies arising from pressure loss.

The ground deposit pattern produced by the sprayer was measured by a number of methods. With the sprayer held in a stationary horizontal position, 50cm from the ground, a row of test tubes evenly spaced along a ruler was used to evaluate a cross-section through the deposit. Eveness of radial distribution was measured using eight inclined collecting vessels placed in a circle around the sprayer.

After a certain spraying time the contents of each bucket was then carefully poured into a measuring cylinders to give the total fluid emitted in that segment.

Ground deposit was also measured, both with the sprayer stationary and moving, by use of water sensitive cards, placed at intervals from the centre or centreline, and an Optomax image analysis system (Last and Parkin, 1986). The water sensitive cards used (Turner and Huntingdon, 1970) are manufactured by Ciba Geigy Limited, and consist of rigid paper with a specially coated yellow surface which is stained dark blue by aqueous droplets impinging on it. A number of stains were then calibrated against other similar sized droplets measured in in silicone oil using a microscope, and a spread factor of 2 ± 0.1 was verified, for droplets greater than 100µm.

The data was then processed using an existing program for lane separation analysis (called "Overlaps", written originally for aerial spraying). The program presents a single swath pattern, and then calculates peak deposit and coefficient of variation for different lane separations. The user can also choose any particular lane separation and the actual deposit pattern produced by that lane separation will be calculated. The results for this particular exercise are presented in Chapter 7.

Figure 5.2 Apparatus for rotary atomisation experimentation

5.3 The PMS laser droplet sizing system

The system used to measure particle size distribution was an Optical Array Cloud Droplet Spectrometer Probe model OAP-260X (Knollenberg, 1970 and 1976, Parkin, Wyatt and Wanner, 1980) and a Data Acquisition System model PDS-300 both manufactured by Particle Measuring Systems, Boulder, Colorado. This type of probe was originally designed to be mounted on an aircraft for measuring the particle size within clouds. The system has been interfaced with a Hewlett Packard 80 computer for data storage and handling.

The probe consists of a linear array of photodiodes illuminated by a low power He-Ne laser. When a particle crosses a laser beam it casts a shadow on the array as shown in Figure 5.3. The photodiode array is switched on and off at a very fast rate so the probe measures "slices" of the particle as it passes through the beam. The diameter of the particle is given by the maximum number of array elements obscured during the passage of the particle. The optical array consists of 64 photodiodes, located on 200um centres. The probe used incorporated a lens system which magnified the shadow so that each diode was equivalent to 15um and covers the range 15um-930um in 62 size classes. The two end elements are used to check if the particle is totally within the sample area.

A particle will be rejected for one of two reasons. Firstly, small particles can produce a diffuse shadow pattern when out of focus, this results in only partial occlusions of the photodiodes. To assess if a particle is in focus, a two-stage comparator is included in the detection system. The diameter of the particle is measured on the basis of the number of photodiodes that are 50% obscured, but to be classed as in focus at least one diode must be 67% obscured. Thus small droplets have a low probability of being accepted by the probe. The second reason for rejection occurs when droplets obscure the end elements making their size indeterminate. Thus large droplets have a low probability of passing through the probe without obscuring an end element.

The size of each particle measured is stored in the Data Acquisition System (PDS-300) and during sampling the size distribution histogram is displayed on a small CRT screen which is updated with each new piece of data. This gives a useful indication that the system is operating correctly; sudden changes in histogram shape generally indicate contamination of the optics. Termination of a sample is achieved either automatically or manually, upon which the data can downloaded to a printer. The data may then be stored on a computer for later retreival, stastical analysis and plotting.

The field of view variation imposed by the optics result in different probabilities involved in counting each particle size. Correction factors therefore have to be applied to the data, depending on the length of sample volume used. For spinning disc work, sampling may be limited to the central portion of the laser by means of two shrouds. For all dropsize measurements in this thesis, a reduced length of sample volume of 10mm, as opposed to the maximum value of 61mm was used.

The software also may be set to eliminate spurious droplet counts, so long as they are are separated from the main population by at least two empty bins. With all the droplet spectra presented, this feature has been included as a matter of course, although the occurrance of spurious counts was rare.

Due to their volume, printouts of all the corrected bin data and statistics for the Spinning Groove, Micron Herbi and Waterwheel dropsize experiments have not been included in this thesis. If required, they may be obtained from Dr. C.S.Parkin, Engineering for Agriculture, Silsoe College, in hardcopy form or as files on computer disc.

Results for the two most commonly used spectral parameters, Number Median Diameter and Volume Median Diameter are included in the Droplet Data Summaries. Details of how all the the various spectral parameters are calculated will now be introduced.

In calculating droplet statistics, values referred to as percentiles are calculated from the bin data, corrected for the sample volume used. A percentile X may be defined as a particular diameter below which X% of the spray is composed, either in terms of number, length, area or volume. Percentile values for 5, 10, 16, 25, 50, 75, 84, 90 and 95% of the spray are presented.

Following percentiles, the following droplet spectra parameters are presented:

Parameter	Abr.	Notation
Number Median Diameter	NMD	$D_{n\ 0.5}$
Number Average Diameter	NAD	$D_{1,0}$
Volume Average Diameter	VAD	$D_{3,0}$
Sauter Average Diameter	SAD	$D_{3,2}$
Volume Median Diameter	VMD	$D_{v\ 0.5}$

Number Median Diameter is defined as the drop diameter which divides the spray sample in half by number. It is infact the 50% percentile for number. Similarly, Volume Median Diameter divides the spray sample in half by volume and corresponds to the 50% percentile for volume.

The PMS dropsizing system measures droplets by counting the maximum number of photodiodes occluded as a droplet passes through the laser beam. The data system then places that droplet into a size bin, the bottom (D_b), mean (D_m) and top (D_t) diameters of which are given in Table 6.4.1c.

In calculating a particular percentile, say 50% by number, (ie NMD) size bin j is selected so that the following condition is true:-

i) the number of droplets contained size bins up to and including j-1, n_{j-1}, is less than half the total number of droplets, n in the sample
i) the number of droplets contained size bins up to and including j, n_j, is more than half the total number of droplets, n.

Size bin j therefore contains the diameter corresponding to NMD, so

$$D_{tj-1} < NMD < D_{tj} \qquad (140)$$

NMD is then calculated using a linear interpolation over the interval D_{tJ-1} to D_{tJ} as follows:

$$NMD = D_{tj-1} + \left[D_{tj} - D_{tj-1} \cdot \frac{.5n - n_{j-1}}{n_j - n_{j-1}} \right] \qquad (141)$$

where

n = total number of droplets
n_j = number of droplets upto and including size bin j
n_{j-1} = number of droplets upto and including size bin j-1

Similarly, for Volume Median Diameter

$$VMD = D_{tj-1} + \left[D_{tj} - D_{tj-1} \cdot \frac{.5v - v_{j-1}}{v_j - v_{j-1}} \right] \qquad (142)$$

where v = total volume of droplets

Number Average Diameter, or number mean diameter is simply the arithmetic mean diameter of all of the droplets in the spray.

$$NAD = \frac{n_1 D_{m1} + n_2 D_{m2} + n_3 D_{m3} + \cdots n_x D_{mx}}{n} \quad (143)$$

where:

$n_1, n_2, \cdots n_x$ = numbers of droplets in size bins 1 to x

$D_{m1}, D_{m2}, \cdots D_{m3}$ = $(D_t - D_b)/2$ for size bins 1 to x.

Volume Average Diameter, or volume mean diameter is where $\pi(D_{3,0})^3/6$ is the average of the volumes of the individual droplets of the spray. Therefore :

$$VAD = \left[\frac{n_1 D_{m1}^3 + n_2 D_{m2}^3 + n_3 D_{m3}^3 + \cdots n_x D_{mx}^3}{n} \right]^{1/3} \quad (144)$$

Sauter Average Diameter is defined as the diameter of the drop which has the same volume to surface area ratio as that of the whole spray sample. Therefore:

$$SAD = \left[\frac{n_1 D_{m1}^3 + n_2 D_{m2}^3 + n_3 D_{m3}^3 + \cdots n_x D_{mx}^3}{n_1 D_{m1}^2 + n_2 D_{m2}^2 + n_3 D_{m3}^2 + \cdots n_x D_{mx}^2} \right] \quad (145)$$

SAD is rarely used in pesticides application technology, although it is commonly used in other fields such as combustion where sprays are more commonly sampled spatially rather than temporally as with the PMS probe. .

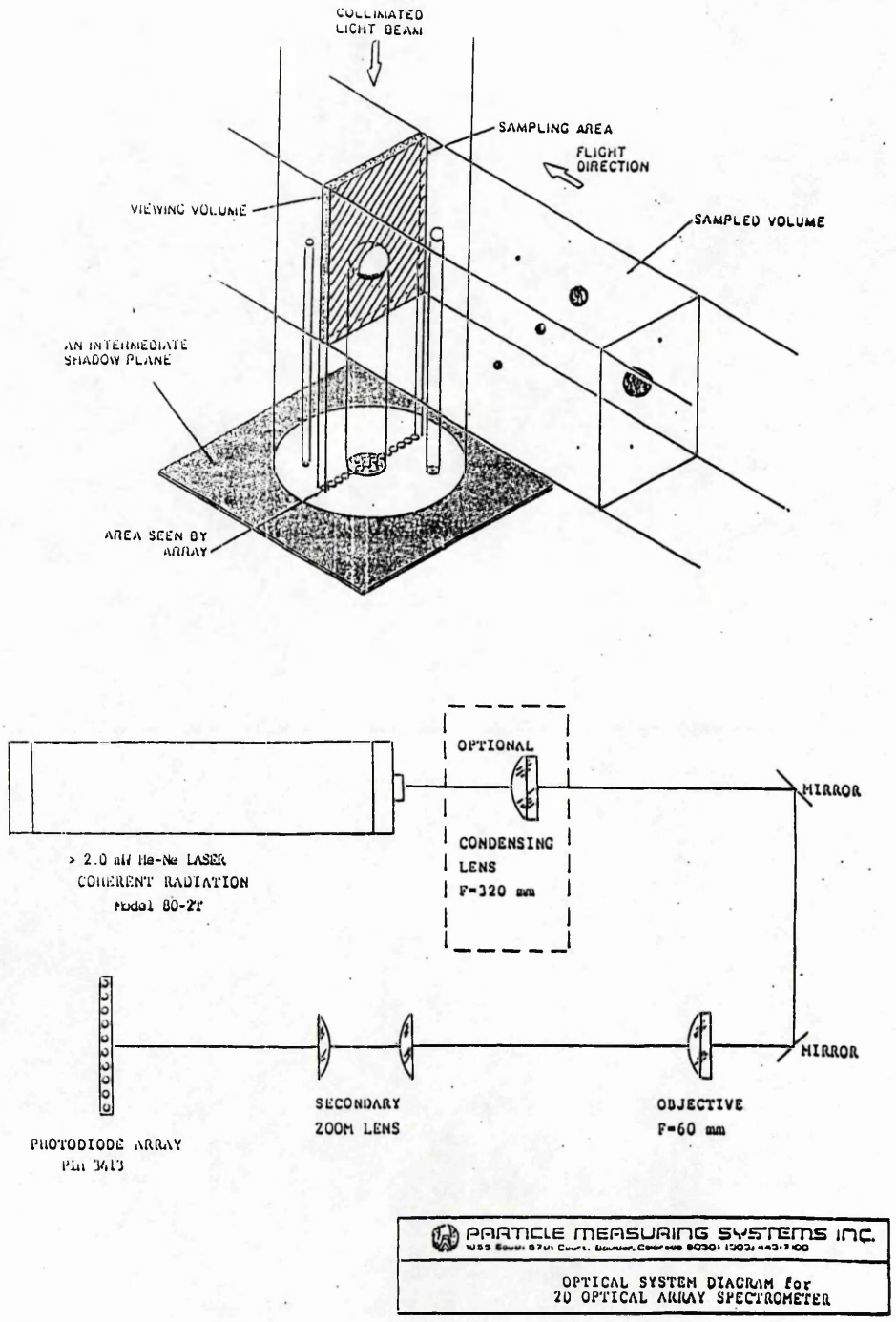

Figure 5.3 Laser droplet sizing system (PMS OAP-260x)

5.4 Tests on a single groove issuing point system.

Figure 5.4 shows the single groove/issuing point system used for observational studies to examine the effect of slippage (section 4.4.2) and for basic rotary atomisation dropsizing tests. The spinning groove has a distinct advantage over circular discs with several emitting points in that flowrate to the tooth is known, and can be controlled very accurately by means of a syringe pump.

Referring back to Table 2.7 which summarises power indices for the relationship between dropsize and various physical quantities, there seems to be some disparity between workers. This has frequently been attributed to variation in disc design. For example, workers may have stated that they have used a certain flowrate of fluid to the disc. However, variation in the number of teeth on the discs, from about 45 to ∞ (ie. smooth edged disc) will lead to different values of flowrate per tooth (q), which may lead to disparity in results. In addition, if the feed to each tooth is less than even, different dropsizes will be produced by each tooth resulting in a wider overall droplet spectra. This may act to obscure relationships which the experimenter is trying to detect.

Results of three experiments carried out with the spinning groove are presented in Droplet Data Summaries 1 - 3. Droplet Data Summaries are tables summarising the dropsize experiments carried out, and record at least the following imformation:

i) Rotation Rate, N, (RPM)
ii) Flowrate, Q, (ml/min)
iii) Number Median Diameter (μm)
iv) Volume Median Diameter (μm)
v) VMD/NMD ratio
vi) File Number and Record Number

(raw numbers and spectral statistics for each Record may be located in Appendix II)

Three different experiments were carried out on the spinning groove:

1) Effect of rotation speed on dropsize for various flowrates
2) Effect of rotation speed on dropsize for two groove lengths
3) Effect of flowrate on dropsize at four different rotation speeds

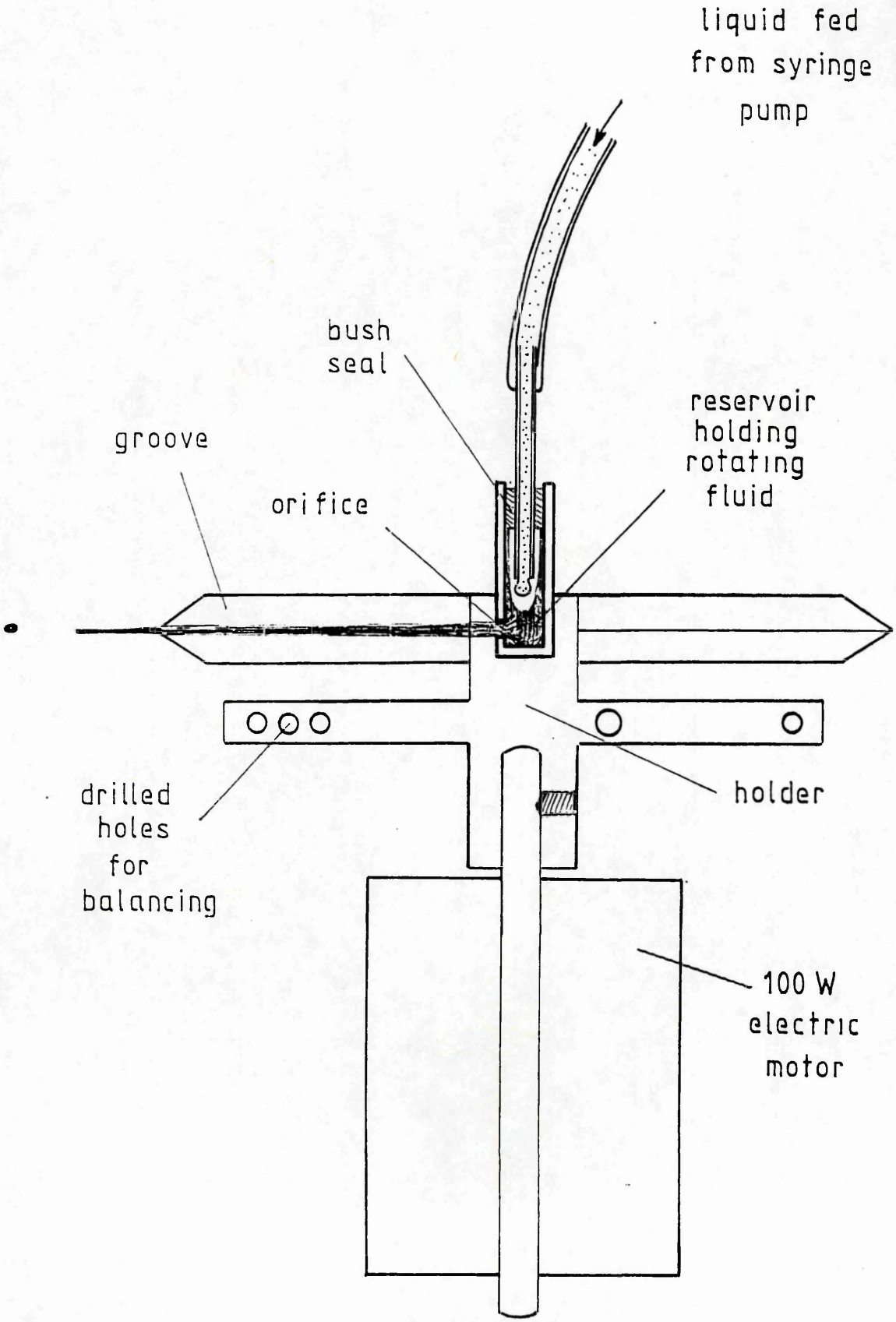

Figure 5.4 **Experimental single groove / issuing point system**

Figure 5.4a summarises the relationship between dropsize and rate of rotation for tap water with the spinning groove. The figure consists of two graphs, the upper expressing dropsize in terms of Number Median Diameter, the lower in terms of Volume Median Diameter (refer to nomenclature). Figure 5.4b consists of the same information expressed as log values to the base 10.

In Figures 5.4c and d, three curves are presented for three different flowrates:- 0.2 ml/min, 1.0 ml/min and 5.0 ml/min. When multiplied by the number of teeth on a CDA spinning disc atomiser (typically between 120 and 360), these flowrates would be considered as low, medium to high, and very high respectively. For example, with the Micron herbi disc with 360 teeth, corresponding flowrate values would be 72 ml/min, 360 ml/min, and 1800 ml/min. In fact a flowrate of 1800 ml/min would be too high for a conventionally designed spinning disc, and severe flooding with poor atomisation would be the result. One objective with the spinning groove was to observe the true effect of rotation speed on droplet size at higher flowrates per groove than could be obtained with a conventional disc.

Referring to the curves Figure 5.4.c, as one would expect droplet size is seen to decrease with increasing RPM for all three flowrates. The NMD curves have a similar form to the VMD curves for the lower two flowrates. However, NMD values are significantly lower than VMD values with the highest flowrate indicating that the spectral width of the spray is large.

If log values are plotted as in Figure 5.4d, the slopes of the different curves may be compared. An important feature which arises is that the dependancy of dropsize on rotation speed is not the same for different flowrates.

The VMD curves approximate to nearly straight lines which enable mean gradients to be measured and power relationships estimated. Relationships between VMD and N (RPM) are as follows:

$$VMD \propto N^{-0.85} \qquad 0.2 \text{ ml/min}$$

$$VMD \propto N^{-0.65} \qquad 1.0 \text{ ml/min}$$

$$VMD \propto N^{-0.25} \qquad 5.0 \text{ ml/min}$$

It is important to note that the decrease in gradient does not occur with the NMD curve at 5.0 ml/min. This is due to an increase in width of the droplet spectrum.

Thus, for flowrates per tooth above 1.0 ml/min, VMD may not be the best indicator of dropsize, since it is biased towards the coarse end of the droplet spectrum. The occurence of a few very large drops at high flowrates, unrelated in size to the main population, may be largely independant of N.

A power indice of -0.5 is what one would expect for ligament breakup if dropsize was strictly proportional to undisturbed ligament diameter, and ligament diameter was inversely proportional to radial velocity of the fluid (which was directly proportional to disc RPM). At low flowrates and rotational speeds, there is insufficient fluid momentum for ligaments to be produced, and droplets are formed directly. Consideration of surface tension opposing centrifugal force on a pendant drop leads to a prediction of -1 for direct droplets (Walton and Prewitt, 1949). In this case, fluid radial velocity is small, and its effect may be negligable compared to surface tension forces.

It is the opinion of the author, that there is an interplay of the two mechanisms at intermediate flowrates, and therefore there is unlikely to be a sudden transition between -1 and -0.5 for the N power index. It is more likely that there is a gradation of values, for the intermediate stages between direct droplet production and fully developed ligament disintergration.

Droplet Data Summary 2 contains imformation of a similar nature to DDS 1, except this time flowrate has been varied for four different constant values of RPM. Experimental time allocated to the aquisition of this particular data set was insufficient to establish the curves of Figure 5.4.4 with very great confidence. However, the few points obtained indicate the likely degree of complexity involved with the dropsize flowrate relationship near to the direct droplet/ligament transition. The 4000 RPM, 6000 RPM, and probably 8000 RPM curve as well, appear to have minima at around 0.5 ml/min. One can immediately draw the conclusion that there is unlikely to be a simple power relationship between VMD and Q below flowrates (q) of around 1 ml/min/emitting point.

At the lowest rotational speed of 2000 RPM, transition is apparent in Figure 5.4c, with a sudden reduction in VMD between 0.2 and 0.5 ml/min. The first three points represent direct droplets having VMDs of around 250 to 300 μm and very low VMD/NMD ratios. Dependancy on flowrate for the thick ligament represented by the next three points appears to be lower than for thinner ligaments produced at higher speeds. However the following relationship may be cautiously drawn for values of q above 1 ml/min, which appears to be

consistant with the values obtained by other workers (Table 2.7) :-

$$VMD \propto Q^{0.1 - 0.4} \quad (146)$$

Although a sizable body of empirical data exists, (Frost, 1981) there is a requirement for more fundamental work to be carried out, beyond the scope of this thesis, to establish from first principles how dropsize is effected by rotational speed and flowrate. Such investigation would also have to incorporate liquid properties such as viscosity and surface tension in one model.

A hypothesis based on first principles has however been proposed to to explain the effect of disc radius on droplet size (Section 4.4). The theory involves a consideration of the viscous drag experienced by a fluid subject to centrifugal forces . Droplet data summary 3 provides some experimental data to support this theory.

The two graphs in each of the Figures 5.4e to i, show NMD and VMD data for 2 lengths of groove:- i)50mm and ii)20mm. Dropsize data for a number of groove lengths would be ideal, and would be necessary if further work were to be carried out in this area. However, the two lengths do represent maximum and minimum radii of typical spinning discs currently available for pesticides application. 50mm would represent the radius of a large spinning disc, for example the Microcide Attila and the Horstine Farmery Lancelot; similarly 20mm is typical of the smallest discs generally available, for example, the Agritechnics 250, and the Nomix discs (section 2.6).

As one would expect, Figure 5.4e shows that the longer of the two grooves produces smaller droplets for the same RPM. However, this effect decreases towards higher RPM values. Taking logarithms, one can tentatively derive the following empirical relationship:

$$VMD \propto r_{(DISC)}^{-0.3} \quad \text{for} \quad N < 4000 \text{ RPM} \quad (147)$$

This agrees well with data obtained by Oyama (1953), but with none of the other workers in Table 2.7. One would expect $VMD \propto r_{(DISC)}^{-0.5}$ if dropsize was only dependant on peripheral velocity of the disc, an understandable assumption if viscosity of the fluid is ignored. The lower power index of -0.3 obtained indicates that this is unlikely to be a safe assumption, especially when flowrates and disc radii are such that viscosity becomes an important factor.

Figure 5.4f shows the same data expressed in log form. Measurement of the gradients provides additional support for the N index as follows: :

$$VMD \quad \alpha \quad N^{-0.66} \qquad 50mm \text{ groove} \qquad (148)$$

$$VMD \quad \alpha \quad N^{-0.6} \qquad 20mm \text{ groove} \qquad (149)$$

An alternative method of analysing the data is to replace the x-axis with tangential velocity at the tip, V_T, rather than rate of rotation, RPM. Infact the experimental data was originally taken choosing RPM values so that dropsize could be compared directly for the same tip velocity experienced by each groove. The maximum tip velocity obtainable with the shorter groove was 20.94 ms^{-1} since the maximum rotation rate of the electric motor used was 10000 RPM. With the longer groove however, 8000 RPM could be reached providing a a maximum V_T in excess of 40 ms^{-1}.

Notable at V_T greater than 20 ms^{-1} is a sudden increase in dropsize, effecting VMD more than NMD. This may represent the onset of assymetric ligament instability due to air disturbance above a certain Reynolds Number (Crowther, 1986). The Reynolds Number ($\rho Vd/\mu$) of a 90μm ligament in a 20 ms^{-1} airstream is approximately 10^5.

If dropsize was simply a direct function of velocity, one would expect that for the same V_T, an identical dropsize would be obtained for both 50mm and 20mm groove lengths. Figure 5.4g shows the data plotted in log form, and illustrates the fact that there are two clearly separated lines for each groove length ie. the longer groove is clearly producing larger droplets for the same V_T.

Of course, centrifugal acceleration w^2r is greater for the 20mm groove compared to the 50mm groove by a factor of 5/2 which may be having an effect on ligament behavior and therefore on dropsize. Surface tension opposes centrifugal force acting to keep the ligament attached to the disc. Greater centrifugal force with the smaller radius will lead to a greater rate of thinning of the ligament. If the breakup point is at all time dependant, breakup of the ligament will not occur until a thinner diameter has been reached. A reduced dropsize is therefore likely.

However, this effect is considered by the author to be negligable with fully developed ligament formation. It may be the parameter controlling the size of direct droplets (Walton and Prewitt, 1949) in which case $d \alpha w^{-1}$. With the present flowrate however $d \alpha w^{-0.6}$, implying that dropsize is likely to be more dependant on a velocity term. The effect may however explain why the index is - 0.6 rather than 0.5.

Particularly at the higher flowrates per emitting point with which this study is concerned, and therefore thicker ligaments with greater momentum, the effects of surface tension are less. The ligament may therefore be considered as acting freely or outside the influence of the disc soon after it has left it.

The main factor controlling dropsize is likely to be the initial thickness of fluid on the disc just prior to detachment. The main control on this is likely to be the radial velocity of the fluid.

Assuming inviscid flow, radial velocity of the fluid at the tip is equal in magnitude to V_T (section 4.4). Since flowrate Q is known and remains constant at every point along the groove (Continuity), ligament thickness $d_{(LIG)}$, assuming no contraction, may be predicted as follows:-

$$Q = V_T A$$

therefore $$\pi/4.d_{(LIG)}^2 = Q/V_T$$

and $$d_{(LIG)} = (4Q/\pi V_T)^{0.5} \qquad (150)$$

Figure 5.4h shows dropsize data plotted against $d_{(LIG)}$ assuming no fluid viscosity. The dotted line is simply $d_{(DROP)} = 2\ d_{(LIG)}$ for ease of reference (section 2.7).

Reduction of $V_{(RADIAL)}$ due to viscous drag, from the inviscid value of V_T, may be calculated (section 4.4.2) as follows:

With the following constants:

$k = 3$ for a parabolic profile
$\nu = 1 \times 10^{-6}\ m^2s^{-1}$
$Q = 1$ ml/min
$q = 0.0167 \times 10^{-6}\ m^3s^{-1}$

from equation (115c)

$$b = 4.\sqrt{2}.k\nu/q$$

$$= 5.657 \times \frac{3 \times 1 \times 10^{-6}}{0.0167 \times 10^{-6}}$$

$$= 1018.26$$

The value of b greatly exceeds 5 indicating that fluid viscosity is an important effect. The formula for calculating $V_{(RADIAL)}/wr$ is therefore

from equation (129)

$$V_R/wr = \frac{2}{br}\left[1 - \frac{1}{br}\right]^{1/2}$$

for 50mm groove

$$V_R/wr = 0.196 \qquad (151)$$

for 20mm groove

$$V_R/wr = 0.306 \qquad (152)$$

The theory is therefore predicting that the radial velocity for the 20mm groove is 1.56 times greater than that for the 50mm groove, for the same V_T. This would lead to the shorter groove producing drops smaller by a factor of $\sqrt{1.56}$ or 1.25. This is supported by the the NMD lines of Figure 5.4h. The difference in VMD is slightly larger at around 1.4.

If dropsize is plotted directly against predicted ligament diameter including the viscous effect, the result is that the two lines converge and become one (Figure 5.4i). This therefore is strong evidence to suggest that the theory is correct, and that dropsize is directly a function of radial velocity of the fluid, upon which the effects of fluid viscosity are important.

Droplet data summary : 1 EFFECT OF ROTATION RATE ON DROPSIZE
Effect of rotation speed on droplet size for various flowrates

Atomiser : 50 mm SPINNING GROOVE WITH SINGLE EMITTING POINT
Fluid : Tap water

N (RPM)	NMD (um)	VMD (um)	Span	Ratio	no. drops	File Record
Flowrate 0.2 ml/min, 02/07/88						
1500						
2000	258	260	.12	1.01	99	1,260
2500	168	196	.40	1.16	297	1,261
3000	144	174	.49	1.21	291	1,262
3500	108	131	.76	1.21	682	1,263
4000	99	121	1.58	1.23	901	1,264
4500	87	106	1.72	1.22	2048	1,265
5000	82	96	.56	1.17	2048	1,266
5500	77	95	1.23	1.23	2047	1,267
6000	72	85	.66	1.18	2048	1,268
7000	65	80	.76	1.23	2048	1,269
8000						
Flowrate 0.5 ml/min, 02/07/88						
1500						
2000	172	252	.62	1.46	336	1,295
2500	139	156	.54	1.12	1098	1,296
3000	125	142	.71	1.14	1176	1,297
3500	122	141	.76	1.16	1460	1,298
4000	100	112	.46	1.12	3451	1,299
4500						
5000	81	92	.45	1.13	4096	1,300
5500						
6000	79	90	.48	1.15	4095	1,301
7000	63	78	.68	1.24	4096	1,303
8000	57	73	.74	1.26	4096	1.303
Flowrate 0.75ml/min, 30/08/89						
1500	234	261	.39	1.11	1317	2,399,400
2000	186	224	.44	1.20	4674	2,396,397
2500						
3000	139	193	.46	1.38	10582	2,394,395
3500						
4000	118	139	.44	1.18	6109	2,392,393
4500						
5000	83	107	.62	1.29	7265	2,390,391
5500						
6000						

Droplet data summary : 1 continued
Effect of rotation speed on droplet size for various flowrates

Atomiser : 50 mm SPINNING GROOVE WITH SINGLE EMITTING POINT
Fluid : Tap water

N (RPM)	NMD (um)	VMD (um)	Span	Ratio	no. drops	File Record
Flowrate 1 ml/min. 26/08/88 (extrapolated from DDS3, 26/08/88)						
1500	230	270				
2000	180	230				
2500	155	195				
3000	135	170				
3500	120	155				
4000	110	140				
4500	105	135				
5000	100	130				
5500						
6000						
Flowrate 5 ml/min. 30/08/89						
1500	239	317	.63	1.33	749	2,398
2000	254	287	.49	1.13	1611	2,383
2500						
3000	85	261	.40	3.08	4569	2,384,385
3500						
4000	68	234	.46	3.42	13524	2,386,387
4500						
5000	58	229	.57	3.92	5354	2,389
5500						
6000						

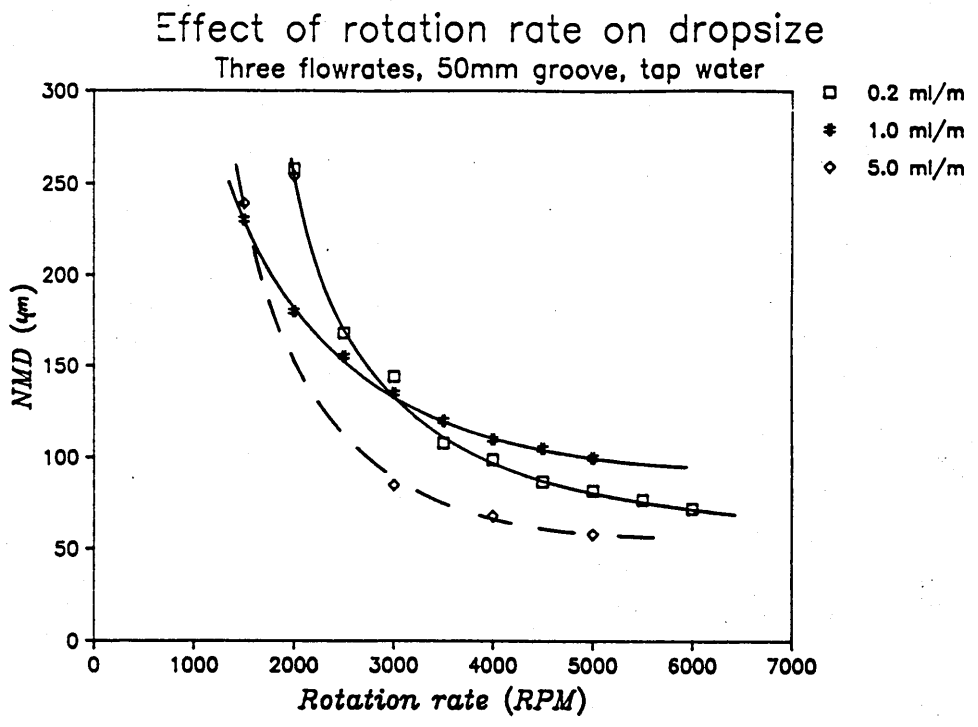

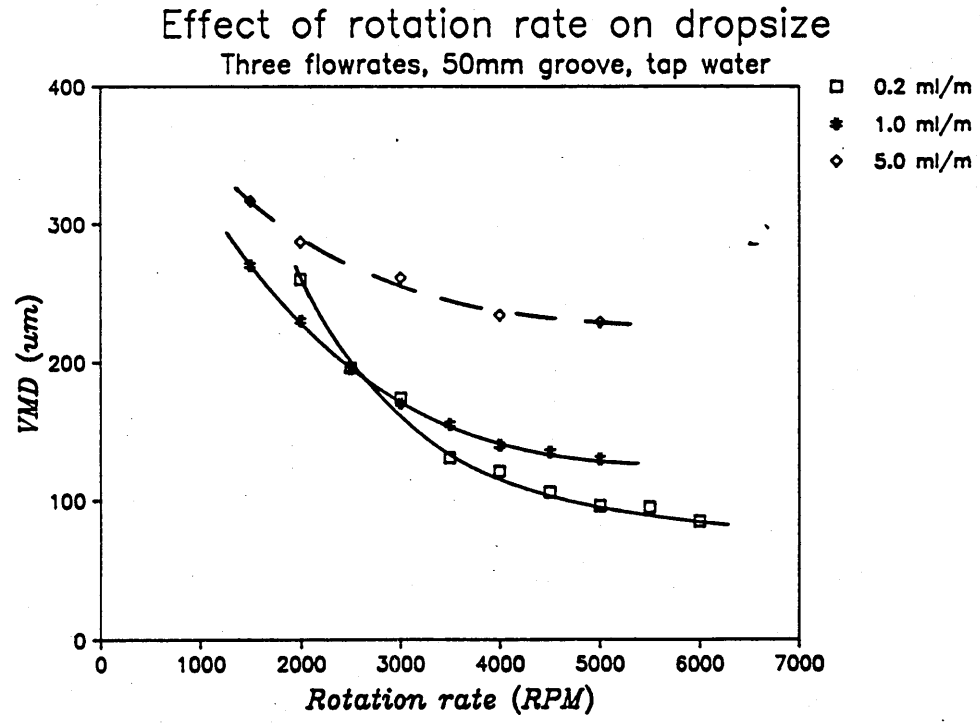

Figure 5.4a Single groove; effect of N (RPM) on dropsize

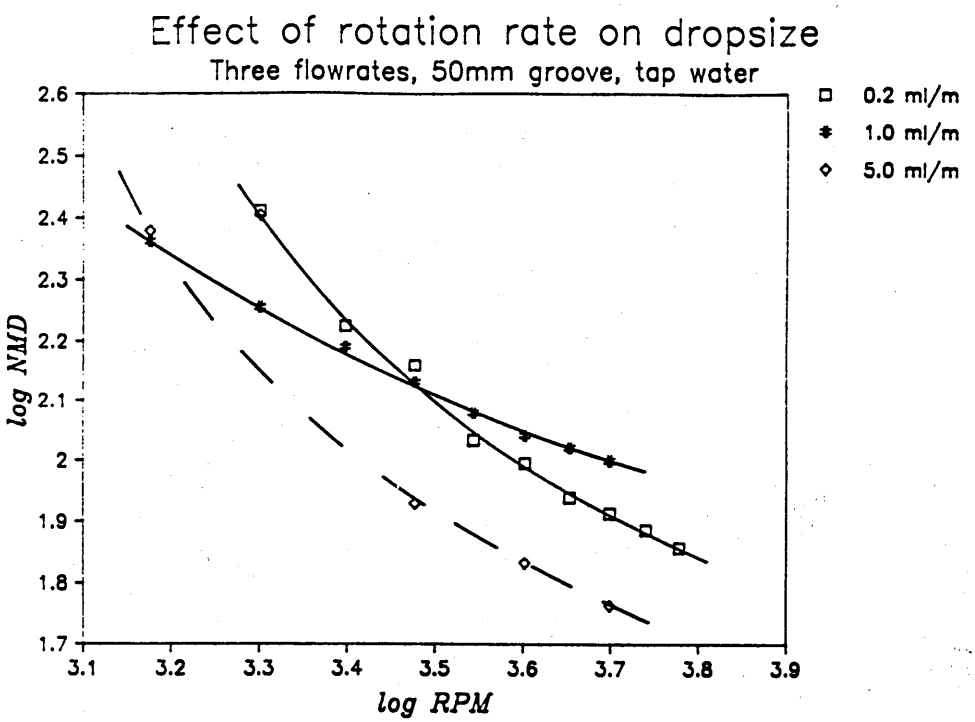

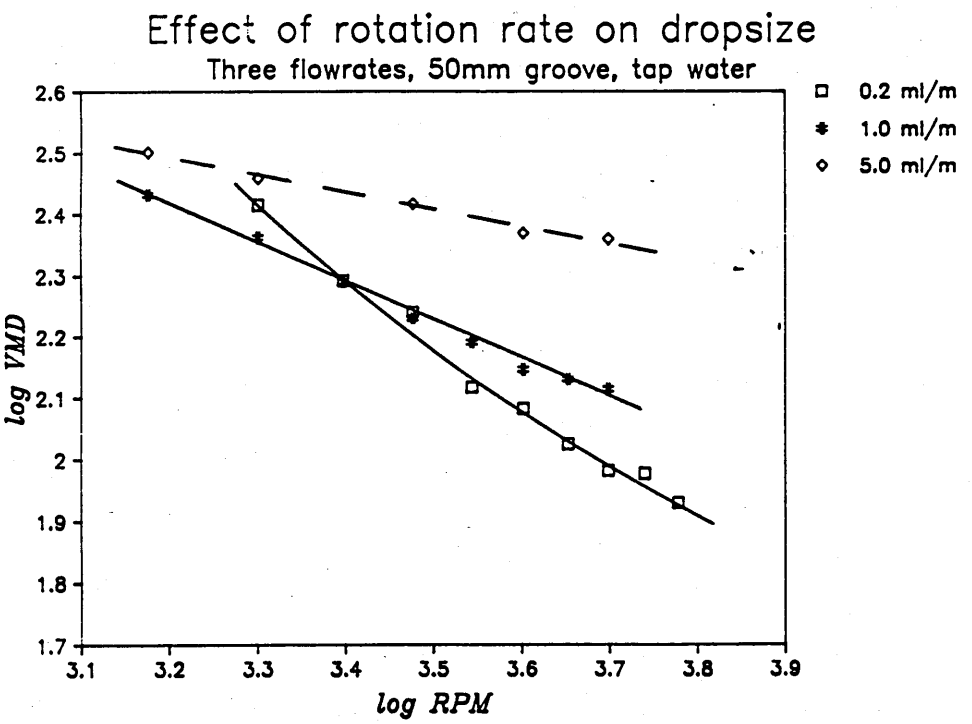

Figure 5.4b Single groove; effect of N (RPM) on dropsize

Droplet data summary : 2 EFFECT OF FLOWRATE ON DROPSIZE
Effect of flowrate on droplet size at four different rotation speeds

Atomiser : 50mm SPINNING GROOVE WITH SINGLE EMITTING POINT
Fluid : Tap water

Q (ml/min)	NMD (um)	VMD (um)	Span	Ratio	no. drops	File Record
2000 RPM, 03/07/88						
.05	281	283		1.01		
.10	256	264		1.03		
.20	244	252	.20	1.03	44	1.257
.50	165	191	.49	1.15	183	1.256
1.00	177	198	.45	1.12	265	1.258
2.00	163	210		1.28		
4000 RPM, 03/07/88						
.05	123	128	.28	1.05	155	1.289
.10	116	122	.34	1.05	275	1.290
.20	92	105	.56	1.14	111	1.278
.50	101	115	.46	1.14	590	1.291
1.00	110	124	.51	1.13	4096	1.292
2.00	145	164	1.04	1.13	2445	1.293
6000 RPM, 03/07/88						
.05	89	93	.33	1.04	460	1.282
.10	78	91	.49	1.16	743	1.284
.20	66	79	.50	1.21	964	1.281
.50	73	87	.74	1.19	1949	1.285
1.00	106	122	.94	1.16	4095	1.286
2.00	118	139	.97	1.17	2385	1.287
8000 RPM, 03/07/88						
.05	52	66		1.27		
.10	51	64		1.25		
.20	54	69	.66	1.29	1097	1.271
.50	55	71	.78	1.29	2048	1.272
1.00	90	112				ns
2.00	106	132	1.06	1.24	16376	1.274

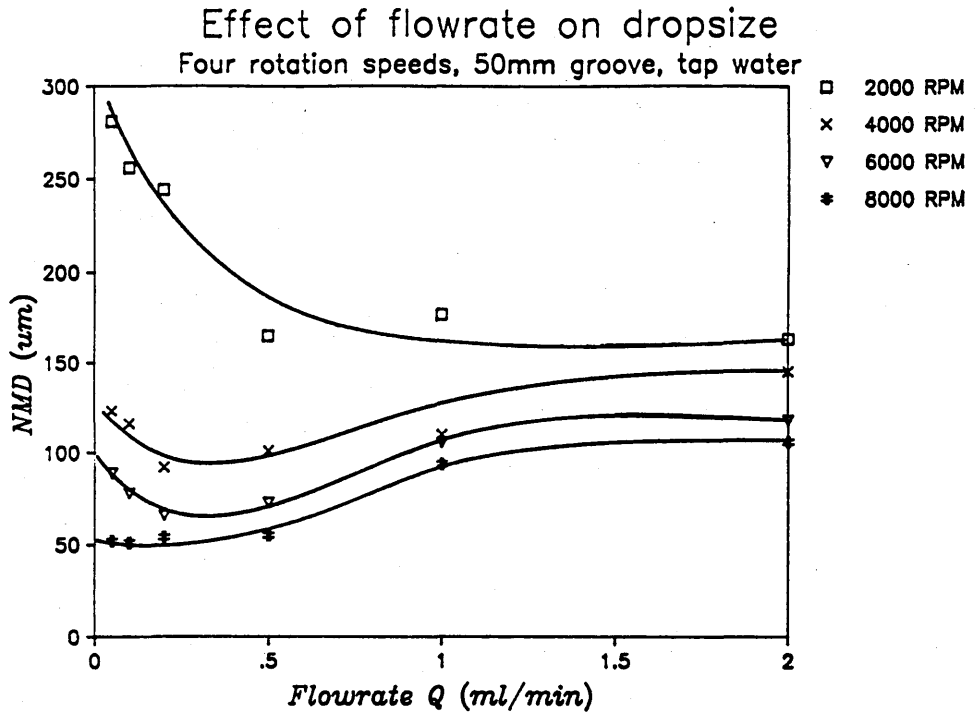

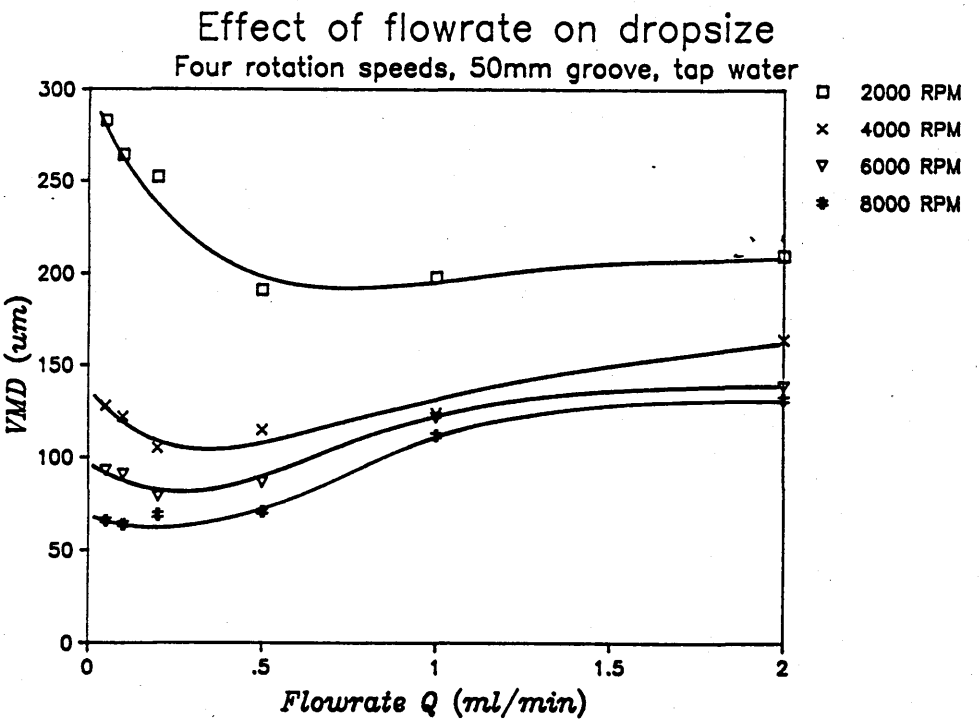

Figure 5.4c Single groove; effect of Q (ml/m) on dropsize

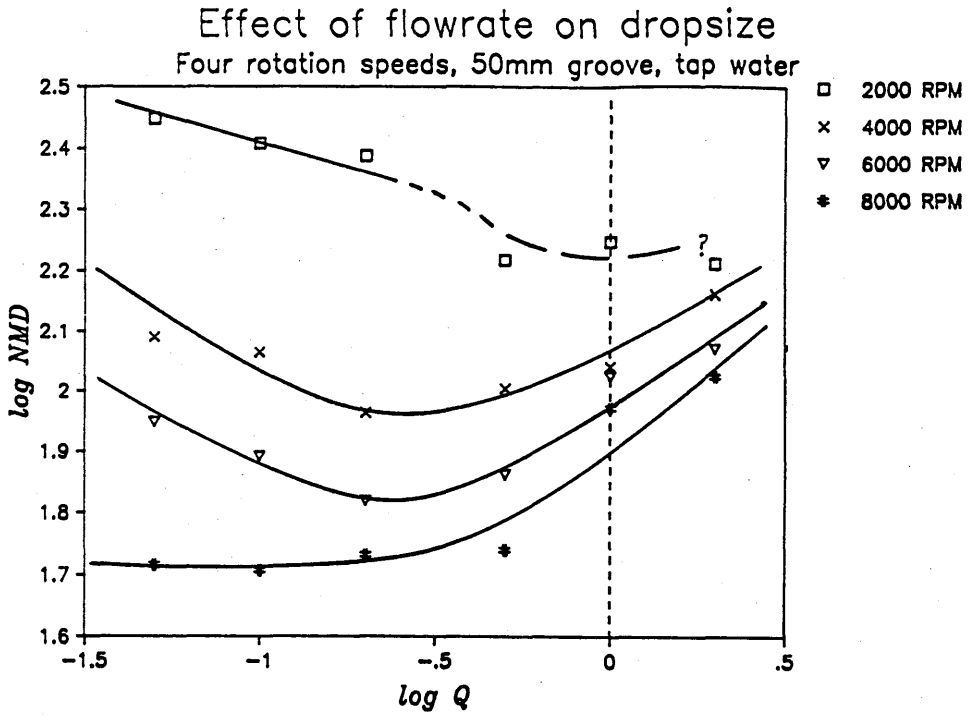

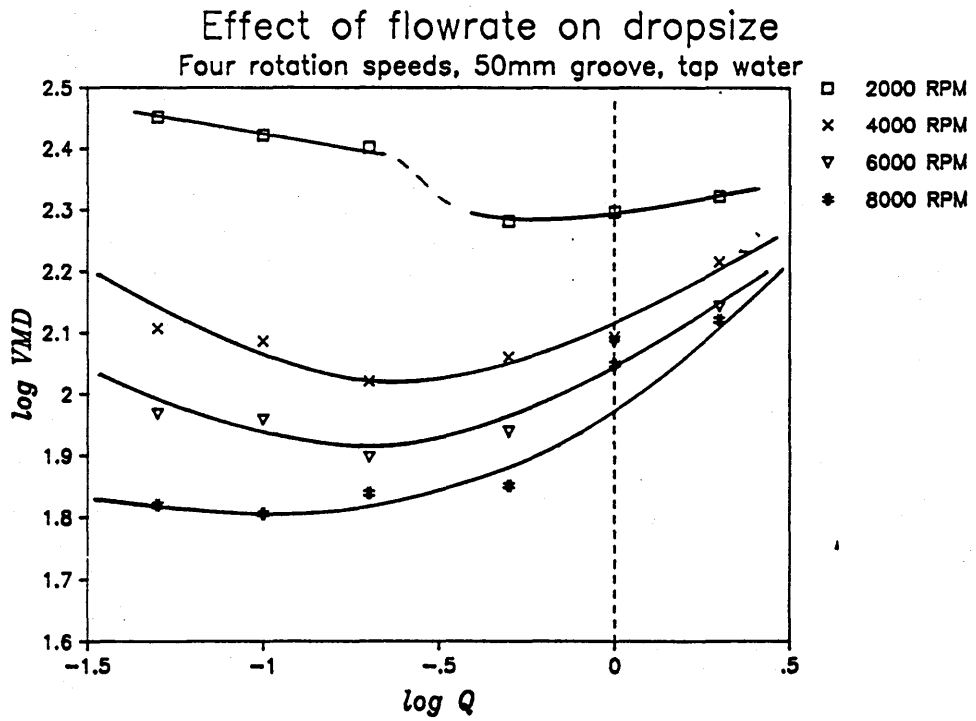

Figure 5.4d Single groove; effect of Q (ml/m) on dropsize

Droplet data summary : 3 EFFECT OF RADIUS ON DROPSIZE
Effect of rotation speed on droplet size for two groove lengths

Atomiser : SPINNING GROOVE WITH SINGLE EMITTING POINT
Flowrate : 1 ml/min
Fluid : Tap water

50mm radius, 26/08/88

N (RPM)	Vt (m/s)	NMD (um)	VMD (um)	Span	Ratio	File Record
1000	5.24	373	400	.41	1.07	1,350
1200	6.28	257	307	1.09	1.19	1,347
1400	7.33	231	282	.54	1.22	1,351
1600	8.38	213	257	.95	1.21	1,346
2000	10.47	175	228	.95	1.30	1,338
2400	12.57	163	201	1.01	1.23	1,367
2800	14.66	145	175	1.15	1.21	1,372
3200	16.76	128	160	1.02	1.25	1,366
3600	18.85	118	150	1.34	1.27	1,373
4000	20.94	111	165	1.36	1.48	1,361
5000	26.18	110	167	1.25	1.50	1,360
6000	31.42	106	122	.94	1.16	1,286
8000	41.89	94	121	1.04	1.28	1,273

20mm radius, 26/08/88

N (RPM)	Vt (m/s)	NMD (um)	VMD (um)	Span	Ratio	File Record
2500	5.24	228	250	.39	1.10	1,349
3000	6.28	202	224	.48	1.11	1,348
3500	7.33	171	210	.75	1.23	1,352
4000	8.38	168	189	.46	1.13	1,344
5000	10.47	145	165	.57	1.14	1,341
6000	12.57	130	145	.41	1.11	1,369
7000	14.66	116	135	1.16	1.17	1,371
8000	16.76	112	128	.60	1.14	1,365
9000	18.85					ns
10000	20.94	96	108	.55	1.13	1,364

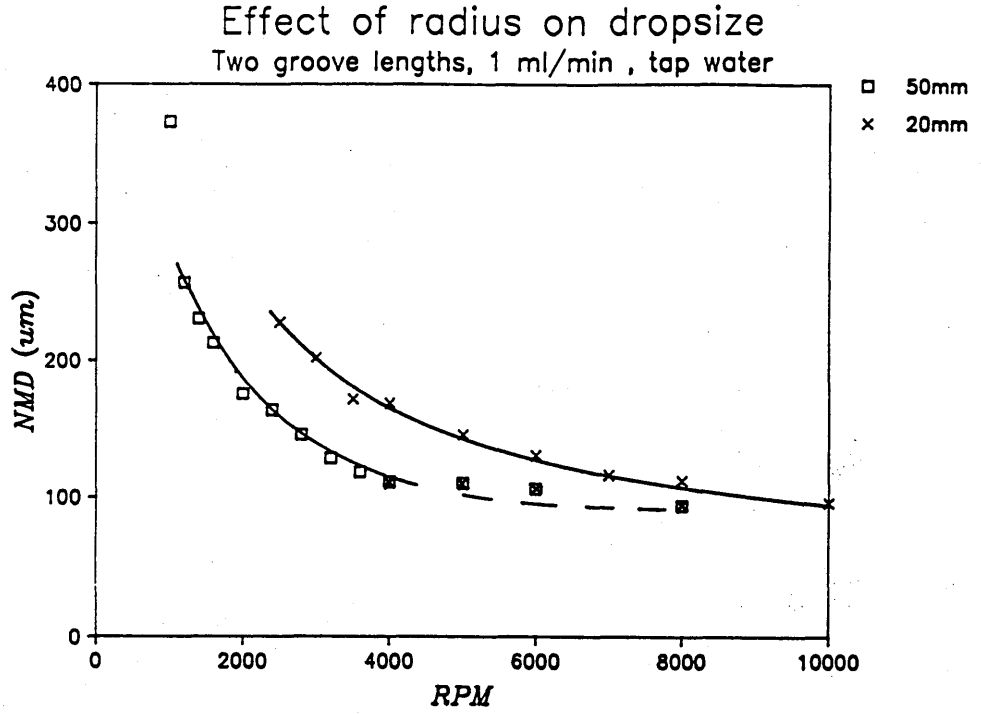

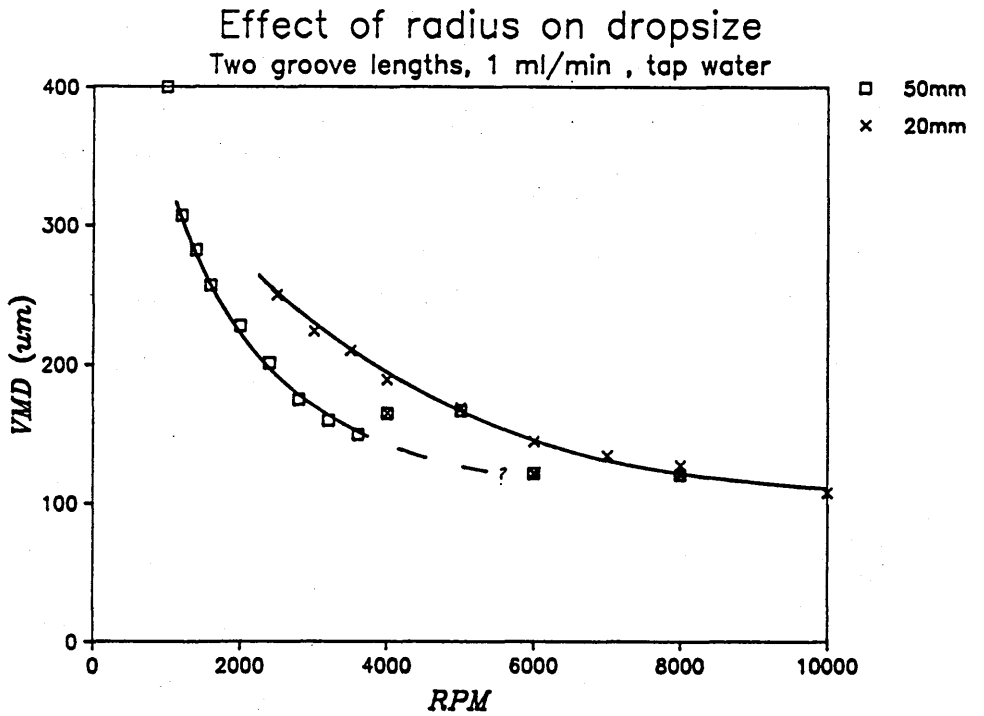

Figure 5.4e Single groove; effect of radius on N vs d

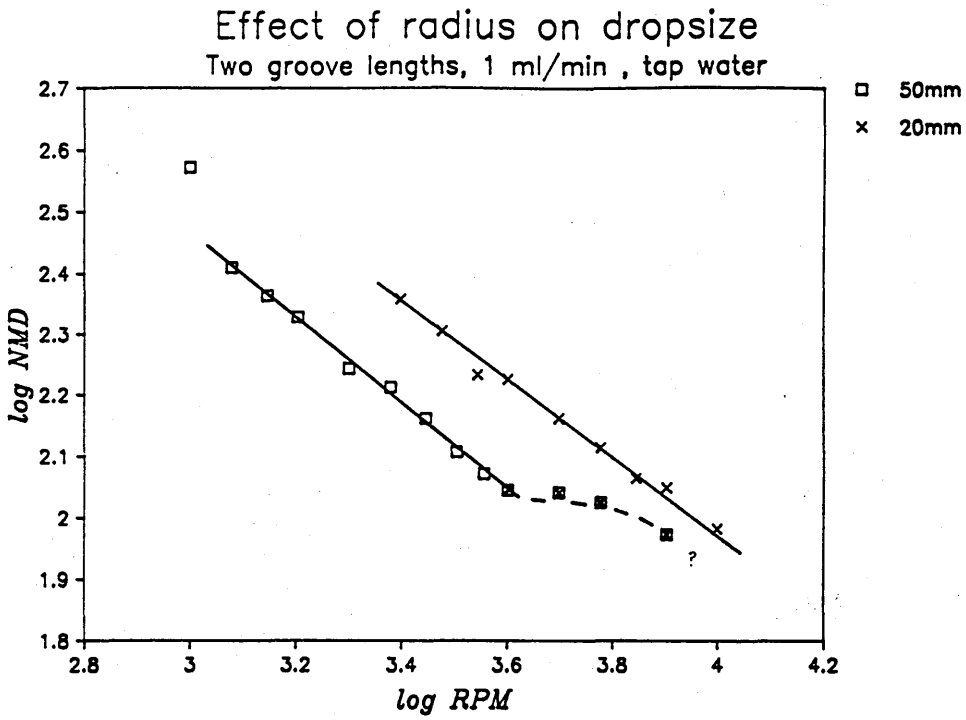

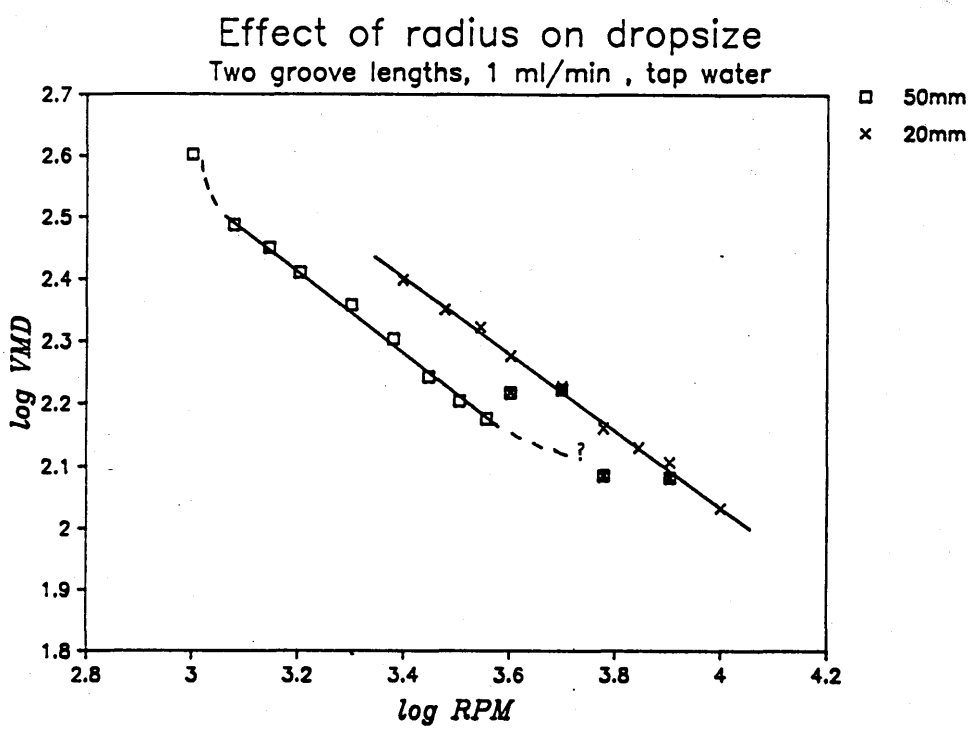

Figure 5.4f Single groove; effect of radius on N vs d

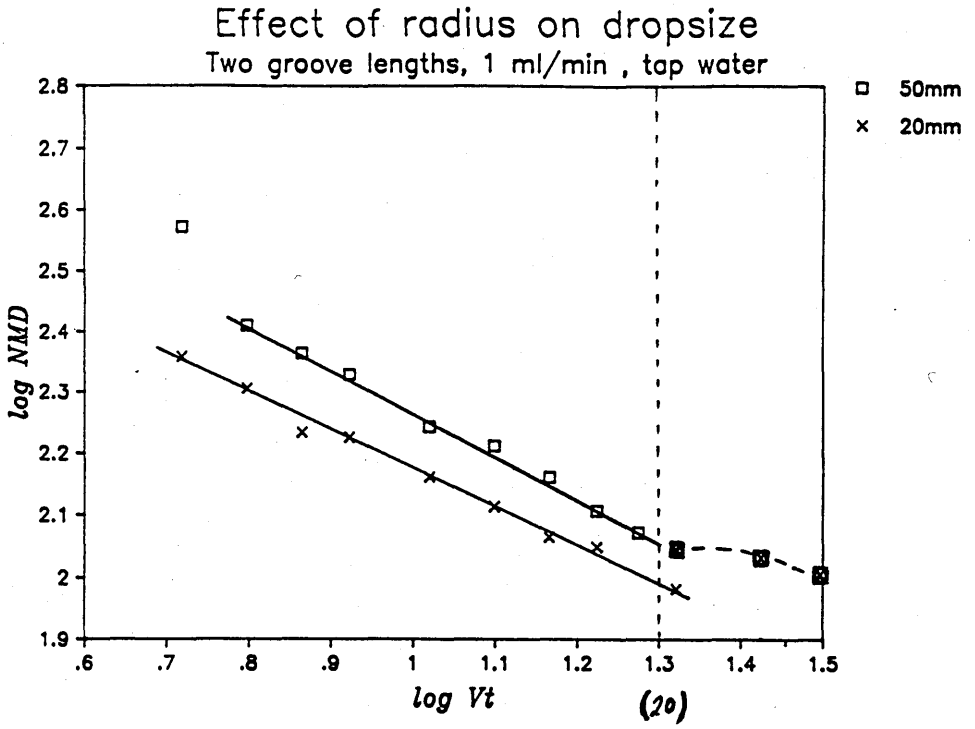

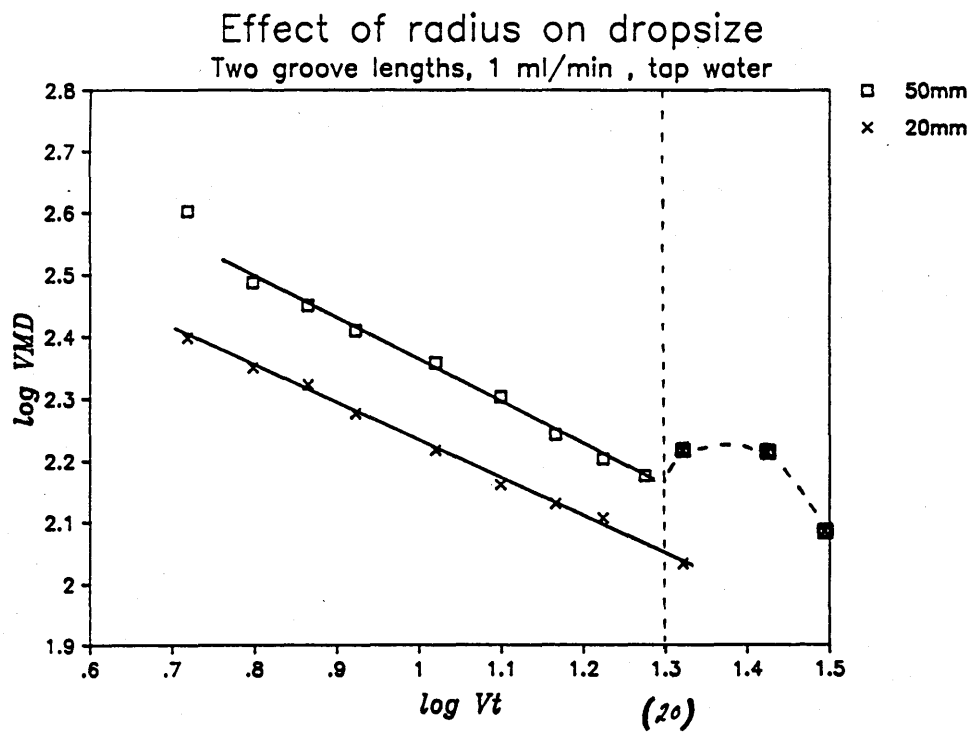

Figure 5.4g Single groove; dropsize vs tip velocity, V_T

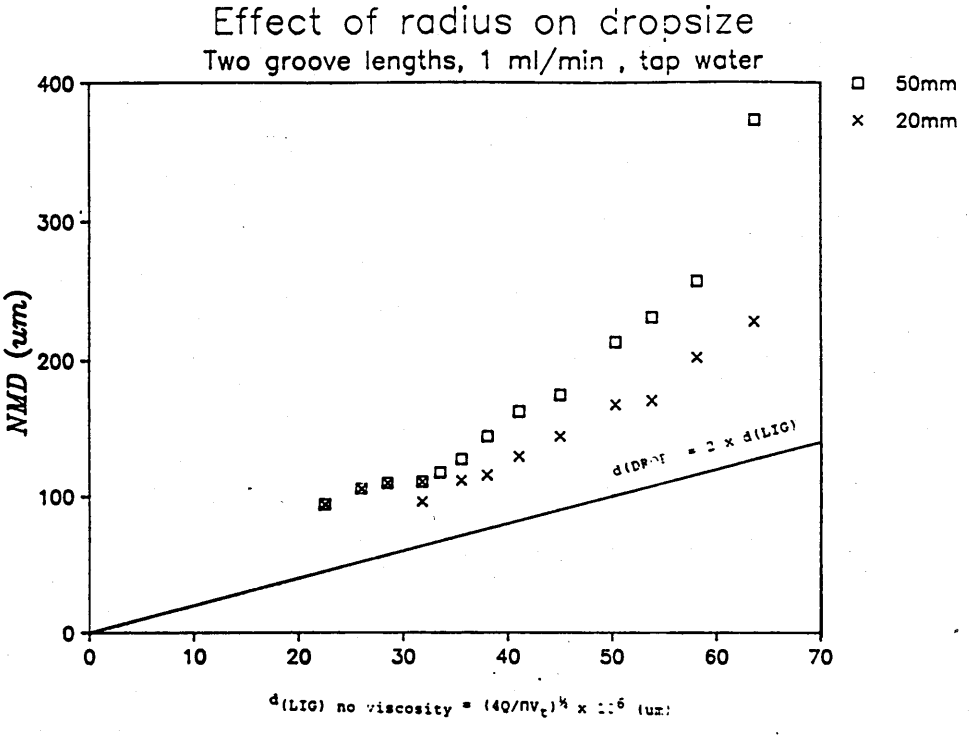

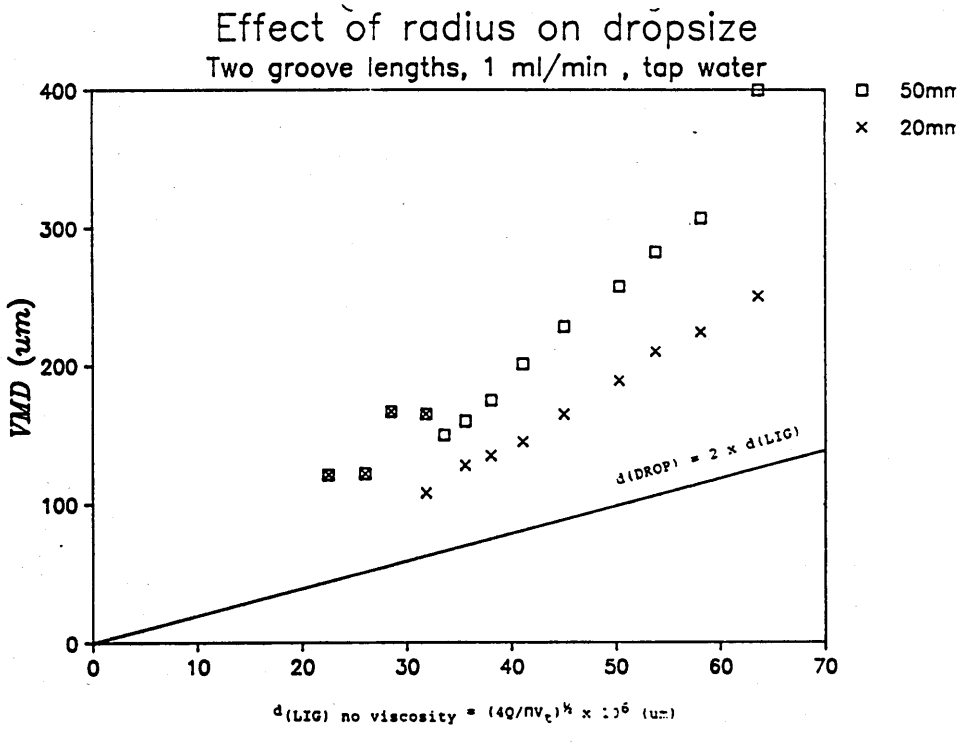

Figure 5.4h Single groove; dropsize vs theoretical ligament diameter $d_{(LIG)}$, calculated from inviscid fluid radial velocity.

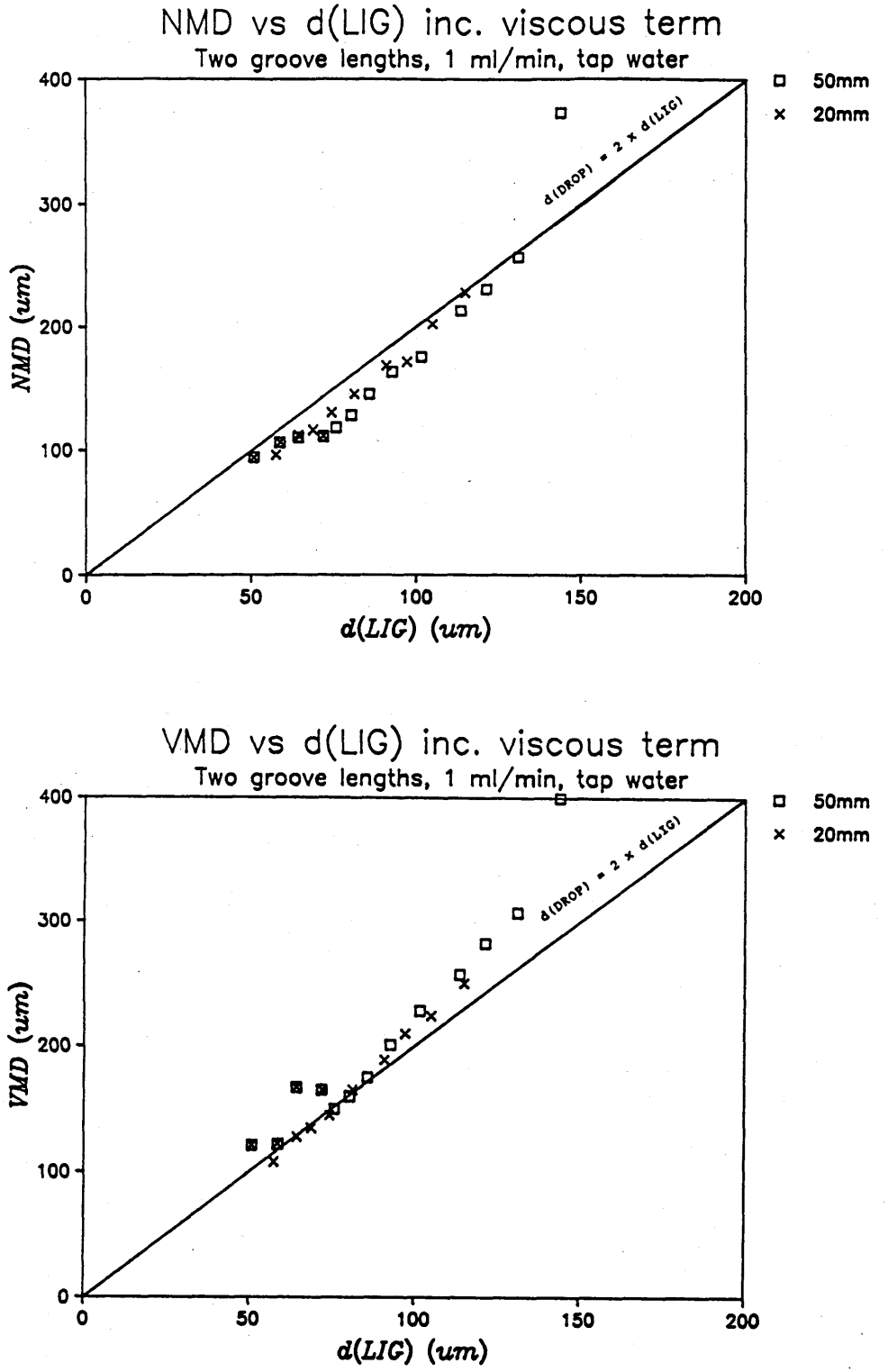

Figure 5.4i Single groove; dropsize vs theoretical ligament diameter $d_{(LIG)}$, calculated from fluid radial velocity, including losses due to viscosity.

5.5 Tests carried out on the Micron Herbi, a standard CDA rotary atomiser for herbicide application.

Four dropsize tests were carried out on the Micron Herbi, and are summarised in Droplet Data Summaries 4 to 7. For a description of the Herbi atomiser refer to Section 2.6.

The main purpose of the tests was to provide droplet spectra for later comparison with Waterwheel data, rather than to establish the relationships between dropsize and various parameters.

Each test was carried out using a different formulation as follows:

i) Tap water
ii) 0.01% Agral in tap water
iii) 20% Butyldigol in water
iv) 100% Butyldigol

A standard Herbi atomiser head was connected to a constant current supply rather than the dry cell batteries contained in the handle, so that RPM could be maintained constant over long time periods. Droplet spectra measurements for each test were taken at 250 RPM intervals from 1500 to 3000 RPM. This would be repeated with a number of different flowrates, typically 60, 120, 180, 240 and 360 ml/min. The Herbi disc has 360 teeth, so the feedrate values per tooth for the above flowrates are 0.166, 0.333, 0.5, 0.666, and 1 ml/min/tooth respectfully.

Figures 5.5a to 5.5d show dropsize data against RPM for various flowrates and liquids. Unfortunately the number of points available are not sufficient to establish definite curves in every case. Trends are present, although they are in general less predictable than with the spinning groove with single emitting point.

This is probably due to a sampling error associated with the fact that we are dealing with a more complex system. Unlike with the spinning groove, flowrate to each tooth is not exactly known. Droplet sampling with the laser (section 5.3) takes place at one point only with respect to rotating disc. If the feed to the periphery of the disc is less than completely uniform, this will lead to unpredictability in results obtained. Feed is less likely to be uniform at low flowrates, and with formulations without a surfactant to promote thorough wetting of the disc.

Figure 5.5e shows data for ligament disintegration at a flowrate of 120 ml/min expressed in log form. To this data, corresponding values for 240 ml/min were then added (not shown since they were similar). The mean slope of both sets of curves lead to an approximate power index for the relationship between VMD and RPM, for q between $0.33 \leq q \leq 0.66$ ml/min/tooth :

$$VMD \quad \alpha \quad N^{-0.75} \tag{153}$$

The value -0.75 agrees well with the experiments of Frost (1980), and Kinnersley (1987). The value of -0.75 was expected since it lies between -0.85 and -0.65, the values obtained by the single groove, for q = 0.2 and 1.0 ml/min groove respectfully. This may provide evidence for a relationship between the power index itself and q. This would provide a useful empirical formula for operators of spinning discs. More accurate prediction of dropsize for a particular disc is likely, compared to assuming constant value for the power index over a wide range of flowrates.

Droplet data summary 4

Atomiser MICRON HERBI
Fluid description Tap Water
Test carried out 06/02/89

N (RPM)	NMD (um)	VMD (um)	Span	Ratio	% vol. < 145um	File, Record
Flowrate = 60 ml/min						
1500	275	389	.89	1.41	.32	2.35
1750	236	363	.91	1.53	.75	2,36,40
2000	208	254	.78	1.22	1.91	2,33,34
2250	176	219	.92	1.24	4.05	2.87
2500	165	199	.89	1.21	6.28	2.38
2750	151	202	.80	1.34	13.32	2.88
3000	146	201	.77	1.37	16.60	2.89
Flowrate 120 ml/min						
1500	269	405	.74	1.50	.25	2.42
1750	269	382	.81	1.42	.28	2.41
2000						ns
2250	328	335	.24	1.02	.14	2,45
2500	292	307	.34	1.05	.65	2.43
2750	258	274	.31	1.06	1.53	2.90
3000						
Flowrate 240 ml/min						
1500	464	472	.36	1.02	.01	2.50
1750	401	415	.47	1.04	.05	2.46
2000	278	369	.60	1.33	.27	2.47
2250	196	329	.63	1.68	1.45	2.49
2500	172	288	.72	1.68	3.72	2.48
2750						ns
3000	140	195	.91	1.39	20.76	2.91
Flowrate 360 ml/min						
1500	464	478	.36	1.03	.03	2.53
1750						ns
2000	271	372	.46	1.37	.31	2,51
2250	194	313	.71	1.61	1.72	2,54
2500						
2750						
3000						

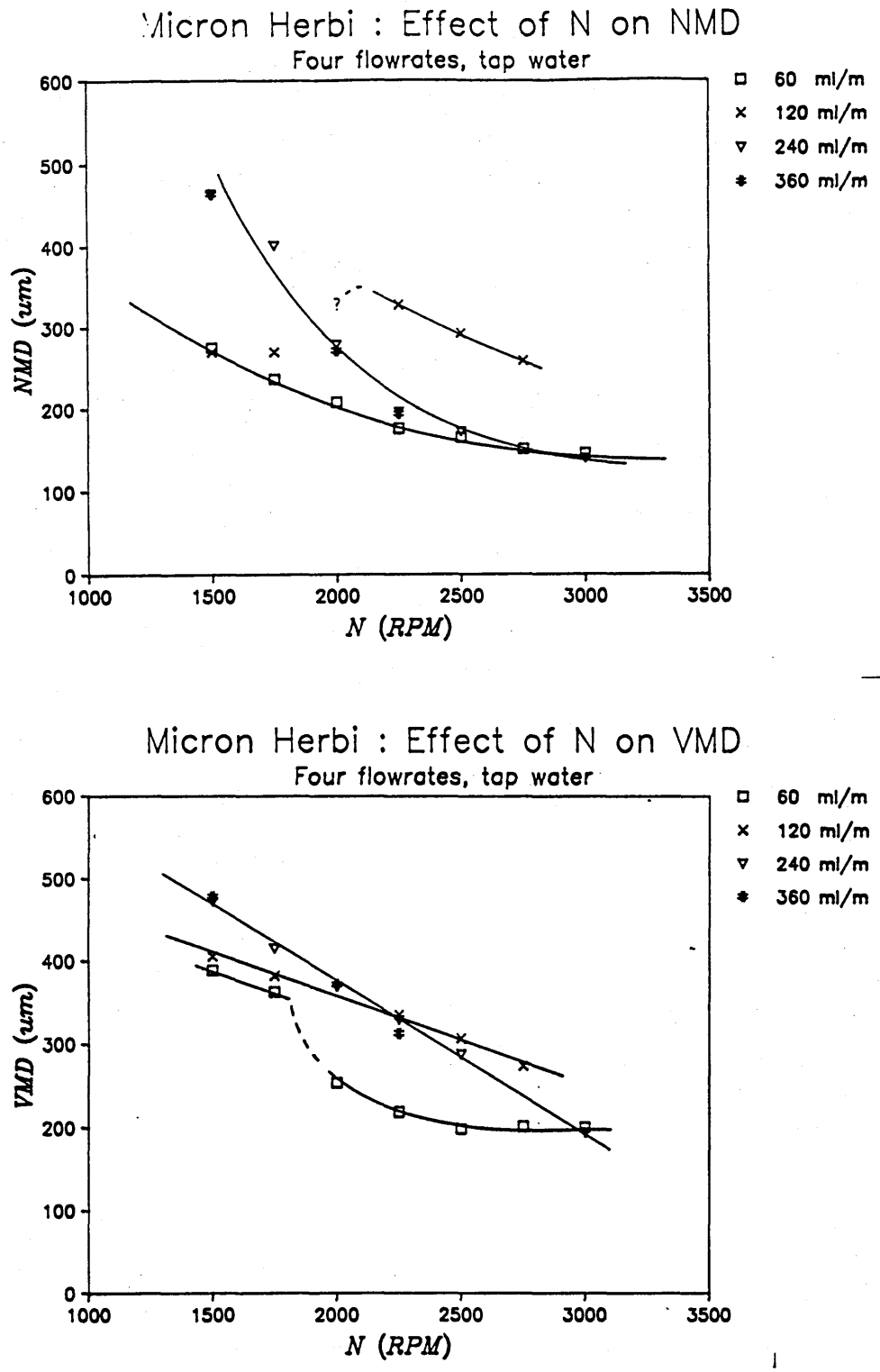

Figure 5.5a **Micron Herbi; effect of rotation rate on dropsize, tap water**

Droplet data summary 5

Atomiser MICRON HERBI
Fluid description 0.01% Agral in tap water
Test carried out 06/02/89

N (RPM)	NMD (um)	VMD (um)	Span	Ratio	% vol. < 145um	File, Record
Flowrate 60 ml/min						
1500	248	394	.84	1.59	.54	2,65
1750	219	272	.91	1.24	1.34	2,66
2000	194	227	.81	1.17	2.78	2,63
2250	180	211	.86	1.18	4.09	2,67
2500	165	193	.82	1.17	7.02	2,64
2750	148	177	.92	1.19	17.28	2,84
3000	143	174	.89	1.22	21.89	2,68
Flowrate 120 ml/min						
1500						
1750	409	417	.14	1.02	.07	2,74
2000	373	377	.14	1.01	.04	2,70
2250	342	347	.15	1.01	.07	2,73
2500	304	314	.24	1.03	.19	2,69
2750	243	288	.47	1.18	1.19	2,72
3000	225	279	.47	1.24	2.57	2,83
Flowrate 180 ml/min						
2000	217	397	.75	1.83	.76	2,75
Flowrate 240 ml/min						
1500	285	512	.74	1.80	.17	2,80
1750	251	466	.71	1.86	.37	2,81
2000	240	396	.75	1.65	.63	2,78
2250	258	358	.47	1.39	.65	2,76
2500	166	274	.90	1.65	5.07	2,79
2750	157	231	.98	1.47	7.77	2,82
3000	151	226	.93	1.50	12.14	2,77

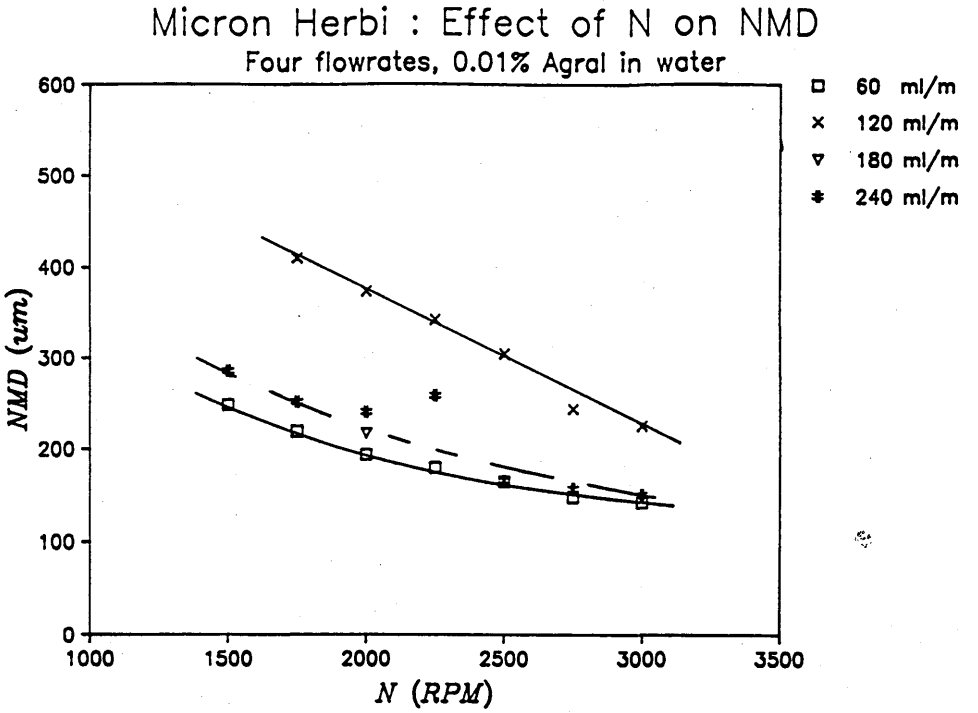

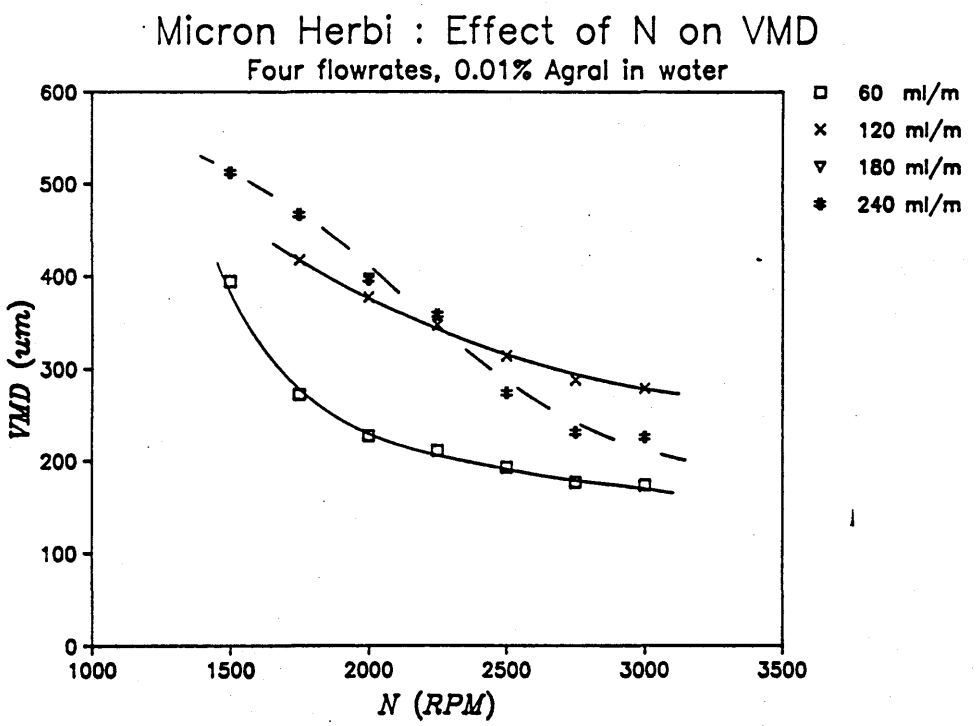

Figure 5.5b Micron Herbi; effect of rotation rate on dropsize, 0.01% Agral in tap water

Droplet data summary 6

Atomiser MICRON HERBI
Fluid description 20 % Butyldigol in water
Test carried out 06/02/89

N (RPM)	NMD (um)	VMD (um)	Span	Ratio	% vol. < 145um	File. Record
Flowrate 60 ml/min						
1500						
1750	327	328	.11	1.00	.05	2,93
2000	293	295	.09	1.01	.06	2,94
2250	270	272	.13	1.01	.10	2.95
2500	245	247	.16	1.01	.14	2,96
2750	226	229	.18	1.07	.31	2,97
3000	209	212	.17	1.01	.59	2.92
Flowrate 120 ml/min						
1500						
1750	333	339	.11	1.02	.23	2,98
2000	300	311	.28	1.04	.60	2,99
2250	254	275	.26	1.09	2.83	2,101
2500	139	255	.62	1.83	11.70	2,100
2750	115	218	.80	1.90	25.90	2,102
3000	108	197	.82	1.82	31.06	2,103
Flowrate 240 ml/min						
1500						
1750	173	265	1.15	1.53	4.42	2,104
2000	158	254	1.16	1.60	7.71	2,105
2250	147	224	1.12	1.53	13.86	2,106
2500	139	217	1.06	1.56	17.34	2,107
2750	135	214	1.00	1.59	18.61	2,108
3000						

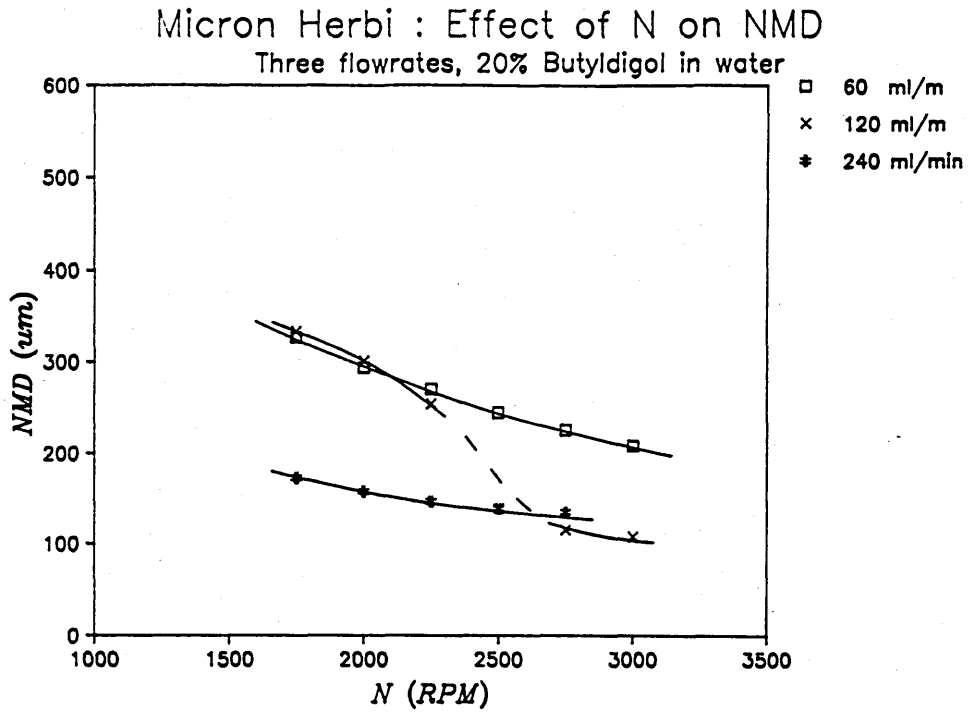

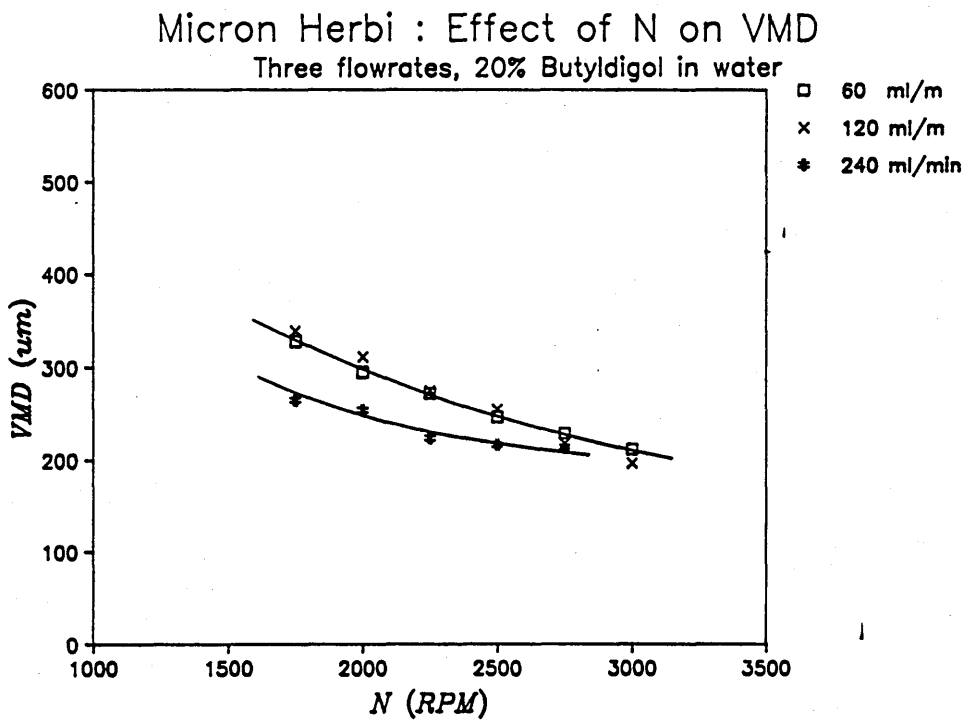

Figure 5.5c Micron Herbi; effect of rotation rate on dropsize, 20% Butyldigol in tap water

Droplet data summary 7

Atomiser MICRON HERBI
Fluid description 100 % Butyldigol
Test carried out 06/02/89

N (RPM)	NMD (um)	VMD (um)	Span	Ratio	% vol. < 145um	File, Record
Flowrate 60 ml/min						
1500						
1750	317	341	.09	1.07	2.21	2,110
2000	276	291	.01	1.05	2.80	2,109
2250	256	274	.29	1.07	3.10	2,111
2500	235	251	.17	1.06	3.38	2,112
2750	123	233	.22	1.89	7.46	2,113
3000	105	206	.72	1.96	29.33	2,114
Flowrate 120 ml/min						
1500						
1750	169	247	.97	1.46	5.47	2,115
2000	146	273	.79	1.88	12.30	2,116
2250	148	188	1.00	1.27	15.79	2,117
2500	138	178	1.01	1.28	22.07	2,118
2750	139	179	1.01	1.29	21.15	2,119
3000						
Flowrate 240 ml/min						
2000	181	252	1.20	1.39	3.35	2,121
2500	156	220	1.12	1.42	9.22	2,120
RPM constant at 2000 RPM						
Q (ml/min)	NMD (um)	VMD (um)	Span	Ratio	% vol. < 145um	File, Record
30	282	288	.12	1.02	.94	2,122
15	276	284	.14	1.03	1.13	2,123
5	266	274	.14	1.03	.78	2,124

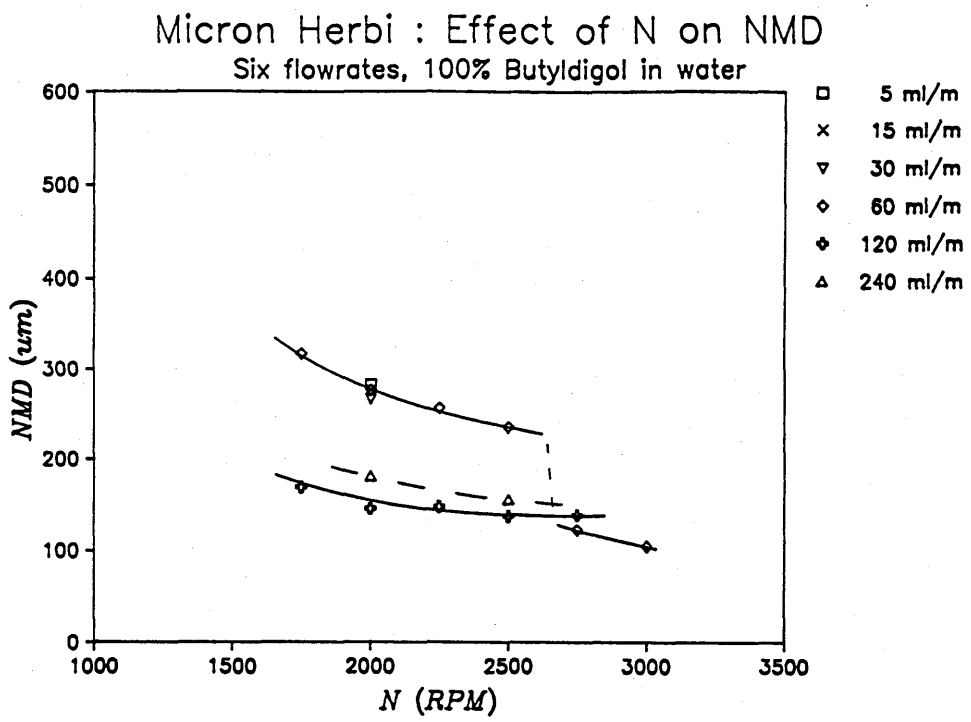

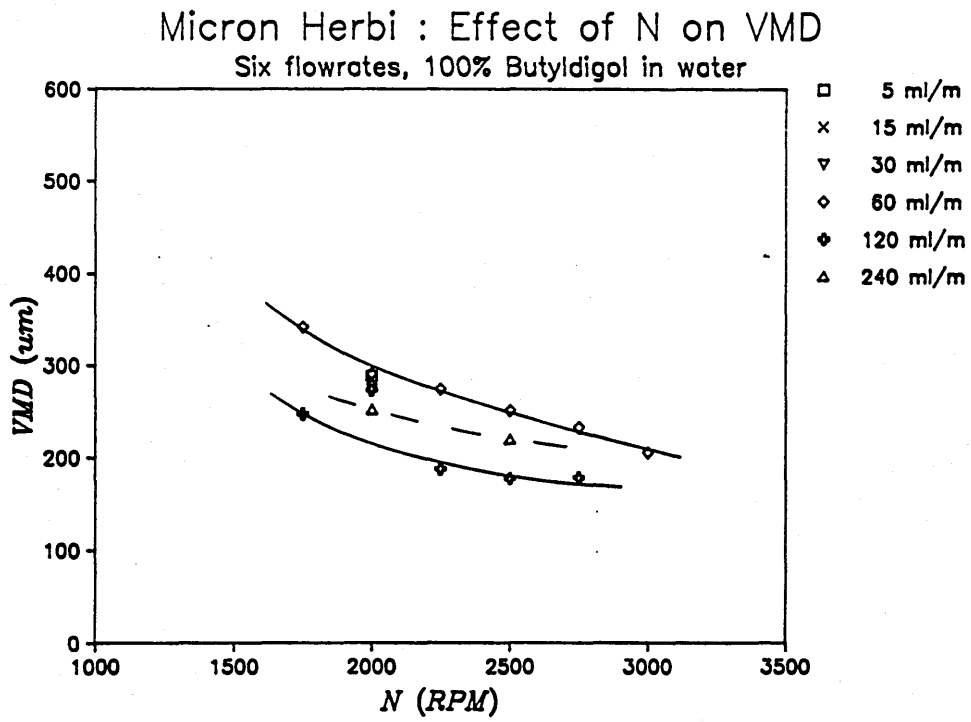

Figure 5.5d **Micron Herbi; effect of rotation rate on dropsize, 100% Butyldigol**

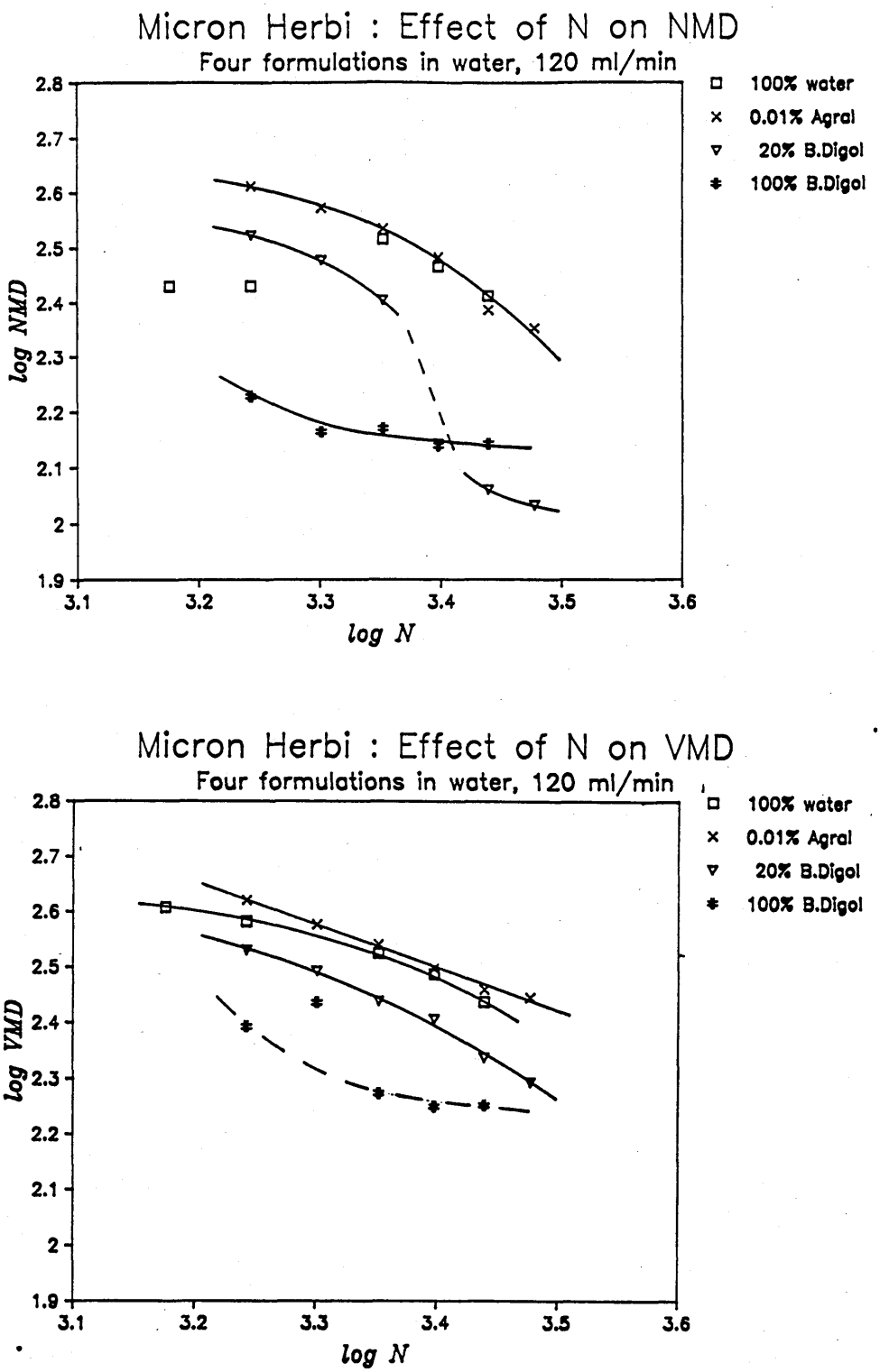

Figure 5.5e Micron Herbi; effect of rotation rate on dropsize for four formulations, 120 ml/min.

Chapter Six

PROTOTYPE EXPERIMENTAL RESULTS

6.1 Summary of development and test programme

Progressive modification of various features of the Waterwheel were carried out in conjunction with tests to assess performance. The experiments were devised in order to increase understanding of the processes involved and progress progress towards an optimum in design.

Flowrate and rotation speed were noted at various supply pressures and at the same time measurements of the droplet spectra were recorded. Analysis of the results at each stage of development would lead on to the next design modification.

For ease of reference, the different versions have been designated prototype numbers 1 to 12. In total, three basic designs were manufactured, each with a different size and bearing arrangement. The first two were machined primarily from aluminium alloy, the last from PVC plastic.

Four variations of each design were tested with the PMS dropsizing equipment, and for ease of reference are described respectfully as prototypes 1 to 4, 5 to 8, and 9 to 12 (Table 6.1).

Prototypes 1 to 4 had an internal cup diameter of 70mm and the tip to tip diameter of the disc was 83mm. Prototypes 1 and 2 were tested prior to the commencement of this study (Kinnersley 1987), but the results are included for completion.

Prototype 3 is essentially identical to 2 except that the external air motor bearing was replaced with the plain bearing of an electric motor. Tests with Mk.3 involved altering nozzle orifice diameter to assess the effect of flowrate on droplet spectra. Mk.3 was tested with plain tap water, and also with 0.01% agral surfactant in tap water.

Mk.1, Mk.2 and Mk.3 were found to produce relatively wide droplet spectra. The reason was identified as fluid slippage from tooth to tooth as described in section 4.4.1. This led to the design of a similar disc but with deeper grooves for Mk.4. However, slippage was still noted to occur at all flowrates except the very lowest obtainable for satisfactory rotation ie nozzle diameter equal to 0.38mm.

Prototypes 5 to 8 were of smaller size, the inner wall diameter being only 44mm. External diameter of the disc from tip to tip was 56mm. Such a size reduction led to a requirement for low bearing friction, which was facilitated by means of lubricated dual miniature ball races.

The disc consisted of grooves with one vertical face, which delayed fluid exitting the groove until the tip of the tooth was very nearly reached (section 5.4). Atomisation was therefore satisfactory up to nozzle orifice diameters of about 0.65mm. Mk.5 had a nozzle orifice diameter of 0.62mm; with Mk.6 to 8 it was 0.5mm which provided the desired flowrate of 0.25 litres per minute at 3 bar, for a 40 litre per hectare application (section 6.5).

Mk.5 was also tested with 0.01% Agral in water, 10% Butyldigol in water and 100% Butyldigol. Mk.6 was tested with a formulation likely to be used commercially with the Waterwheel for weed control, consisting of 20% (v/v) heavy glyphosate acid + surfactant in water. Photographs showed that higher than expected VMD values were due to foaming of the formulation. Mk.6 was also tested with alternative designs of disc including one with cylindrical channels instead of grooves for flowrates higher than 0.25 l/min.

Rounding off the end of the nozzle, and increasing clearance from the inner wall from 1.5 to 3mm led to greater rotation speeds and therefore smaller droplets for Mk.7 and 8. The problem of reduced rotation speeds when using a surfactant was also alleviated, leading to the production of acceptable droplet spectra with 20% (v/v) heavy glyphosate acid + surfactant (Roundup^{tm}, Monsanto) in water, and concentrations of Agral surfactant of up to 0.1% (v/v).

The effect of weirs in redistributing fluid evenly was investigated by progressively removing the weirs of Mk.7, replacing each weir with a plain ring. The Waterwheel with a completely smooth inner wall was designated Mk.8.

The primary intention with Mk.9 to 11 was to investigate the possibility of using a PTFE plain bearing which would be less costly to produce on a commercial scale. Internal diameter was therefore increased to 60mm so that there was sufficient torque from the jet to overcome the increased friction from such a bearing. Nozzle orifice diameter also had to be increased to 0.65mm inorder to achieve satisfactory rotation speeds. With Mk 10 and 11, the central portion of the shaft was reduced in diameter inorder to reduce surface area in contact with the PTFE, which led to a significant improvement in rotation speed. With Mk.11, two nozzles with 0.5mm orifices replaced the single nozzle, to investigate whether rotation speed was increased, and also if peripheral distribution without the weiring system was improved. Results show that neither of these hypothesis actually appeared to be the case.

With Mk.12, the plain bearing was replaced with a single ballrace with an increased internal diameter of 5mm, inorder to investigate the effect of increasing shaft strength to survive impact from dropping.

Table 6.1 Summary of fluid driven prototypes tested (denoted Waterwheel or WW Mk. 1 - 12).

Mk.	G've shape	D_{int} (mm)	D_{ext} (mm)	H_{int} (mm)	Nozzle (mm)	Weirs	Bearing type
1	v	70	83	14	0.45	no	ext. ballraces
2	v	70	83	22	0.45	yes	ext. ballraces
3	v	70	83	22	varied	yes	ext. plain
4	V	70	83	22	0.38	yes	ext. plain
5	7	44	56	22	0.62	yes	min. ballraces
6	7	44	56	22	0.5	yes	min. ballraces
7	7	44	56	22	0.5*	yes	min. ballraces
7a-g	7	44	56	22	0.47*	yes	min. ballraces
8	7	44	56	22	0.5*	no	min. ballraces
9	7	60	80	30	0.65	no	plain bearing
10	7	60	80	30	0.65	no	plain bearing [1]
11	7	60	80	30	2x0.5	no	plain bearing [1]
12	7	60	80	30	0.5	yes	min. ballrace

Notes

* modified nozzle

1 skimmed shaft

7a-g have 0.47mm nozzle, with the exception of 7d

6.2 Performance data with water

Section 6.2 consists of a list of droplet data summaries corresponding to experiments with water on the Waterwheel. The primary aim of this particular set of data was to assess the effect of supply pressure on rotational performance and droplet size.

Data obtained by Kinnersley for Mk.1 and 2, 1987, was taken at intervals of pressure corresponding to multiples of 5 PSI (pounds per square inch). For purposes of direct comparison the present author continued using these intervals for Mk.3, Mk.5 and 6. For ease of handling these pressures have been converted to Bar (corresponding to 10^5 Pascals). Later tests with Mk.6, tests with Mk.4,7,8 and Mk.9-11 were carried out at 0.5 Bar, or 1 bar intervals, depending on the sensitivity required.

Basic features of the Waterwheel tested, liquid sprayed and date of the test have been listed at the top of each summary. Against each pressure is listed mean rotational speed in Revolutions per minute, calibrated flowrate in ml per minute, meaned Number Median Diameter and Volume Median Diameter in micrometers or microns (μm), the NMD / VMD ratio for an indication of spectral width, and finally the File and the Record Number under which the raw droplet data is stored on computer disc.

NMD and VMD may have been derived from a Record, or more than one record. In the latter case the droplet counts have been added together to produce a mean result. The file and record number may be used to locate processed data and droplet statistics for the reading concerned, in Appendix 2.

The individual record numbers indicate the chronological order in which the readings were taken. The reader may note that these are rarely in ascending or descending order of pressure, primarily so that consistancy could be checked regularly, so to avoid time dependant errors arising from steady changes in bearing friction, and therefore rotational speed of the atomiser.

Atomiser prototype	WW Mk. 1
Internal diameter of cup	70mm
Disc type and diameter	> shaped shallow grooves, 83mm
Nozzle orifice size	0.45mm
Bearing	external air motor (min. ballraces)
Substance sprayed	Water
Test carried out	1987, (R.P.Kinnersley)

P (PSI)	P (Bar)	N (RPM)	Q (ml/min)	NMD (um)	VMD (um)	R
25	1.72	385	133.8			
30	2.07	704	148.2	322	432	1.34
35	2.41	969				
40	2.76	1172	174.0			
45	3.10	1407				
50	3.45	1586	203.4			
55	3.79	1777				
60	4.13	1943	225.0	199	293	1.47
65	4.48	2108				
70	4.82	2227	242.4			
75	5.17	2375				
80	5.51	2472	257.4			
85	5.86	2607				
90	6.20	2725	273.6	151	254	1.68
95	6.55	2809				
100	6.89	2840	293.4			

DDS 9

Atomiser prototype	WW Mk. 2
Internal diameter of cup	70mm
Disc type and diameter	> shaped shallow grooves, 83mm
Nozzle orifice size	0.45mm
Bearing	external air motor (min. ballraces)
Substance sprayed	Water
Test carried out	1987, (R.P.Kinnersley)

P (PSI)	P (Bar)	N (RPM)	Q (ml/min)	NMD (um)	VMD (um)	R
25	1.72		133.8			
30	2.07	1634	148.2	234	300	1.28
35	2.41					
40	2.76		174.0			
45	3.10					
50	3.45	2259	203.4	169	249	1.47
55	3.79					
60	4.13		214.8			
65	4.48					
70	4.82		238.2			
75	5.17					
80	5.51	3122	253.8	218	109	2.00
85	5.86					
90	6.20		270.0			
95	6.55					
100	6.89		277.8			

DDS 10

Atomiser prototype	WW Mk. 3
Internal diameter of cup	70mm
Disc type and diameter	> shaped shallow grooves, 83mm
Nozzle orifice size	.55mm
Bearing	external air motor (min. ballraces)
Substance sprayed	Water
Test carried out	13/05/88

P (PSI)	P (Bar)	N (RPM)	Q (ml/min)	NMD (um)	VMD (um)	R
25	1.72					
30	2.07	1910	240	163	302	1.85
35	2.41					
40	2.76	2250	276	201	289	1.44
45	3.10					
50	3.45	2570	294	197	282	1.43
55	3.79					
60	4.13	2925	321	181	270	1.49
65	4.48					
70	4.82	3235	342	151	258	1.71
75	5.17					
80	5.51	3440	354	130	261	2.01
85	5.86					
90	6.20	3590	375	133	277	2.08
95	6.55					
100	6.89					

DDS 11

Atomiser prototype WW Mk.4

Internal diameter of cup 70mm

Disc type and diameter > shaped grooves, 83mm, deep

Nozzle orifice size 0.38mm

Bearing external electric motor (plain)

Substance sprayed water

Test carried out 09/08/89

P (Bar)	N (RPM)	Q (ml/min)	NMD (um)	VMD (um)	Ratio	File, Record
.5						
1.0						
1.5						
2.0	500	105	493	755	1.53	2,206
2.5	940	115	374	451	1.21	2,199
3.0	1200	122	362	412	1.14	2,200
3.5	1420	132	316	379	1.20	2,204,5
4.0	1780	140	262	309	1.18	2,201,2,3
4.5	2000	148	230	279	1.21	2,207
5.0	2100	154	230	280	1.22	2,208

DDS 12

Atomiser prototype	WW Mk.5
Internal diameter of cup	44mm
Disc type and diameter	7 shaped grooves, 56mm
Nozzle orofice size	0.62mm
Bearing	minature ball races
Substance sprayed	water
Test carried out	02/02/89

P (Bar)	N (RPM)	Q (ml/min)	NMD (um)	VMD (um)	Ratio	File, Record
1.72	1810	290	325	375	1.16	2,007
2.07	2000	320	308	352	1.14	2,008,6
2.41	2230	340	330	377	1.14	2,009
2.76	2450	362	280	327	1.17	2,010,5
3.10	2610	380	269	325	1.21	2,011
3.45	2770	395	264	318	1.20	2,012,14,4
3.79	2990	410	257	315	1.22	2,013
4.13	3150	425	257	315	1.24	2,015,16,3
4.48	3320	440	243	319	1.31	2,018
4.82	3500	450	234	307	1.31	2,017

DDS 13

Atomiser prototype	WW Mk.6
Internal diameter of cup	44mm
Disc type and diameter	7 shaped grooves, 56mm
Nozzle orifice size	0.5mm
Bearing	minature ball races
Substance sprayed	water
Test carried out	23/03/89

P (Bar)	N (RPM)	Q (ml/min)	NMD (um)	VMD (um)	Ratio	File, Record
1.72	1450	195	328	397	1.21	2,152
2.07	1680	210	295	351	1.19	2,151
2.41	2000	220	278	337	1.21	2,153
2.76	2280	230	255	314	1.23	2,150
3.10	2412	238	247	302	1.22	2,154
3.45	2680	245	235	298	1.27	2,149
3.79	2840	253	224	288	1.29	2,155
4.13	3000	260	222	295	1.33	2,145
4.48	3180	265	212	280	1.32	2,156
4.82	3410	270	206	290	1.41	2,146

DDS 14

Atomiser prototype	WW Mk.6
Internal diameter of cup	44mm
Disc type and diameter	7 shaped grooves, 56mm
Nozzle orifice size	0.5mm
Bearing	miniature ballraces
Substance sprayed	tap water
Test carried out	

P (Bar)	N (RPM)	Q (ml/min)	NMD (um)	VMD (um)	Ratio	File, Record
2.0	1380	200	372	449	1.21	2,275-6
2.5	1750	220	316	362	1.15	2,277
3.0	1965	235	294	331	1.13	2,273-4
4.0	2550	260	261	304	1.17	2,267-9
5.0	2960	280	237	290	1.22	2,270-2

DDS 15

Atomiser prototype	WW Mk.7 (a) water
Internal diameter of cup	44mm
Disc type and diameter	7 shaped grooves, 56mm
Nozzle orifice size	0.48mm, modified
Bearing	miniature ballraces, lubricated
Substance sprayed	tap water
Test carried out	27/11/90

P (Bar)	N (RPM)	Q (ml/min)	NMD (um)	VMD (um)	R.Span	Ratio	File, Record
.5							
1.0							
1.5							
2.0	3470	164	190	233	.83	1.22	4,024,25
2.5	3890	185	181	228	.85	1.26	4,023,26
3.0	4305	200	171	217	.87	1.27	4,022,27
3.5	4730	218	168	217	.84	1.30	4,028
4.0	5050	230	165	212	.83	1.28	4,021,29
4.5							
5.0	5800	260	159	204	.82	1.28	4,020,30

DDS 16

Atomiser prototype	WW Mk.7 e
Internal diameter of cup	44mm
Disc type and diameter	7 shaped grooves, 56mm
Nozzle orifice size	0.48mm, modified
Bearing	miniature ballraces, dry
Substance sprayed	tap water
Test carried out	16/11/90
Other information	BARC out

P (Bar)	N (RPM)	Q (ml/min)	NMD (um)	VMD (um)	Ratio	File, Record
1.0	900	125				
1.1	1500	130	549	576	1.05	3,038
1.2	1640	135	423	530	1.25	3,039
1.3	1730	139	301	482	1.60	3,040
1.4	1860	143	277	427	1.54	3,041
1.5	1970	147	258	316	1.22	3,042,23,36
1.6	2050	152	253	302	1.20	3,043
1.7	2250	157	245	288	1.18	3,044
1.8	2300	161	238	276	1.16	3,045
1.9	2380	164	233	273	1.17	3,046
2.0	2520	169	227	270	1.19	3,018,19,22,47
2.5	3070	185	208	252	1.21	3,021,34,48
3.0	3530	205	194	247	1.27	3,002-4,8,20,24,33,4
3.5	3870	218	187	249	1.30	3,020,25,32,50,
4.0	4200	236	179	257	1.43	3,005-7,26,31,51
4.5	4480	249	175	268	1.54	3,027,30,52
5.0	4840	265	172	270	1.57	3,028,29,53

DDS 17

Atomiser prototype	WW Mk.8
Internal diameter of cup	44mm
Disc type and diameter	7 shaped grooves, 56mm, reversed
Nozzle orifice size	0.5mm, modified
Bearing	miniature ballraces
Substance sprayed	water
Test carried out	28/02/90

P (Bar)	N (RPM)	Q (ml/min)	NMD (um)	VMD (um)	Ratio	File Record
.5	1400	102	388	587	1.51	1,034
1.0	2150	140	245	284	1.16	1,016,17
1.5	2750	166	201	231	1.15	1,018,19
2.0	3340	190	177	204	1.15	1,013,14,20,21
2.5	3700	210	167	190	1.14	1,022,33
3.0	4140	230	163	184	1.13	1,011,12,23,24
3.5	4600	246	160	183	1.14	1,025,26
4.0	5060	264	158	181	1.15	1,027,28
4.5	5400	282	158	184	1.16	1,029,30
5.0	5700	295	157	186	1.18	1,031,32

DDS 18

Atomiser prototype	WW Mk.9
Internal diameter of cup	60mm
Disc type and diameter	7 shaped grooves, 80mm
Nozzle orifice size	0.65mm
Bearing	plain PTFE, 3mm shaft, unmodified
Other information	no weirs
Substance sprayed	water
Sample position	270 behind nozzle
Test carried out	14/03/90

P (Bar)	N (RPM)	Q (ml/min)	NMD (um)	VMD (um)	Ratio	File, Record
.5		180				
1.0		250				
1.5	100	300	(1000)	(1500)		
2.0	750	340	314	338	1.08	1,114
2.5	1350	380	292	316	1.08	1,113
3.0	1750	410	269	304	1.13	1,111-115
3.5	2000	440				
4.0	2380	470	254	287	1.13	1,110
4.5	2600	500				
5.0	2790	525	236	279	1.18	1,103,106

(water sensitive paper)

6.3 Operational Parameters

The primary factor which can be readily altered by the operator to control flowrate, rotational speed and to a certain extent droplet size, is the pressure to which the spray fluid is subjected prior to discharge from the nozzle. Information about how each of the above parameters varies with supply pressure is therefore vital for a clear understanding of the processes involved.

6.3.1 Flowrate

Table 6.3.1 shows flowrates, arranged from left to right in order of ascending nozzle orifice diameter. These flowrates have been measured directly by discharging into a measuring cylinder, rather than indirectly using the calibrated flowmeter.

To assess the effect of orifice characteristics on discharge efficiency, two extra values have been included which correspond to normal and reversed flow at 3 bar, through a .54mm diameter orifice with rounded inlet. The diameter of this nozzle was determined using a microscope.

Figure 6.3.1a shows the flowrate values plotted against supply pressure. Note that the curves for the Mk.6 and the Mk.8 nozzle orifice are slightly different. This may be due to alteration of the nozzle shape during modification

Figure 6.3.3b shows Coefficient of Discharge, C_d, values calculated using the following formula:

$$C_d = \frac{Q}{A\ (2\delta P/p)^{1/2}} \qquad (154)$$

where Q = flowrate, m^3/s
A = orifice area, m^2
P = supply pressure, bar
p = fluid density. kg/m^3

The curves show C_d values around 0.8 ± .1. The spread is probably due to inaccuracy in assessment of orifice area. The values decrease with increasing pressure initially, although the curves tend become flatter at higher pressures.

Figure 6.3.1c shows the same data plotted against inverse square root supply pressure, and with a larger scale on the y axis. As expected, C_d values for the 0.38 mm diameter nozzle are clearly lower than the rest, due to increased viscous losses associated with the smaller nozzle. Similarly, higher C_d values are obtained with the largest diameter nozzle (ie 0.65mm).

Figure 6.3.1c also shows that the effect of rounding the inlet to the nozzle is to increase C_d at 3 bar, from around 0.8, to 0.9, an increase of just over 10% . This may be desirable from the viewpoint of obtaining maximum efficiency. However, it may be the case that a larger diameter orifice with a low C_d may be less prone to blockage than a smaller orifice with rounded inlet, therefore reducing filtration requirements (Chapter Four). Since the generation of a surplus supply pressure of 20% or so is unlikely to be a problem with existing knapsack equipment, it is the opinion of the author that orifice shape is not an important factor.

Measured flowrates from the main nozzle sizes used

Expt	Mk.4	Mk.2	Mk.7	Mk.8	Mk.3	Mk.5	Mk.9	noz1	noz2
d (mm)	.38	.45	.47	.5	.55	.62	.65	.54	.54
P (Bar)	measured Q values (ml/min)								
.5				102			180		
1		120	125	140	180	225	250		
1.5		142	149	166	210	270	300		
2	105	160	169	190	235	310	340		
2.5	115	175	185	210	258	340	380		
3	122	190	205	230	280	365	410	305	260
3.5	132	205	218	246	296	395	440		
4	140	218	236	264	314	420	470		
4.5	148	230	249	280	330	440	500		
5	154	240	263	295	345	460	525		

Table 6.3.1 Summary of flowrate data for the various sizes of nozzle used with the Waterwheel, with water.

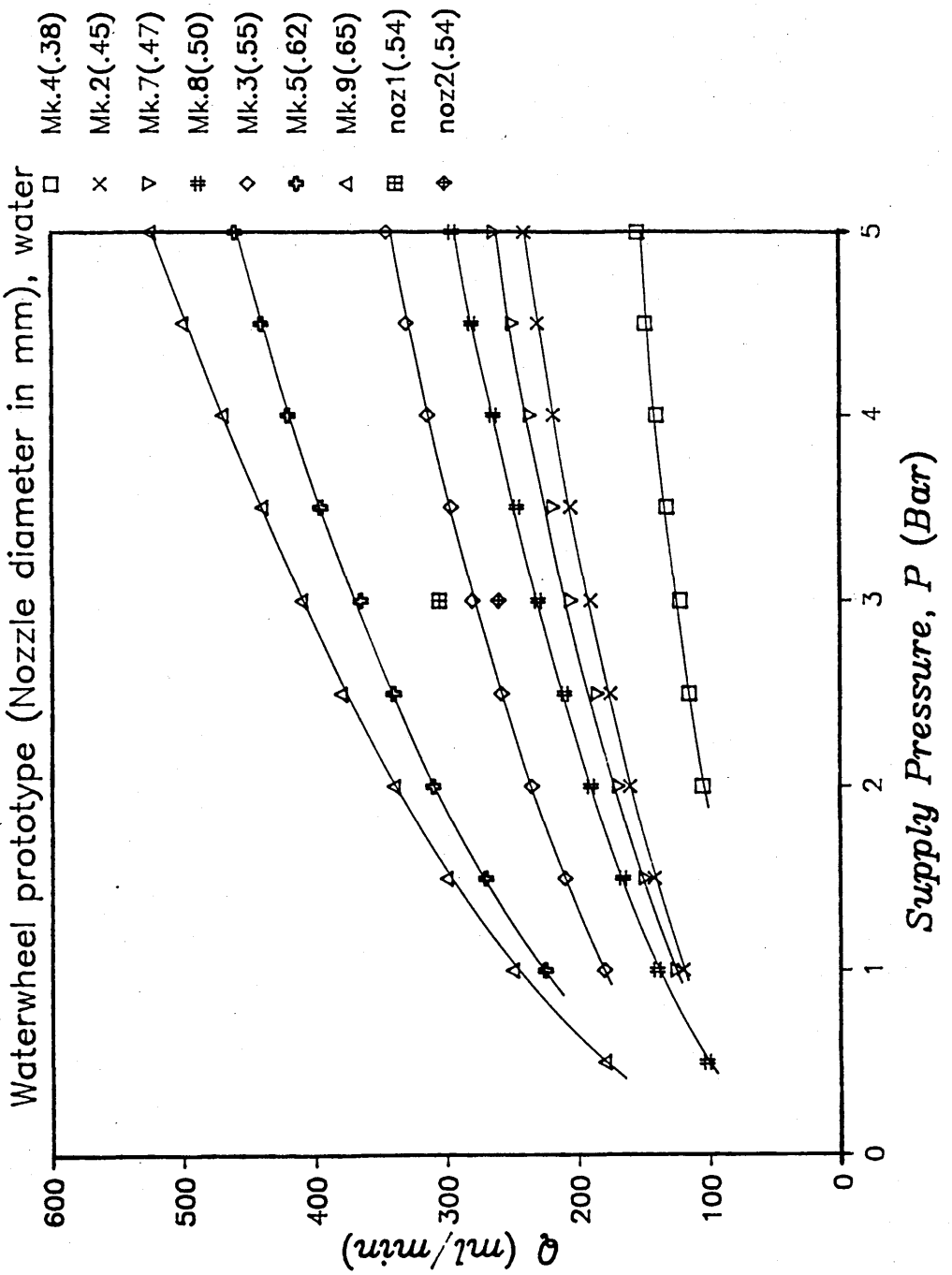

Figure 6.3.1a Measured flowrates vs supply pressure for the nozzles used in Waterwheel tests

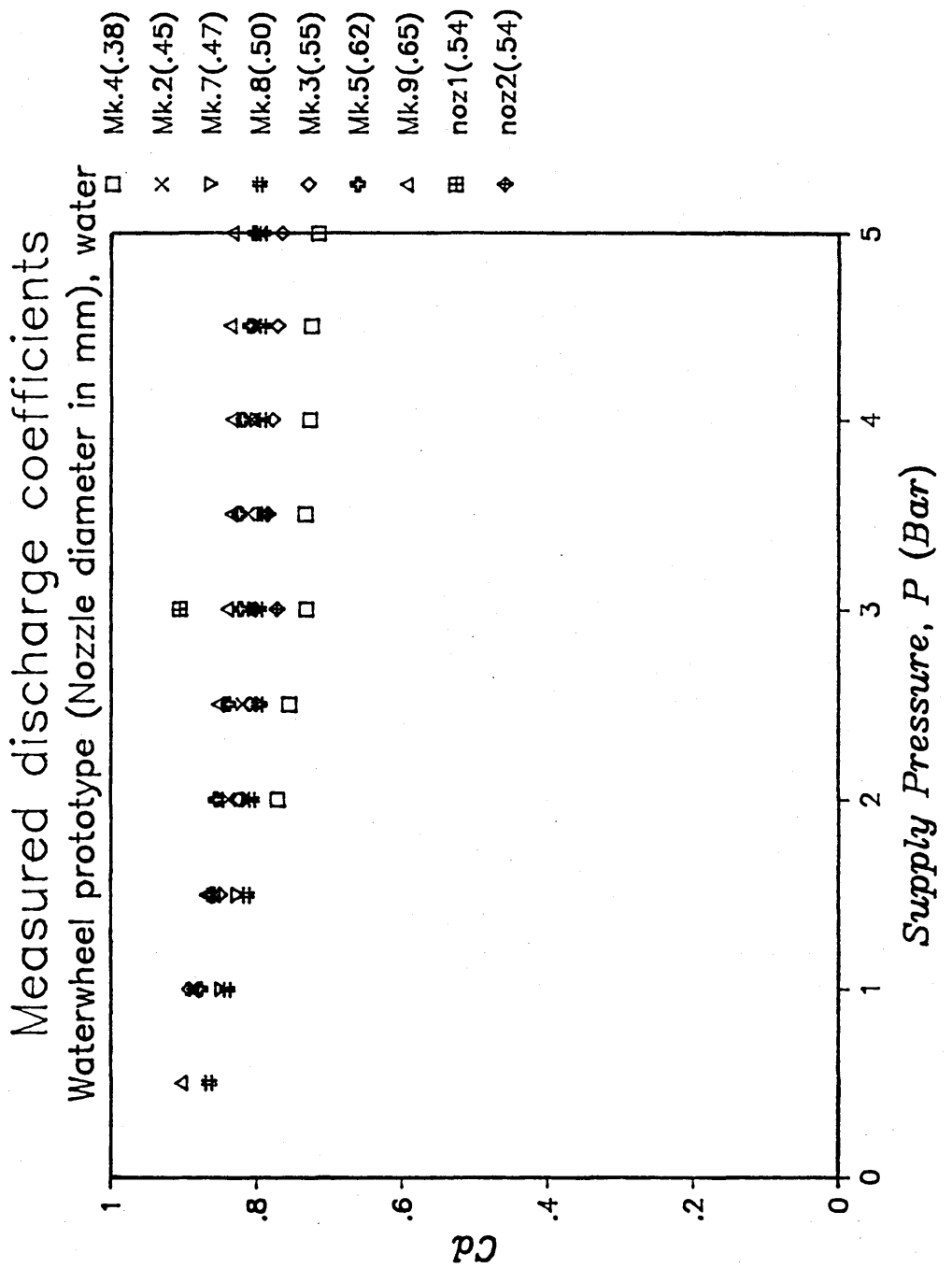

Figure 6.3.1b Coefficients of discharge vs supply pressure for the nozzles used in Waterwheel tests

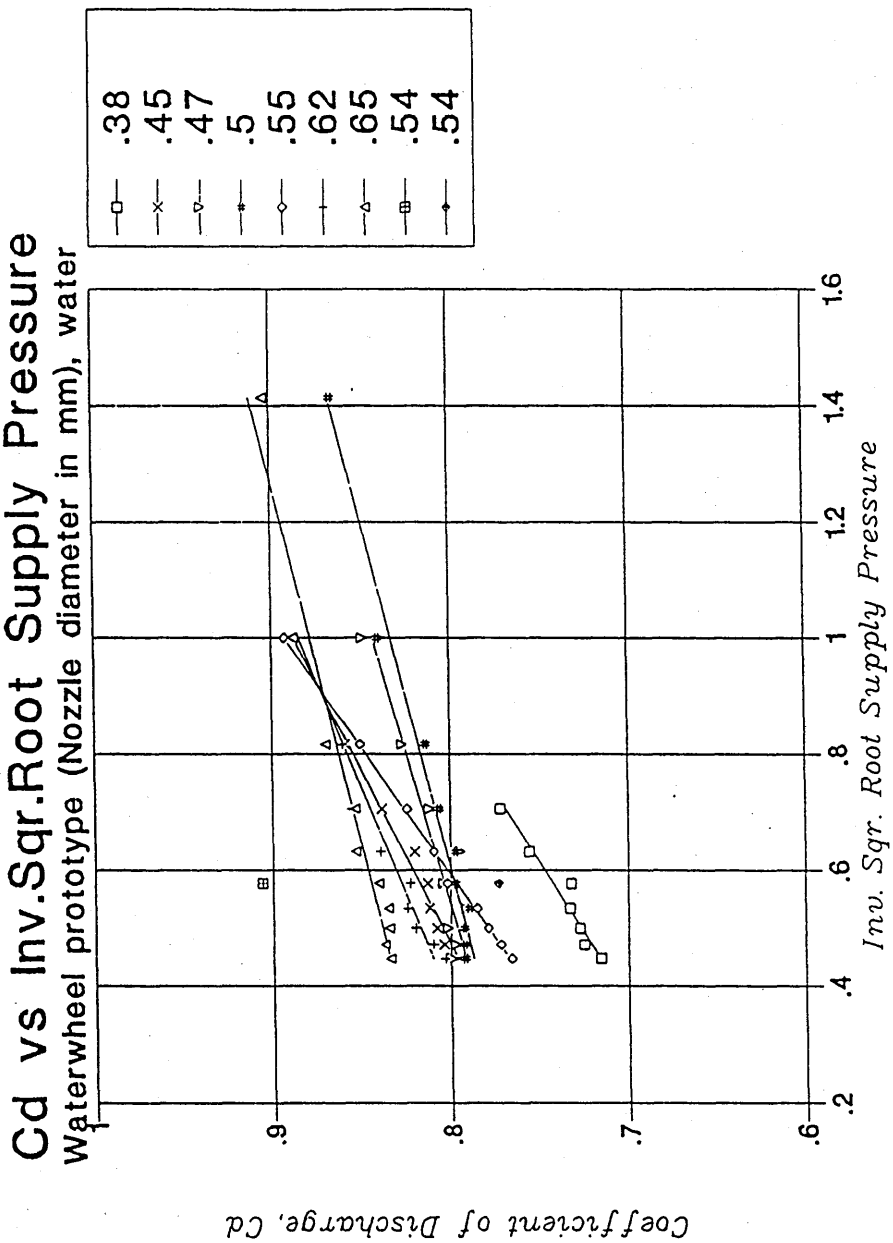

Figure 6.3.1c Linear regression lines of Coefficients of Discharge vs inverse square root Supply Pressure, for nozzles used in Waterwheel tests

6.3.2 Rotation rate

Figures 6.3.2a-c illustrate rotation speeds plotted against supply pressure for the first, second and third group of prototypes described in section 6.1.

Refering to Figure 6.3.2a, the curve designated Mk.1 and the two points for Mk.2 are taken from Kinnersley, (1987). Increasing nozzle orifice diameter from 0.45mm to 0.55mm and using a different bearing resulted in rotation rates depicted by the Mk.3 curve. Reducing nozzle orifice diameter to 0.38mm (Mk.4) resulted in lower rotation rates, and a curve similar to that of Mk.1.

Figure 6.3.2b consists of similar curves for the smaller diameter versions Mk.5-8. Rotation speeds for Mk.7 and 8 are clearly higher than those for the earlier Mk.5 and 6 primarily because nozzle clearance was increased resulting in less fluid drag, but also because friction in the dual miniature ballraces decreased with operation time.

Rotation speeds are somewhat lower for Mk.6 compared to Mk.5; particularly so at low supply pressures. This is due to the fact Mk.5 had a larger nozzle diameter (0.62mm) compared to Mk.6 (0.5mm) so was capable of delivering more torque at low speed. At higher pressures, energy expenditure overcoming bearing friction becomes less as a proportion of the total energy provided by the jet, so the rotational speeds are similar.

The curves for Mk.7 and 8 are quite similar; the reason why rotational speeds for Mk.8 slightly exceed those for Mk.7 may be due to due to absence of the fluid distribution system. This would lead to reduced cup weight and therefore slightly less bearing friction.

Rotational speeds for the larger diameter prototypes Mk.9 to 11 are presented in Figure 6.3.2c. With Mk.9 the plain PTFE bearing was relatively very stiff and no rotation was possible below about 2 bar, even when adequate lubrication was provided (a mixture of light oil and grease). Skimming of the central portion of the 3mm shaft resulted in reduced contact area and a substantial decrease in friction; the resultant rotation speeds are represented by the Mk.10 curve.

The single 0.65mm nozzle of Mk.10 was replaced by two 0.5mm nozzles resulting in a slightly larger overall flowrate. This resulted in only marginally increased rotational speed as illustrated by the curve designated Mk.11.

Figures 6.3.2d-f represent the same information but plotted against the square root of the supply pressure. For Figures 6.3.2g-i the x-axis of the graphs has been replaced jet velocity calculated from available flowrate imformation taken at the same time as when the rotational speeds were measured. The y-axis has also been replaced with the inner wall velocity, V_i (product of the rotation rate w, and the radius to inner wall, r_i) for the prototype concerned.

The dotted line in Figures 6.3.2g-i represents the equation $V_i = ½ V_j$ which according to Pelton Wheel theory (Chapter 3) represents the condition for maximum efficiency assuming no friction. The ratio V_i/V_j will now be referred to simply as the velocity ratio.

At the highest pressures attainable (5 bar) the Mk.3 curve approaches the $V_i = ½ V_j$ line. However, as pressure is reduced the curve falls away indicating that the Waterwheel is operating reduced efficiency. At a jet velocity of around 12 m/s, the atomiser is not rotating, and starting friction is equal to mV_j. With Mk.4, m is reduced so $V_i = 0$ at a higher jet velocity. With, Mk.1 and Mk.4, the nozzle diameter used is clearly not sufficient for the friction of the bearing used, and the velocity ratio curves remain well below the $V_i = ½ V_j$ line.

Velocity ratio curves for Mk.5-8 are more linear due to the extremely low friction of the dual miniature ball races used. The Mk.7 and Mk.8 lines follow $V_i = 1/2 V_j$ closely except they have a slightly steeper gradient. High V_i values for Mk.8 actually exceed ½ Vj.

Finally, Figure 6.3.2 illustrates velocity ratios for the large plastic Waterwheel. Due to the high friction of the unmodified plain bearing the the Mk.9 curve is well below the ½ Vj line. Modification of the bearing resulted in improved in efficiency for Mk.10 and Mk.11.

Unfortunately, the flowrate necessary for this efficiency is unrealistically high for the intended application rate for the atomiser. The exceptionally low friction offered by miniature ball bearings makes their use highly advisable if the design aim is satisfactory rotation speeds at low flowrates.

Table 6.3.2

Summary of Waterwheel Rotation Rates with Water

	RPM										
	Mk.1	Mk.2	Mk.3	Mk.4	Mk.5	Mk.6	Mk.7	Mk.8	Mk.9	Mk.10	Mk.11
Inner cup dia.(mm)	70	70	70	70	44	44	44	44	60	60	60
Nozzle dia. (mm)	.45	.45	.55	.38	.62	.5	.5	.5	.65	.65	.5x2
P(Bar)											
.5							1100	1400		250	1000
1.0			400		1000	500	1970	2150		1380	1720
1.5	110		1200		1620	1260	2580	2750		1870	2080
2.0	650	1600	1700	500	1990	1660	3110	3340	750	2250	2400
2.5	1020		2100	940	2290	2040	3520	3700	1350	2570	2710
3.0	1380		2380	1200	2580	2400	3860	4140	1750	2800	3000
3.5	1620	2300	2610	1500	2820	2700	4320	4600	2000	3100	3250
4.0	1890		2860	1780	3090	2950	4670	5060	2380	3310	3400
4.5	2108		3090	2000	3310	3200	4960	5400	2600	3550	3730
5.0	2310		3290	2100	3600	3400	5260	5700	2790	3800	4000

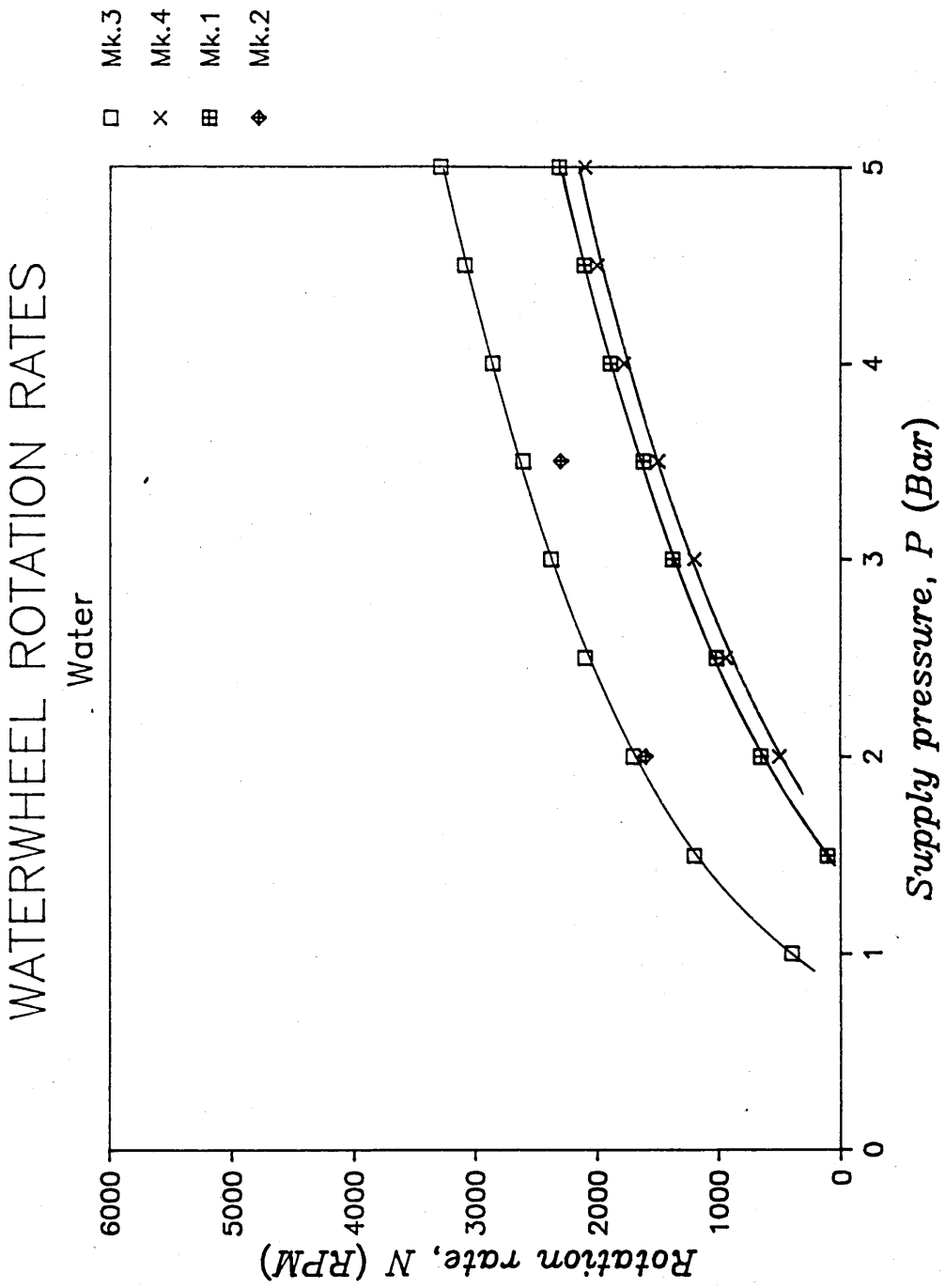

Figure 6.3.2a Prototypes Mk.1-4; rotation rate vs supply pressure

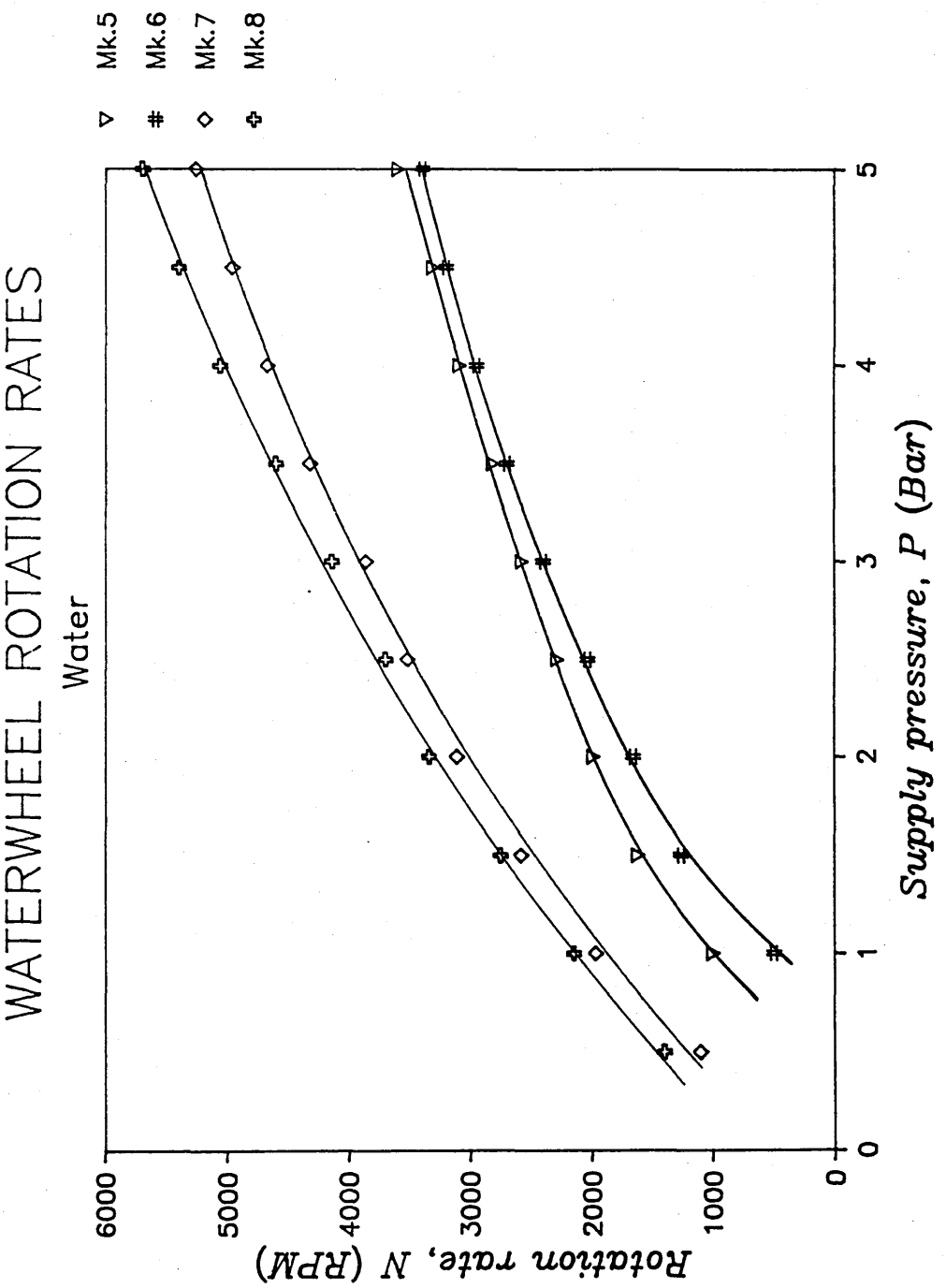

Figure 6.3.2b Prototypes Mk.5-8; rotation rate vs supply pressure

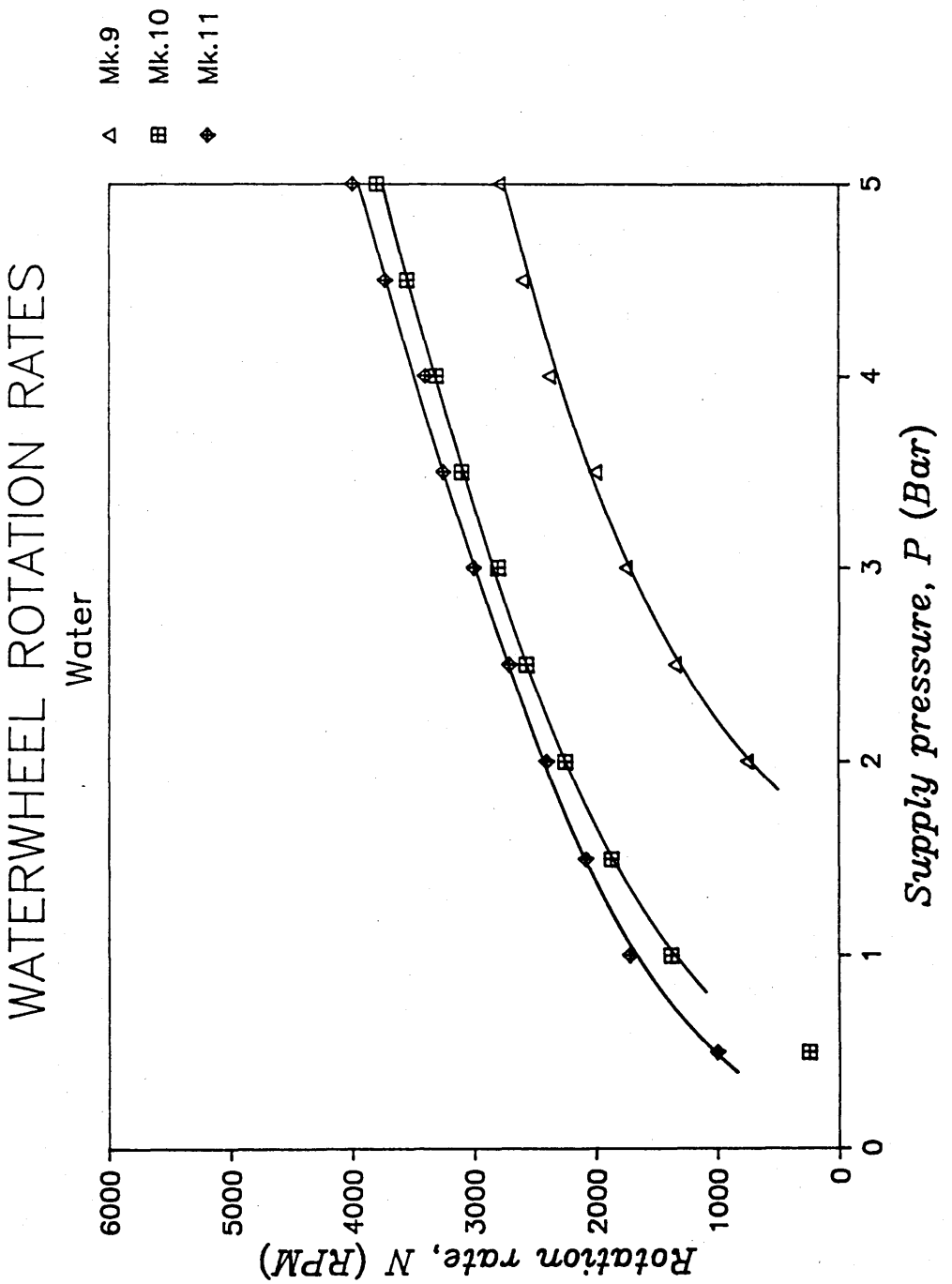

Figure 6.3.2c Prototypes Mk.9-11:
rotation rate vs supply pressure

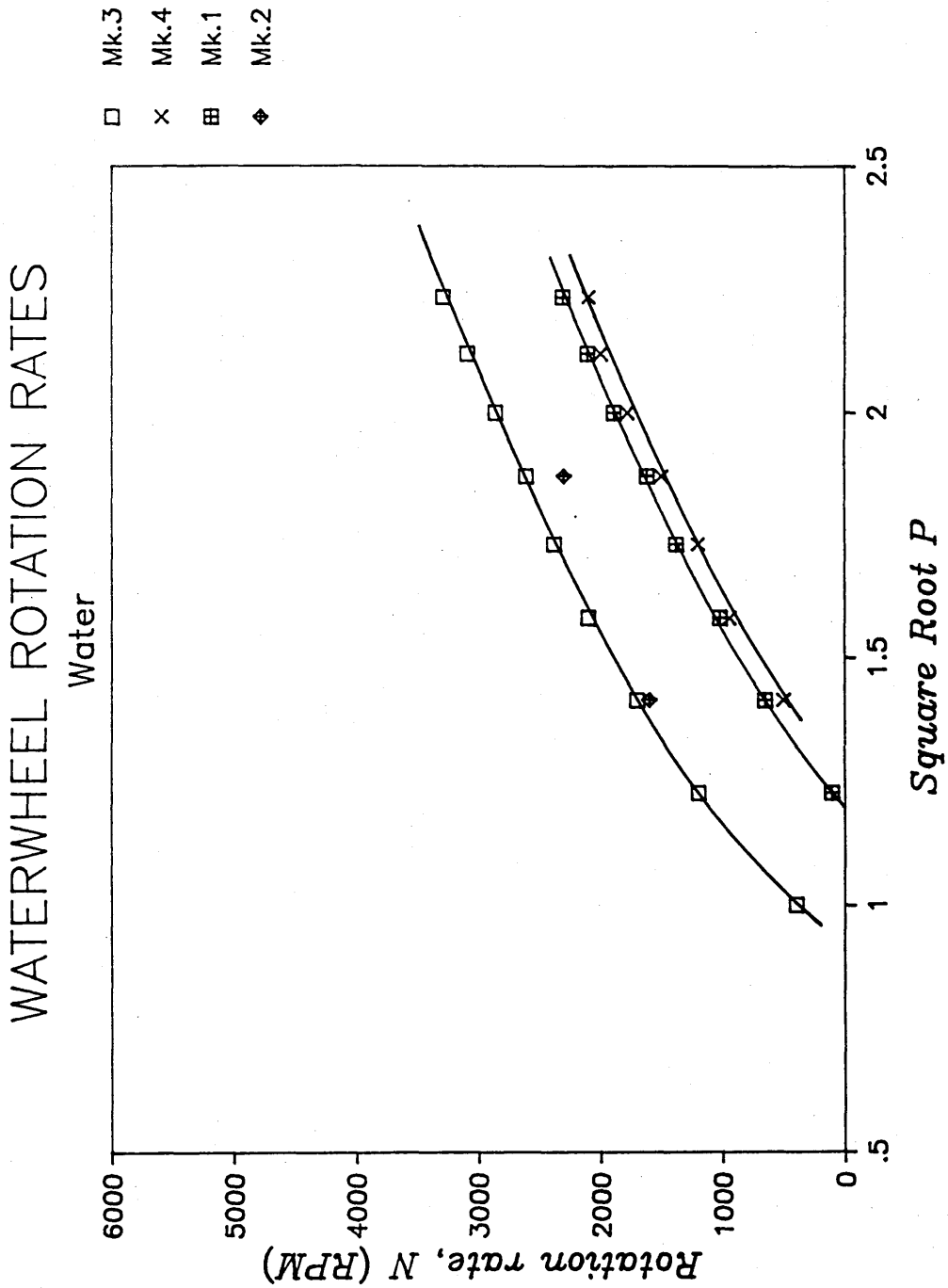

Figure 6.3.2d Prototypes Mk.1-4;
rotation rate vs square root pressure

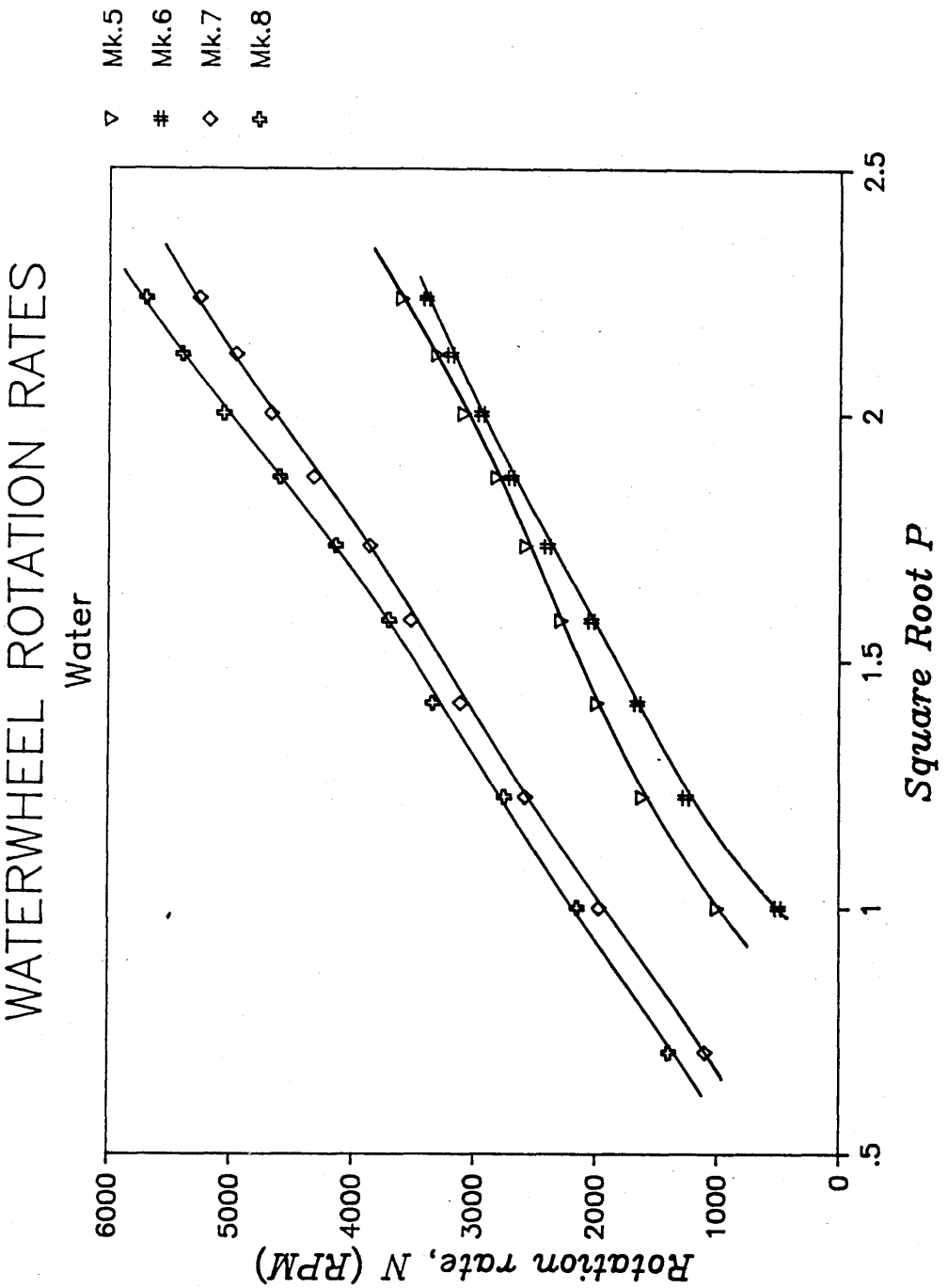

Figure 6.3.2e Prototypes Mk.5-8;
rotation rate vs square root pressure

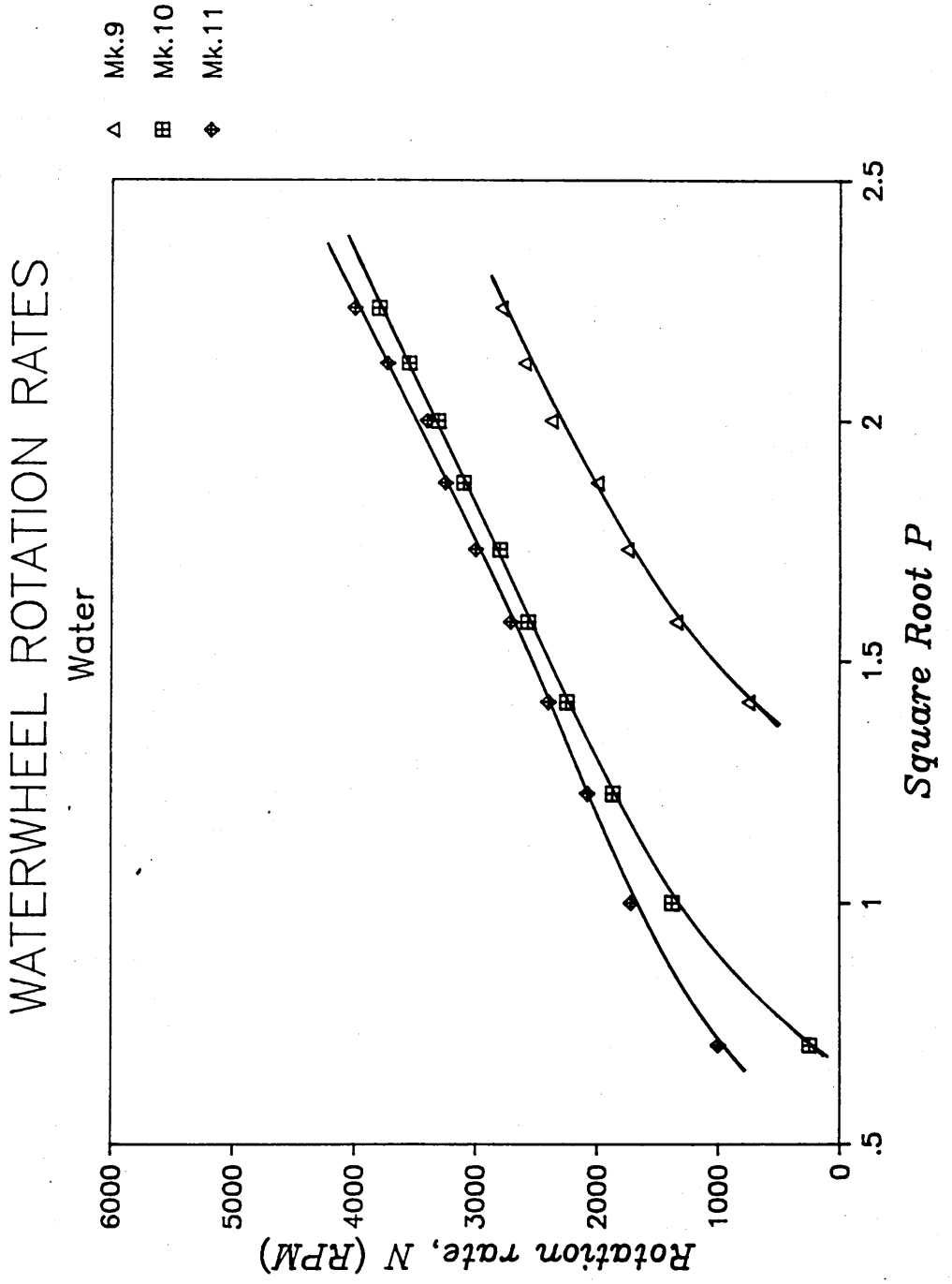

Figure 6.3.2f Prototypes Mk.9-11;
rotation rate vs square root pressure

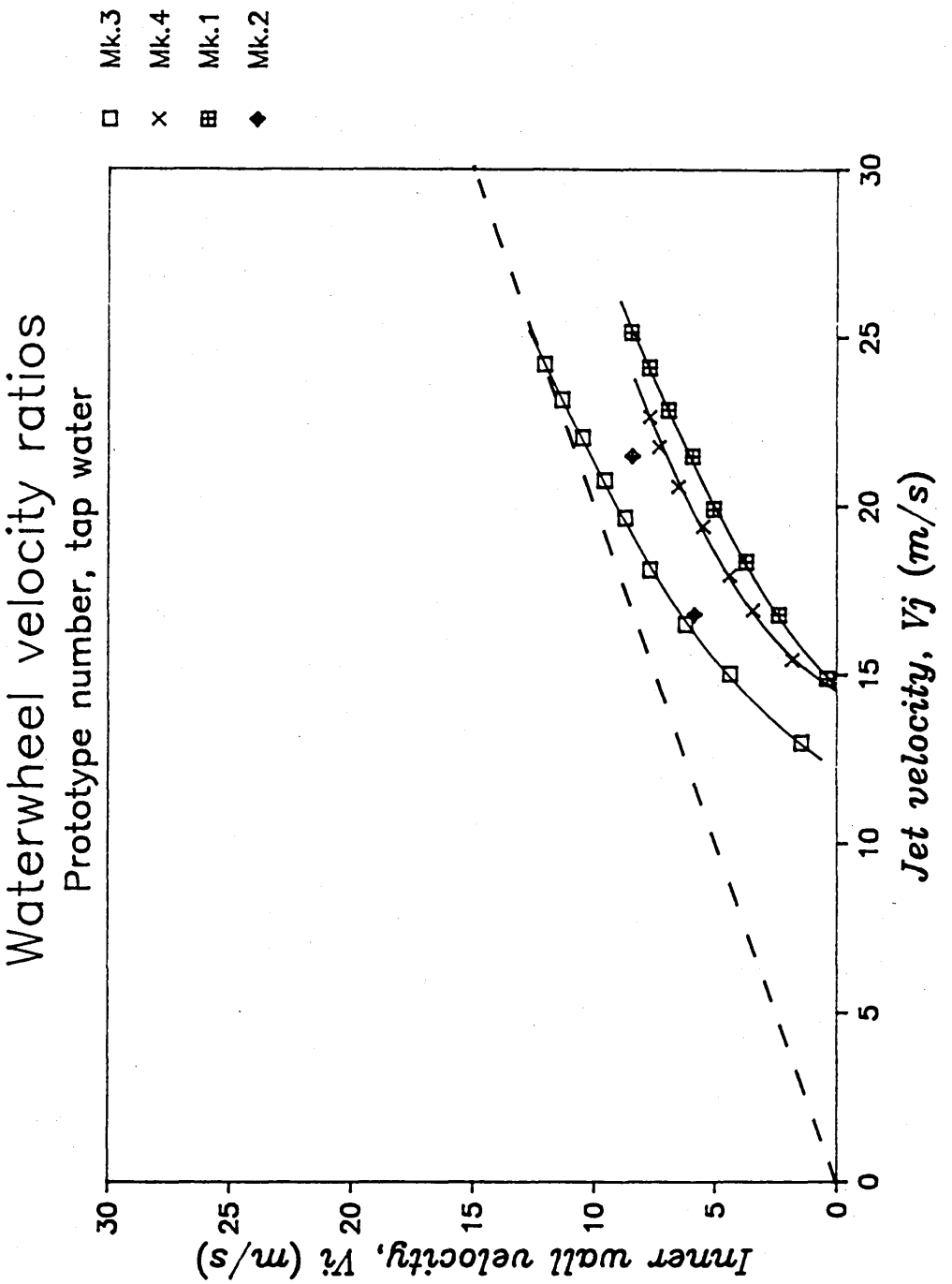

Figure 6.3.2g Prototypes Mk.1-4;
velocity at inner wall of cup vs jet velocity

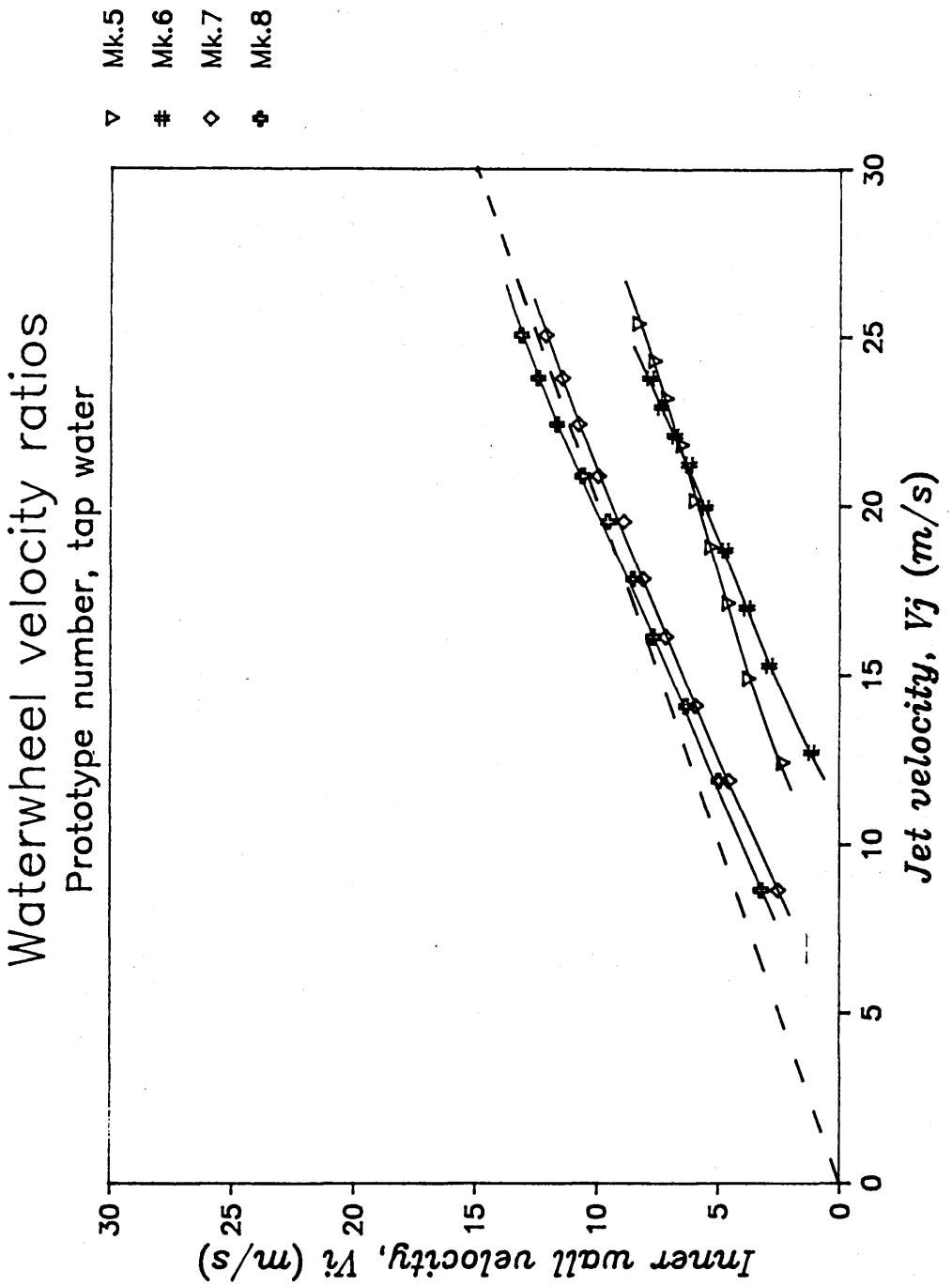

Figure 6.3.2h Prototypes Mk.5-8;
velocity at inner wall of cup vs jet velocity

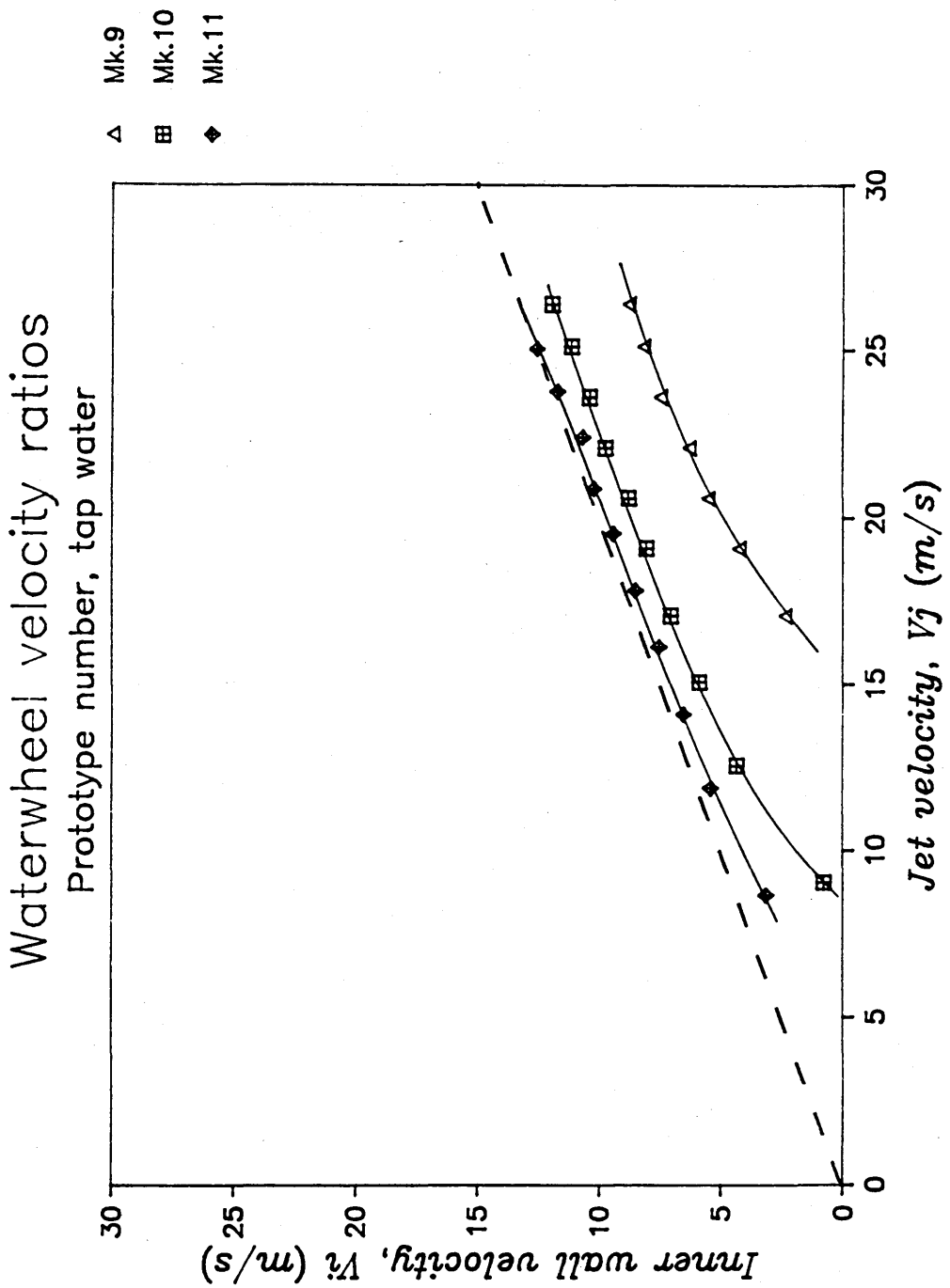

Figure 6.3.2i Prototypes Mk.9-11;
velocity at inner wall of cup vs jet velocity

6.3.3 Droplet size

Two parameters have been listed in the Droplet Data Summaries and Table 6.3.3 expressing droplet size. These are Number Median Diameter (NMD) and Volume Median Diameter (VMD). For statistical definitions of these parameters, refer to section 5.3.

Figure 6.3.3a shows NMD values, and Figure 6.3.3b shows VMD values for several of the prototypes tested with water. The NMD results show similar trends in that with increasing pressure and therefore rotational speed of the atomiser, there is in general a decrease in the droplet sizes produced. The VMD curves behave slightly differently in that they tend to flatten out at the higher pressures: VMD actually starts to increase with some of the prototypes.

Decrease in droplet size with supply pressure is steeper initially, but tends to level out the higher pressures. This is probably due to the fact that flowrate is increasing as well as rotational speed. This may be interpreted as an attractive feature since droplet size will not vary markedly with fluctuations in supply pressure. However, application rate will vary, so pressure regulation at source is still desirable.

This "flattening" characteristic is more pronounced with Mk.7 and Mk.8, the prototypes which rotate the fastest and therefore produce the smallest droplets. Figure 6.3.3c shows that the cut-off in pressure below which satisfactory atomisation does not take place is 1.5 Bar for Mk.7e. With the Mk.7e tests the bearing was not lubricated which reduced speeds at the lower pressures. With the Mk.7a and b tests the bearing was lubricated which enabled satisfactory atomisation as low as 0.5 bar. In all tests with Mk.7 and 8 there appears to be only a small decrease in droplet size above 2 bar.

With increasing rotational speeds and flowrates per tooth, atomisational quality tends to diminish with droplet spectra becoming broader. This is expressed by an increase in the VMD/NMD ratio with increasing pressure. Optimum supply pressure is therefore probably between 2 and 2.5 Bar for Mk.7 and 8.

Table 6.3.3 Summary of dropsize data obtained for the Waterwheel, with water

NMD (um)

P(Bar)	Mk.1 70 .45	Mk.2 70 .45	Mk.3 70 .55	Mk.4 70 .38	Mk.5 44 .62	Mk.6 44 .5	Mk.7 44 .5	Mk.8 44 .5	Mk.9 60 .65
.5								388	
1.0								245	
1.5								201	
2.0				493			190	177	314
2.5				374			181	167	292
3.0				362			171	163	269
3.5				316			168	160	
4.0				265			165	158	254
4.5				230				158	
5.0				230			159	157	236
1.72					325	328			
2.07	322	234	163		308	295			
2.41					330	278			
2.76			201		280	255			
3.10					269	247			
3.45			197		264	235			
3.79					257	224			
4.13	199	169	181		252	222			
4.48					243	212			
4.82			151		234	206			
5.17									
5.51			130						
5.86									
6.20	151	218	133						

VMD (um)

.5								587	
1.0								284	
1.5								231	
2.0				755			233	204	338
2.5				451			228	190	316
3.0				412			217	184	304
3.5				377			217	183	
4.0				308			212	181	287
4.5				279				184	
5.0				280			204	186	279
1.72					375	397			
2.07	432	300	302		352	351			
2.41					377	337			
2.76			289		327	314			
3.10					325	302			
3.45			282		318	298			
3.79					315	288			
4.13	293	249	270		315	295			
4.48					319	280			
4.82			258		307	290			
5.17									
5.51			261						
5.86									
6.20	254	109	277						

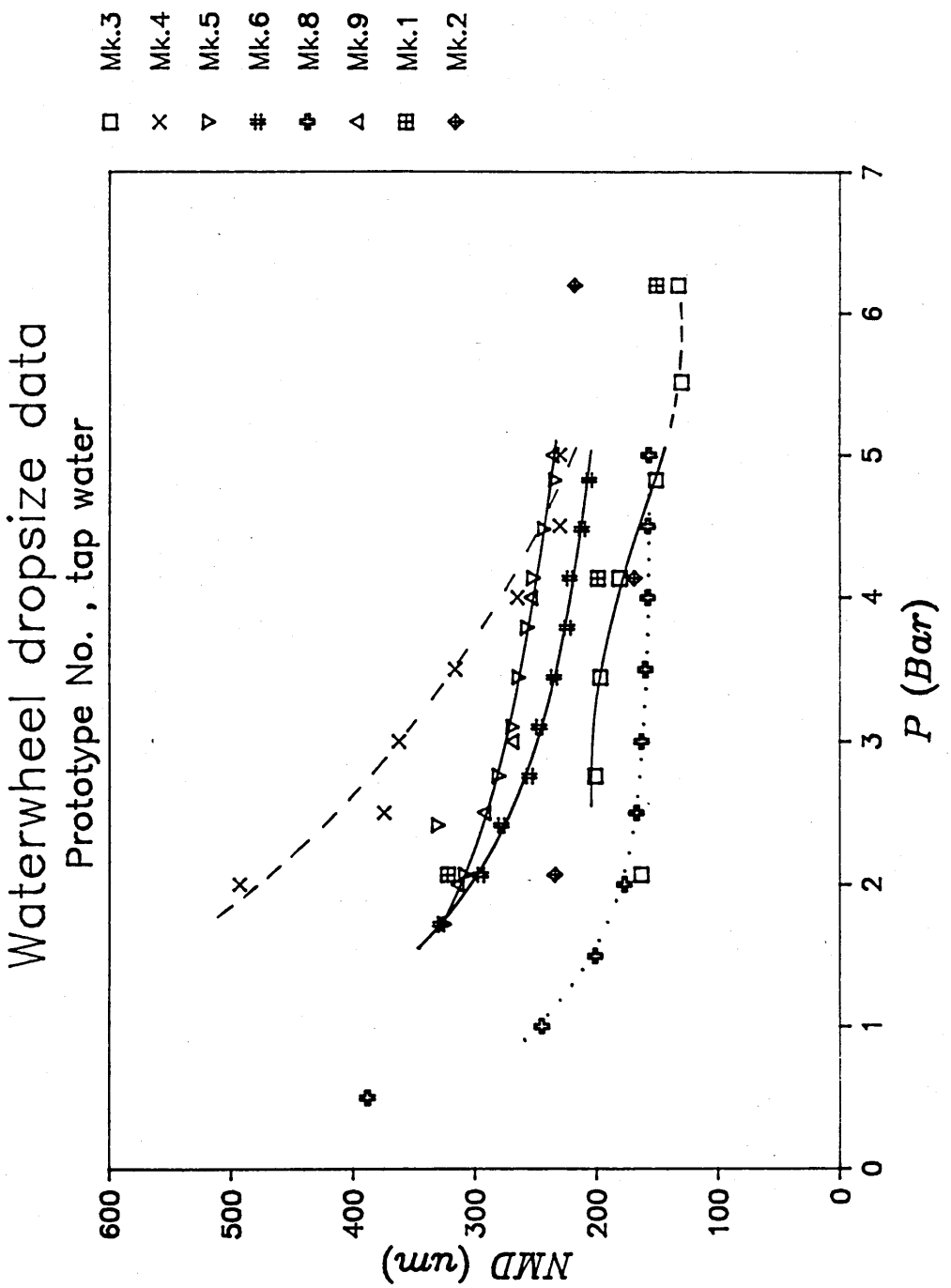

Figure 6.3.3a Number Median Diameter (μm) vs supply pressure for prototypes tested with tap water

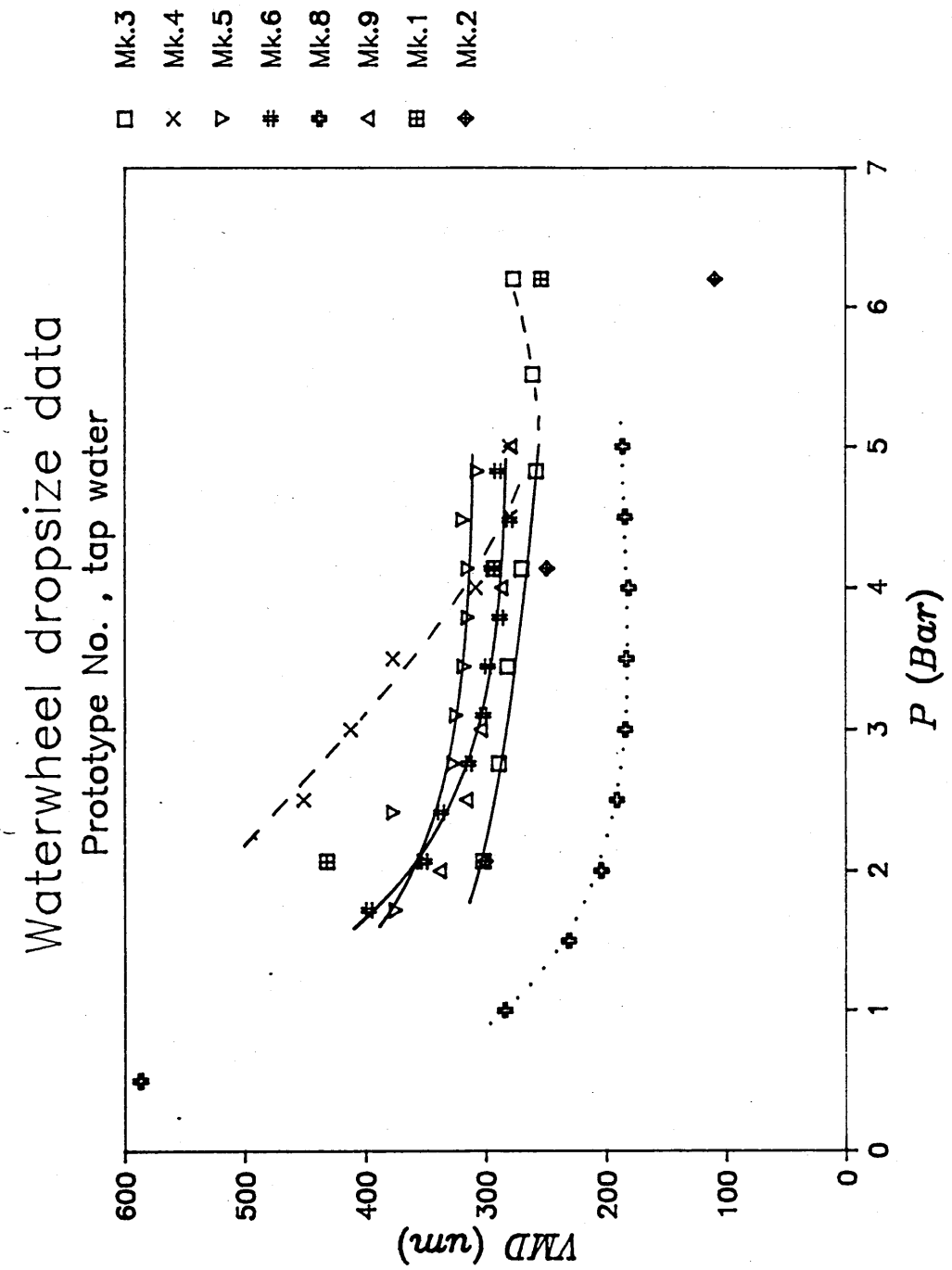

Figure 6.3.3b Volume Median Diameter (µm) vs supply pressure for prototypes tested with tap water

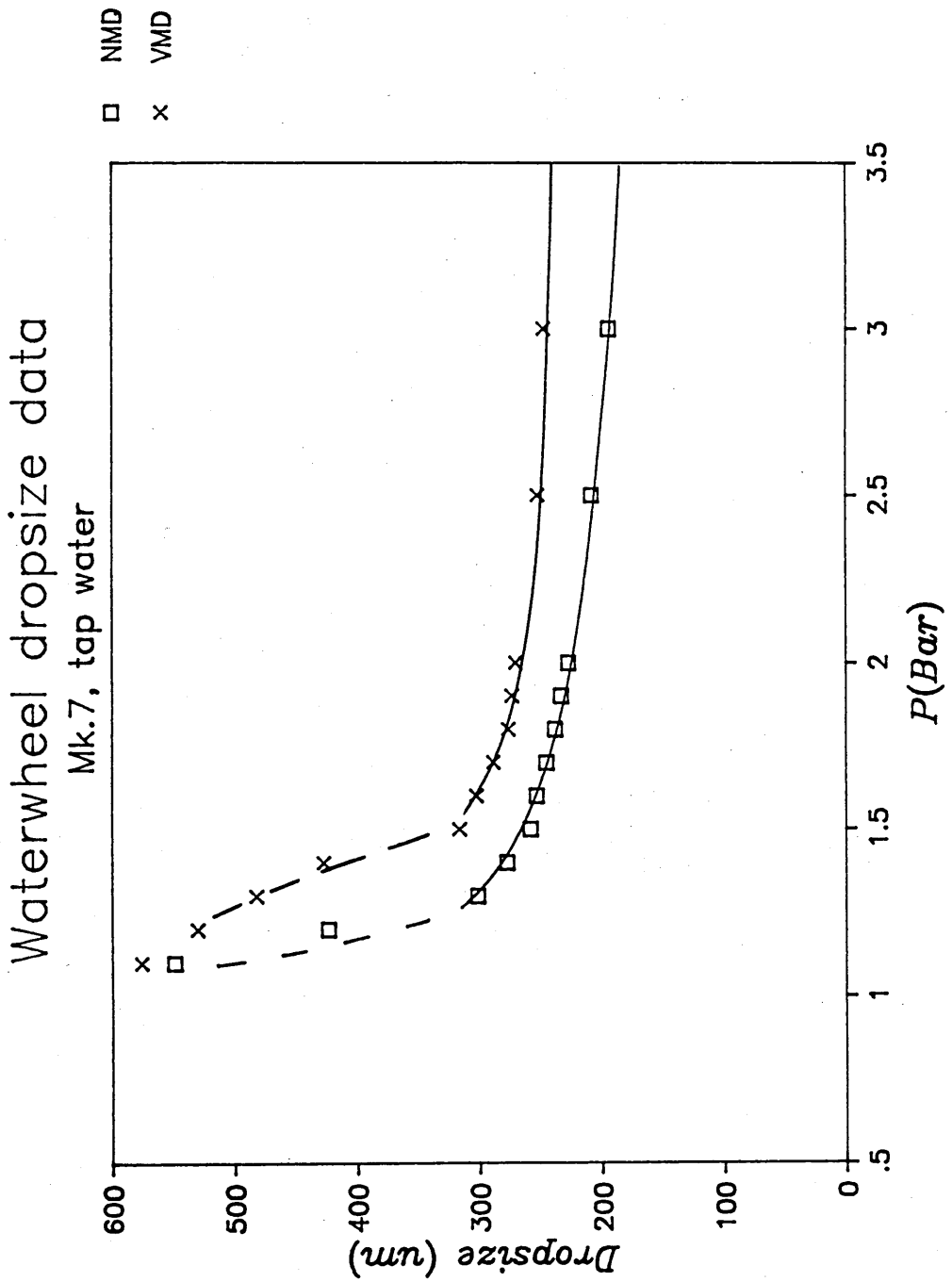

Figure 6.3.3c Dropsize vs supply pressure for Mk.7e, dry bearing. (shows typically "flat" relationship with a "cut-off" at around 1.5 bar).

6.4 Atomisation characteristics

6.4.1 Typical droplet spectra with water

Table 6.4.1 is a computer printout of the meaned droplet spectra and statistics of Record Numbers 273 and 274 of File "craig2". These records have been selected using the appropriate droplet data summary, and correspond to Waterwheel Mk.6 operating with tap water at 3 bar, rotating at 1965 RPM, with a total flowrate 210 ml per minute. Printouts of all the other Record Numbers are contained in Appendix II.

Following the atomiser description are percentile values for 5,10,16,25,50,75,84,90 and 95% of the spray, in terms of number, length, area and volume. For example, 5% of the total number of droplets in the spray are less then 170.4 µm in diameter (so $D_{v0.05}$ = 170.4) and 95% are less than 401.6 µm in diameter. Similarly, 5% of the total volume of the spray is composed of droplets less than 226.5 µm in diameter, and 95% of the volume is less than 559.3µm in diameter.

After percentiles, the following droplet spectra parameters are presented:

Parameter	Abr.	Notation
Number Median Diameter	NMD	$D_{n\ 0.5}$
Number Average Diameter	NAD	$D_{1,0}$
Volume Average Diameter	VAD	$D_{3,0}$
Sauter Average Diameter	SAD	$D_{3,2}$
Volume Median Diameter	VMD	$D_{v\ 0.5}$

Number Median Diameter is defined as the drop diameter which divides the spray sample in half by number. It is infact the 50% percentile for number. Similarly, Volume Median Diameter divides the spray sample in half by volume and corresponds to the 50% percentile for volume. Mathematical expressions for all of the above are to be located in section 5.3.

Following on from the droplet spectra parameters are four indicators of spectral width of the spray sample. These are as follows:

i) span
ii) relative span
iii) VMD/NMD ratio
iv) sigma g (num),(vol)

Span in this case is defined as the difference between the 90% percentile and the 10% percentile by volume. Relative span is simply this quantity divided by the VMD :

$$\text{relative span} = \frac{V_{.90} - V_{.10}}{V_{.50}}$$

Relative span is probably the best single indicator of spectral width when comparing droplet spectra between different atomisers and when dealing with the full range of droplet sizes between 10µm and 900µm.

However, VMD/NMD ratio is the most commonly quoted parameter in pesticide application indicating the spectral width of a spray, and therefore has been included in the droplet data summaries. It also has the advantage that when looking out for the occurance of small droplets ie less than 100µm, it is more sensitive than relative span.

For example when comparing certain droplet spectra from a the Waterwheel, and a typical hydraulic nozzle spectrum (section 6.4.2), both may have relative spans of around 1.0 or 1.2. However the VMD/NMD ratio may be less than 1.5 for the Waterwheel and anything between 5 and 10 for the hydraulic nozzle.

VMD/NMD ratio has a disadvantage however in that it relies on an accurate measurement of NMD. Droplet counts for the smallest size bins have been noted to be unreliable when there is a high concentration of small droplets in the sample. This could be due to the large sample volume correction factor required for out of focus droplets. It could also be due to diffractional effects causing secondary interferance shaddowing.

With the present study dealing with droplet spectra for herbicide application, drops less than 100µm in diameter are relatively rare, and therefore VMD/NMD is thought to be a satisfactory parameter.

Alternatively, sigma g (num),(vol), the lower half of the geometric standard deviation for the number and volume distribution has been included ie

$$\text{sigma g (num)} = D_{n0.5} / D_{n0.159}$$

$$\text{sigma g (vol)} = D_{v0.5} / D_{v0.159}$$

For the purposes of the present study, one of the aims of the study was to produce a herbicide spray with a narrow

droplet spectrum with no droplets less than 100µm (Chapter 2). Figures for percentage volume of spray less than 100µm and 145µm are provided inorder to assess the drift potential of the spray. Total number of raw droplets counted, and sample time have also been included.

The second half of Table 6.4.1a consists of smoothed and corrected bin data (section 5.3) expressed in both frequency and cumulative form for number,length area and volume. This facilitates plotting of the droplet spectra in any of the above forms.

Figure 6.4.1a shows the droplet spectra of Record 2,273,274 plotted in histogram form with % Number freqency on the y axis. The histogram shows that there are no droplets less than 100µm and few greater than 500µm, and that the most frequently occuring droplet size is 300µm.

Number frequency histograms are preferred by the present author to volume frequency, since a very small number of spurious counts at the coarse end of the spectra form a pronounced tail (Figure 6.4.1b). Workers dealing with finer droplets tend to prefer % volume so to reduce the tail at the fine end!

Probably the best way to represent droplet spectra is to use accumulated percentage curves for both number and volume plotted upon the same graph. Distance between the lines gives an indication of spectral width, and where they intersect 50%, provide a graphical solution for NMD and VMD.

Typical droplet spectra for Mk.7 and Mk.8 have also been included, this time at 2 bar since rotational speeds are significantly greater than for Mk.6. Due to the increased speed, more smaller droplets are produced and the volume of spray below 100µm becomes a few percent.

The Mk.7e spectra show more pronounced tails than usual, probably due to the fact that Bulk Area Rejection Circuit was left out of the probe during this particular set of measurements. The Bulk Area Rejection Circuit (BARC) assesses the shape of the droplet by comparing the width and length of the pulse produced by it. If this ratio is not within certain limits the droplet is rejected as non-spherical or coincident with another droplet.

Usually with droplet sizing with rotary discs there are usually no coincident droplets since the disc produces all the droplets in one plane. However with the Waterwheel Mk.7e test run, an occasional ligament formed on the cup beneath the disc due to a small amount of leakage at the holes which contain the disc retaining bolts. Coincident droplets, which would otherwise be eliminated with the BARC in place are more apparent in the droplet spectra produced at high

flowrates and rotation speeds, and may well explain why VMD is seen to increase slightly towards higher pressures with Mk.7e.

The Mk.8 data also has to be treated with caution due to the fact there are no weirs in the device to ensure even peripheral distribution of fluid. The precise flowrate at the sampling point is therefore not known. The sample position of 90^{o} behind the nozzle was chosen since it gave the tightest droplet spectrum. From independant measurement of the peripheral fluid distribution without weirs, the local flowrate at this point is estimated to be around three quarters that of the mean ie approximately 150 ml/min at 2 bar. Due to likely shifting of the peripheral fluid distribution pattern with increasing pressure, the relationship between droplet size and pressure is likely to be unpredictable for a single sample position.

The spectra for Mk.8 has been included however to demonstrate the effect of reducing local flowrate on spectral width. Note that some of the droplet spectra such as this one are plotted with a log scale for droplet size.

This particular spectrum for the prototype without weirs, taken at the point where local flowrate is lowest, may be useful if a design of fluid driven atomiser with shrouding and fluid recycling was contemplated. Although outside the brief of this particular thesis, the accumulated volume curve for Mk.8 shows that a droplet spectra with a VMD as low as 200µm, still with no droplets less than 100µm may be possible.

Droplet Spectrum Analysis Cranfield Institute of Technology

FILE :- craig2 MEANED RECORD NUMBERS :- 273 274

Atomiser Parameters

Atomiser Type	:- WW Mk.6
Pressure (Bar)	:- 3.0
Disc Speed (RPM)	:- 1965
Flow Rate (ml/min)	:- 210
Fluid Description	:- tap water

Percentiles - µm Diameter

	5%	10%	16%	25%	50%	75%	84%	90%	95%
Number	170.4	191.6	211.2	241.1	293.9	331.5	350.9	371.5	401.6
Length	188.2	211.8	237.4	267.4	306.8	345.1	366.8	390.4	428.9
Area	205.8	235.8	262.9	283.2	318.6	360.4	386.0	415.4	473.8
Volume	226.5	259.3	278.9	295.1	331.0	379.4	412.1	456.8	559.3

Droplet Spectra Parameters

Number Median Diameter	= 293.9	µm
Number Average Diameter	= 289.5	µm
Volume Average Diameter	= 308.2	µm
Sauter Average Diameter	= 327.6	µm
Volume Median Diameter	= 331.0	µm

Spectrum Width

Span (ASTM)	= 197.5	
Relative Span (ASTM)	= 0.60	
V.M.D./N.M.D. Ratio	= 1.13	
sigma g (num), (vol)	= 1.39	1.19
Volume of Spray <100 µm	= 0.00	%
Volume of Spray <145 µm	= 0.12	%
Total Number of Raw Drops	= 150836	
Sampling Time (secs)	= 682	

Table 6.4.1a Typical droplet spectrum for the Waterwheel with water; (i) droplet spectrum analysis.

Table 6.4.1b ii)

Frequency and Accumulated Spectrum Data

FILE :- craig2 **MEANED RECORD NUMBERS :- 273 274**

Bin no.	Diam. µm	Number %		Length %		Area %		Volume %	
1	25.5	0.0	0.0	0.0	0.0	0.0	0.0	0.0	0.0
2	40.3	0.0	0.0	0.0	0.0	0.0	0.0	0.0	0.0
3	55.2	0.0	0.0	0.0	0.0	0.0	0.0	0.0	0.0
4	70.1	0.0	0.1	0.0	0.0	0.0	0.0	0.0	0.0
5	84.9	0.0	0.1	0.0	0.0	0.0	0.0	0.0	0.0
6	99.6	0.1	0.2	0.0	0.0	0.0	0.0	0.0	0.0
7	114.3	0.3	0.4	0.1	0.1	0.0	0.0	0.0	0.0
8	129.1	0.6	1.0	0.2	0.4	0.1	0.1	0.0	0.0
9	145.2	0.8	1.8	0.4	0.8	0.2	0.3	0.1	0.1
10	158.9	1.3	3.1	0.7	1.5	0.3	0.7	0.2	0.3
11	173.4	2.3	5.5	1.3	2.8	0.7	1.4	0.4	0.6
12	188.3	3.5	9.0	2.2	5.0	1.3	2.7	0.7	1.4
13	203.0	4.4	13.4	3.0	8.0	1.9	4.6	1.1	2.5
14	217.8	4.6	18.1	3.4	11.4	2.3	6.9	1.5	4.0
15	232.5	4.4	22.5	3.5	14.8	2.5	9.4	1.7	5.7
16	247.5	4.3	26.9	3.6	18.4	2.8	12.2	2.0	7.8
17	262.5	5.0	31.9	4.4	22.9	3.7	15.9	2.9	10.6
18	277.5	6.9	38.8	6.5	29.3	5.6	21.5	4.7	15.3
19	292.5	10.2	49.0	10.0	39.3	9.2	30.7	8.0	23.3
20	307.5	10.8	59.8	11.2	50.5	10.9	41.6	9.9	33.2
21	322.5	10.2	69.9	11.1	61.6	11.3	52.9	10.9	44.1
22	337.5	8.4	78.4	9.6	71.2	10.3	63.2	10.3	54.5
23	352.5	6.3	84.7	7.5	78.7	8.4	71.6	8.9	63.3
24	367.5	4.4	89.1	5.5	84.2	6.5	78.1	7.1	70.4
25	382.5	3.2	92.4	4.2	88.4	5.0	83.1	5.8	76.2
26	397.5	2.2	94.6	3.0	91.4	3.8	86.9	4.6	80.8
27	412.5	1.5	96.1	2.0	93.5	2.7	89.6	3.3	84.1
28	427.5	1.0	97.0	1.4	94.9	2.0	91.6	2.5	86.6
29	442.5	0.7	97.8	1.1	96.0	1.5	93.1	2.0	88.6
30	457.5	0.5	98.2	0.7	96.7	1.1	94.2	1.5	90.1
31	472.5	0.3	98.6	0.5	97.2	0.8	95.0	1.1	91.2
32	487.5	0.2	98.8	0.3	97.6	0.5	95.5	0.7	91.9
33	502.5	0.2	98.9	0.3	97.8	0.5	95.9	0.7	92.6
34	517.5	0.1	99.1	0.3	98.1	0.4	96.4	0.7	93.3
35	532.5	0.1	99.2	0.2	98.3	0.4	96.7	0.6	93.9
36	547.5	0.1	99.3	0.2	98.5	0.4	97.1	0.6	94.5
37	562.5	0.1	99.4	0.2	98.7	0.4	97.5	0.6	95.1
38	577.5	0.1	99.5	0.2	98.9	0.4	97.8	0.6	95.8
39	592.5	0.1	99.6	0.2	99.2	0.4	98.2	0.7	96.5
40	607.5	0.1	99.7	0.2	99.3	0.3	98.5	0.6	97.1
41	622.5	0.1	99.8	0.1	99.5	0.3	98.8	0.5	97.6
42	637.5	0.1	99.8	0.1	99.6	0.2	99.1	0.5	98.0
43	652.5	0.0	99.9	0.1	99.7	0.2	99.2	0.4	98.4
44	667.5	0.0	99.9	0.1	99.7	0.2	99.4	0.4	98.8
45	682.5	0.0	99.9	0.1	99.8	0.2	99.6	0.3	99.1
46	697.5	0.0	100.0	0.1	99.9	0.2	99.8	0.4	99.5
47	712.5	0.0	100.0	0.0	99.9	0.1	99.9	0.2	99.7
48	727.5	0.0	100.0	0.0	100.0	0.1	99.9	0.1	99.8
49	742.5	0.0	100.0	0.0	100.0	0.0	99.9	0.0	99.9
50	757.5	0.0	100.0	0.0	100.0	0.0	100.0	0.0	99.9
51	772.5	0.0	100.0	0.0	100.0	0.0	100.0	0.1	100.0
52	787.5	0.0	100.0	0.0	100.0	0.0	100.0	0.0	100.0

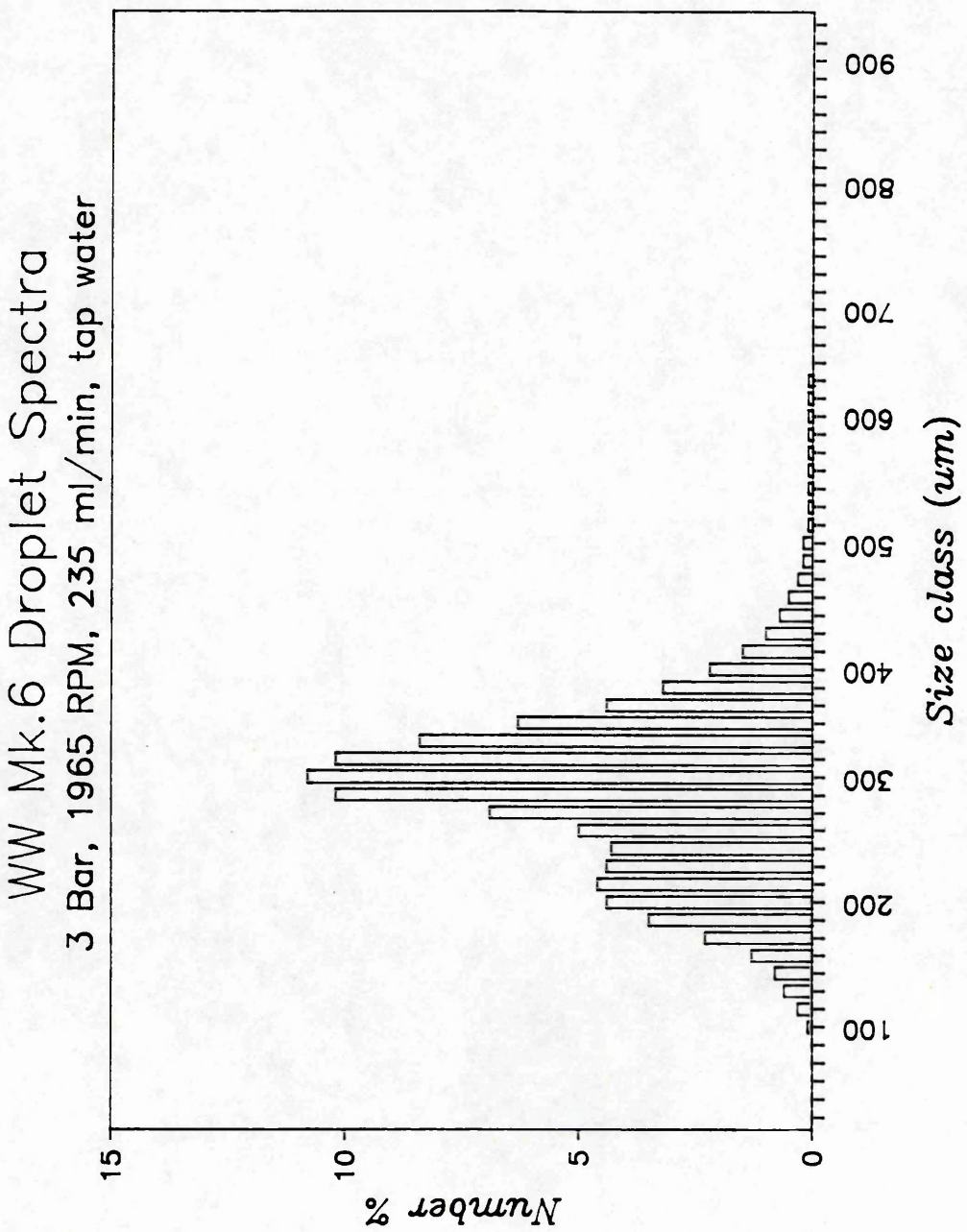

Figure 6.4.1a Number frequency histogram for typical droplet spectra with water

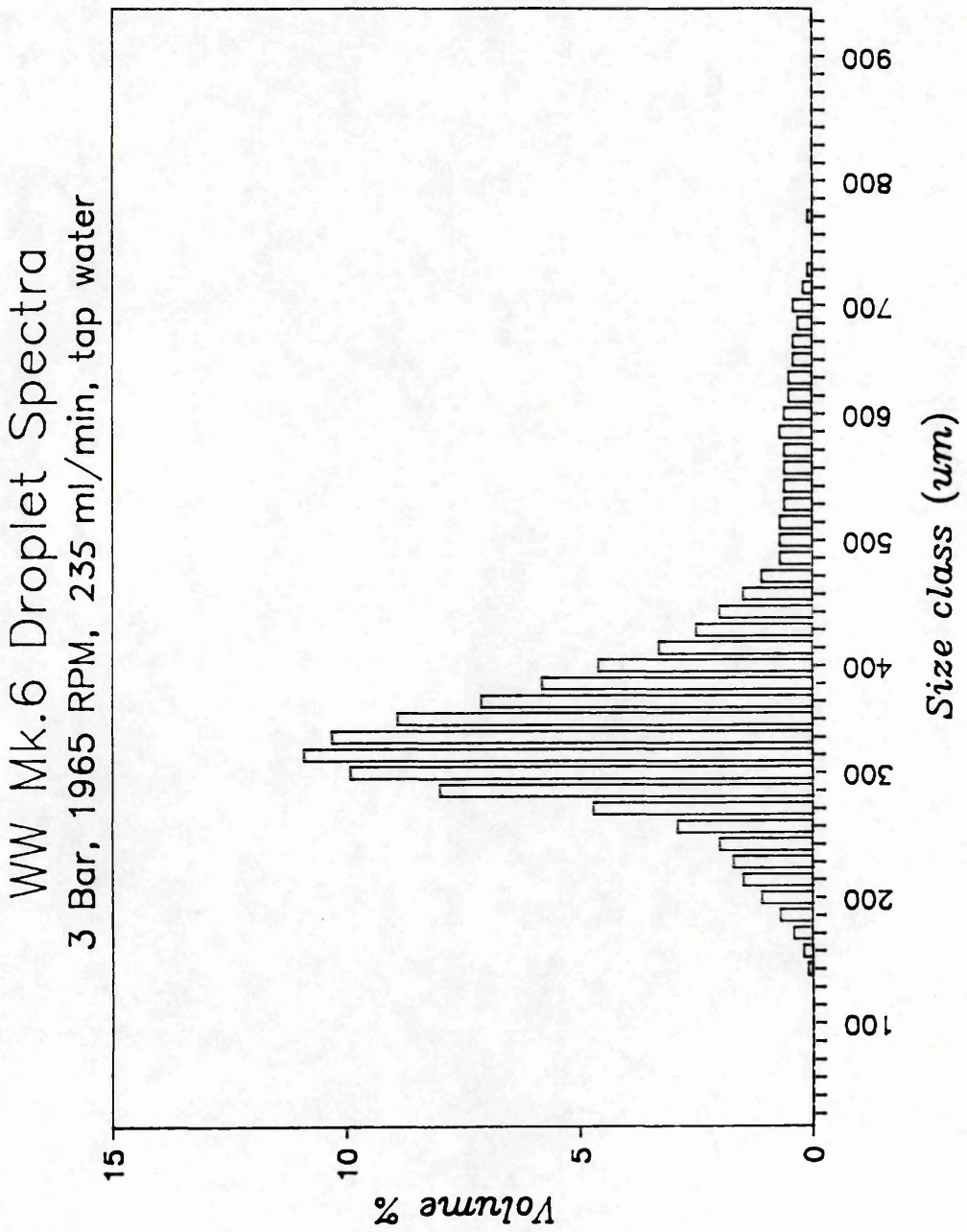

Figure 6.4.1b Volume frequency histogram for typical droplet spectra with water

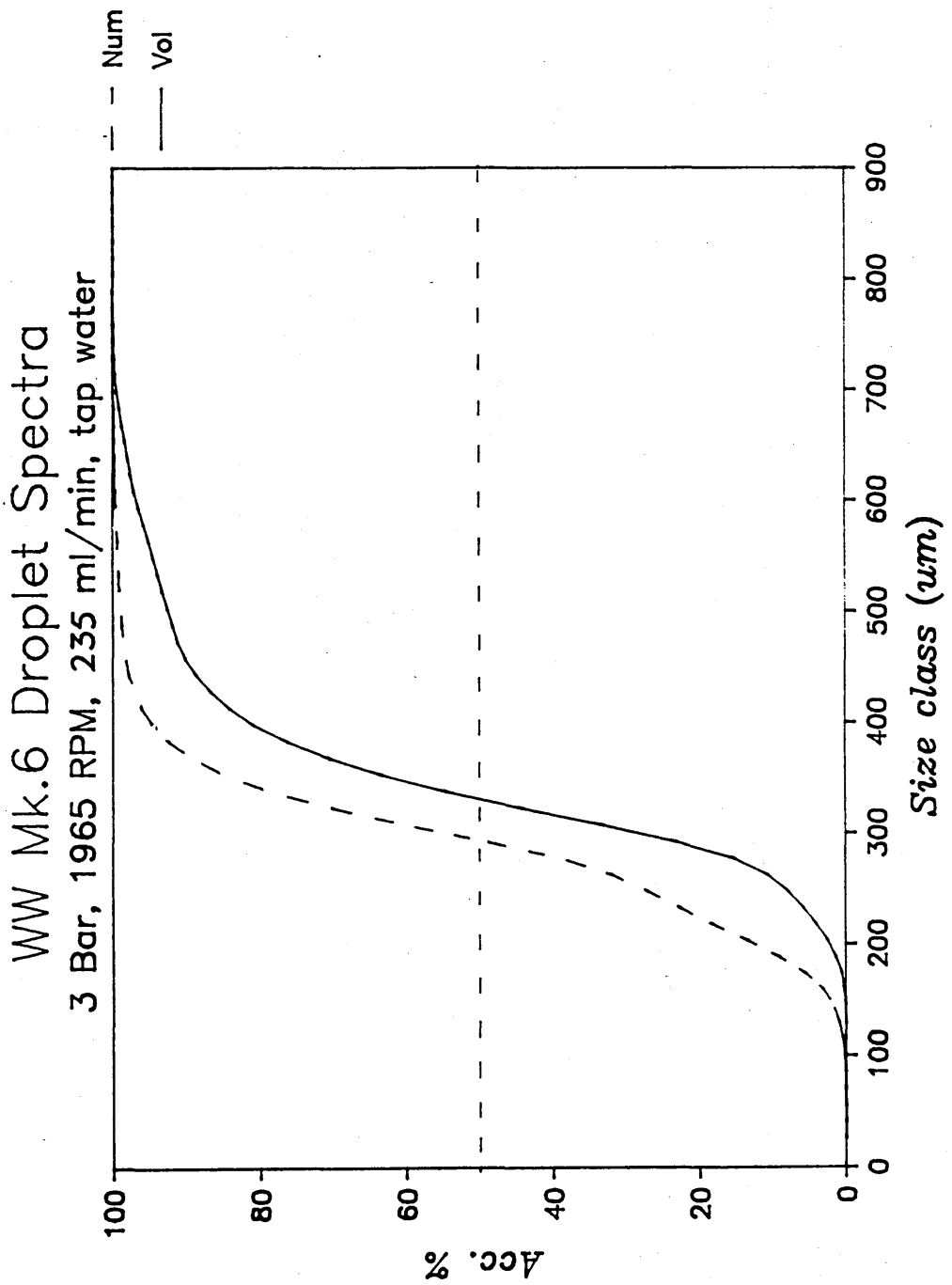

Figure 6.4.1c Accumulated number and volume curves for typical droplet spectra with water

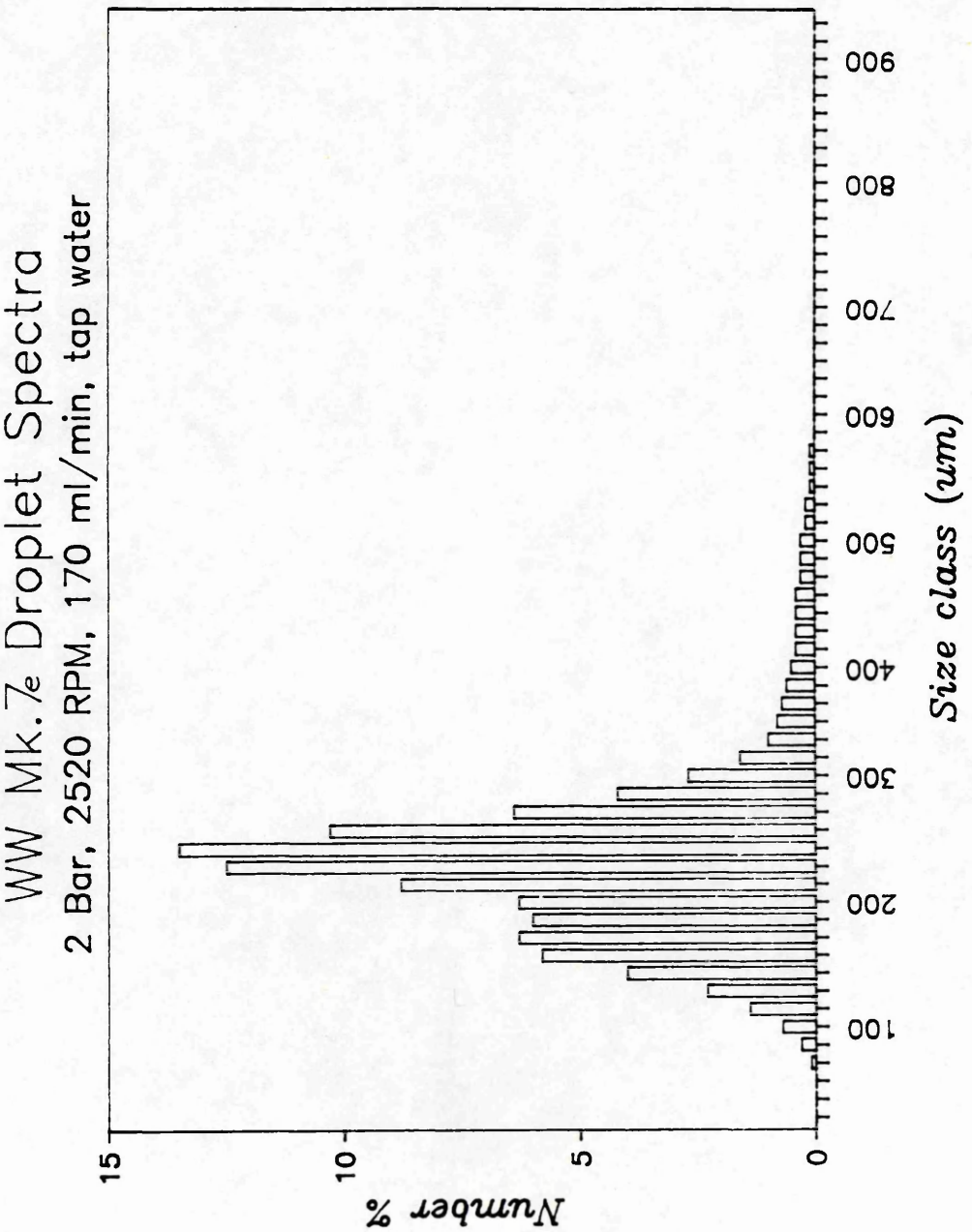

Figure 6.4.1d Number frequency histogram for Mk.7e, water

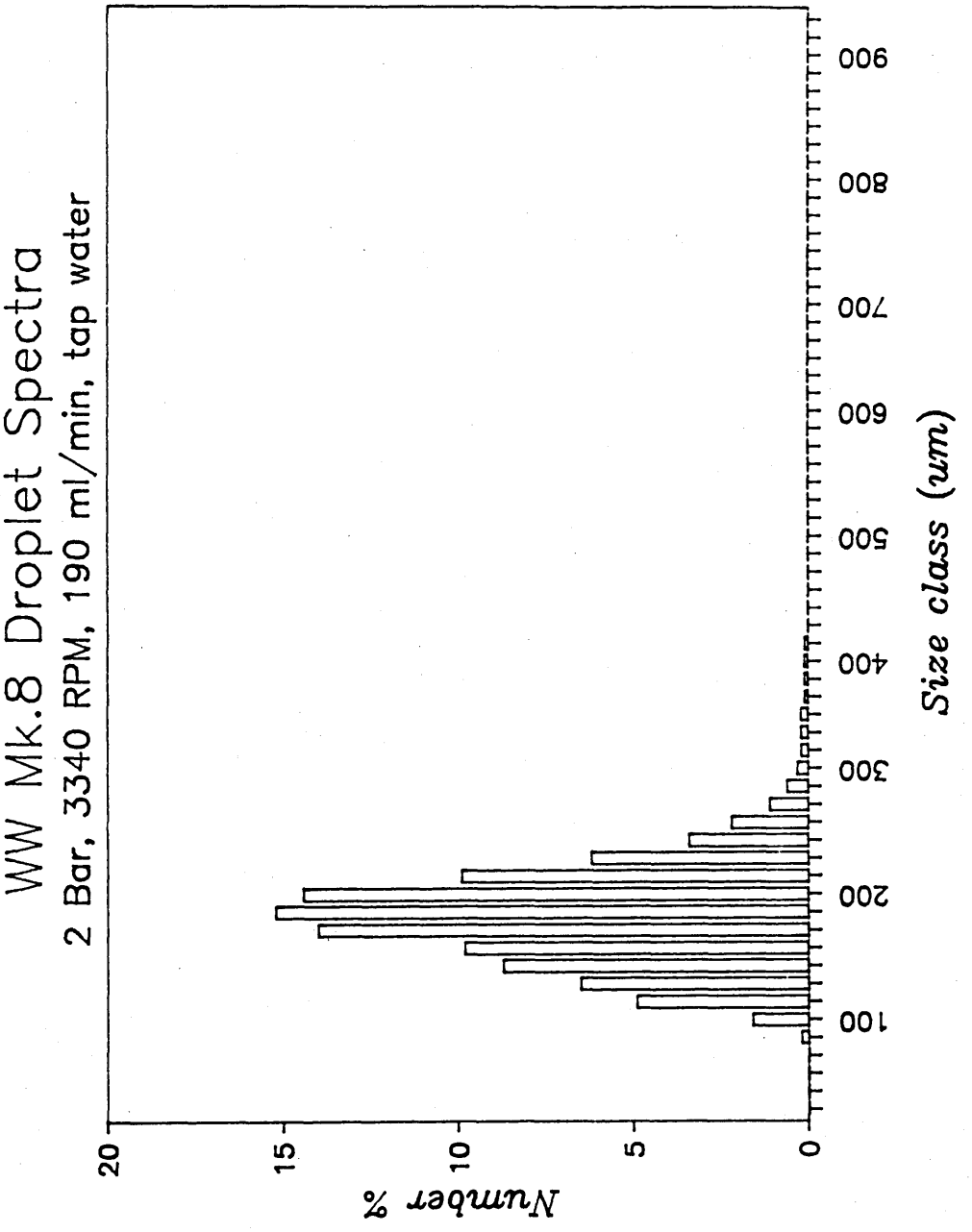

Figure 6.4.1e Number frequency histogram for Mk.8 (no weirs)

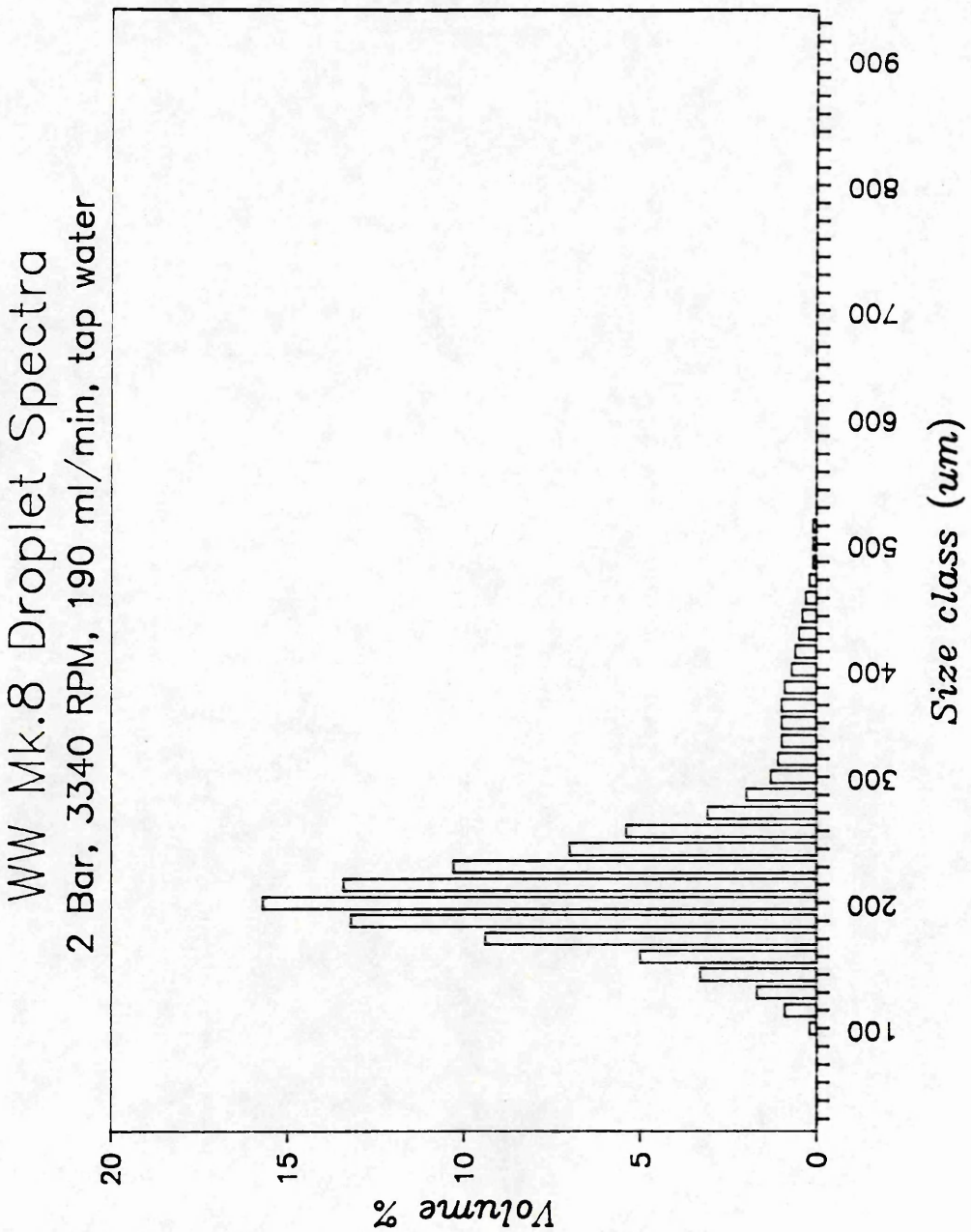

Figure 6.4.1f Volume frequency histogram for Mk.8 (no weirs)

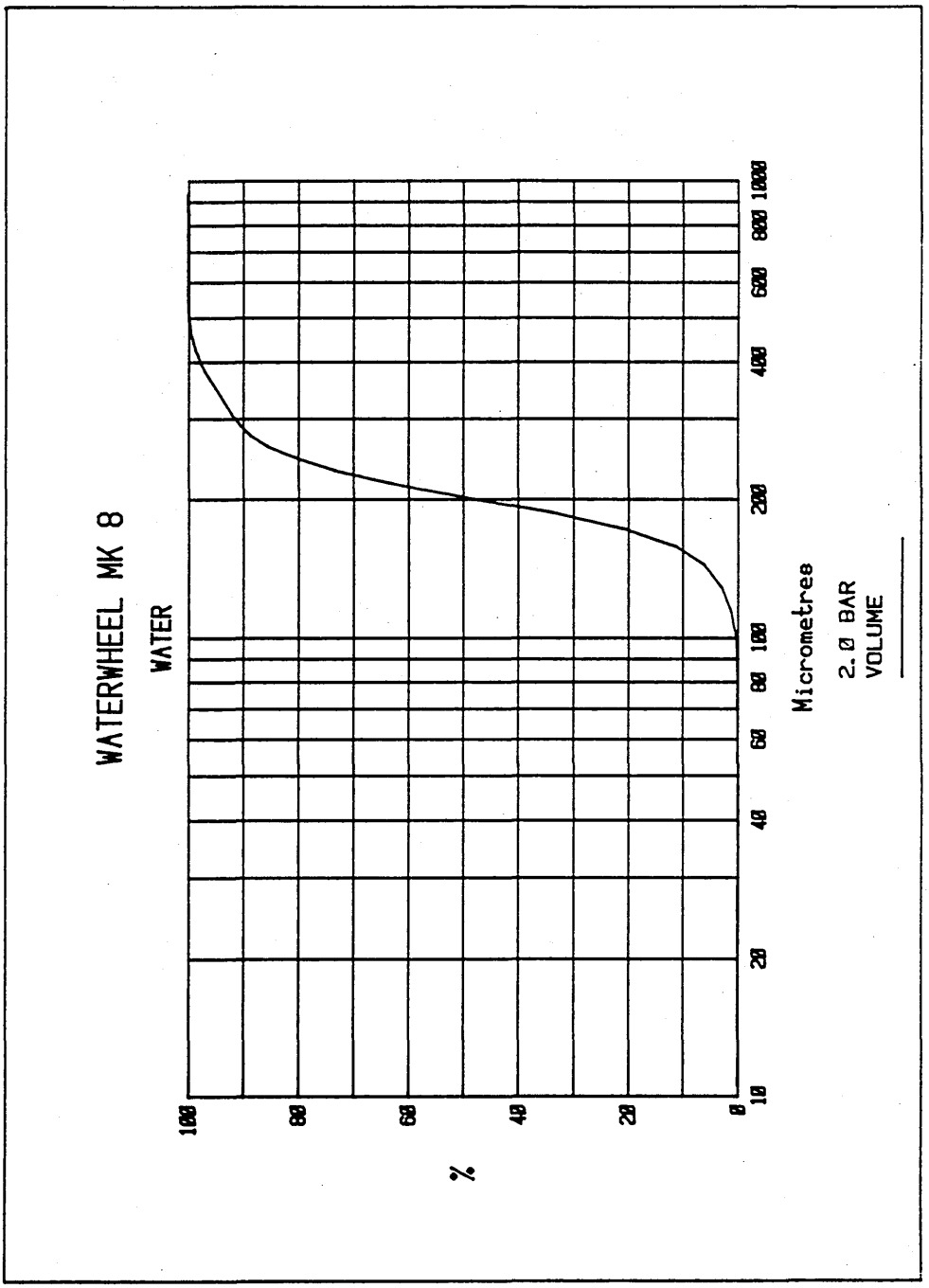

Figure 6.4.1g Accumulated volume curve for Mk.8 (no weirs)

6.4.2 Comparison with droplet spectra from a Micron Herbi and other atomisers

Figure 6.4.2a shows a comparison between Record 2,273,274 for Waterwheel Mk.6 and Record 2,047 for the Micron Herbi (Droplet Data Summary 4, Chapter 5). These particular records were chosen since they correspond to similar flowrates with tap water, and similar rotational speeds.

Although the two spectra have different NMD and VMD values, the general range of droplet sizes present are broadly similar. As is frequently characteristic with water droplet spectra, the two disributions show a degree of bimodality, although this is more pronounced with the Herbi spectra.

A point of interest is that Number Average Diameter only differs by 2.3µm (289.5 µm and 287.2µm respectively). Also the relative spans are identical at 0.6. One can conclude therefore, that the two spectra are roughly comparable.

Figure 6.4.2b shows a comparison between the Waterwheel Mk.7b (2 bar, 2340 RPM, 170 ml/min, Record 4,036,42) and a typical spectrum from a 80015 flat fan hydraulic nozzle at 2.5 Bar (Merritt, 1985, unpublished report MON 208/7, International Centre for the Application of Pesticides, Cranfield Institute of Technology). The spray fluid in both cases is a solution of glyphosate in water. Although the concentrations are different (4% and 20% respectfully), they are both intended for an application rate on the ground of 4.0 litres a.i. per hectare. VMD values for the two distributions are identical at 234µm.

The spectra are remarkably similar at the coarse end. However at the fine end of the droplet spectra they are noticeably different. The percentage of droplets by volume less than 100µm for the hydraulic nozzle is 6.6 % , which compares to less than 0.3% for the Waterwheel.

Figure 6.4.2c shows droplet spectra from a higher flowrate hydraulic nozzle (8005 Flat Fan) which produces a coarser spray compared to the 80015. As is apparent from the accumulated volume curves, VMD has increased to around 400µm inorder that no droplets are less than 100µm by volume.

A similarly coarse droplet spectrum produced by the Waterwheel (Mk.5, 2000 RPM, 320 ml/min, Record 2,006,8) has been superimposed for purposes of comparison. The percentage volume of spray under 150µm is less than 0.1%, compared to 3 or 4 % for the hydraulic nozzle.

Droplet Spectrum Analysis Cranfield Institute of Technoloc

FILE :- craig2 RECORD NUMBER :- 47

Atomiser Parameters

Atomiser Type	:- Micron Herbi
Pressure (Bar)	:-
Disc Speed (RPM)	:- 2000
Flow Rate (ml/min)	:- 240 ml/min
Fluid Description	:- tap water

Percentiles - µm Diameter

	5%	10%	16%	25%	50%	75%	84%	90%	95%
Number	144.0	178.5	196.7	216.9	277.7	366.0	378.0	388.5	405.
Length	179.3	201.0	218.8	242.0	340.4	375.9	386.7	397.0	431.
Area	198.9	221.2	242.2	276.3	359.8	382.6	395.1	414.9	482.
Volume	217.8	243.6	273.6	324.6	368.9	391.4	410.2	463.5	538.

Droplet Spectra Parameters

Number Median Diameter	= 277.7	µm
Number Average Diameter	= 287.2	µm
Volume Average Diameter	= 314.2	µm
Sauter Average Diameter	= 341.6	µm
Volume Median Diameter	= 368.9	µm

Spectrum Width

Span (ASTM)	= 219.9	
Relative Span (ASTM)	= 0.60	
V.M.D./N.M.D. Ratio	= 1.33	
sigma g (num), (vol)	= 1.41	1.35
Volume of Spray <100 µm	= 0.02	%
Volume of Spray <145 µm	= 0.27	%
Total Number of Raw Drops	= 19589	
Sampling Time (secs)	= 860	

Table 6.4.2a Droplet spectrum analysis for the Micron Herbi with water (DDS 4).

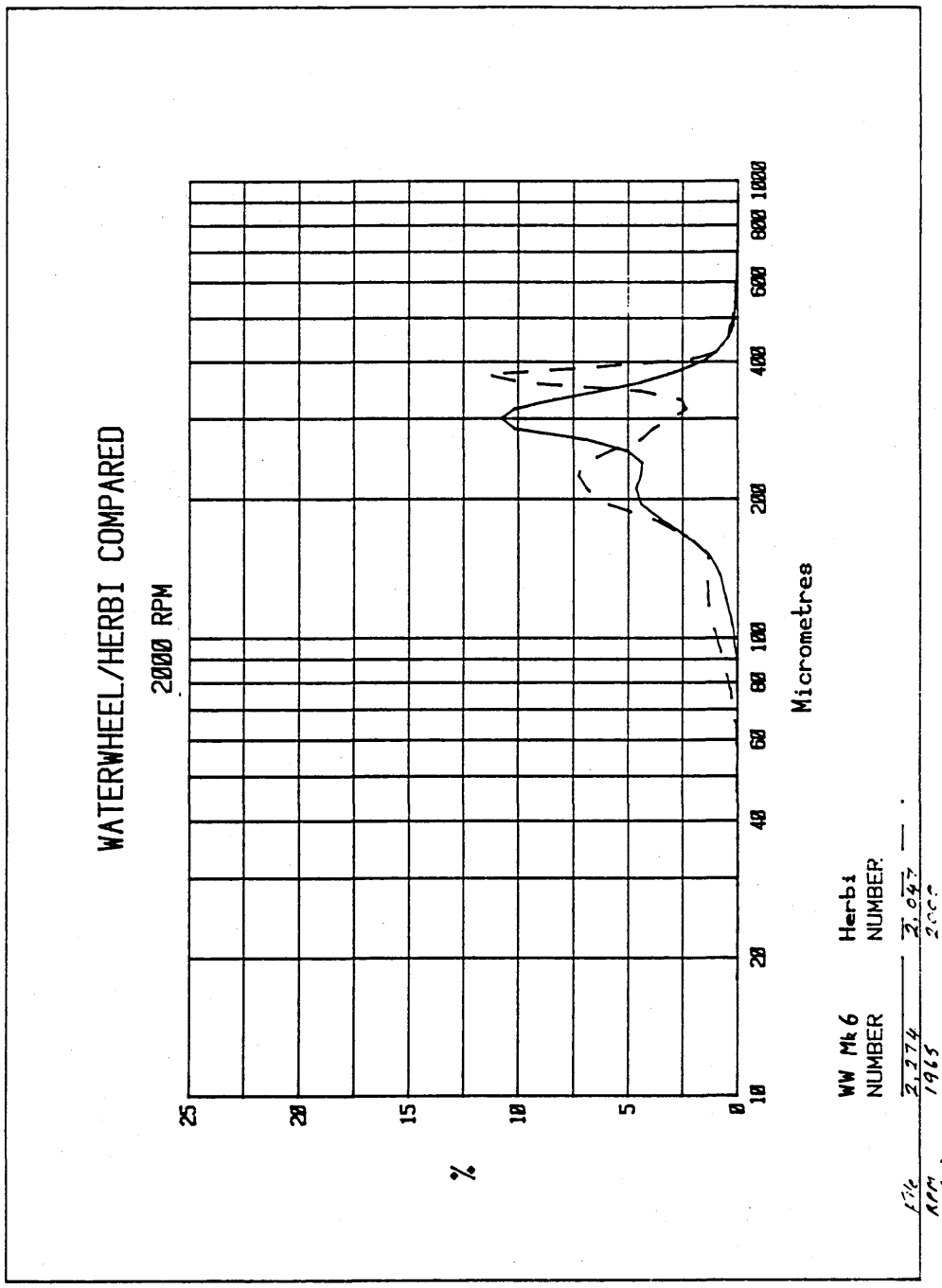

Figure 6.4.2a Comparison with typical droplet spectrum from a Micron Herbi spinning disc atomiser; tap water

Number = (0)
Length = (1)
Area = (2)
Volume = (3)

	PERCENTILES um			
(%<)	(0)	(1)	(2)	(3)
10.0	14.0	21.1	61.7	118.6
15.9	16.0	27.9	83.0	147.8
25.0	19.1	41.7	113.4	178.8
50.0	31.1	93.9	190.9	234.0
75.0	65.9	183.6	250.0	293.2
84.1	96.5	221.4	281.6	335.0
90.0	134.7	248.0	311.7	370.4

Droplet Spectra Parameters

NUMBER MEDIAN DIAMETER	31.1 um
NUMBER AVERAGE DIAMETER	55.4 um
VOLUME AVERAGE DIAMETER	108.0 um
SAUTER AVERAGE DIAMETER	190.7 um
VOLUME MEDIAN DIAMETER	234.0 um

Spectrum Width

sigma g	(0)	(3)	1.9	1.6
SPAN (ASME)			1.1	
'R'	(VMD/NMD)		7.5	

DROP #/ LITRE	1.52E+09
TOTAL DROPLET NUMBER COUNTED	14038

Table 6.4.2b Droplet spectrum analysis for Spraying Systems 80015 Flat Fan hydraulic nozzle at 2.5 bar, with 4% (w/v) glyphosate plus surfactant in water. (Monsanto Report 208/7, File Number #: E204, ICAP Spectral Analysis, Oct. 1985, Cranfield).

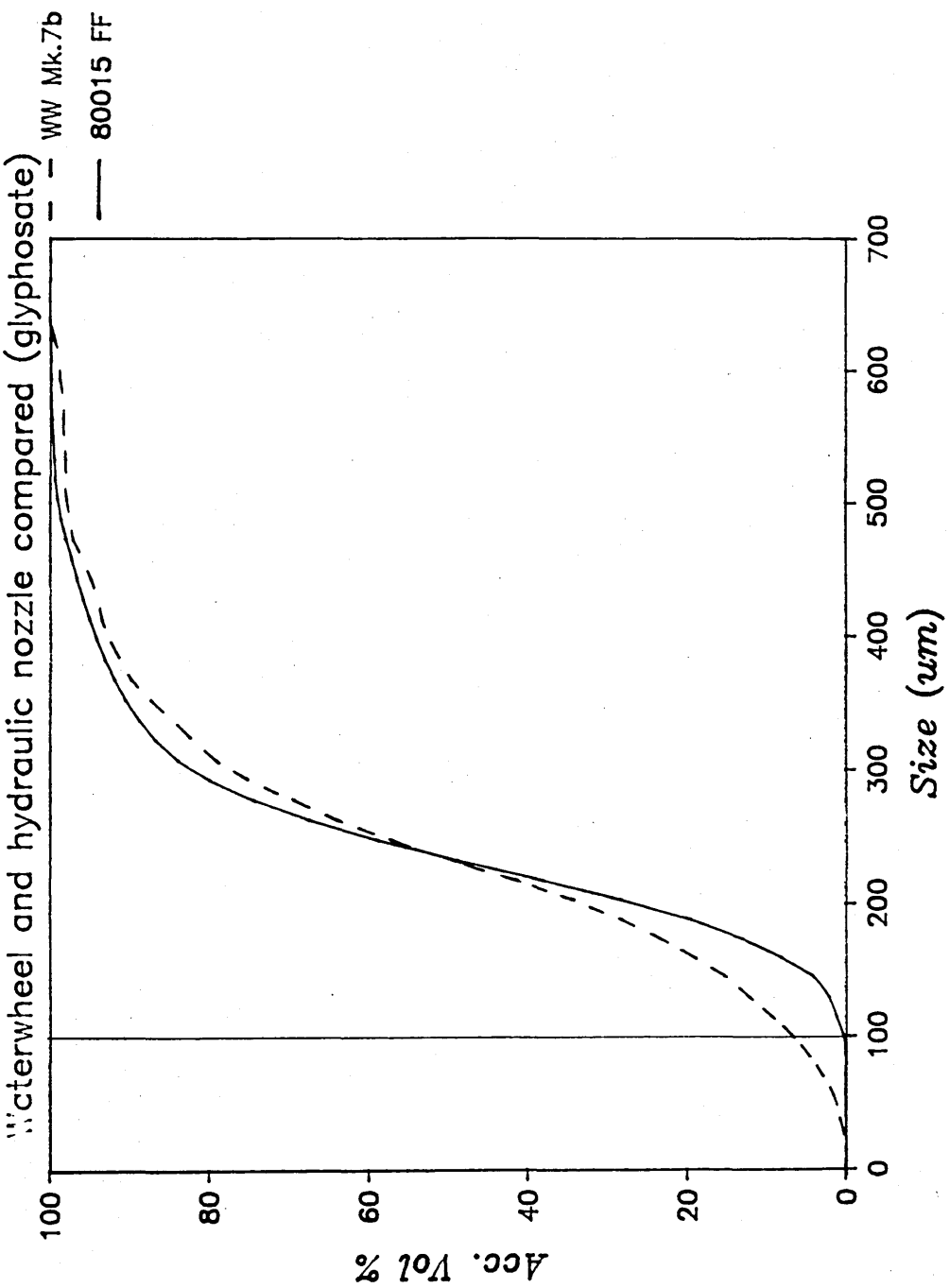

Figure 6.4.2b Comparison with droplet spectrum from a hydraulic nozzle (FF 80015); glyphosate plus surfactant, low flowrate

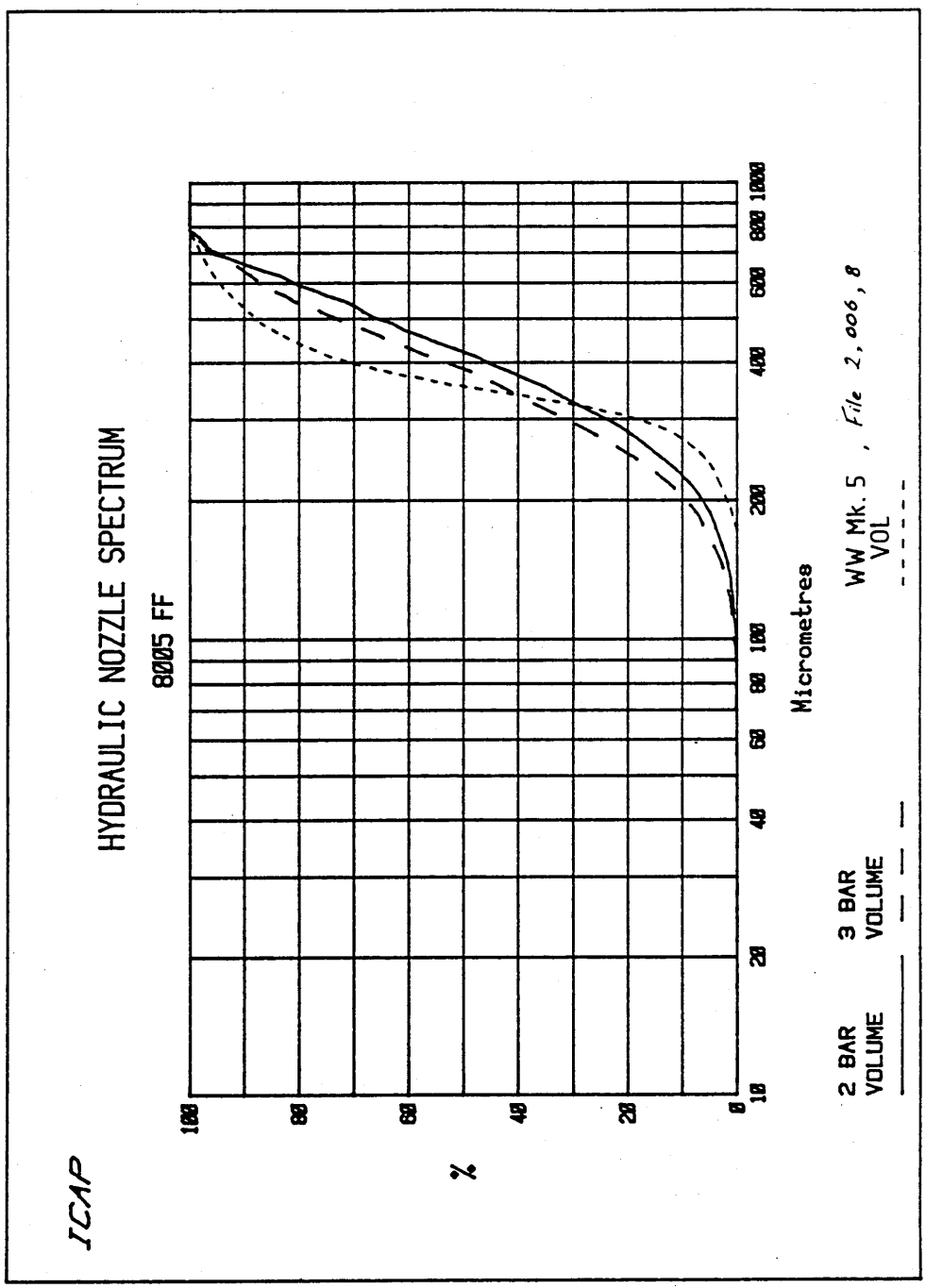

Figure 6.4.2c Comparison with droplet spectrum from a hydraulic nozzle (FF 8005); tap water, high flowrate

Droplet Spectrum Analysis Cranfield Institute of Technoloc

FILE :- craig2 MEANED RECORD NUMBERS :- 6 8

Atomiser Parameters

Atomiser Type	:- WW Mk.5
Pressure (Bar)	:- 2.07
Disc Speed (RPM)	:- 2000
Flow Rate (ml/min)	:- 320
Fluid Description	:- tap water

Percentiles - µm Diameter

	5%	10%	16%	25%	50%	75%	84%	90%	95%
Number	179.4	199.0	218.6	250.3	307.7	348.7	371.5	395.7	435.
Length	194.9	219.4	247.2	278.6	322.4	365.5	392.7	423.1	479.
Area	213.4	246.5	273.9	297.0	336.5	386.6	420.7	464.6	550.
Volume	237.4	271.6	293.0	311.5	352.0	415.2	466.3	532.2	623.

Droplet Spectra Parameters

Number Median Diameter	= 307.7	µm
Number Average Diameter	= 305.3	µm
Volume Average Diameter	= 327.4	µm
Sauter Average Diameter	= 351.0	µm
Volume Median Diameter	= 352.0	µm

Spectrum Width

Span (ASTM)	= 260.5	
Relative Span (ASTM)	= 0.74	
V.M.D./N.M.D. Ratio	= 1.14	
sigma g (num), (vol)	= 1.41	1.20
Volume of Spray <100 µm	= 0.00	%
Volume of Spray <145 µm	= 0.05	%
Total Number of Raw Drops	= 52675	
Sampling Time (secs)	= 1053	

Table 6.4.2c Droplet spectrum analysis for Waterwheel Mk.5 with water (DDS 12).

6.4.3 Effect of supply pressure on droplet size distribution

Figure 6.4.3a and 6.4.3b show droplet spectra for Mk.5 (Droplet Data Summary 12) and for Mk.6 (Droplet Data Summary 13) taken with water at supply pressures of 25, 30, 40, 50, and 60 PSI. The spectra are plotted with a log scale for dropsize. All the spectra take on a remarkably similar form with a progressive shift leftwards with increasing pressure. A graph summarising their VMDs is located in 6.4.5.

The shift towards the small end is due to rotational speed increasing with increasing supply pressure. There is a very slight broadening out of the spectra with increasing pressure due to the fact that flowrate is increasing. VMD/NMD ratios increase from around 1.15 to 1.3 for Mk.5, and from 1.2 to 1.4 for Mk.6.

The Mk.6 spectra have tails at the coarse end implying that the BARC was left out during this particular set of tests. The resultant accumulated % volume curves therefore exhibit a kinked appearance compared to Mk.5. This may also explain why the VMD/NMD ratios are slightly higher for Mk.6, when one would otherwise expect slightly lower values with the overall lower flowrates involved.

This was indeed shown to be the case with a later test carried out on Mk.6 with the BARC in. VMD/NMD ratio in this case is seen to decrease to 1.15 initially, rising to 1.22 at 5 bar.

A neatly arranged set of spectra such as those in Figures 6.4.3a and b is by no means the case with other Waterwheel prototypes. With the faster rotating Mk.7 and 8 for example, droplet spectra is seen to hardly change above pressures of about 2 bar.

With the high bearing friction prototypes such as Mk.3, Mk.4 and Mk.9-11, there tends to be a more profound increase in spectral width at the lower pressures. Droplet spectra are generally coarser anyway, due to the increased flowrate required to overcome bearing friction. The spectral widening at low pressure is probably due to there being insufficient rotational speed at these higher flowrates for the production of stable ligaments and uniform atomisation.

Spectra for Mk.4, which had an exceptionally well lubricated plain bearing and flowrate reduced to a minimum, are included for 2, 3, 4, and 5 bar (water) in Figure 6.4.3c. As one can see from the accumulated curves there is almost a complete break down in atomisation at 2 bar.

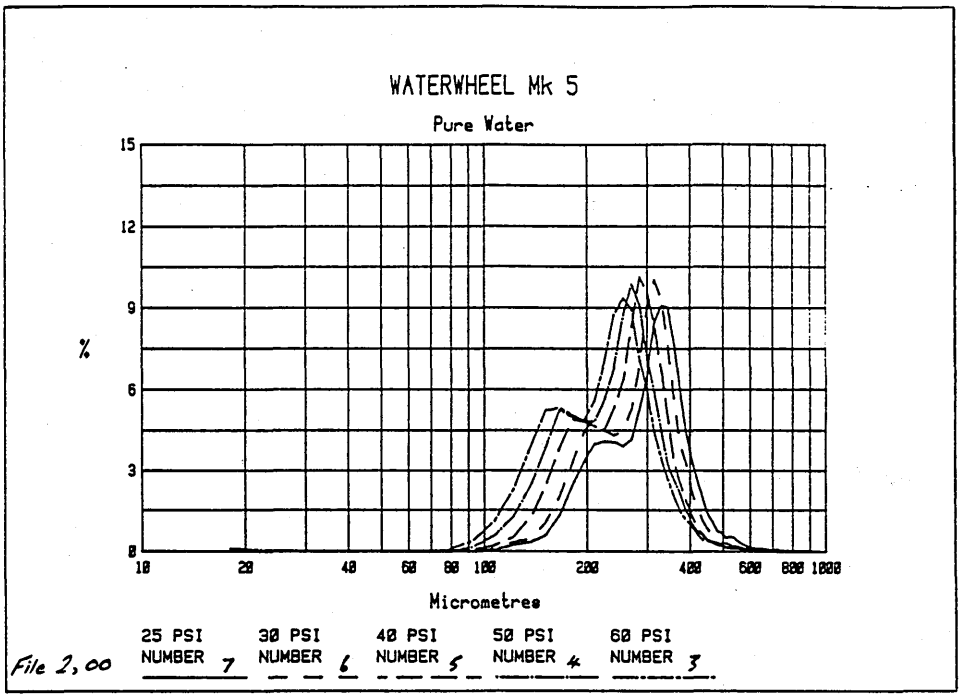

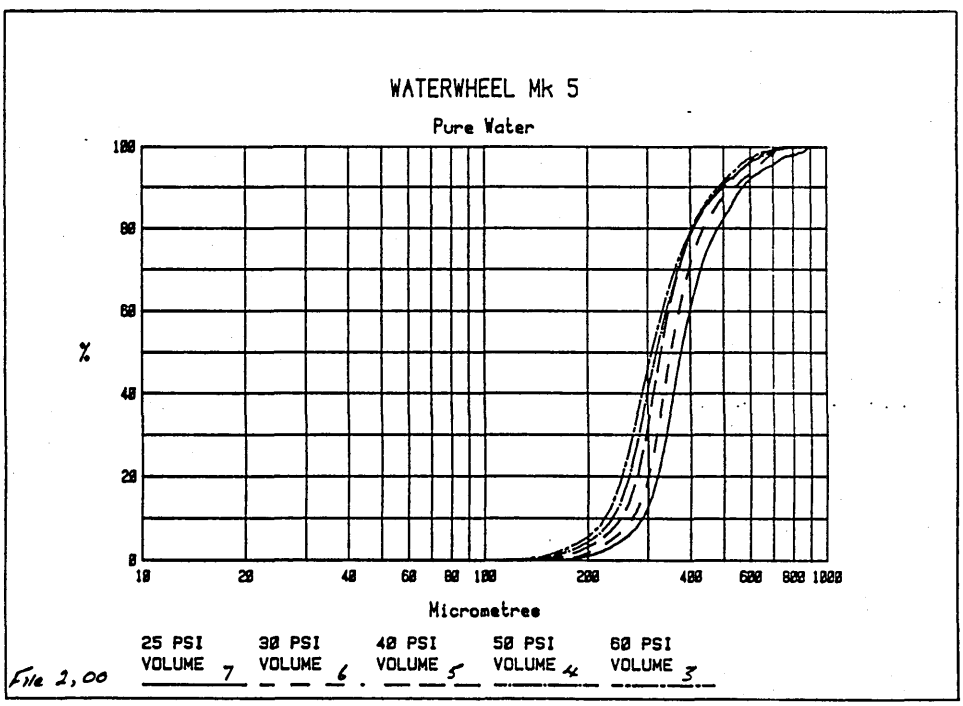

Figure 6.4.3a Effect of supply pressure on Waterwheel Mk.5 droplet spectra with tap water

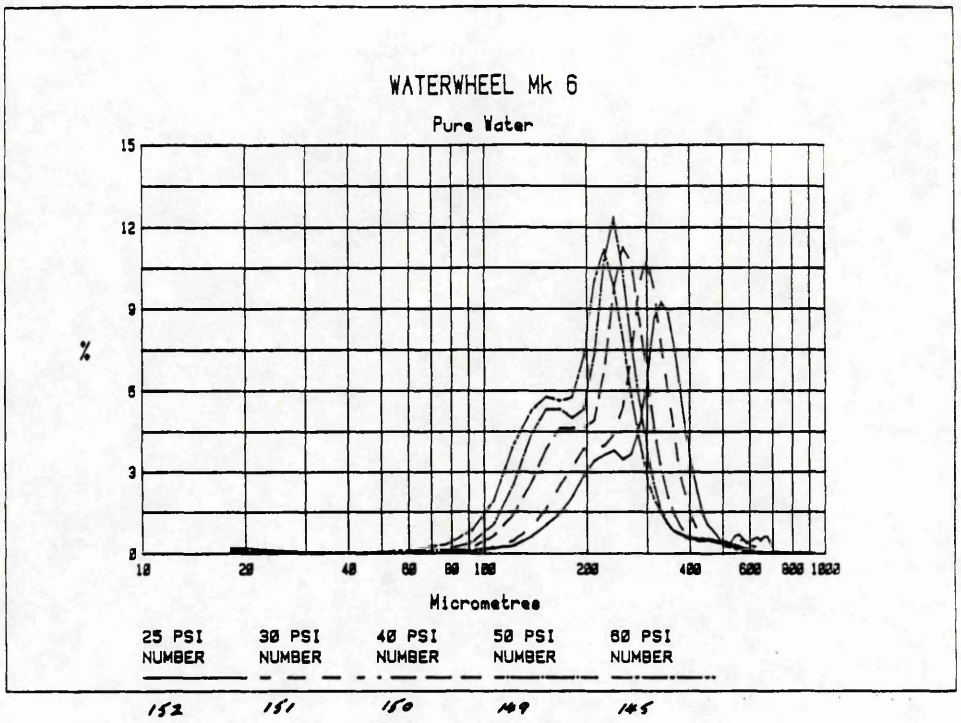

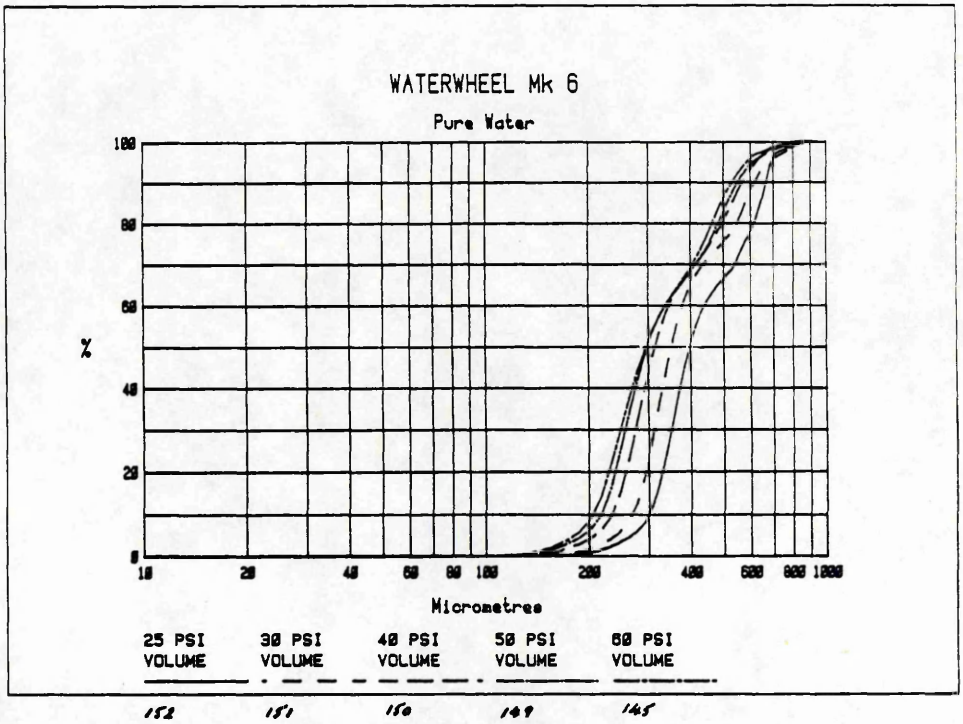

Figure 6.4.3b Effect of supply pressure on Waterwheel Mk.6 droplet spectra with tap water

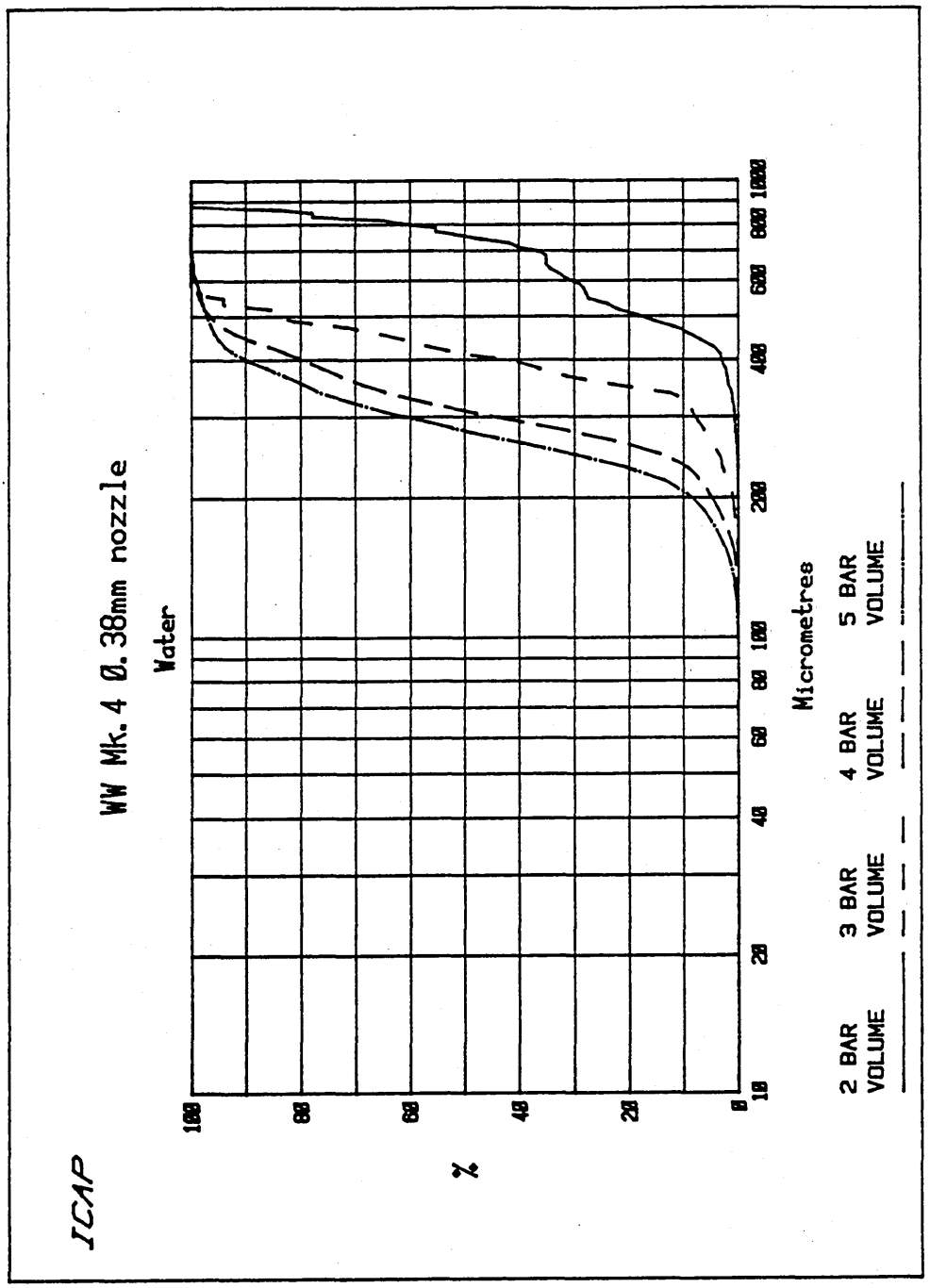

Figure 6.4.3c Effect of supply pressure on Waterwheel Mk.4 droplet spectra with tap water

6.4.4 Droplet spectra with various formulations

For the purposes of standard developmental work, tests took place with water since this was the most convenient fluid to handle. However, most of the prototypes were also tested with different fluids. A list of all the formulations used is as follows; all concentrations are expressed as:

B plus 100 x vol A / (vol A + vol B) %

1) tap water
2) tap water plus 0.005% Agral surfactant
3) tap water plus 0.01% Agral surfactant
4) tap water plus 0.05% Agral surfactant
5) tap water plus 0.1% Agral surfactant
6) tap water plus 20% Butyldigol
7) Butyldigol
8) tap water plus 10% H.Glyphosate*
9) tap water plus 10% H.Glyphosate plus 0.01% Midox antifoam
10 tap water plus 20% H.Glyphosate
11) tap water plus 20% H.Glyphosate plus 0.01% Midox antifoam
12) tap water plus 20% H.Glyphosate plus 0.02% Midix antifoam

Notes

Agral manufactured by ICI Agrochemicals, Farnham, Surrey

Heavy Glyphosate produced by Monsanto plc and sold under the trade name Roundup^{tm}.

containing:

480 g/Litre glyphosate acid

60 g/Litre surfactant
(corresponding to approximately 0.01% concentration of surfactant in a 20% glyphosate in water formulation)

code LLN 84/38 date 10/04/85

Midox ^{tm} antifoam agent (dimethylpolysiloxane) manufactured by Albright and Wilson plc.

The first tests with a fluid other than water was with Mk.3. Two concentrations of Agral, a standard surfactant for general use in pesticide formulations were used; 0.01% and 0.05% and compared to pure water.

Dropsize results with the surfactant were initially interpreted as disappointing, with the production of very coarse drops if the concentration of surfactant exceeded 0.01%. The reasons for the poor droplet spectra are as follows:

i) the performance of Mk.3 was at the best marginal, even if pure tap water was used, since the plain bearing used was too stiff resulting in low rotational speed. A characteristic of Mk.3 was that the fluid layer thickness behind the first weir was large. The jet in striking the inner wall had to firstly penetrate this thick fluid layer, resulting in further wastage of energy. With the introduction of surfactant, this made matters much worse since the production of foam was encouraged. If nozzle clearance was insufficient the foaming would cause the atomiser to stop rotating completely. With the nozzle further out a further loss in efficiency also occurred. Under low rotatonal speed the foam would persist on its journey through the weirs and out onto the atomising disc, resulting in a foamy appearance to the spray. The coarse droplet spectra was probably due to the laser probe measuring foam bubbles as well as normal spherical droplets.

ii) with the increased wetting of the atomising disc with surfactant, fluid slippage took place more readily between grooves which were shallow and "open" in nature (ie "v" shaped).

Accumulated volume curves for Mk.3, 0.4mm nozzle, for 0%, 0.01% and 0.05% Agral are included in Figure 6.4.4a

Increasing nozzle orifice size improved matters slightly in that rotational speed was increased resulting in a thinner inner wall fluid layer and more energy was available for the expulsion of foam. VMD/NMD ratios however are still unacceptably high because of the very high flowrate involved (up to 0.5 litre/min).

Droplet spectra for Mk.5 and 6 were also relatively wide, although not as wide as those obtained with Mk.3. The performance of Mk.5 appeared to markedly deteriorate with a surfactant concentration as low as 0.005% (Figure 6.4.4b).

Mk.5 spectra with 20% Butyldigol in water, and 100% Butyldigol were broader than for water, although would be considered exceptable for most herbicide applications (Figure 6.4.4c and d).

Figure 6.4.4e shows that results for 20% glyphosate in water with Mk.6 were similar to those obtained with 0.005% Agral (MK.5). This lead to the conclusion that it must be surfactant in the formulation causing a slowing of rotational speed, and therefore wide droplet spectra.

One solution to the problem was removal of the weirs and their replacement with a cylindrical ring which ensured a smooth inner wall from base to top. This enabled more rapid exit of fluid, a thinner inner wall fluid layer and the problem of foaming was avoided. However, the peripheral distribution of the fluid was nolonger even; that is the subject of section 6.4.7. Removal of the weiring system was not a practical solution.

The problem of slowing with surfactant was caused by the nozzle dipping into the fluid layer inside the cup and exerting a drag force opposing rotation. The edge of the nozzle facing the oncoming fluid was square. This edge was therefore carefully rounded to produce a more streamlined profile using a needle file. Rotational performance tests were then repeated.

The effect on rotational speeds obtained by modifying the nozzle was profound; comparison with rotation rate data in Droplet Data Summary 14 shows that speeds for tap water alone were nearly doubled. Even with no surfactant, nozzle drag must have occured with the unmodified nozzle.

Figure 6.4.4f compares rotational speeds obtained with various formulations for Mk.6 with rounded nozzle, with and without the fluid distribution system. The upper diagram shows that with the weirs there is a still a noticable speed reduction with increasing concentrations of surfactant, for example with 20% glyphosate curve (resulting in a total concentration of surfactant in the water + glyphosate mixture of just over 0.01%) rotational speeds are reduced by over half. The lower diagram shows that with exactly the same atomiser without the weirs, there was no such reduction in velocity.

The next stage in the development of the Waterwheel was to eliminate the effect of fluid drag altogether by moving the nozzle further away from the inner wall. Nozzle clearance was increased from 1.5 to 3mm. This gave rise to the Mk.7 (with weirs) and Mk.8 (without weirs) prototypes.

Figure 6.4.4g shows that the concentration of Agral in water with Mk.8 could now be increased to 0.1% without any substantial decrease in rotational speed and atomisational quality, although the Agral spectra is somewhat coarser. Exceptable spectra with 20% concentration of glyphosate plus surfactant in water could also be produced.

The next stage was to replace the weirs, now Mk.7, and repeat the tests. The quality of atomisation with Agral concentrations of up to 0.1% appeared to be satisfactory as shown by Droplet Data Summary 25. The VMD/NMD ratios are slightly coarser than they would be if the BARC was fitted,

but the objective of the test was to detect non-spherical droplets, so was performed with the BARC removed

However, with 0.1% agral, marked slowing of the atomiser occured below pressures of around 2.5 bar, and below about 2 bar atomisation broke down completely. The slowing rate with no liquid was also measured and found to be a little greater than previous measurements for Mk.7, implying that the bearing was a little stiffer than usual, and may have been contributing to the problem.

Following identical slowing rate measurements, the rotational speed with water was compared to that with 0.1% Agral, and found to be over 600 RPM faster at 2 bar (2520 RPM compared to 1915 RPM). It was therefore concluded that a slightly stiffer bearing and a particularly high surfactant concentration were combining to produce a degredation in performance and complete foaming up of the atomiser at low supply pressures.

Under stroboscopic illumination the foamy nature of the spray was apparant with all surfactant concentrations exceeding 0.01% , with agral and with glyphosate. Once the atomiser had stopped due to foaming, it was often impossible to restart, even with 5 bar pressure.

Addition of a small quantity of an antifoam agent (Midox^{tm}), however, brought about an immediate solution to the problem, and no foamy droplets could be detected above pressures of about 1.5 bar with 0.01% surfactant in water. A little lubricant was also added to the bearing which resulted in atomisational breakdown being delayed to below pressures of 0.5 bar. Figure 6.4.4i shows the extremely flat nature of the NMD and VMD curves for Mk.7b 20% glyphosate + 0.02% antifoam, against supply pressure in bar.

Figure 6.4.4j shows a typical droplet spectra taken at 2 bar. The reader may note that it is very similar to the droplet spectra produced by Mk.7 and Mk.8 with water at 2 bar.

Finally, Droplet Data Summary 27 shows some tests designed to ascertain the amount of antifoam agent required to ensure that no foaming occurs at any pressure. Studying the results it appears that the amount of Midox needed in a water plus glyphosate formulation is is approximately 0.001 times the quantity of glyphosate, or about double that of the surfactant. Reducing the concentration of antifoam to approximately the same as that of the surfactant allowed foaming to stop the atomiser at pressures below 2 bar.

DDS 19

EFFECT OF SURFACTANT ON DROPLET SPECTRA, LOW FLOWRATE

Atomiser prototype	WW Mk.3
Internal diameter of cup	70mm
Disc type and diameter	> shaped grooves, 83mm
Nozzle orifice size	0.4mm
Bearing	external electric motor (plain)
Substance sprayed	0%, 01%, 0.05% Agral in water
Test carried out	12/09/89

P (Bar)	N (RPM)	Q (ml/min)	NMD (um)	VMD (um)	Ratio	File, Record
0 % Agral in water						
3	1310	122	315	442	1.40	2,216
4	1750	138	247	291	1.18	2,215
5	2065	154	228	274	1.20	2,213,4
0.01% Agral in water						
3	1270	122	319	491	1.54	2,219
4	1720	138	254	303	1.19	2,218
5	2080	154	225	276	1.22	2,217
0.05% Agral in water						
3	1150	122	328	733	2.24	2,210
4	1340	138	291	697	2.39	2,211
5	1940	154	283	695	2.45	2,209

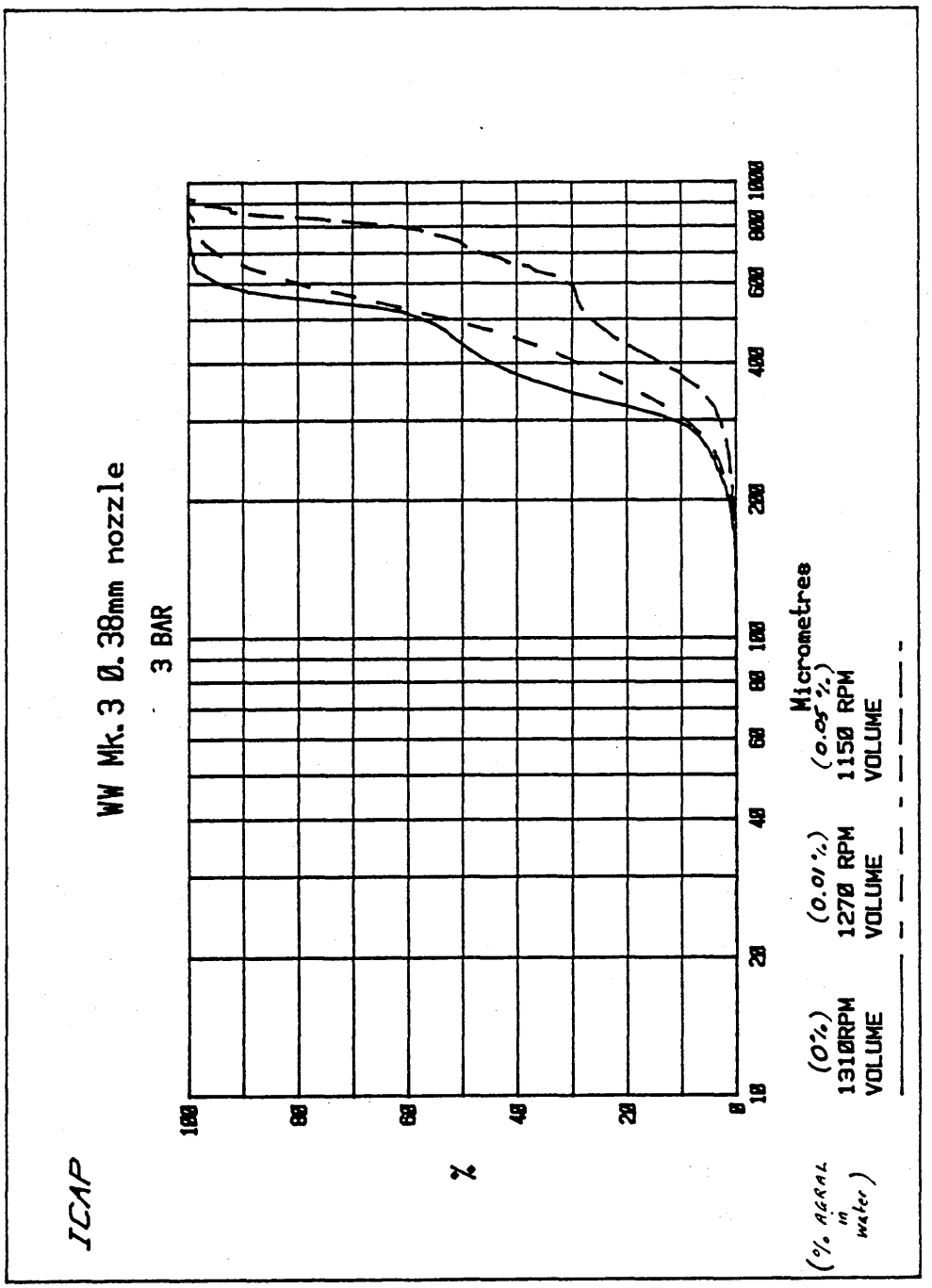

Figure 6.4.4a Effect of increasing surfactant concentration in water on droplet spectra for Mk.3, 3 bar

DDS 20

EFFECT OF SURFACTANT ON DROPLET SPECTRA, HIGH FLOWRATE

Atomiser prototype	WW Mk.3
Internal diameter of cup	70mm
Disc type and diameter	> shaped grooves, 83mm
Nozzle orifice size	0.6mm
Bearing	external electric motor (plain)
Substance sprayed	0%, 01%, 0.05% Agral in water
Test carried out	12/09/89

P (Bar)	N (RPM)	Q (ml/min)	NMD (um)	VMD (um)	Ratio	File, Record
0 % Agral in water						
3	1870	366	298	363	1.22	2,253
4	2410	420	231	339	1.36	2,254,5
5	2860	512	227	328	1.45	2,256
0.01% Agral in water						
3	2050	366	293	380	1.30	2,258
4	2540	464	260	362	1.39	2,257
5	2820	512	247	354	1.43	2,259,6
0.05% Agral in water						
3	1300	380	294	655	2.23	2,263
4	2540	464	239	443	1.85	2,261
5	2970	508	193	442	2.29	2,266

DDS 21

EFFECT OF VARIOUS FORMULATIONS ON DROPLET SPECTRA

Atomiser prototype WW Mk.5

Internal diameter of cup 44mm

Disc type and diameter 7 shaped grooves, 56mm

Nozzle orofice size 0.62mm

Bearing minature ball races

Test carried out 09/08/89

P (Bar)	N (RPM)	Q (ml/min)	NMD (um)	VMD (um)	Ratio	File, Record
.01% Agral in water						
2.07						
2.76	2400	366	326	565	1.73	2,023
3.45	2960	426	291	479	1.65	2,020
4.13	3370	450	277	468	1.69	ns
20% Butyldigol in water						
2.07	1830	320	271	390	1.44	2,136
2.76	2210	362	258	384	1.49	2,135
3.45	2670	395	238	379	1.59	2,134
4.13	3000	425	237	390	1.64	2,133
100% Butyldigol						
2.07	1300	206	300	352	1.17	2,128, 129
2.76	1650	240	290	333	1.15	2,127, 130
3.45	2000	270	254	365	1.43	2,126, 131
4.13	2800	290	210	314	1.49	2,125, 132

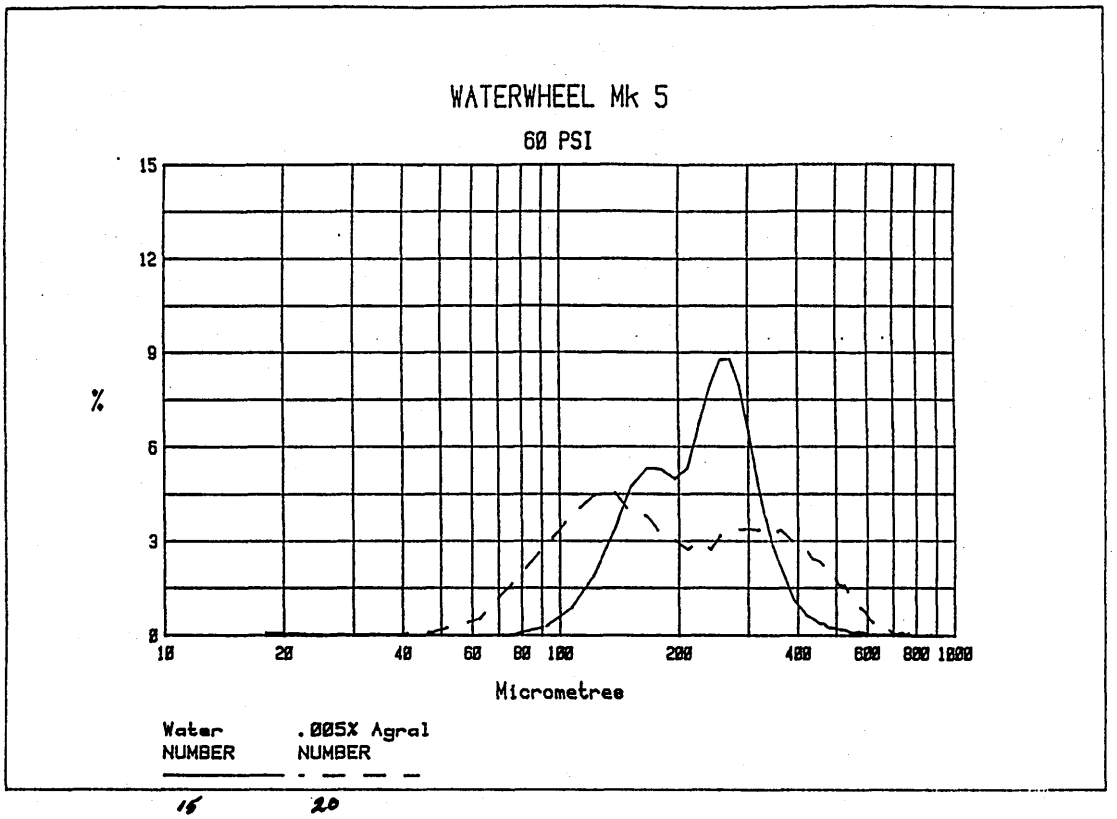

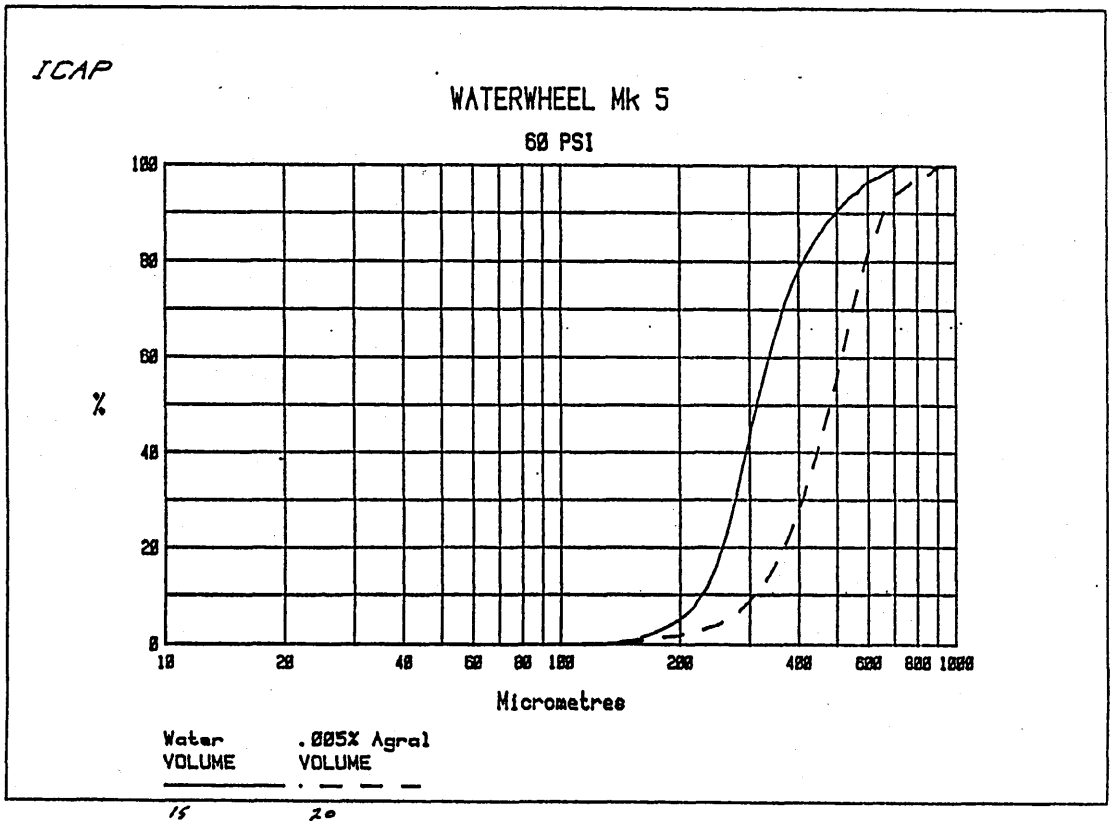

Figure 6.4.4b Effect of low surfactant concentration on droplet spectra of Mk.5

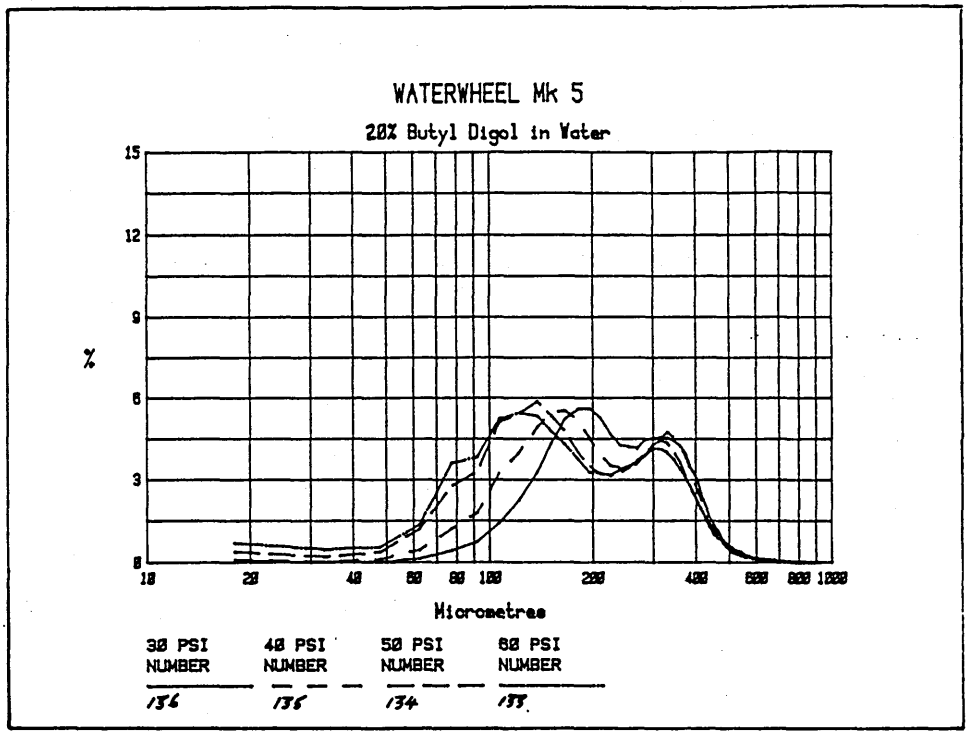

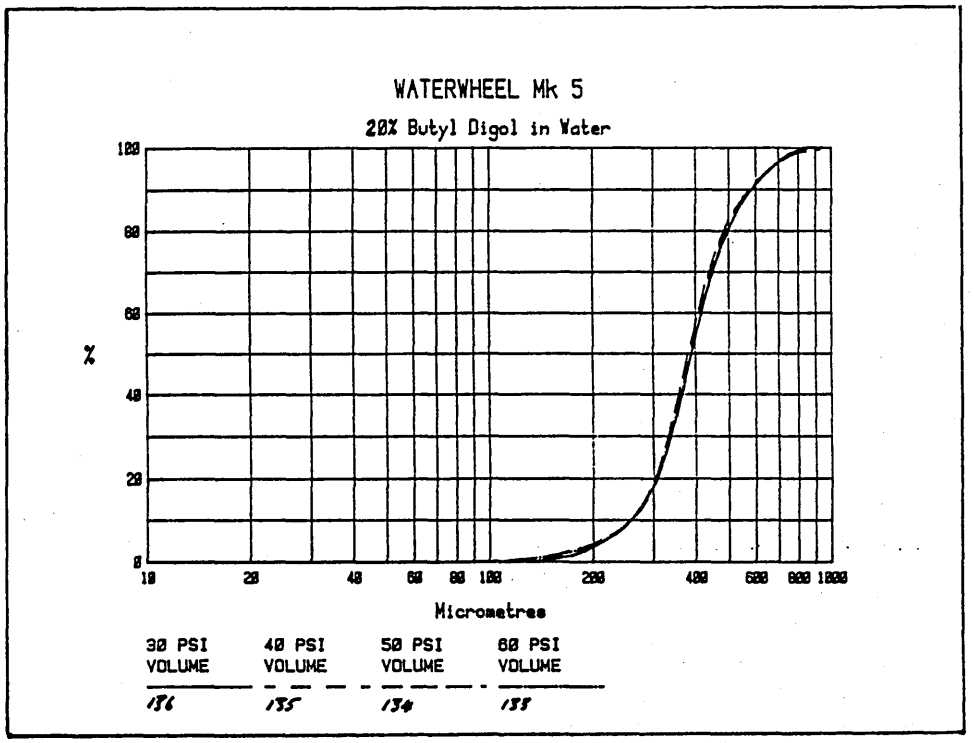

Figure 6.4.4c Droplet spectra for Mk.5 with 20% (v/v) Butyldigol in tap water

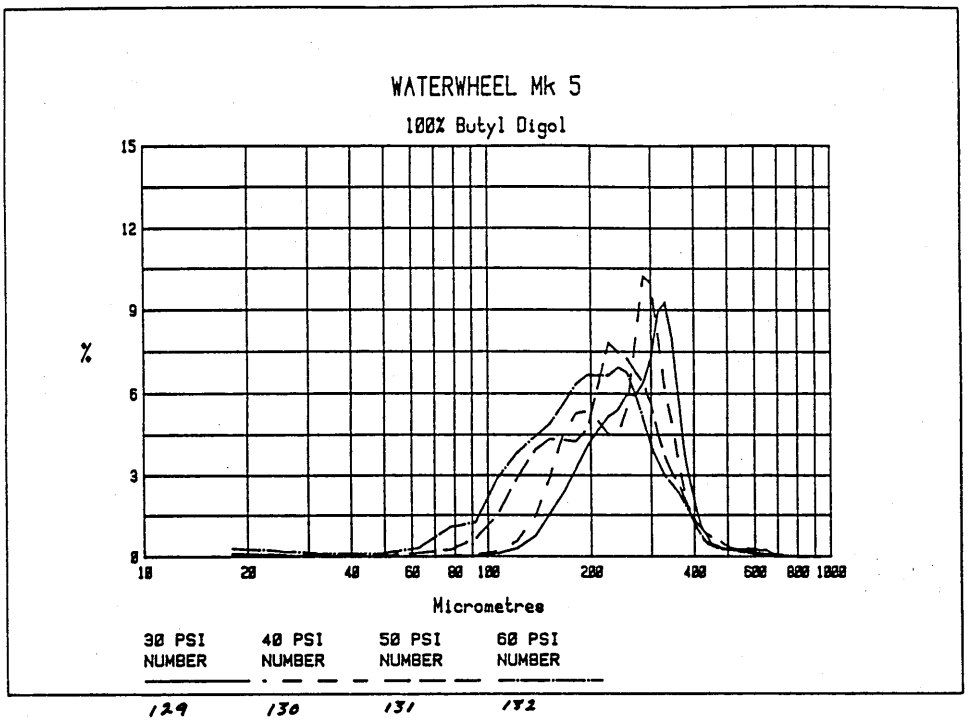

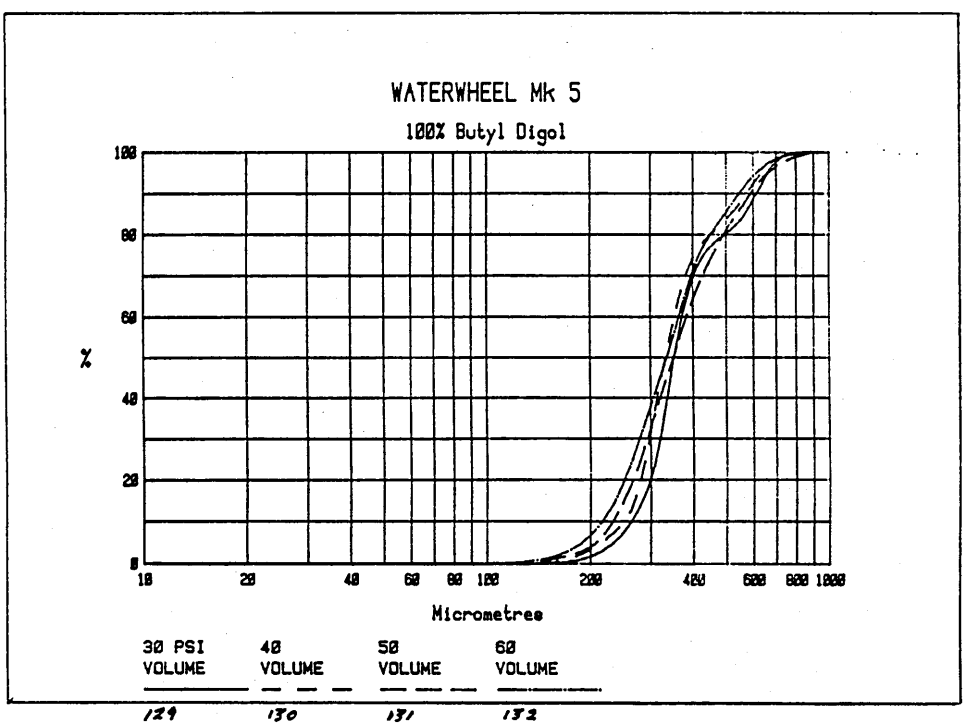

Figure 6.4.4d Droplet spectra for Mk.5 with 100% (v/v) Butyldigol in tap water

DDS 22

20% (v/v) HEAVY GLYPHOSATE ACID + SURFACTANT IN WATER

Atomiser prototype	WW Mk.6
Internal diameter of cup	44mm
Disc type and diameter	7 shaped grooves, 56mm
Nozzle orifice size	0.5mm
Bearing	miniature ballraces
Substance sprayed	20% glyphosate in water
Test carried out	21/03/89

P (Bar)	N (RPM)	Q (ml/min)	NMD (um)	VMD (um)	Ratio	File, Record
.5						
1.0						
1.5						
2.0	1180	200	328	681	2.00	2,157,162
2.5						
3.0	1620	235	292	687	2.35	2,158
3.5	1820	250	280	651	2.32	2,159
4.0	2400	260	216	663	3.07	2,160
4.5						
5.0	2630	280	204	642	3.15	2,161

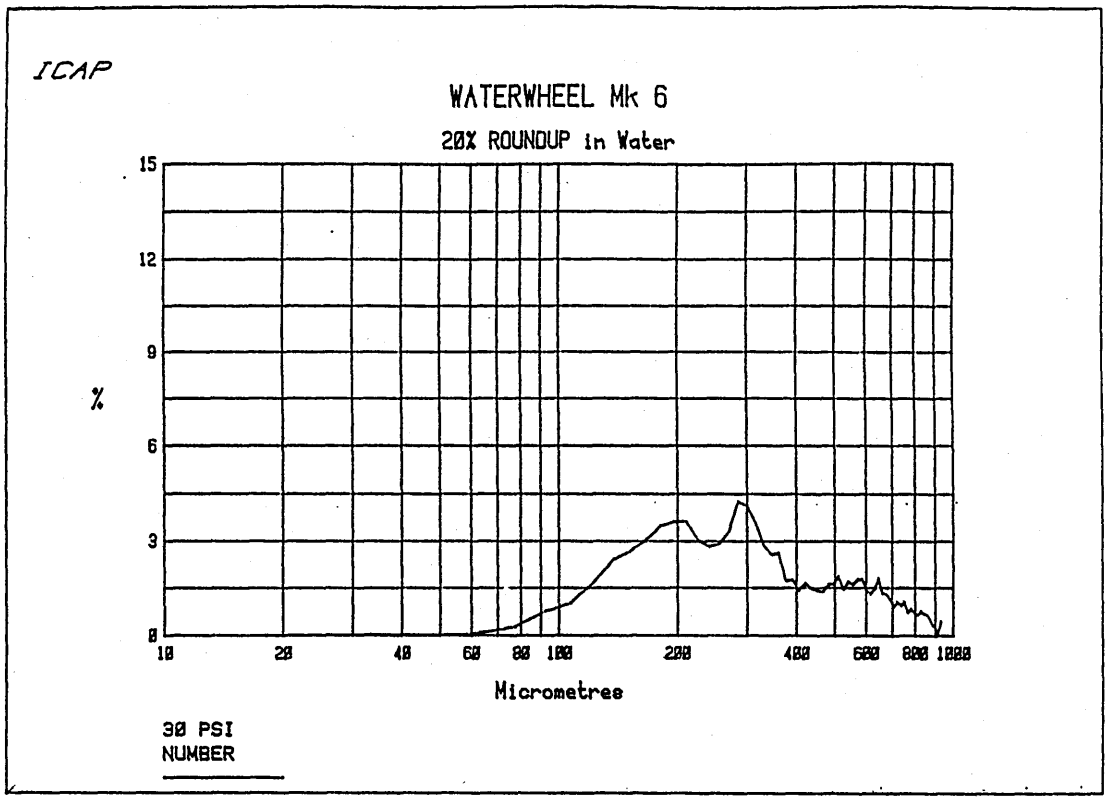

157

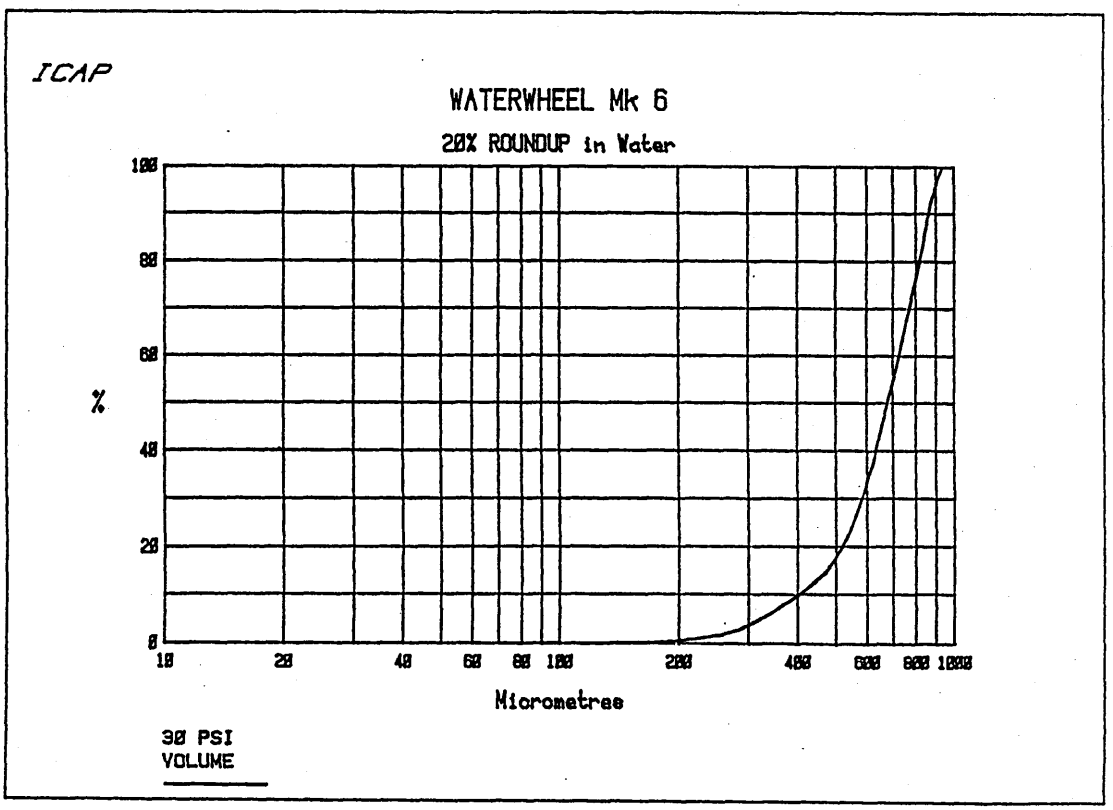

157

Figure 6.4.4e Droplet spectra for Mk.6 with 20% (v/v) glyphosate in tap water

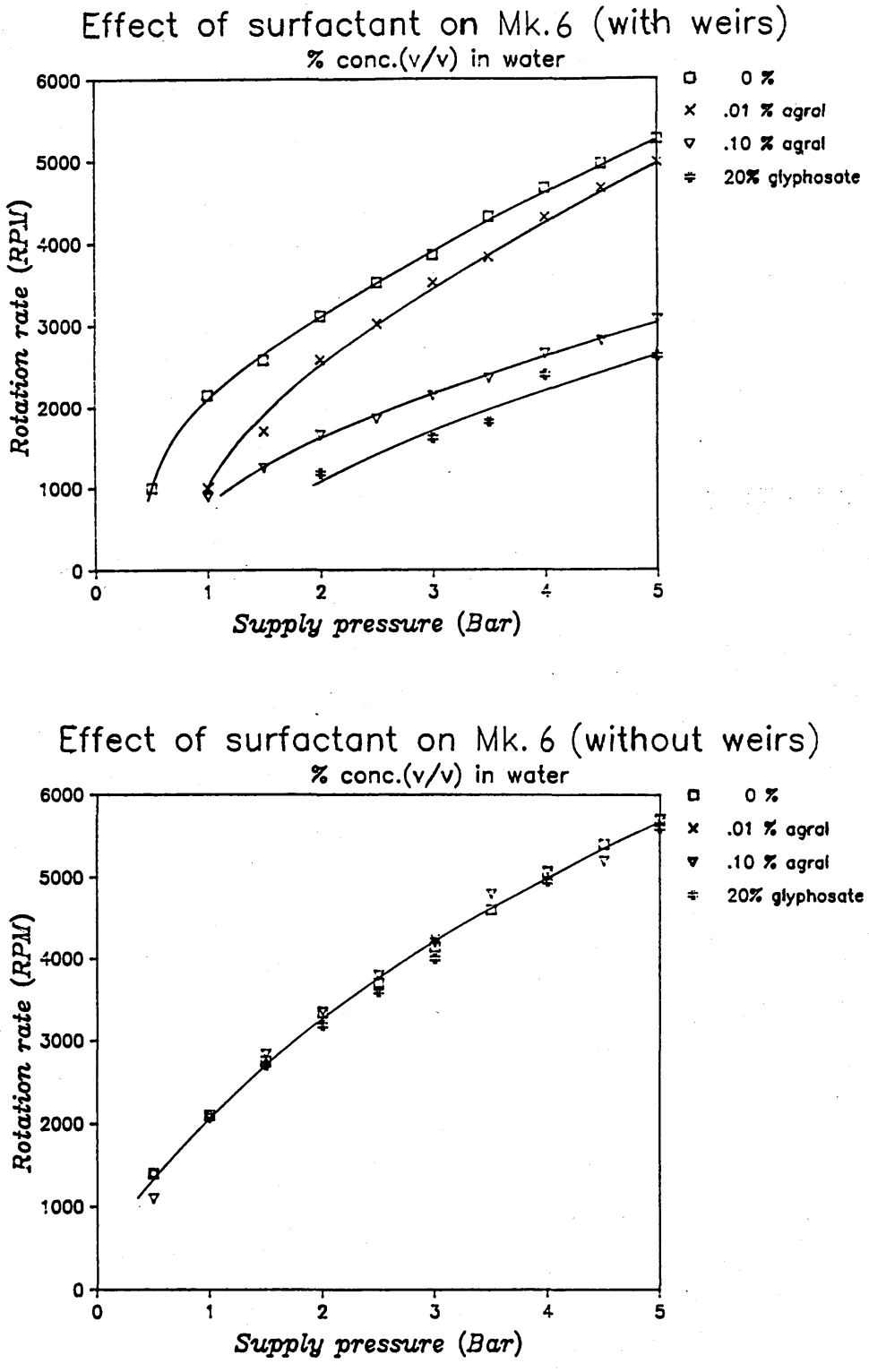

Figure 6.4.4f Effect of surfactant on rotational performance of Mk.6, with and without weirs

DDS 23

0.1 % AGRAL IN WATER

Atomiser prototype	WW Mk.8
Internal diameter of cup	44mm
Disc type and diameter	7 shaped grooves, 56mm, reverse
Nozzle orifice size	0.5mm, modified
Bearing	miniature ballraces
Substance sprayed	0.1 % Agral in water
Test carried out	28/02/90

P (Bar)	N (RPM)	Q (ml/min)	NMD (um)	VMD (um)	Ratio	File, Record
.5	1100	102	376	515	1.37	1,046
1.0	2070	140	222	280	1.26	1,043
1.5	2840	166	216	263	1.22	1,045
2.0	3360	190	207	259	1.25	1,044
2.5	3800	206	193	241	1.15	1,041,42
3.0	4200	225	187	243	1.15	1.035,36
3.5						
4.0	5080	264	172	230	1.34	1,037,38
4.5						
5.0	5700	300	169	230	1.36	1,039,40

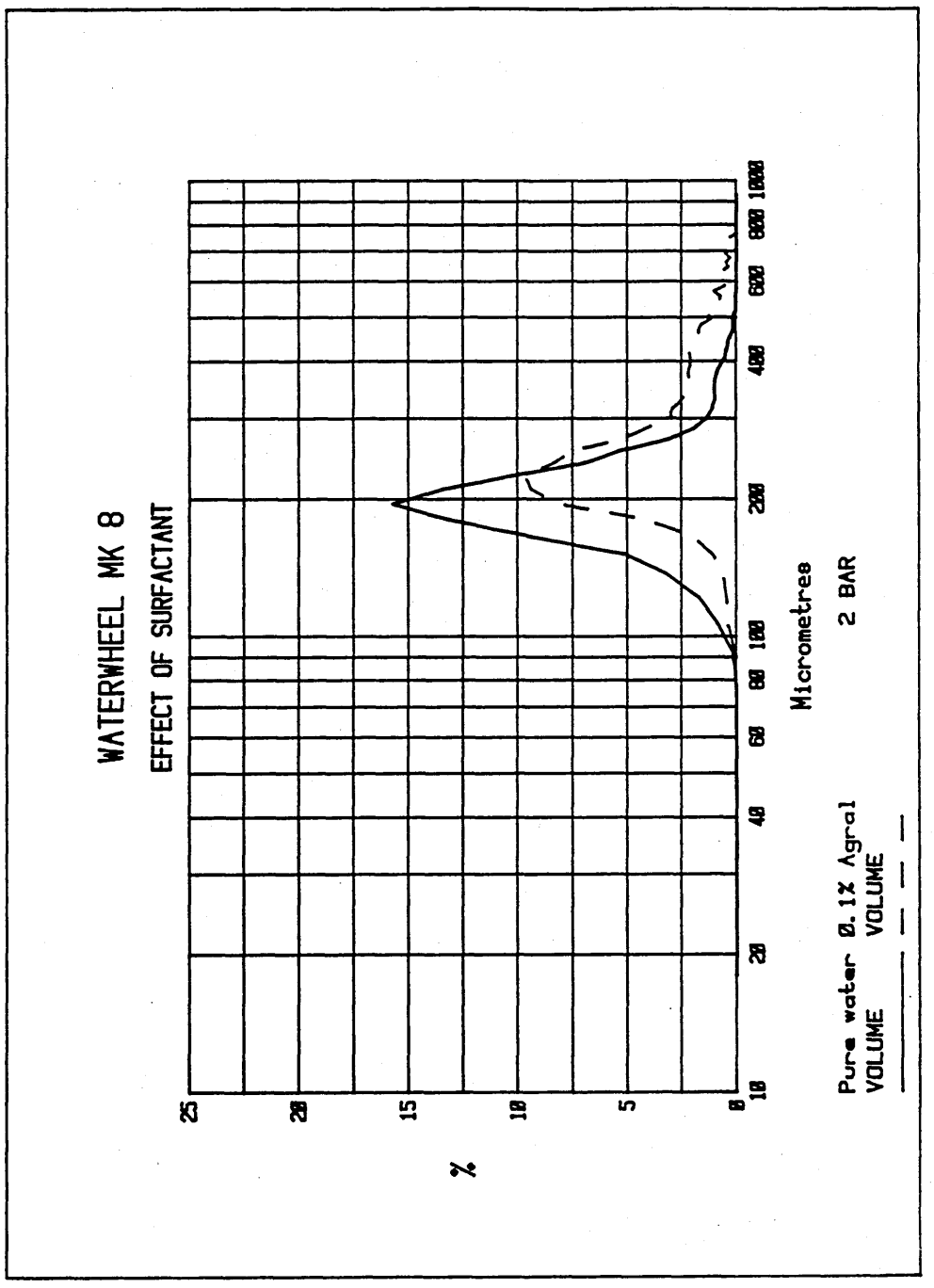

Figure 6.4.4g Minimal effect of high surfactant concentration on droplet spectra for Mk.8 (no weirs)

DDS 24

20% (v/v) HEAVY GLYPHOSATE ACID + SURFACTANT IN WATER

Atomiser prototype	WW Mk.8
Internal diameter of cup	44mm
Disc type and diameter	7 shaped grooves, 56mm, reversed
Nozzle orifice size	0.5mm, modified
Bearing	miniature ballraces
Substance sprayed	20% glyphosate in water
Test carried out	08/03/90

P (Bar)	N (RPM)	Q (ml/min)	NMD (um)	VMD (um)	Ratio	File, Record
.5						
1.0	2100	140	234	352	1.51	1,064
1.5	2710	165	213	369	1.73	1,065
2.0	3190	190	192	267	1.39	1,063
2.5	3600	210	187	283	1.51	1,066
3.0	4000	230	179	262	1.47	1,062
3.5						
4.0	4950	265	158	238	1.51	1,067
4.5						
5.0	5600	295	152	242	1.59	1,068

DDS 25

Atomiser prototype	WW Mk.7 (f) foaming with surfactant
Internal diameter of cup	44mm
Disc type and diameter	7 shaped grooves, 56mm
Nozzle orifice size	0.48mm, modified
Bearing	miniature ballraces, dry
Substance sprayed	0.1% Agral in tap water
Test carried out	16/11/90
Other information	BARC out

P (Bar)	N (RPM)	Q (ml/min)	NMD (um)	VMD (um)	R.Span	Ratio	File, Record
.5							
1.0							
1.5							
2.0	1915	170	274	388	.90	1.42	3,057,67
2.5	2750	185	201	267	1.15	1.33	3,058,66
3.0	3530	206	182	255	1.19	1.41	3,056,59
3.5	3860	218	174	255	1.17	1.46	3,064
4.0	4160	236	178	263	1.17	1.47	3,060,63
4.5	4550	254					
5.0	4880	266	163	270	1.27	1.66	3,061

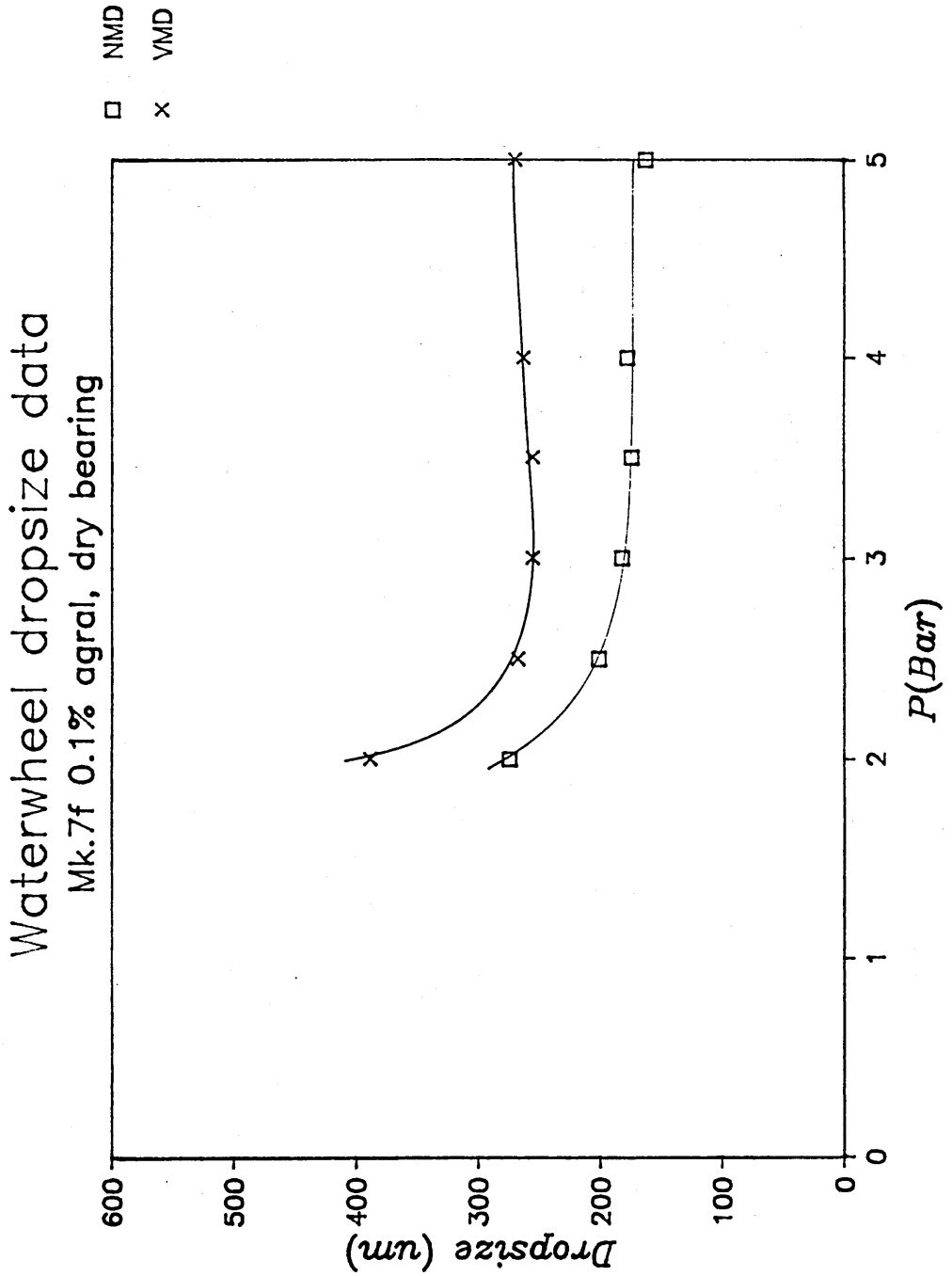

Figure 6.4.4h Dropsize vs supply pressure for Mk.7f with 0.1% surfactant in water:- foaming stops rotation below 2 bar pressure

DDS 26

Atomiser prototype	WW Mk.7 (b) glyphosate + midox
Internal diameter of cup	44mm
Disc type and diameter	7 shaped grooves, 56mm
Nozzle orifice size	0.48mm, modified
Bearing	miniature ballraces, lubricated
Substance sprayed	20% glyphosate + .02% m.antifoam in w
Test carried out	27/11/90

P (Bar)	N (RPM)	Q (ml/min)	NMD (um)	VMD (um)	R.Span	Ratio	File, Record
.5	1500	109	251	300	.87	1.20	4,039
1.0	2310	128	218	256	.75	1.17	4,038,40
1.5	2870	152	203	251	.82	1.24	4,037,41
2.0	3340	170	187	234	.78	1.25	4,036,42
2.5							
3.0	4200	202	173	223	.78	1.29	4,034,35,
3.5							
4.0	4960	228	167	214	.77	1.28	4,033,44
4.5							
5.0	5610	254	169	209	.80	1.24	4,032

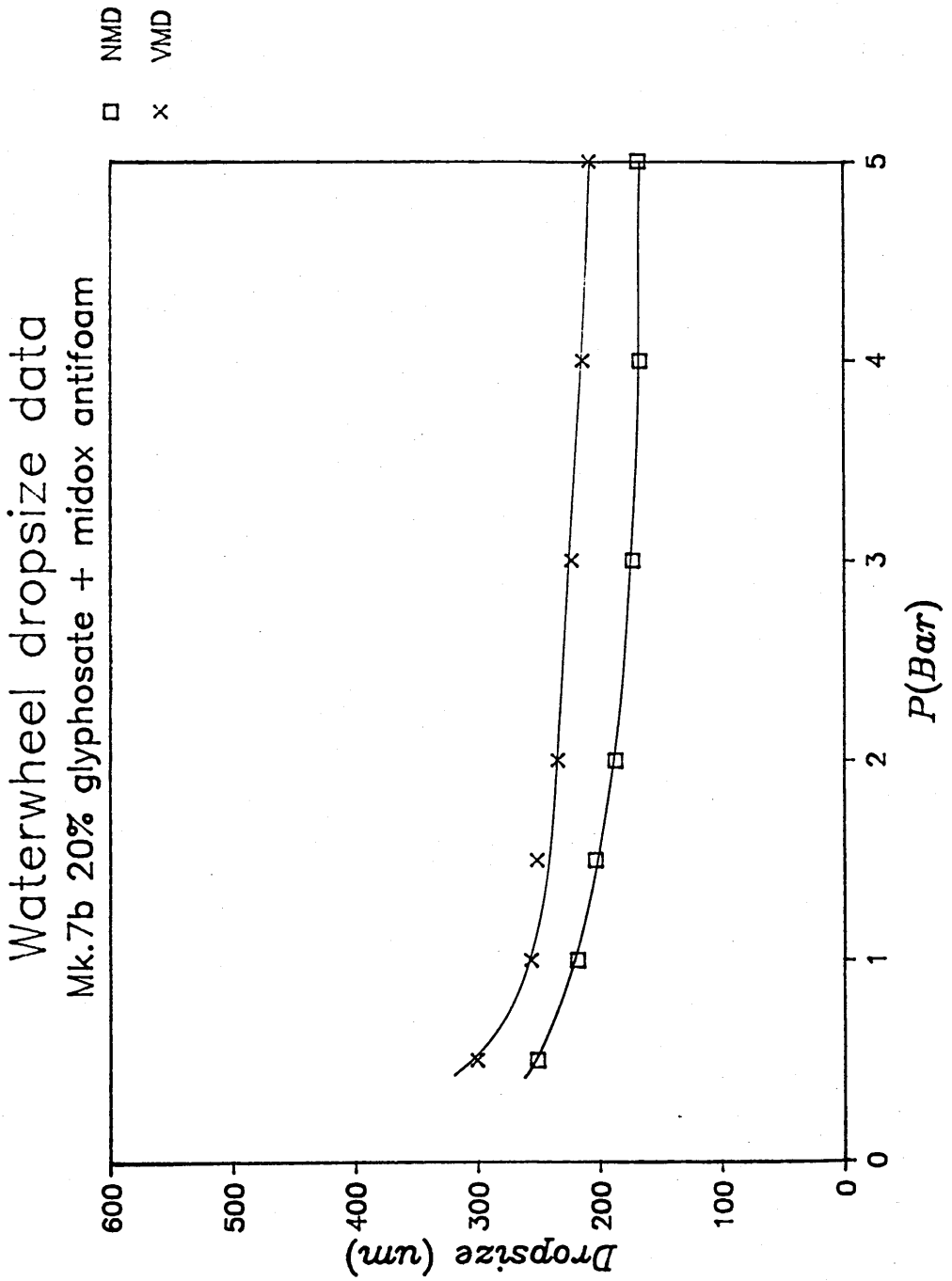

Figure 6.4.4i Dropsize vs supply pressure for Mk.7b; 20% glyphosate plus surfactant in water, with antifoam agent

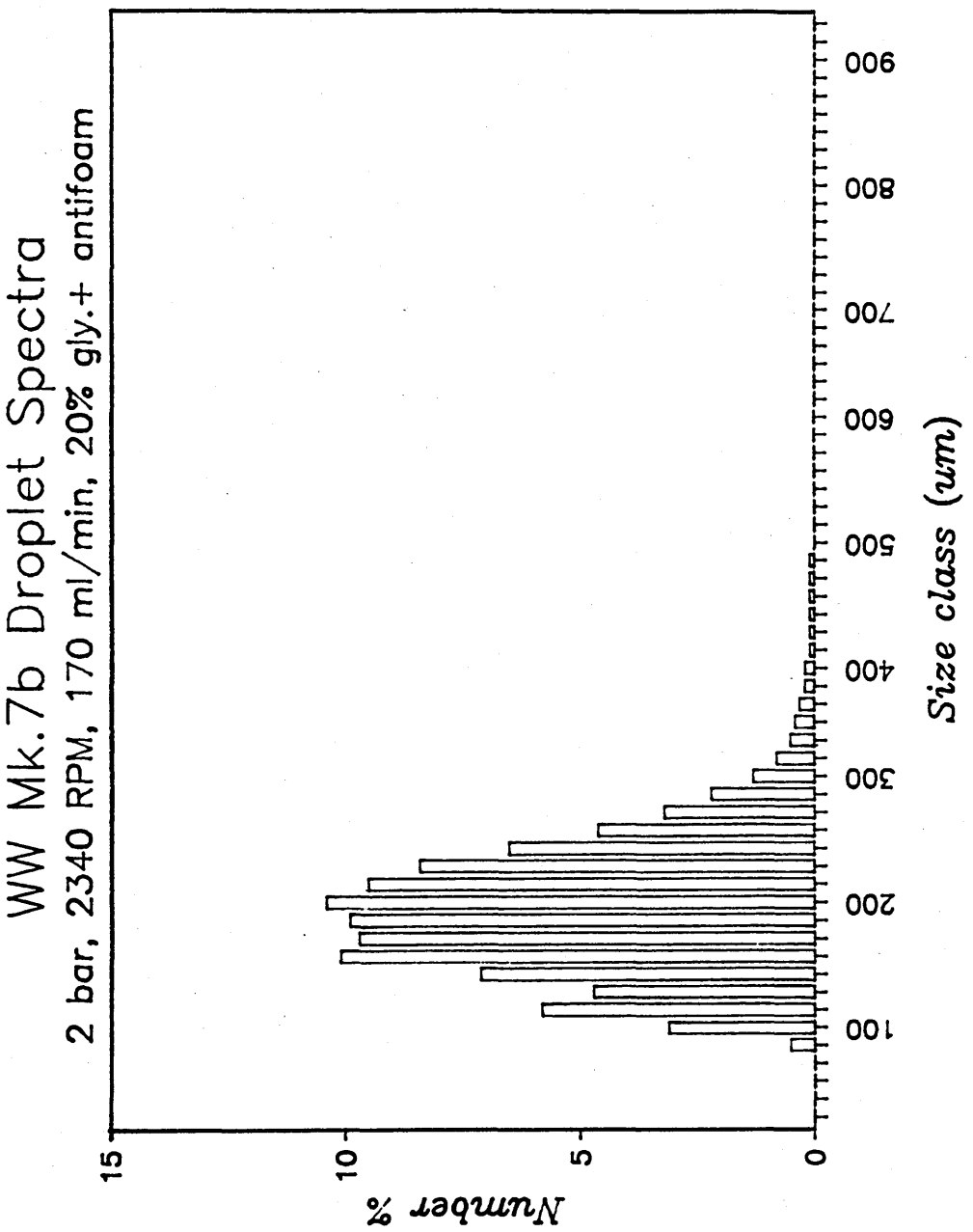

Figure 6.4.4j Droplet spectra produced by Waterwheel spraying glyphosate (Roundup^{tm}) at 2 bar supply pressure

DDS 27

Atomiser prototype	WW Mk.7 (g) effect of antifoam agent
Internal diameter of cup	44mm
Disc type and diameter	7 shaped grooves, 56mm
Nozzle orifice size	0.48mm modified
Bearing	miniature ballraces, dry
Substance sprayed	various
Test carried out	16/11/90
Other information	BARC out

P (Bar)	N (RPM)	Q (ml/min)	NMD (um)	VMD (um)	R.Span	Ratio	File, Record
10% glyphosate in water							
5.0	900	262	449	811	.44	1.81	3,068
10% glyphosate in water + 0.01% Midox antifoam agent							
1.5	1750	133	265	347	.87	1.31	3,071
2.0	2580	154	213	274	1.08	1.29	3,070
2.5	3000	175	200	274	1.07	1.37	3,072
3.0	3500	207	183	260	1.13	1.42	3,073
3.5							
4.0	4240	238	172	258	1.16	1.50	3,074
4.5							
5.0	4860	262	166	262	1.18	1.57	3,075
20% glyphosate in water + 0.01% Midox antifoam agent							
1.5							
2.0			stopped by foaming				
2.5							
3.0	2500	207	241	345	.91	1.43	3,076
3.5							
4.0	3160	238	213	294	1.02	1.38	3,077
4.5							
5.0	4820	262	167	262	1.16	1.57	3,078
20% glyphosate in water + 0.02% Midox antifoam agent							
1.5	1250	123	379	565	.63	1.49	3,082
2.0	1800	154	222	316	.94	1.42	3,083,90
2.5	2340	175	212	300	1.02	1.41	3,084,89
3.0	3500	207	195	285	1.07	1.46	3,079,85,
3.5	3870	223	179	259	1.14	1.45	3,086
4.0	4200	238	176	262	1.15	1.49	3,080
4.5	4500	252	169	258	1.18	1.53	3,087
5.0	4860	262	164	260	1.18	1.57	3,081

6.4.5 Effect of varying flowrate by adjusting nozzle orifice diameter

Droplet Data Summaries 28 and 29 correspond to tests carried out on Waterwheel Mk.3, to investigate the effect of increasing nozzle orifice diameter with both tap water, and 0.1% Agral in tap water. Each test was carried out at three supply pressures :- 3, 4, and 5 bar.

Summary 28 shows that the response of droplet size to increasing supply pressure is greater, the smaller the nozzle. At the lowest flowrate with water, provided by the 0.4mm nozzle, VMD is reduced by 168µm by increasing supply pressure from 3 bar to 5 bar. With the 0.6mm nozzle, this reduction is only 35µm.

Also worthy of note is the fact that the lowest VMD/NMD values are obtained at intermediate flowrates with the 0.5mm nozzle.

Summary 29 shows the same experiment carried out with 0.01% agral in water. Dropsizes in general are much coarser due to the presence of foam and for reasons explained in the previous section. VMD/NMD ratios generally increase towards the larger nozzle sizes. Effect on droplet spectra of increasing nozzle size at 5 bar is illustrated in Figure 6.4.5a.

Figure 6.4.5b show VMDs obtained for Mk.5 (0.62mm nozzle) and Mk.6 (0.5mm nozzle). The curves shows that slightly larger droplet sizes were obtained with the higher flowrate Mk.5 compared to Mk.6, although they are remarkably similar for saying that the flowrates were quite different. As one would expect the curve for the lower flowrate Waterwheel is slightly steeper initially, since bearing friction is playing a more important role.

Droplet Data Summary 30 consists of tests with Mk.7d with a nozzle orifice enlarged to 0.55mm. The data may be compared Mk.7a (0.47mm nozzle), Summary 15. The advantage of this particular comparison is that rotational speeds are almost identical, and therefore any differences in droplet spectra are likely to be due to flowrate alone. As one would expect, increased flowrate results in increased dropsizes.

Table 6.4.5 shows Q, NMD, and VMD data for constant rotational speeds, and from the differences of their logs, approximate power relationships between Q and dropsize are determined.

DDS 28

EFFECT OF NOZZLE ORIFICE DIAMETER ON DROPLET SPECTRA, WATER

Atomiser prototype	WW Mk.3
Internal diameter of cup	70mm
Disc type and diameter	> shaped grooves, 83mm
Nozzle orifice size	.4mm, .5mm, .6mm
Bearing	external electric motor (plain)
Substance sprayed	tap water
Test carried out	10/08/89

P (Bar)	N (RPM)	Q (ml/min)	NMD (um)	VMD (um)	Ratio	File, Record
.4mm nozzle orifice diameter						
3	1310	122	315	442	1.40	2,216
4	1750	138	247	291	1.18	2,215
5	2065	154	228	274	1.20	2,213,4
.5mm nozzle orifice diameter						
3	1200	240	351	412	1.17	2,200
4	1720	255	271	323	1.17	2,201
5	2100	270	230	280	1.22	2,208
.6mm nozzle orifice diameter						
3	1870	366	298	363	1.22	2,253
4	2410	420	230	339	1.36	2,254,5
5	2860	512	227	328	1.45	2,256

DDS 29

EFFECT OF NOZZLE ORIFICE DIAMETER ON DROPLET SPECTRA, AGRAL

Atomiser prototype	WW Mk.3
Internal diameter of cup	70mm
Disc type and diameter	> shaped grooves, 83mm
Nozzle orifice size	.4mm, .5mm, .6mm
Bearing	external electric motor (plain)
Substance sprayed	0.01% Agral in water
Test carried out	10/08/89

P (Bar)	N (RPM)	Q (ml/min)	NMD (um)	VMD (um)	Ratio	File, Record
.4mm nozzle orifice diameter						
3	1270	122	319	491	1.54	2,219
4	1720	138	254	303	1.19	2,218
5	2080	154	225	276	1.22	2,217
.5mm nozzle orifice diameter						
3	1040	170	343	528	1.54	2,222
4	1680	190	285	380	1.33	2,221
5	2010	220	237	318	1.34	2,220
.6mm nozzle orifice diameter						
3	990	450	372	665	1.79	2,225
4	1790	510	254	512	2.02	ns
5	2420	575	199	466	2.34	2,223

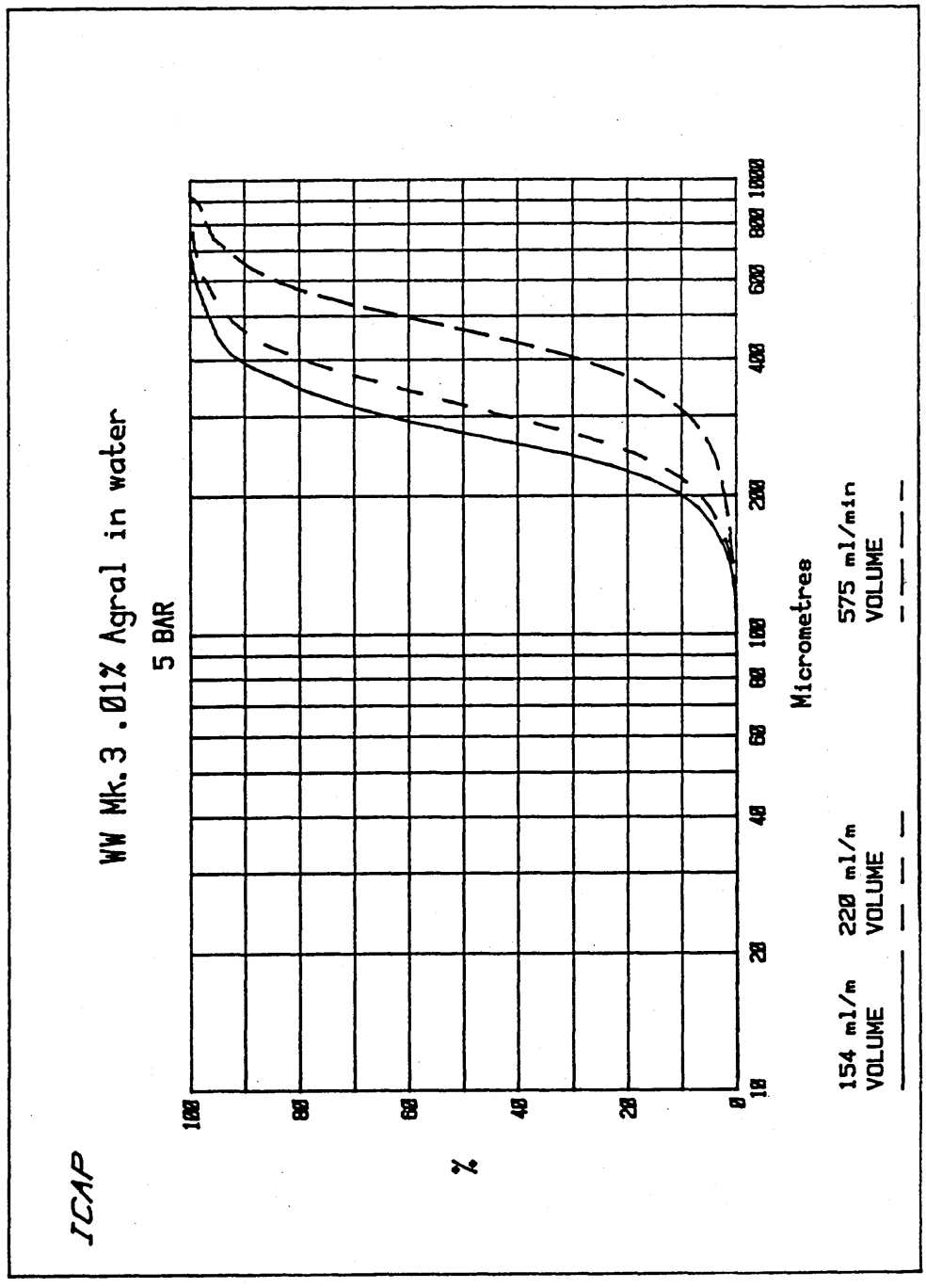

Figure 6.4.5a Effect of increasing nozzle orifice diameter on droplet spectra of Mk.3; 5 bar, 0.01% surfactant in water.

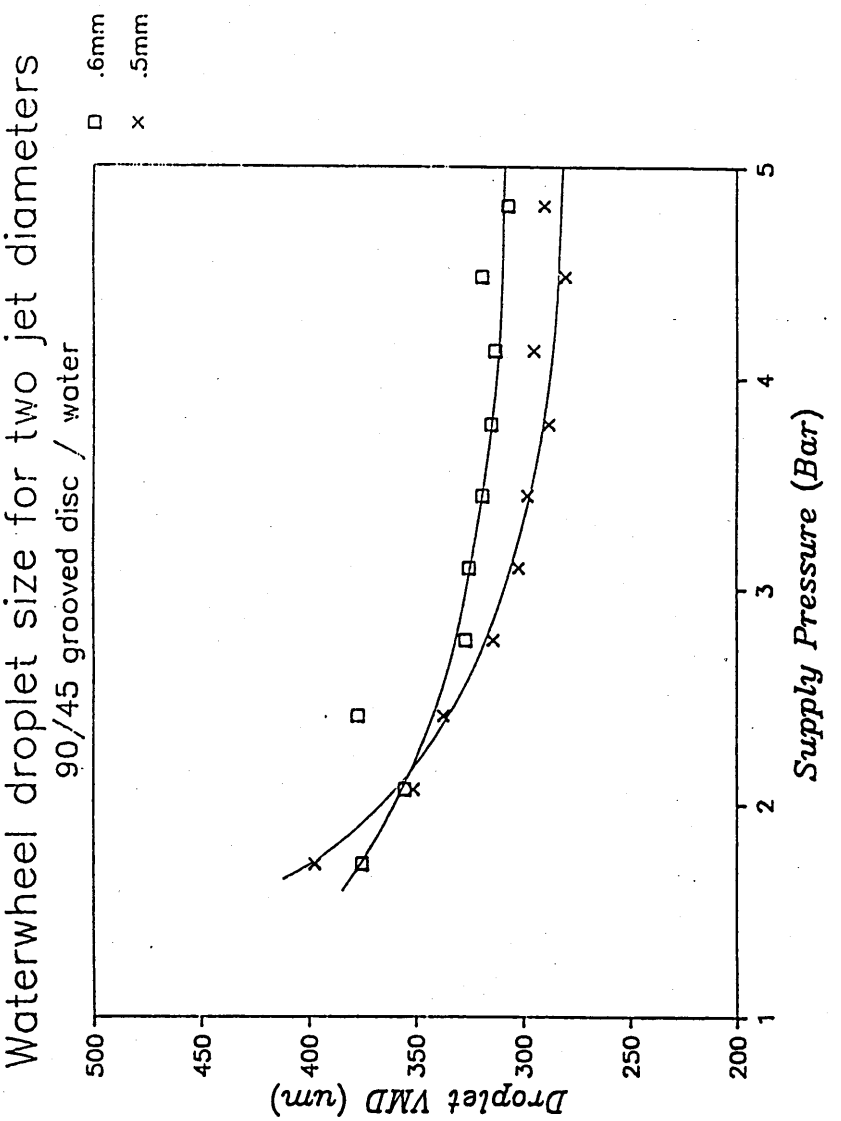

Figure 6.4.5b Droplet VMD vs supply pressure curves for 2 nozzle orifice diameters, tap water

DDS 30

Atomiser prototype	WW Mk.7 (d) enlarged orifice
Internal diameter of cup	44mm
Disc type and diameter	7 shaped grooves, 56mm
Bearing	miniature ballraces
Substance sprayed	tap water
Test carried out	27/11/90

Nozzle orifice diameter enlarged to 0.55mm

P (Bar)	N (RPM)	Q (ml/min)	NMD (um)	VMD (um)	R.Span	Ratio	File, Record
.5							
1.0							
1.5							
2.0	3470	236	203	267	.76	1.32	4,005
2.5	3920	260	192	256	.80	1.33	4,004
3.0	4330	284	184	247	1.02	1.34	4,003
4.0	5020	326	177	231	.81	1.30	4,006,7
5.0	5740	366	167	226	.85	1.35	4,002

Nozzle orifice diameter reduced by blockage

5.0	2780	75	208	250	.68	1.20	4,017

P (Bar)	Q .47mm	Q .55mm	NMD .47mm	NMD .55mm	VMD .47mm	VMD .55mm
2.0	164	236	190	203	233	267
2.5	185	260	181	192	228	256
3.0	200	284	171	184	217	247
4.0	230	326	165	177	212	231
5.0	260	366	159	167	204	226

	Q log diff.	NMD log diff.	VMD log diff.
2.0	.158068	.028742	.059155
2.5	.147802	.025623	.050305
3.0	.152288	.031822	.056237
4.0	.151490	.030489	.037276
5.0	.148508	.021319	.044478

	NMD = Q to power	VMD = Q to power
2.0	.181836	.374239
2.5	.173358	.340356
3.0	.208957	.369281
4.0	.201263	.246064
5.0	.143557	.299501

Table 6.4.5 Experimentally derived approximate power relationships between dropsize and flowrate, constant rotational speed.

6.4.6 Tests on various disc designs

Waterwheels Mk.1 to 3 possessed an atomising ring which had 80 shallow (0.75 mm depth) open "v" shaped grooves. Due to the fact that there was relatively high bearing friction and that high flowrates were required for satisfactory rotational speed, droplet spectra for Mk.1 to 3 were generally wide. VMD/NMD ratios were commonly above 1.4, and exceeded 2 at the higher pressures.

The reason for this behavior was identified visually using stroboscopic illumination. Fluid was not retained within the grooves even at the lower supply pressures. At higher pressures, flooding of the grooves occurred.

A similar disc with deeper grooves (1.5mm depth) was therefore manufactured. The results were still disappointing with VMD/NMD ratios still too high. However, if the bearing was made exceptionally smooth, and flowrates reduced to the minimum, satisfactory VMD/NMD ratios could be achieved, as shown for MK.4, Droplet Data Summary 11.

Initially, the next prototypes Mk.5 and Mk.6 had a disc with shallow "v"grooves. Records available for this disc with Mk.6 (Droplet Data Summary 31) show that atomisation was satisfactory at supply pressures above 3 bar with VMD/NMD about 1.3 to 1.4. However, at low rotational speeds VMD/NMD rose sharply to over 2.

Visual observation of the behavior of fluid accelerating along various rotating "v" section brass rods attached to the shorter of the spinning grooves (section 5.4), lead to the deduction that if the windward facing face of the groove was orientated perpendicularly to the direction of travel, fluid exit could be delayed. A disc with "7" shaped grooves was therefore manufactured and used for future tests with Mk.5 to 8.

A disc with cylindrical channels rather than grooves, which ensured no fluid slippage irrespective of flowrate was also manufactured (section 4.4). Droplet Data Summary 31 shows tests comparing this disc with the "7" shaped groove disc, for two nozzle diameters.

Droplet spectra produced for the two discs with the 0.5mm nozzle are quite similar; any differences are likely due to differences in rotational speed and are bearing related - an eternal problem with such a smooth bearing !. Comparing the results for the two discs with the larger nozzle, again the spectra are similar, with perhaps a marginally greater increase in VMD/NMD for the grooved disc at higher pressures.

One can therefore conclude that at satisfactory rotational speeds, no fluid slippage occured with the "7" grooved disc up to flowrates of 300 ml/min.

DDS 31

COMPARISON BETWEEN DIFFERENT DISC TYPES
WW Mk.6 / internal diameter 44mm / miniature ball races / tap wate:

Low flowrate, nozzle orifice diameter 0.5mm

P (Bar)	N (RPM)	Q (ml/min)	NMD (um)	VMD (um)	R	File, Record
80 (7) shaped grooves, pointed teeth, (24/08/89)						
2.0	1380	200	372	449	1.21	2,275-6
2.5	1750	220	316	362	1.15	2,277
3.0	1965	235	294	331	1.13	2,273-4
4.0	2550	260	261	304	1.17	2,267-9
5.0	2960	280	237	290	1.22	2,270-2
80 (o) cylindrical channels, pointed teeth, (24-09-89)						
2.0	1540	200	323	366	1.13	2,353-4
2.5	1890	220	295	340	1.15	2,355-6
3.0	2040	235	278	322	1.16	2,347-8
4.0	2625	260	258	308	1.20	2,349-5
5.0	2970	280	241	293	1.21	2,351-2

Intermediate flowrate, nozzle orifice diameter 0.55mm

P (Bar)	N (RPM)	Q (ml/min)	NMD (um)	VMD (um)	R	File, Record
80 (7) shaped grooves, pointed teeth, (29/08/89)						
2.0	1765	235	323	389	1.21	2,379-8
2.5	2055	260	291	353	1.21	2,381-2
3.0	2317	280	267	327	1.22	2,377-8
4.0	2810	315	245	314	1.28	2,373-4
5.0	3320	345	223	294	1.32	2,375-6
80 (o) cylindrical channels, pointed teeth, (29-09-89)						
2.0	1625	235	321	369	1.15	2,285
2.5	1950	260	291	337	1.16	2,280,8
3.0	2220	280	273	321	1.18	2,281
4.0	2770	315	261	312	1.19	2,282
5.0	3270	345	220	278	1.26	2,279,8

COMPARISON BETWEEN DIFFERENT DISC TYPES ..... continued
WW Mk.6 / internal diameter 44mm / miniature ball races / tap wate

Low flowrate, nozzle orifice diameter 0.5mm

P (Bar)	N (RPM)	Q (ml/min)	NMD (um)	VMD (um)	R	File, Record
80 (o) disc minus protective ring and distance piece, (29-08-89)						
2.0	1770	200	292	329	1.13	2,367-8
3.0	2350	235	252	298	1.18	2,366
4.0	2840	260	237	291	1.23	2,365
5.0	3330	280	233	283	1.22	2,364
80 > shaped grooves, pointed teeth, (29-08-89)						
2.0	1650	200	287	635	2.21	ns
3.0	2390	235	237	331	1.39	2,369
4.0	2950	260	244	321	1.32	2,370
5.0	3440	280	225	302	1.34	2,371
No disc ! (29-08-89)						
2.0	2000	200	315	754	2.39	ns
3.0	2950	235	305	409	1.34	2,360-1
4.0	3830	260	264	336	1.27	2,357,9
5.0	4760	280	243	319	1.31	2,362

6.4.7 Effect of weirs on droplet uniformity, and peripheral distribution of fluid.

Tables 6.4.7a and b show dropsize measurements, with the PMS probe placed with the laser at various points around the atomiser relative to the position of the nozzle. The precise locations of the 45° interval sample positions are illustrated in Figure 6.4.7.

Variation in dropsize with position is expressed in terms of the standard deviation of the obtained NMD and VMD values. The reader may note that the S.D. values obtained for the weired prototypes (Mk.2, Mk.6 and Mk.7c are significantly lower than those obtained with the weirless versions Mk.8 and Mk.9. VMD values for Mk.6, 8 and 9 are illustrated in the upper diagram of Figure 6.4.7a.

All of the tests took place with water at 3 bar, except the last test with Mk.9. One must conclude that weirs are necessary if peripheral evenness in dropsize is required.

The variation in local flowrate with position was also recorded. Fluid output into eight segments was measured around the Waterwheel using peripherally arranged collectors. Deviation from the mean output with position is expressed in the lower diagram of Figure 6.4.7a and roughly corresponds to the variation in dropsize found with the dropsizing system shown in the upper figure.

Additionally, a series of local flowrate tests took place with differing numbers of weirs in Mk.6 prototype, 3 bar with water. The objective of the tests was to investigate whether less than the full compliment of 4 weirs could be used for the same effect. Where a weir would be missing, the gap left was replaced with a spare ring, to simulate a smooth wall with the same inner radius as that of the lower cup.

Table 6.4.7c summarises the experiments with the weirs in their respective positions, and labelled according to the number of slots each contains. Standard deviation of the local output obtained in each 1/8 th segment is included.

The results with just one weir in place show that the position of this weir is important ie. it has more effect in evening out the flow the lower down the cup it is placed.

Finally, Figures 6.4.7b-g are bar histograms of the flowrate per collector measured over a time period of eight minutes, with 4, 3, 2, 1 and 0 weirs in their correct respective positions. The S.D values obtained are expressed at the top right hand corner of each Figure.

The results show that the optimum number of weirs is obviously the full compliment of four, with ascending numbers of slots of 5, 10, 20 and 40 respectfully, leading to the 80 grooves on the atomising disc.

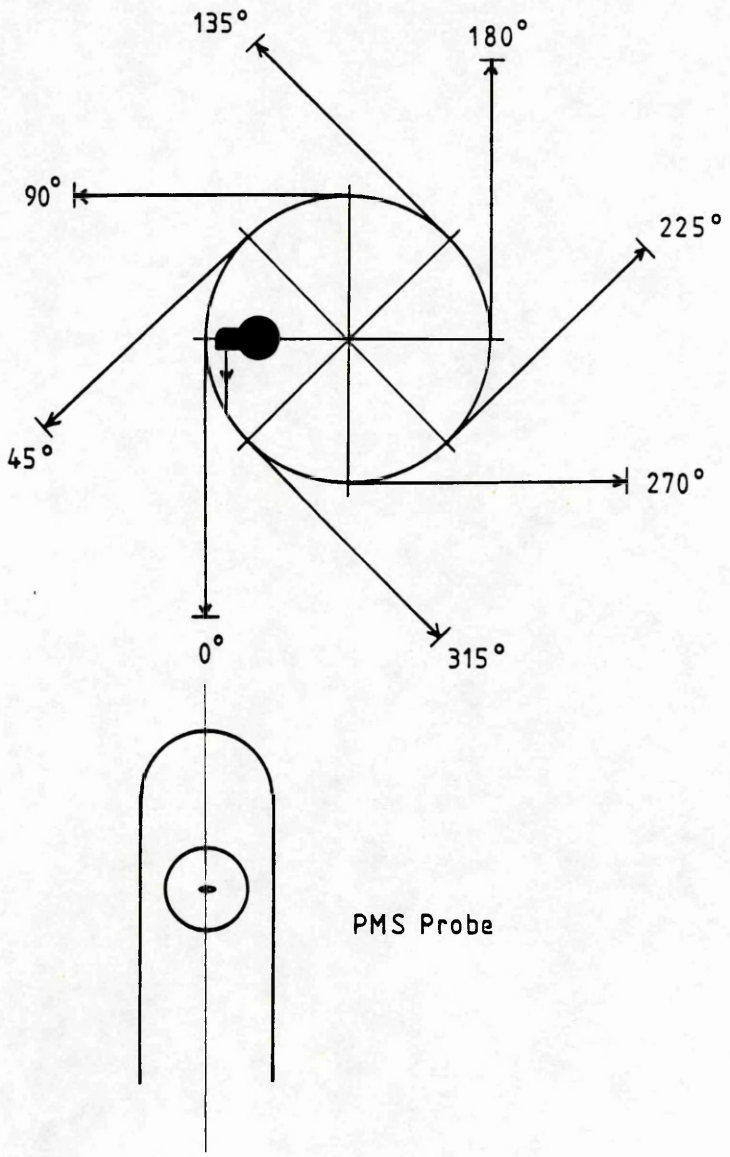

Figure 6.4.7 Peripheral sample positions; degrees behind jet, with respect to direction of rotation

Table 6.4.7a Peripheral variation in dropsize for Waterwheels Mk.2, Mk.6 and Mk.7 with weirs

WW Mk.2 (four weirs) 50 PSI, 2259 RPM, 144 ml/min (Kinnersley)

Sample position behind nozzle	NMD (um)	VMD (um)	R
0	170	248	1.46
45	165	243	1.47
90	179	243	1.36
135	158	257	1.63
180	155	254	1.64
225	180	246	1.37
270	189	249	1.32
315	184	252	1.37
360	170	248	1.46
S.D.	10.92	4.48	.11

WW Mk.6 (four weirs) 3 bar, 3300 RPM, 220 ml/min, water

Sample position behind nozzle	NMD (um)	VMD (um)	R	File Record
0	220	305	1.38	1,151
45		309		
90	217	298	1.36	1,152
135		293		
180	219	293	1.34	1,153
225		294		
270	218	296	1.36	1,154
315		309		
360	220	305	1.38	1,151
S.D.	1.17	6.37	.01	

WW Mk.7c (four weirs) 3 bar, 3520 RPM, 200 ml/min, water

Sample position behind nozzle	NMD (um)	VMD (um)	R	File Record
0	191	245	1.28	3,009
45	192	246	1.28	3,010
90	194	247	1.28	3,011
135	195	248	1.28	3,012
180	195	249	1.28	3,013
225	195	249	1.28	3,014
270	194	249	1.28	3,015
315	193	246	1.28	3,016
360	191	244	1.28	3,017
S.D.	1.56	1.76	.00	

Table 6.4.7b Peripheral variation in dropsize for Waterwheels Mk.2, Mk.6 and Mk.7 without weirs

WW Mk.8 (no weirs) 3 bar, 4180 RPM, 220 ml/min, water

Sample position behind nozzle	NMD (um)	VMD (um)	R	File Record
0	162	225	1.39	1,135,136,143
45	163	204	1.25	1,146
90	162	208	1.29	1,141,142
135	172	218	1.27	1,147
180	174	229	1.32	1,139,140,148
225	184	244	1.32	1,149
270	189	261	1.39	1,137,138,144
315	189	279	1.44	1,150
360	162	225	1.39	1,135,136,143
S.D.	11.05	23.22	.06	

WW Mk.9 (no weirs) 3 bar, 2100 RPM, 300 ml/min

Sample position behind nozzle	NMD (um)	VMD (um)	R	File Record
0	293	373	1.27	1,117,125
45				
90	224	244	1.09	1,118,119
135				
180	263	301	1.15	1,116,120,123-4
225				
270	318	373	1.18	1,121,122
315				
360	293	373	1.27	1,117,125
S.D.	32.22	52.43	.07	

WW Mk.9 (no weirs) 5 bar, 2100 RPM, 300 ml/min

Sample position behind nozzle	NMD (um)	VMD (um)	R	File Record
0	204	227	1.12	1,094
45				
90	222	243	1.10	1,096
135				
180	255	294	1.14	1,097
225				
270	249	283	1.15	1,098
315				
360	206	230	1.12	1,094
S.D.	21.27	27.77	.02	

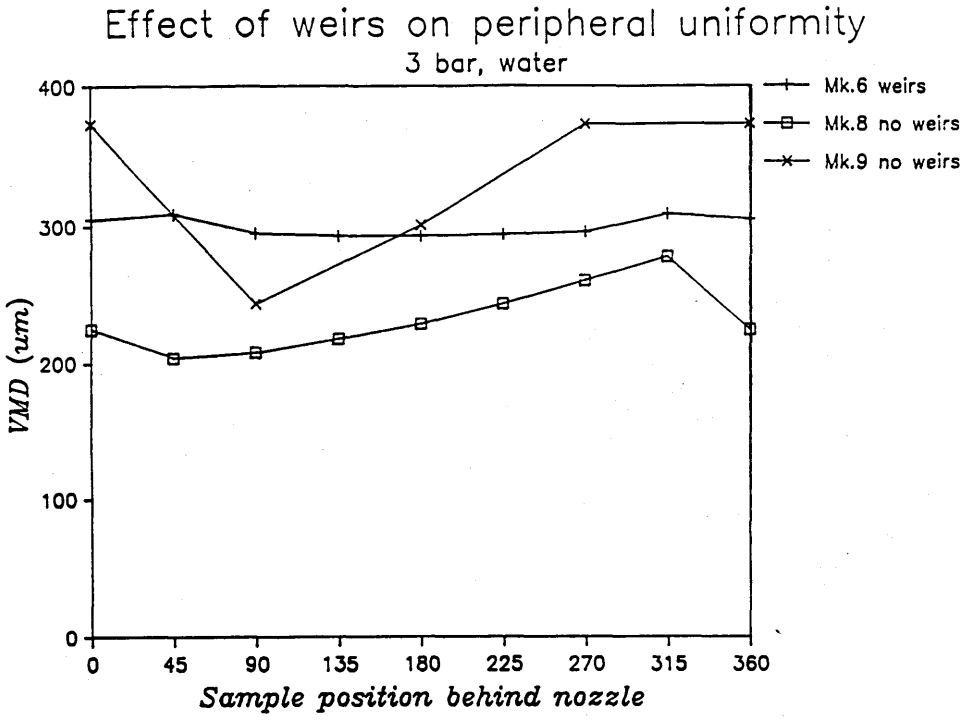

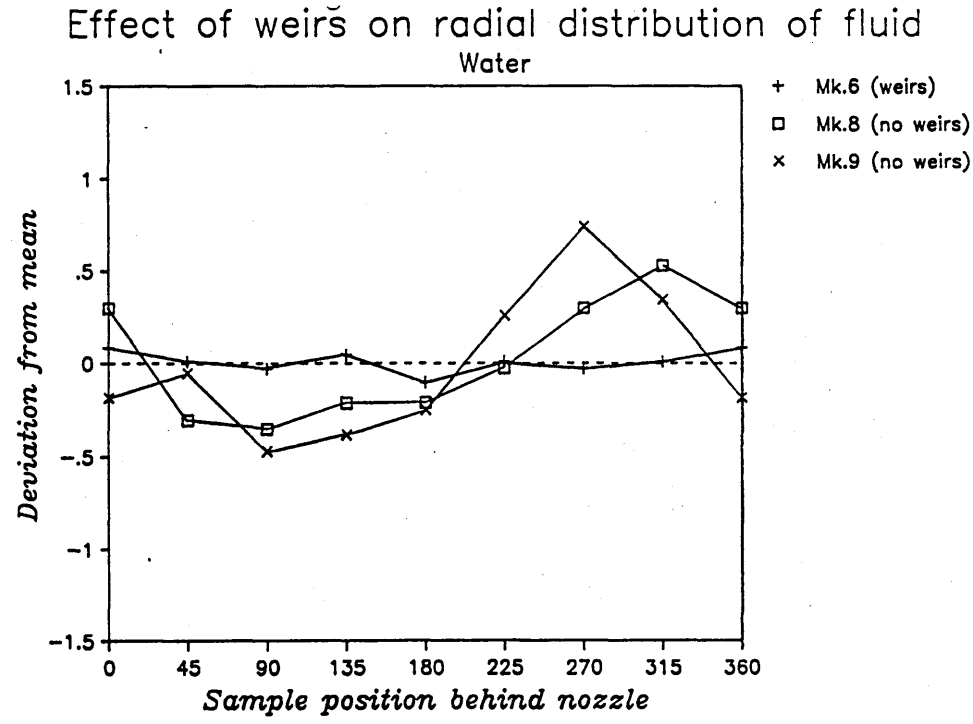

Figure 6.4.7a Peripheral dropsize and fluid distribution measurements for Mk.6, Mk.8, and Mk.9

Expt No.	Base	Top	S.D.
1	4 weirs	(5 10 20 40)	5.79
2	3 weirs	(5 10 20 -)	9.62
3	2 weirs	(5 10 - -)	13.49
4	1 weir	(5 - - -)	24.38
5	no weirs	(- - - -)	34.01
Experiments with one weir			
6	1 weir	(5 - - -)	24.38
7	1 weir	(- 5 - -)	33.26
8	1 weir	(- - 5 -)	40.18
9	1 weir	(- - - 5)	67.97
Experiments with two weirs			
10	2 weirs	(- 40 - 5)	21.81
11	2 weirs	(- 10 - 5)	14.04

Table 6.4.7c Summary of peripheral distribution experiments for WW. Mk.8 with various weir arrangements 3 bar, water

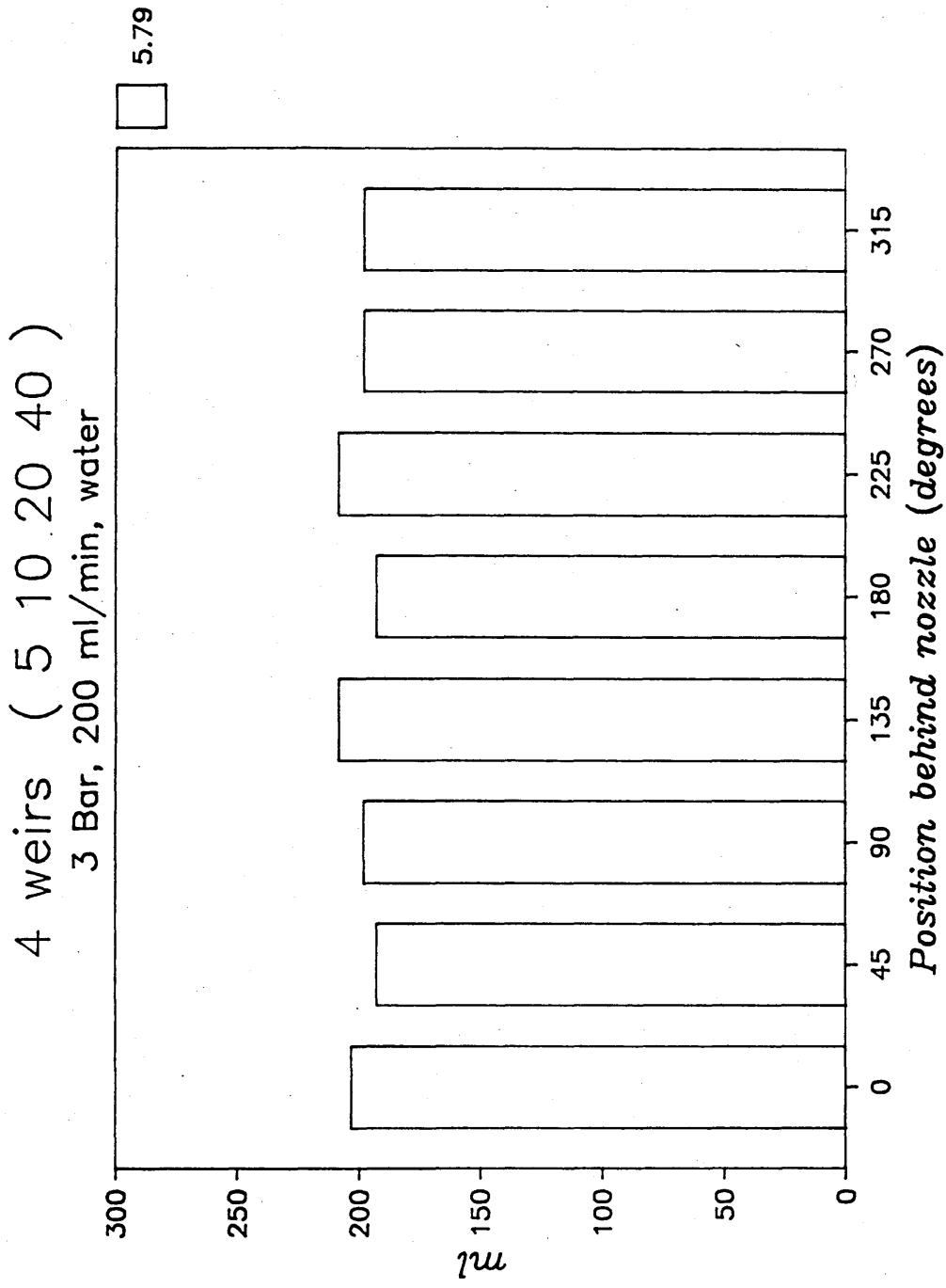

Figure 6.4.7b Peripheral uniformity with 4 weirs

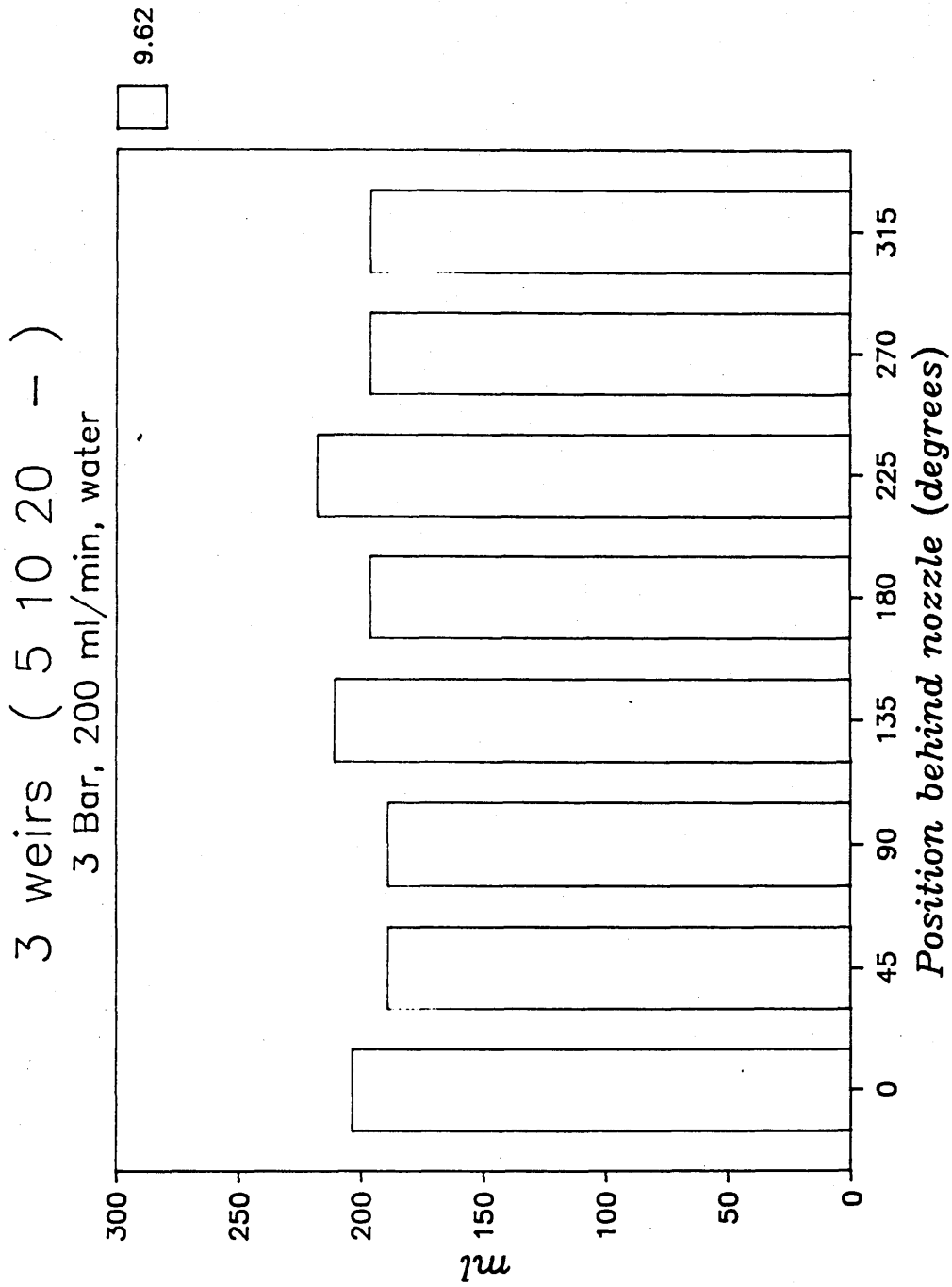

Figure 6.4.7c Peripheral uniformity with 3 weirs

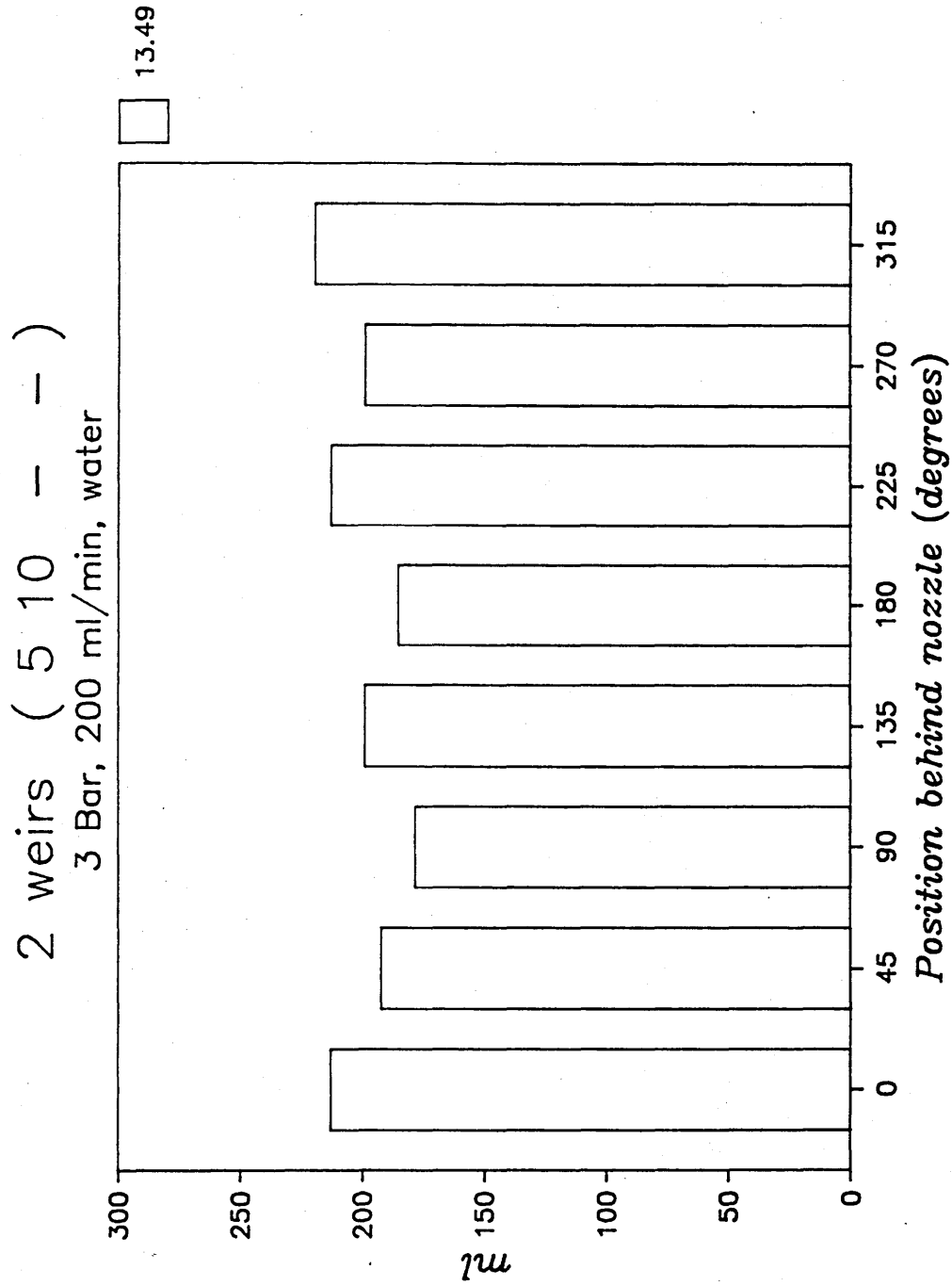

Figure 6.4.7d Peripheral uniformity with 2 weirs

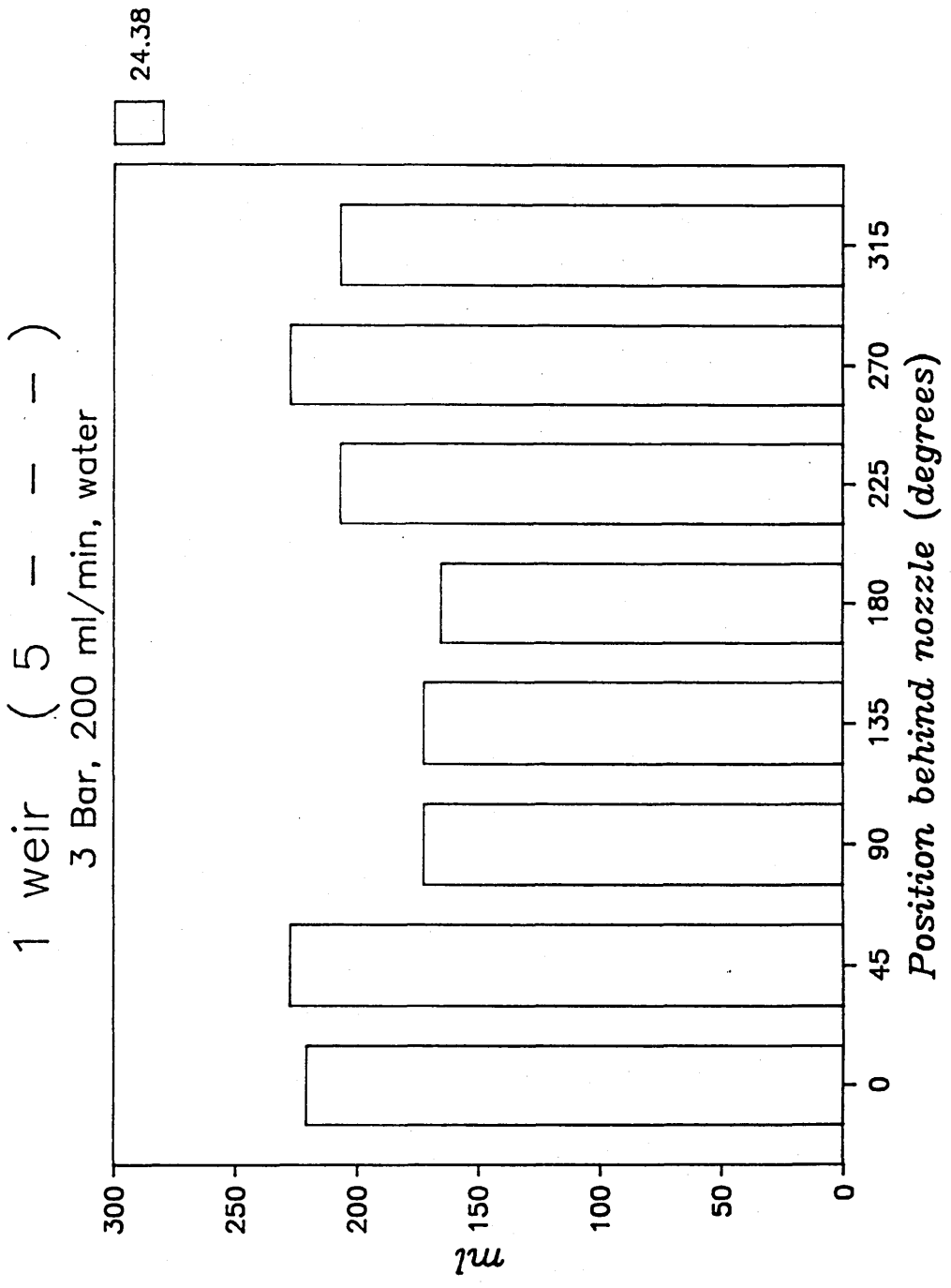

Figure 6.4.7e Peripheral uniformity with 1 weir

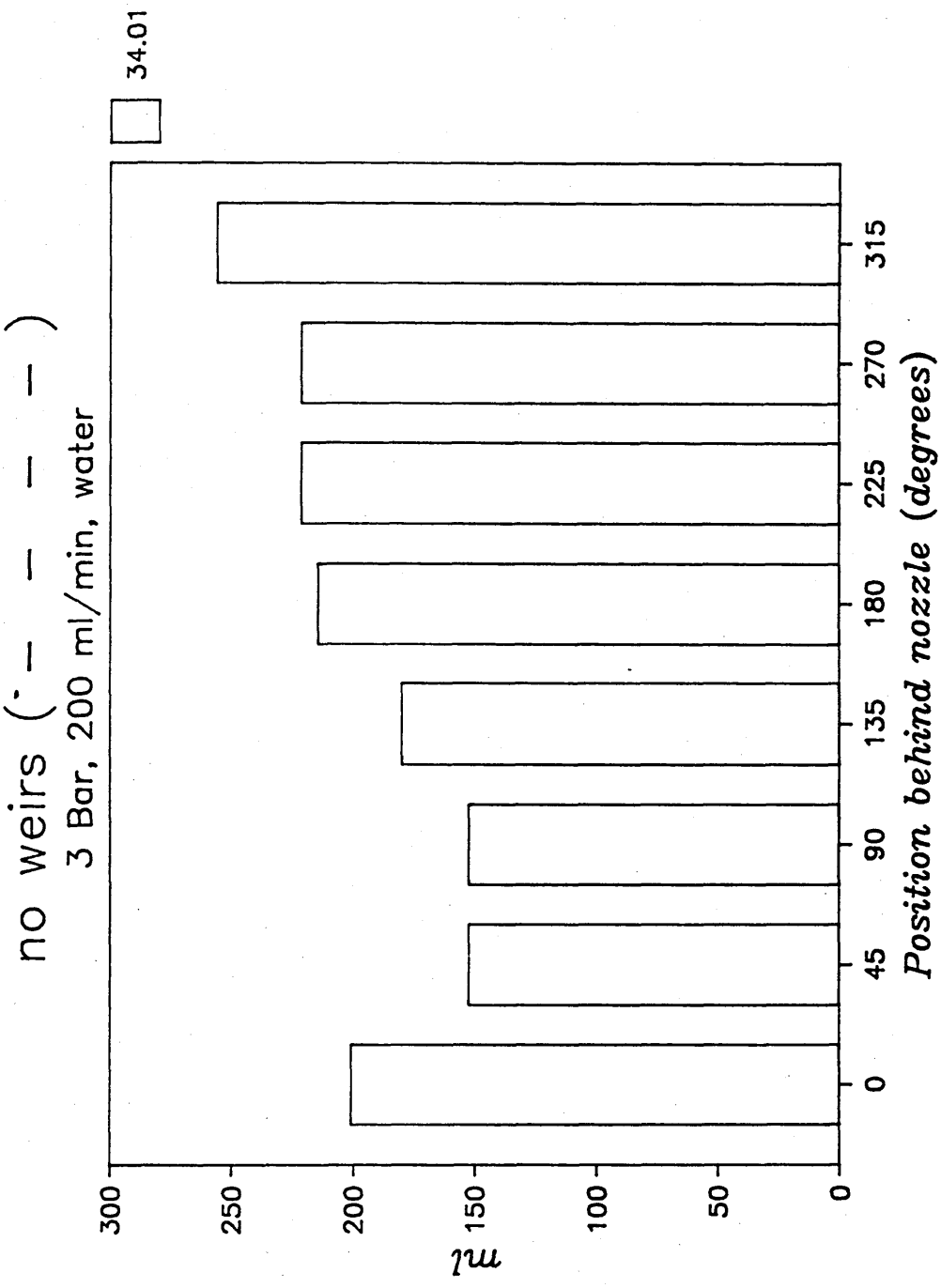

Figure 6.4.7f Peripheral uniformity with no weirs

Chapter Seven

PERFORMANCE MODEL

7.1 Theoretical analysis of Waterwheel performance

In Chapter 3 the theory of Pelton Wheels was discussed, and an expression for the energy provided by change of momentum of the jet as it strikes the inner wall of the cup was derived. Refering to equation (50):

$$\text{Energy input per second} = mV_I(V_J\cos\Theta - V_I)$$

where V_J and V_I are initial and final speeds of the jet, and m is the mass flow per second, which can be expressed ρAV_J, where A = cross sectional area of nozzle exit.

Energy output is associated with fluid leaving the atomiser at an increased speed V_E. V_E is the vector sum of the tangential velocity at the point of emission, wr_o, and the radial velocity there. Assuming no losses, the radial velocity is $w(r_o^2-r_i^2)$. In reality, surface tension and friction effects on the radial flow causes some energy to be lost in heat. However, the disc has been designed so that these losses are reduced to a minimum. For the purposes of a simple model to predict rotation speed and approximate droplet size, they have therefore been ignored.

Thus energy output is equal to :

$$\begin{aligned}
\tfrac{1}{2}mV_E^2 &= \text{Total final K.E.} - \text{Total initial K.E.} \\
&= \tfrac{1}{2}m[w^2r_o^2 + w^2((r_o^2-r_i^2)] - \tfrac{1}{2}mw^2r_i^2 \\
&= \tfrac{1}{2}mw^2[r_o^2 + r_o^2 - r_i^2 + r_i^2] \\
&= mw^2(r_o^2-r_i^2) \qquad (160)
\end{aligned}$$

A further energy loss which cannot be ignored is that associated with friction in the bearing, air resistance or windage, and fluid drag. This combined energy loss may be expressed as the total energy loss, Tw where T is the total non-useful torque.

Balance of energies yields:

Energy transferred by jet	=	Kinetic Energy supplied to liquid	+	Energy lost in bearing

$$mV_I(V_J\cos\theta - V_I) = mw^2(r_o^2 - r_i^2) + Tw \qquad (161)$$

where m = mass flow per second
V_J = velocity of jet
V_I = inner wall velocity
V_T = tip velocity
r_i = inner wall radius
ro = radius at which fluid is shed from teeth
T = total non-useful torque
w = rotation rate

dividing by m

$$V_I(V_J\cos\theta - V_I) = w^2(r_o^2 - r_i^2) + Tw/m \qquad (162)$$

alternatively

$$wr_iV_J\cos\theta - w^2r_i^2 = w^2r_o^2 - w^2r_i^2 + Tw/m \qquad (163)$$

dividing by w

$$r_iV_J\cos\theta = wr_o^2 + T/m \qquad (164)$$

rearranging

$$\boxed{w = \frac{V_Jr_i\cos\theta}{r_o^2} - \frac{T}{mr_o^2}} \qquad (165)$$

If T is zero, is constant with respect to w, or varies linearly with w, equation (165) can be solved directly.

since $V_I = wr_i$

$$V_I = \frac{V_J r_i^2 \cos\Theta}{r_o^2} - \frac{Tr_i}{mr_o^2}$$

$$= V_J \cos\Theta . (r_i/r_o)^2 - \frac{T}{pAV_J} (r_i/r_o^2)$$

$$= V_J \cos\Theta . (r_i/r_o)^2 - \frac{T}{V_J} (r_i/pAr_o^2) \qquad (166)$$

or simply

$$= K V_J - C (T/V_J) \qquad (167)$$

where $K = (r_i/r_o)^2 \cos\Theta$
$C = (r_i/pAr_o^2)$

7.2 Prediction of dropsize based upon viscous fluid radial velocity

Size of droplets produced by the Waterwheel has been related by a simple factor, f_B, to a theoretical prediction of the initial undisturbed ligament radius $d_{(LIG)}$. $d_{(LIG)}$ has been derived from an estimation of final radial velocity of the fluid upon leaving the disc, allowing for viscous losses during acceleration. The method is described fully in section 4.4.4.

In summary, the the relationship between dropsize and viscous fluid radial velocity, V_R, is :

$$d_{(DROP)} = f_B \; d_{(LIG)} \qquad (169)$$

since flowrate per tooth m/n = ρAV

$$d_{(DROP)} = f_B \left[\frac{4m/n}{\rho \pi V_R} \right]^{1/2} \qquad (170)$$

For an inviscid fluid, $d_{(DROP)}$

$$= f_B \left[\frac{4m/n}{p\pi \left[\frac{V_J r_i \cos\Theta}{r_o^2} - \frac{T}{m r_o^2} \right] (r_o^2 - r_i^2)^{1/2}} \right]^{1/2} \quad (171)$$

where: Vj and m are pressure dependant terms.

Accounting for viscous losses during passage of fluid along 45° vertically sided grooves (from equation 132, section 4.4.4), $d_{(DROP)}$ =

$$= f_B \left[\frac{4m/n}{p\pi \left[a/b^2 \{ (br_o - 1) - (br_1 - 1).e^{b(r_1 - r_o)} \} \right]^{1/2}} \right]^{1/2}$$

where $a = 2w^2$, and $b = 4.828\ kv/q$

To predict dropsize in the following model, these f_B values have been used:

for NMD ; $f_B \approx 1.8$ (173)

for VMD ; $f_B \approx 2.2$ (174)

7.3 Simple computer model to predict rotational speed and dropsize

To simulate all the experimentally derived data successfully, the total non-useful torque, T has been treated as a complex function of w. Equation (165) has then been solved iteratively using a spreadsheet program

Table 7.3 is a spreadsheet which acts in a similar fashion to a computer program to predict Waterwheel performance, based upon equation (165). The following are parameters which can be input by the user :

1) exterior diameter of disc, R_o (mm)

2) interior diameter of disc, R_i (mm)

3) nozzle clearance, or distance between centre of jet and inner wall, d_c (mm)

4) supply pressure, P (Bar)

5) linear regression coefficients, b and c, for Coefficient of Discharge, Cd, of the nozzle type used, where:

$$C_d = b\,(P)^{1/2} + c$$

6) liquid density, ρ, (kgm^{-3})

7) nozzle orifice diameter, d_o, (mm)

8) number of teeth on disc, n

9) polynomial regression coefficients A, B, and C for bearing friction, F (Nm), where:

$$F = A(w^2) + B(w) + C$$

10) geometric regression coefficients f and g, for fluid drag on nozzle, D (Nm), where:

$$D = f(w)^g$$

N.B. (F + D) is defined as the total non-useful torque, T

Equation (165) is then solved using iteration, using constants chosen by the user.

Constants b and c were derived for the general nozzle type (section 4.1) by regression performed on the flowrate data in Table 6.3.1c. A linear relationship between Cd and $P^{½}$ was found to have a high correlation coefficient, implying that losses are proportional to jet velocity, V_J.

Constant C may be thought of simply as representing the load independant bearing friction (section 4.2.4). If a constant value for T is all that is required, A, B, f and g can be set to zero.

Constant B may be made negative to provide high starting friction and simulate the effect of lubrication. It may also simulate load dependant friction, caused by weight of fluid in the cup, which is less at higher rotational speeds. This improved agreement between experimental and theoretical results for Mk.9 (Figure 7.1n) which had a stiff, lubricated plain bearing.

Constant A represents the increase in friction suffered by bearings as they reach high rotational speeds, and probably also the effect of windage. However, this does not really come into effect until much higher speeds are reached than those obtainable with the Waterwheel. This therefore generally has a very low value.

The last term $f(w)^g$ makes T increase very suddenly as w reaches small values, so long as g is negative, and represents the fluid layer inside the cup increasing causing fluid drag on the nozzle.

By no means should the equations for non-useful torque be taken as fundamentally correct; they are merely a convenient way of expressing how T must have varied with *w*, to produce the experimental results obtained.

Model predictions

The model has been primarily used to predict performance for a number of supply pressures, so that comparisons can be made with experimental data.

Figure 7.2a shows that with non-useful torque set to zero (ie no energy losses due to bearing friction or fluid drag ie A,B,C,F and g are set to 0), the model predicts a straight line for Vi verses Vj. The line closely corresponds to Vi = ½Vj, agreeing with classical Pelton Wheel theory, Chapter 3. Experimental results for Waterwheel prototype

Mk.7b, which had a well lubricated bearing with friction lie just below this theoretical line for T = 0.

The upper diagram of Figure 7.3b however, shows that the Vi vs Vj fit is improved, if a small constant for bearing friction (F = 0.05mNm) is introduced.

The lower diagram of Figure 7.3b is the predicted energy expenditure budget for Waterwheel Mk.7b. The reader will notice that energy lost in bearing friction is small, and is less than the fluid kinetic energy at all pressures above 0.5 bar.

Figure 7.3c is a dropsize prediction based upon viscous fluid radial velocity (Chapter 5). NMD and VMD values are based upon 1.8 $d_{(LIG)}$ and 2.2 $d_{(LIG)}$ respectively according to Rayleigh theory, Chapter 2. Agreement with experimental data for Waterwheel Mk.7b is close for all pressures above 0.5 bar.

Figure 7.3d shows the predicted effect of increasing total non-useful torque, T, from 0 to 1.5mNm. With increasing constant values for T, the Vi vs Vj lines fall away from Vi = ½Vj, although more so at lower jet velocities. Values for torque are in mNm (equal to 1/1000th Nm)

Figure 7.3 e shows experimental Vi vs Vj points for Mk.7e, which had an unlubricated and therefore slightly stiffer bearing; the theoretical Vi vs Vj line for T = 0.25 mNm has been superimposed for comparison.

Agreement is reasonably close except towards the low energy end, where experimental Vi/Vj suddenly decreases and becomes zero. This represents a breakdown in the theory with T constant at this point.

The reason for this behavior is most likely due to there being insufficient rotational energy for removal of liquid from the cup. The fluid layer therefore builds up in thickness resulting in drag against the nozzle causing further slowing.

Therefore, inorder to obtain better agreement between the theory experimental results where non-useful torque T, was a larger proportion of the total, it was found necessary to treat T as a complex function of *w*.

A statistical package was used to obtain a relationship between T and w, for each experiment. so that when equation (165) was solved iteratively using the relationship, the theoretical Vi vs Vj curve would fit the experimentally obtained data. So in effect, the rotational performance of the Waterwheel was now being used to measure total energy loss, to provide a relationship which could be used for

further predictions. This was a useful approach to take since it provides a means of describing what happens to dropsize if bearing friction is too high.

Figure 7.3f illustrates the statistically derived relationship between rotation rate and non-useful torque. This gives rise to a satisfactory curve fit for Vi vs Vj illustrated in the upper diagram of Figure 7.3g.

The lower diagram of Figures 7.3g illustrates the energy expenditure for Mk.7e. In contrast to Figure 7.3b, it may be observed that non-useful energy is generally a much greater proportion of the total; liquid kinetic energy does not exceed it until a supply pressure of approximately 2 bar is reached. At this point the Waterwheel may be said to be 50% efficient.

Figure 7.3h shows the corresponding dropsize prediction for Mk.7e. 1.8 $d_{(LIG)}$ and 2.2 $d_{(LIG)}$ agree reasonably well above 2 bar. Disagreement below 2 bar however is probably due to tendancy towards atomisation in direct droplet mode. The slight rise in experimental VMD values at higher pressures is due to the measurement of coincident droplets (the BARC was not fitted, Chapter 6). Such an increase is not apparent in other tests for Waterwheel Mk.7 with the BARC in place.

The model is particularly useful to the designer interested in the effects of changing physical dimensions of the various components of the Waterwheel. For example, Figures 7.3i shows predicted effects on Vi vs Vj and rotation rate, of varying nozzle orifice diameter on Mk.7, with a high bearing friction of 0.5mNm.

A similar exercise has been repeated for the latest Waterwheel prototype Mk.9 with lubricated PTFE plain bearing (Figures 7.3j-m), and for the earliest Waterwheel tested, prototype Mk.3 (Figures 7.3o-q). Dropsize predictions are satisfactory indicating that the model is successfully predicting the dropsize from atomisers with differing geometry.

Figure 7.3r shows dropsize predictions for four nozzle sizes for Mk.3. The diagram shows the degree of complexity of the relationship between flowrate and dropsize; the relationship appears to be totally different for each supply pressure used. The model is therefore useful in explaining the experimental results of Mk.3.

The model has also attempted to provide an answer to a very complicated question : "what is the effect of changing the size of the atomiser on dropsize ?" With this question it is assumed that supply pressure, flowrate and bearing friction are held constant, and rotational speed is allowed to vary, since this is dependant on diameter.

Figure 7.3s shows that there is an optimum external disc diameter for minimum dropsize, of around 60mm for the constant value of bearing friction chosen. If a higher friction value was chosen, then this optimum value for diameter would increase.

It is therefore important that the friction of the bearing is known, in the design of any future fluid propelled atomiser. This can be entered into the model, along with the other parameters 1) to 9), inorder to provide a satisfactory performance prediction.

Table 7.3 Spreadsheet model with formulas used to predict Waterwheel performance

Waterwheel Model Mk7a			
w = (Ri.Vj cosθ - T/m)/Ro²			
or			
w = Ri.Vj.cosθ /Ro² - T/mRo²			
GEOMETRY SUB-ROUTINE			
Enter ext. diameter of disc, Do (mm)	56		
Enter int. diameter of cup, Di (mm)	44		
Enter nozzle clearance, d (mm)	3		
Ro (m)		.028	E9/2000
Ri (m)		.022	E10/2000
d (m)		.003	E11/1000
cosθ		.8636364	(F13-F14
Ro²		.000784	(F12)^2
(Rt² + Ri²)		.001268	((F12)^2
c = ƒ(1 - (Ri/Ro)²)		.619	(1-(F13/
ENTER SUPPLY PRESSURE TIMEBASE		3.0	3
JET VELOCITY SUB-ROUTINE			
Enter regression coefficients for Cd			
where Cd = b(JSP) + c			
b	-.045832		
c	.881361		
Cd		.8019776	$E$27*(G21)^.5+$E$28
Enter liquid density (kg/m3)	1000		
Jet velocity, Vj (m/s) =		19.644	$G30*(2*G21*1E5/$E32)^.5
Vj cos θ		16.966	G33*$F15
FLOWRATE SUB-ROUTINE			
Enter nozzle diameter (mm)	.47		
Flowrate, Q, (ml/min) =		204.4913	PI/4*(($E38*1E-3)^2*6033*6041E6
Mass flowrate, m, (kg/s) =		.003408	$E32*PI/4*(($E38*1E-3)^2*G33
Enter tooth number, n	80		
m/n (kg/sec/tooth) =		.0000426	G40/$E41
q (m^3/sec/groove) =		4.260e-8	G39*1E-6

FRICTION SUB-ROUTINE			
Enter regression coefficients for F			
where F = Aw^2 + Bw + C			
A	1e-10		
B	1e-7		
C	2.5e-4		
FLUID DRAG SUB-ROUTINE			
Enter regression coefficients for D			
where D = fw^g			
f	4e0		
g	-2.5e0		
		3	3
ITERATION ROUTINE			
w (no friction) = Ri.Vj cosθ / Ro^2		476.075	$F13$G34/$F16
w (w(nf) to clear, mean value to start)		363.377	G70
T = F(quadratic) + D(geometric)		.0003011	E49$G$66^2+E50$G$66+$E$51+E57$G$66^($E$58)
Torque term = T/(m.Ro^2)		112.698	(G67)/G40/$F16
w (with friction) = w(nf) - T/(m.Ro^2)		363.377	$F13$G34/$F16-G68
mean value		363.377	(G66+G69)/2
PREDICTIONS			
N = w$60/2π		3470	G70/2/PI$60
Vi = wRi		7.994	G70$F13
Vt = wRo		10.175	G70$F12
Max. inviscid velocity, Vr(inv) = w.√(Ro²-Ri²)		6.294	G70$($F1
Waterwheel Mk.7e results with water			
P (Bar)		3	3
N (RPM)		3530	3530
Vi (m/s)		8.133	G85/60$2$PI$$F13
Bearing friction torque, F, Nm		.0002995	$E49$G66^2+$E50$G66+$E51
Fluid nozzle drag torque, D, Nm		.0000016	$E57$G66^($E58)

****

ENERGY EXPENDITURE (in Watts)

Input energy = $mVi(Vj\cos\theta - Vi)$	.2444322	G40*G76*(G34-G76)
Liquid kinetic energy = $mw^2(Ro^2 - Ri^2)$	.1350081	G40*G70^2*($F12^2-$F13^2)
Non-useful energy = Tw	.1094242	G97-G99
Torque (CHECK)	.0003011	G100/G70

****

VISCID FLUID RADIAL VELOCITY ROUTINE

Enter velocity profile factor, k = 3
Enter kinematic viscosity, v .000001

Flowrate localisation factor
q(local)/q 1

a = 2w^2	264085.8	2*(G70)^2
b = 4.828kv/q(local)	339.981	4.828*$E109*$E110/(G43*$E$113)
a/b^2	2.285	G115/(G116)^2
(bRo-1)	8.519476	G116*$F$12-1
(bRi-1)	6.479588	G116*$F$13-1
e^b(Ri-Ro)	.1300433	EXP(G116*($F$13-$F$12))

Equation 132 for annulus (inc. viscosity)
$Vr = [a/b^2\{(bRo-1) - (bRi-1).e^b(Ri-Ro)\}]^{1/2}$ 4.188022 (G117*(G118-(G119*G120)))^.5

DROPSIZE ROUTINE

Ligament diameter, d Lig (μm) = $\sqrt{(4q/\pi Vr)}$		114	((4*G43)/(PI*G123))^.5*1E6
d(DROP)/d(LIG) factor for NMD	1.8	205	$E131*G129
d(DROP)/d(LIG) factor for VMD	2.2	250	$E132*G129

Waterwheel Mk.7e dropsize data		
P (Bar)	3.0	3
NMD (μm)	194	194
VMD (μm)	247	247

TOTAL DROPLET VELOCITY REL. TO AIR

V (drop) = $\sqrt{(Vt^2+Vr^2)}$ 10.42793 (G77^2+G117^2)^.5

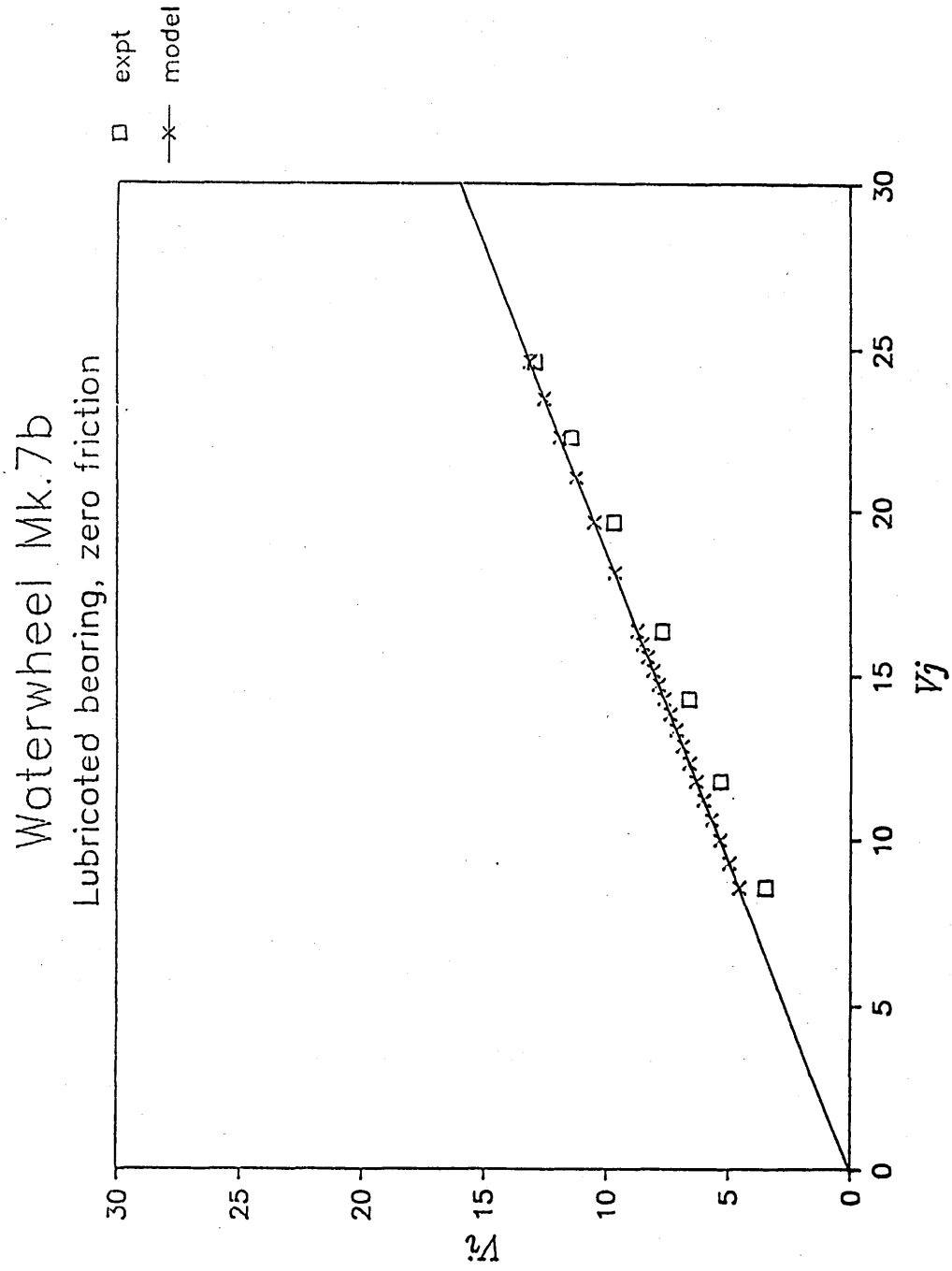

Figure 7.3a Prediction of rotational performance for Waterwheel Mk.7b, with zero frictional torque

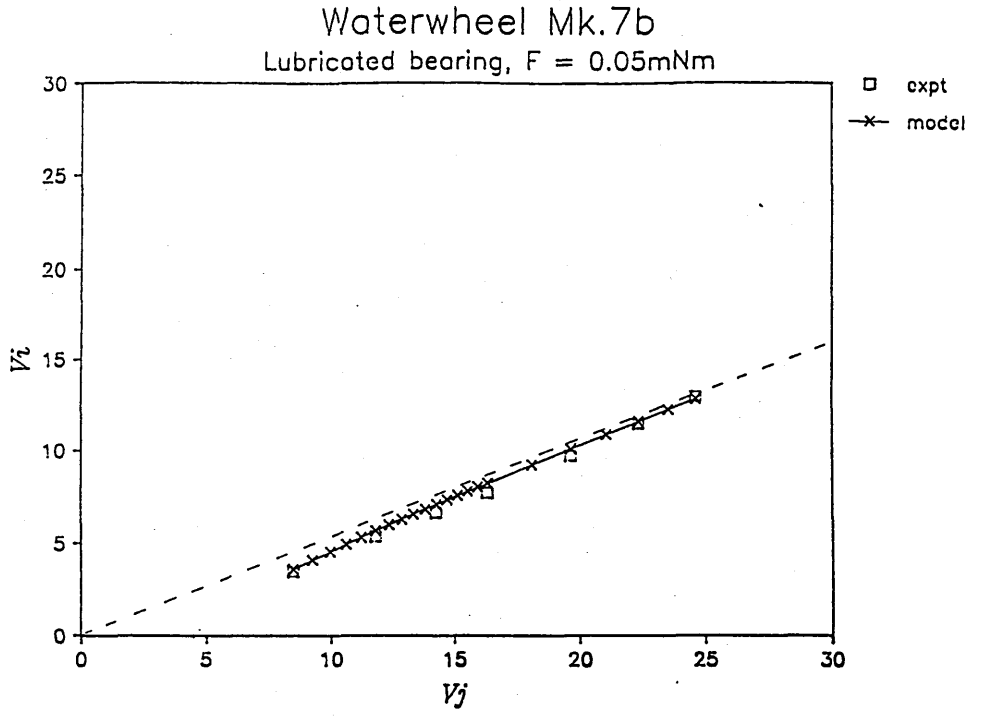

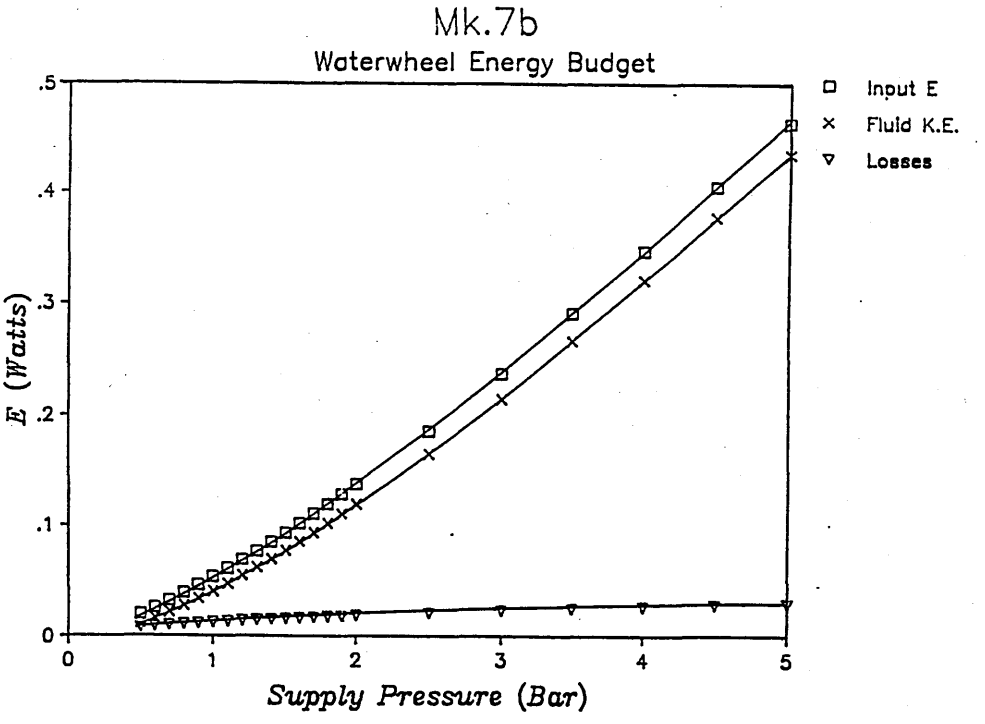

Figure 7.3b Prediction of rotational performance and energy expenditure for Waterwheel Mk.7b, with constant frictional torque

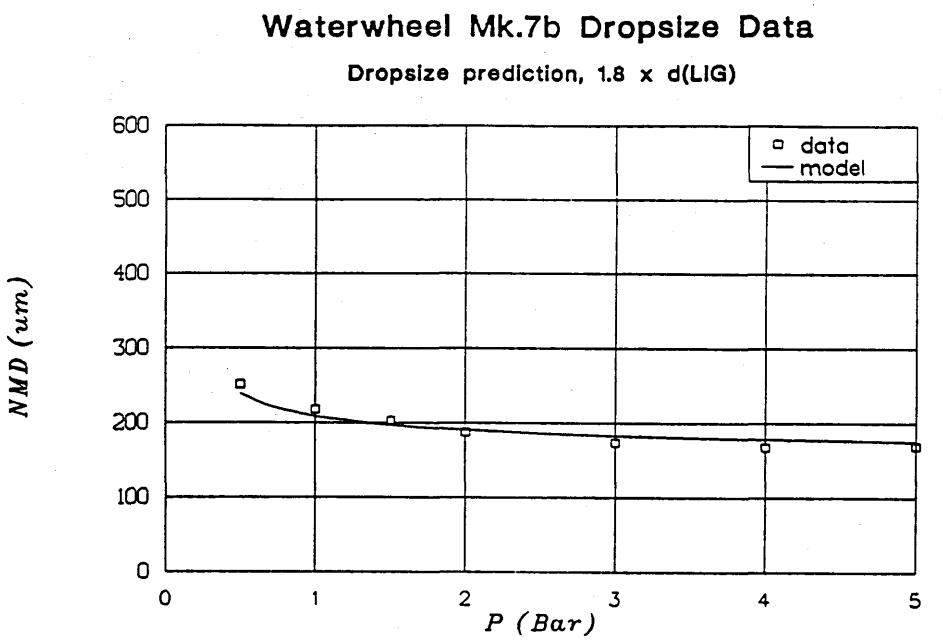

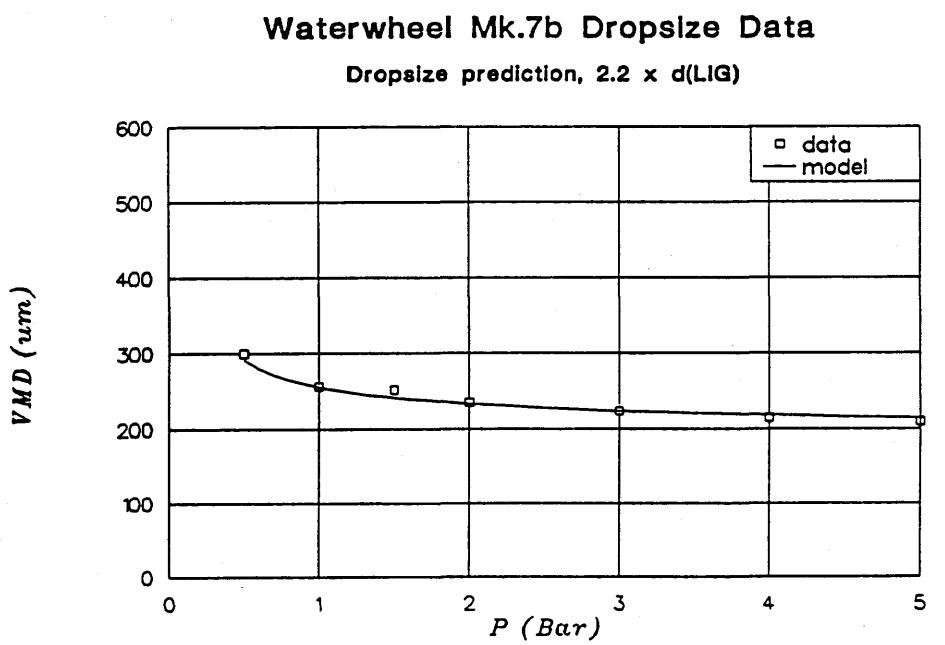

Figure 7.3c Prediction of dropsize for Waterwheel Mk.7b

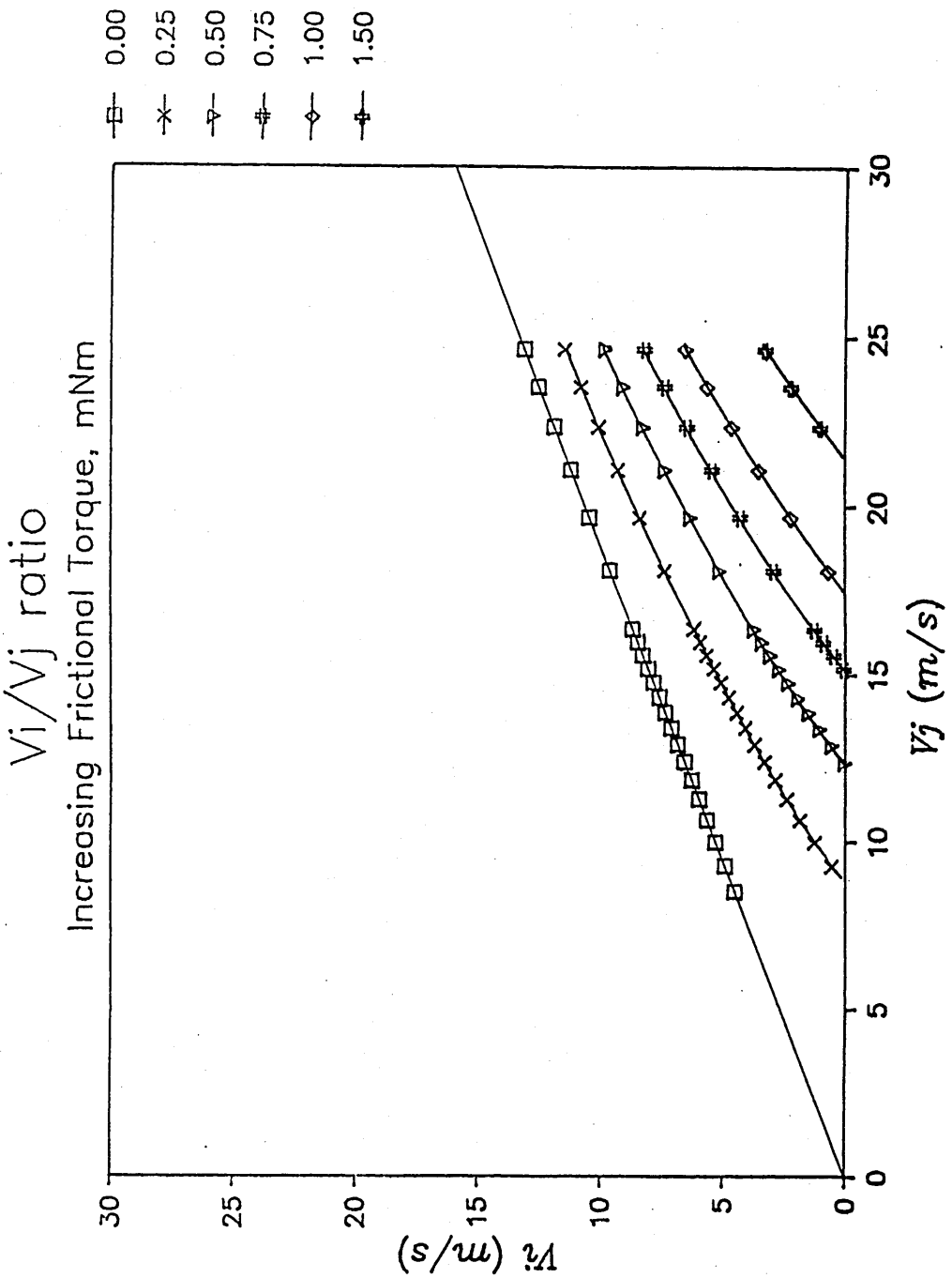

Figure 7.3d Prediction of the effect of increasing frictional torque of the bearing on rotational performance of Mk.7

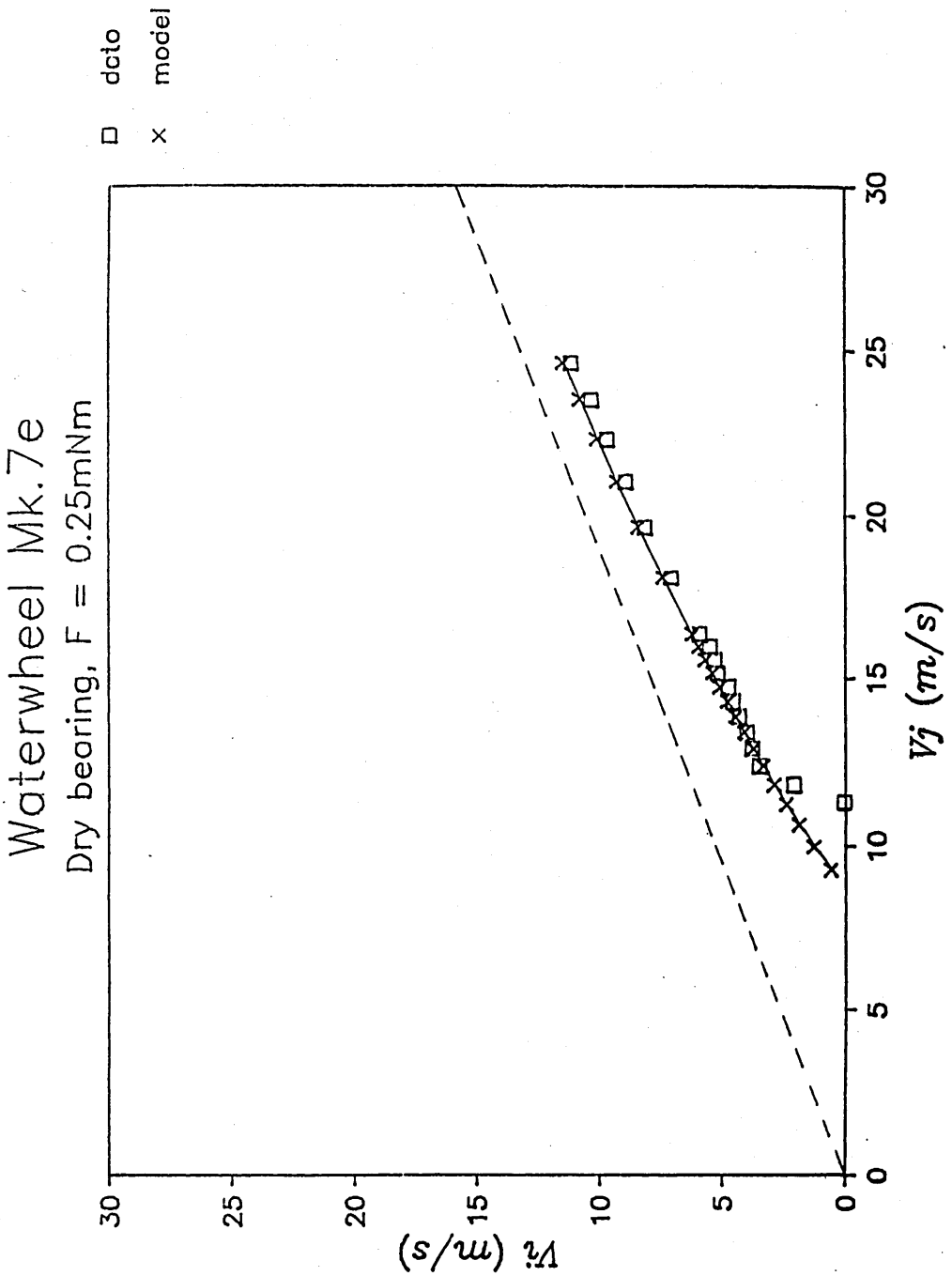

Figure 7.3e Prediction of rotational performance for Waterwheel Mk.7e, with constant frictional torque

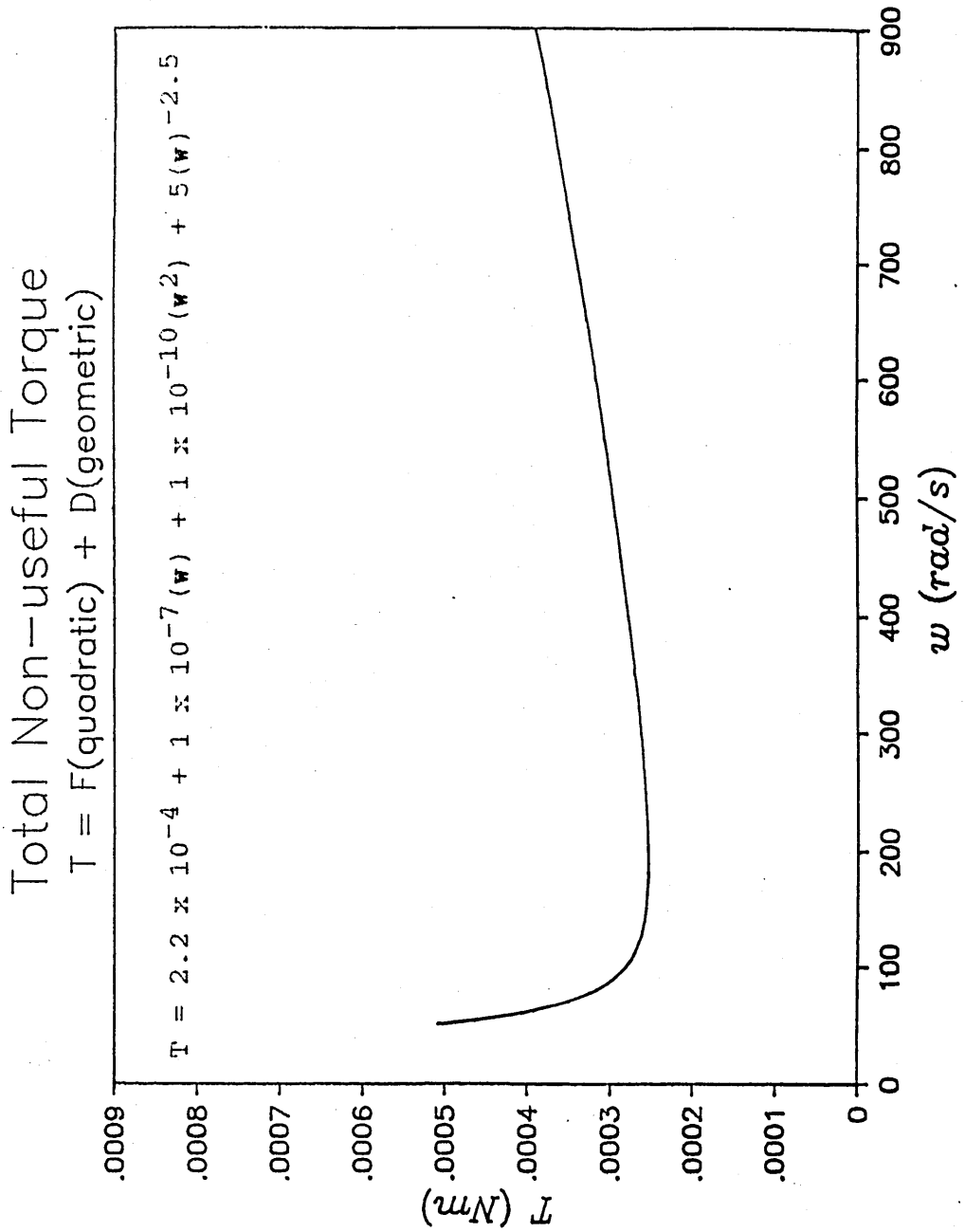

Figure 7.3f Complex relationship between total non-useful torque and rotational speed for Mk.7e

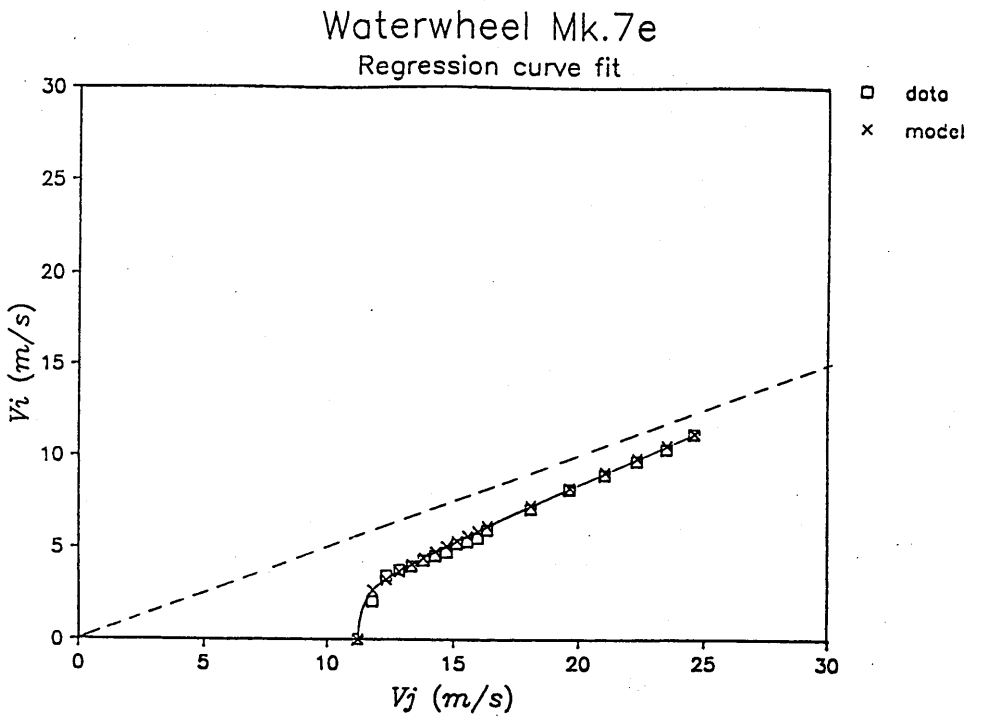

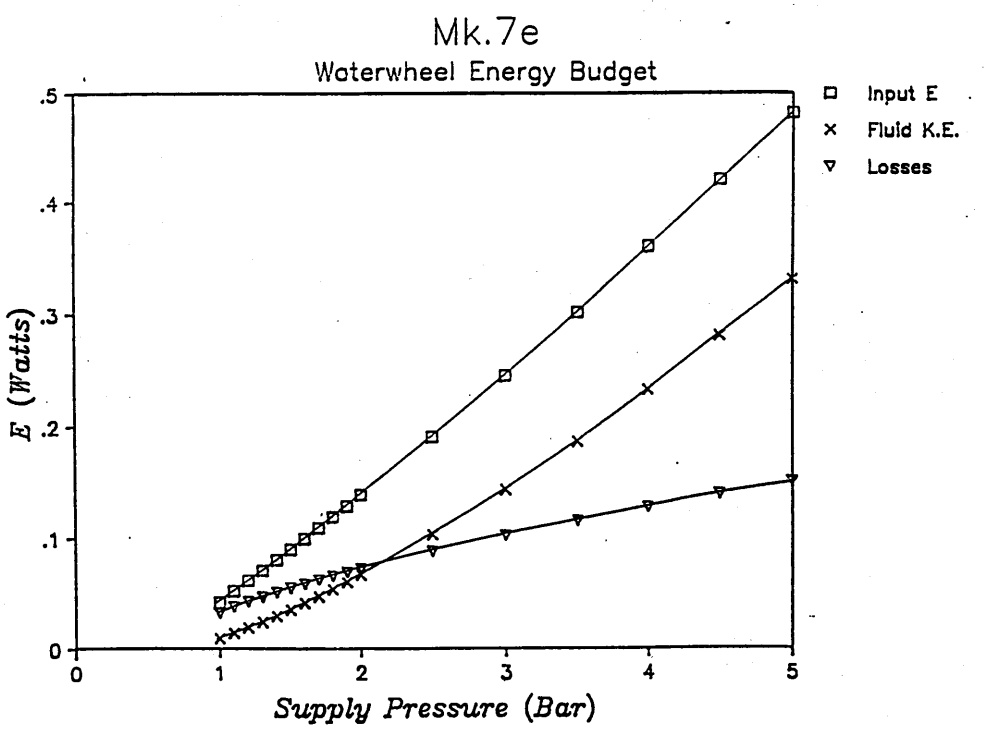

Figure 7.3g Rotational performance and energy expenditure for Waterwheel Mk.7e (with complex T)

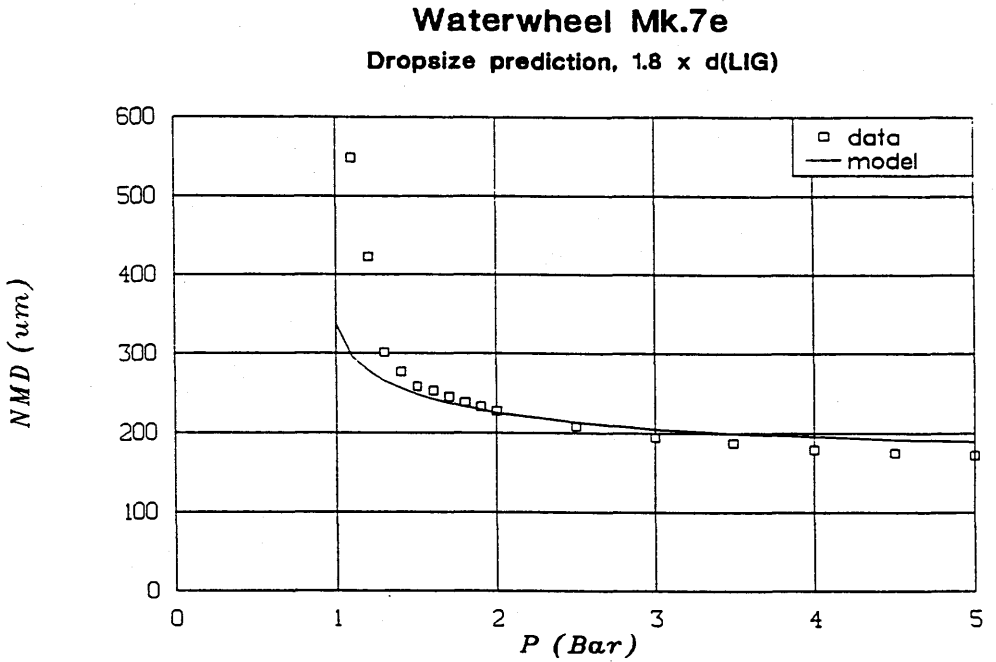

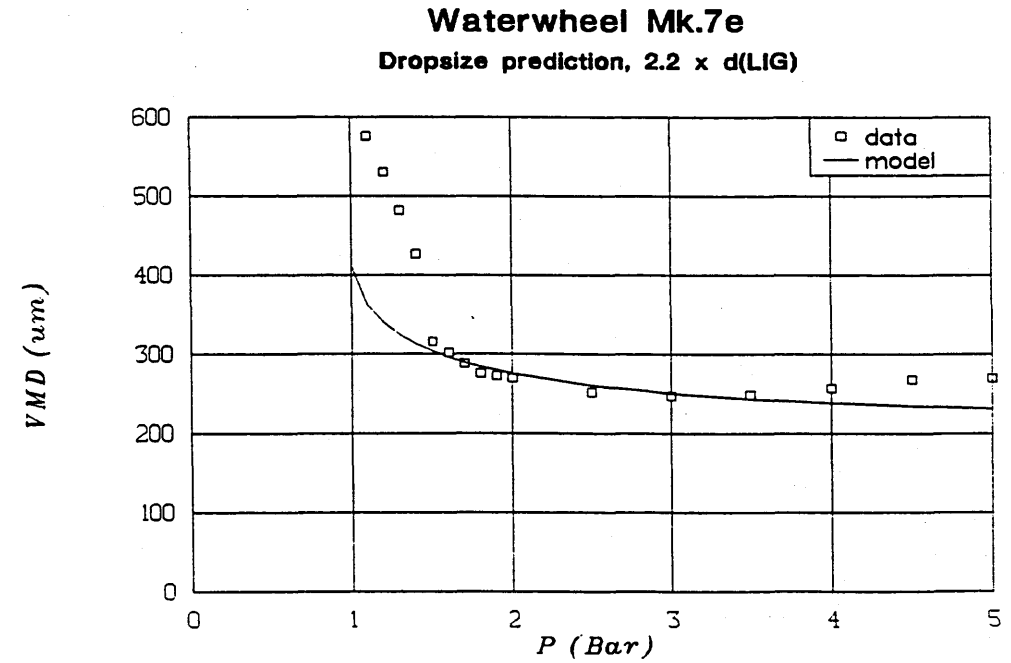

Figure 7.3h Prediction of dropsize for Waterwheel Mk.7e

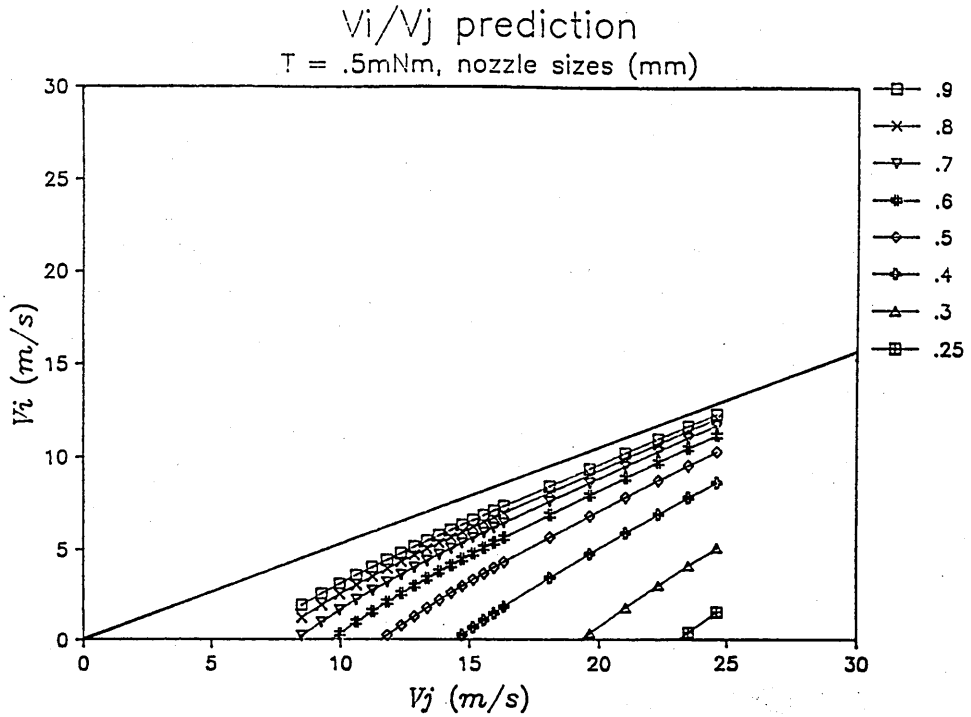

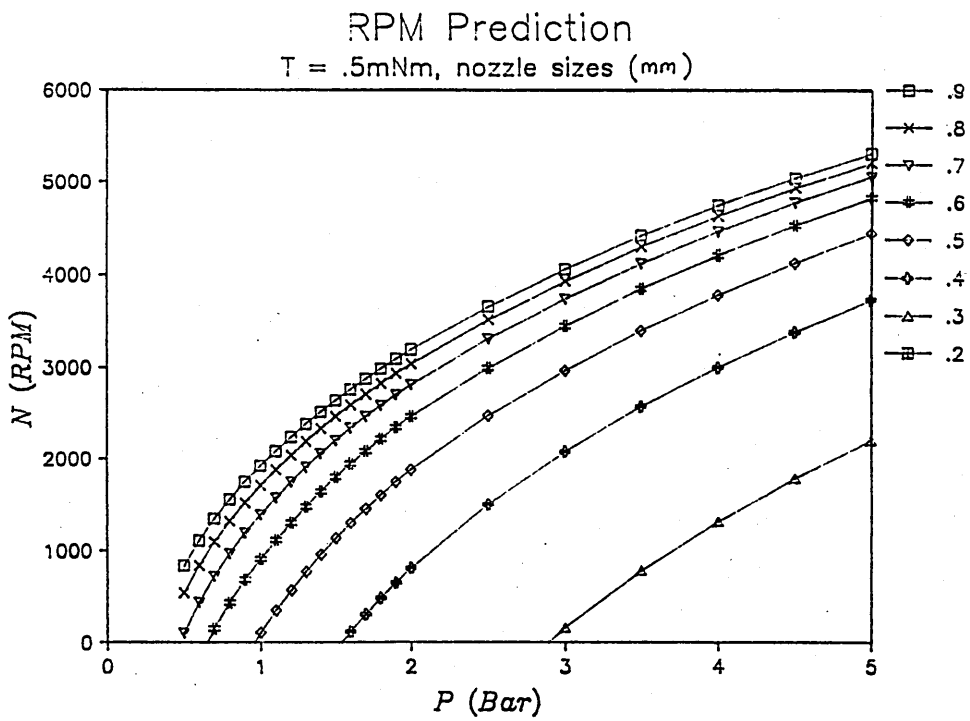

Figure 7.3i Prediction of rotational performance of theoretical Waterwheel Mk.7, with stiff bearing, and various orifice diameters.

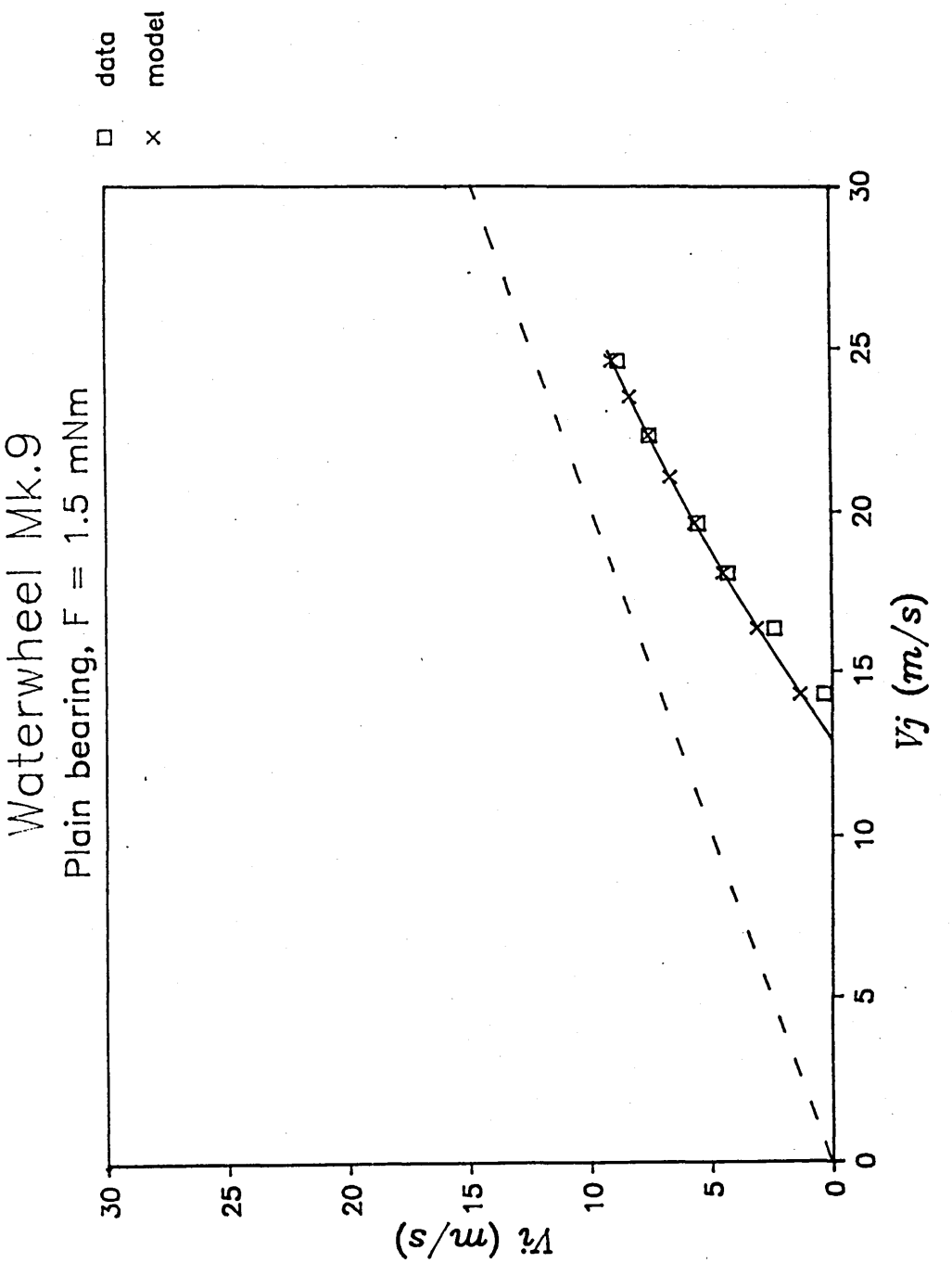

Figure 7.3j Prediction of rotational performance for Waterwheel Mk.9, with constant frictional torque

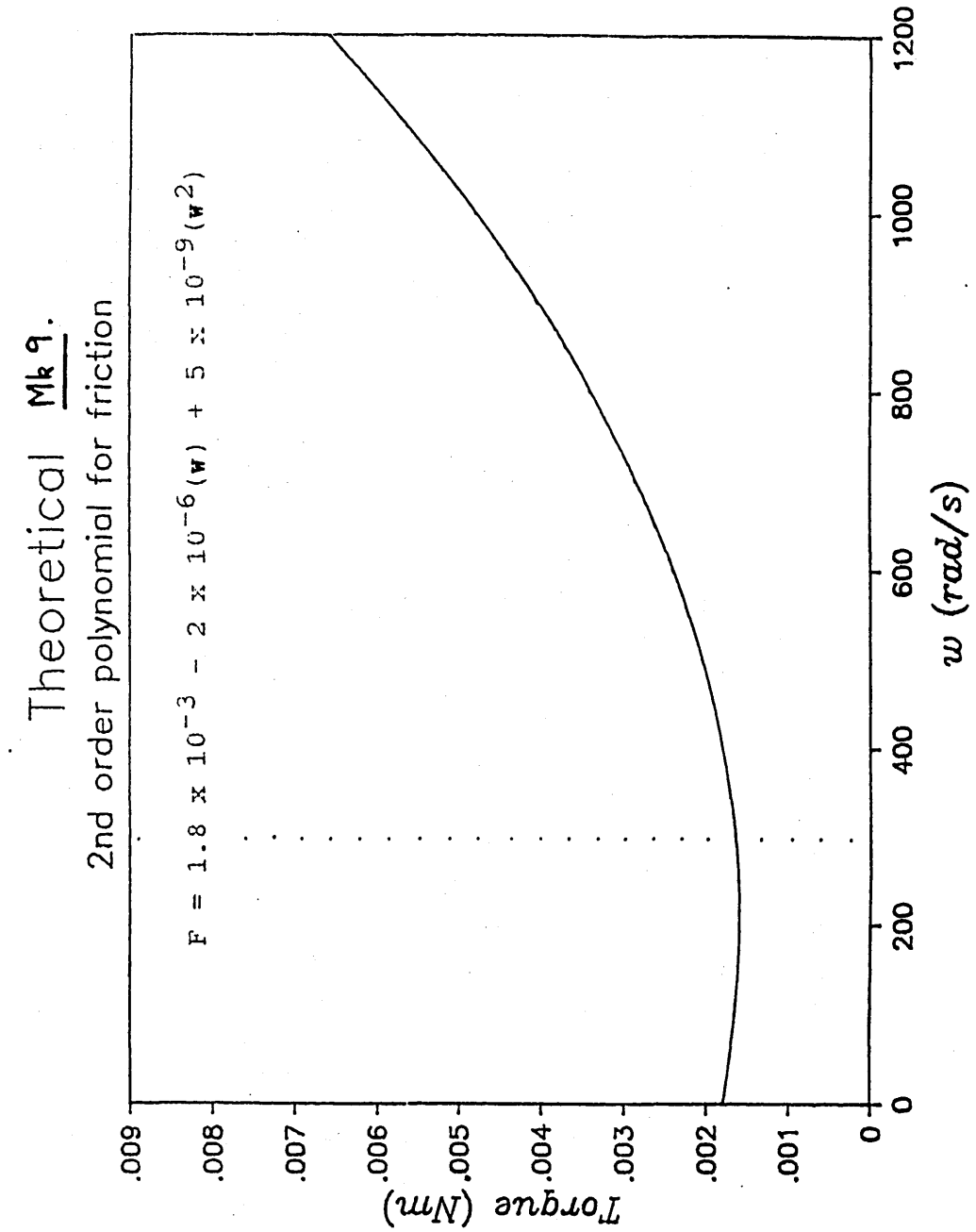

Figure 7.3k Complex relationship between frictional torque and rotational speed for Mk.9, plain lubricated bearing

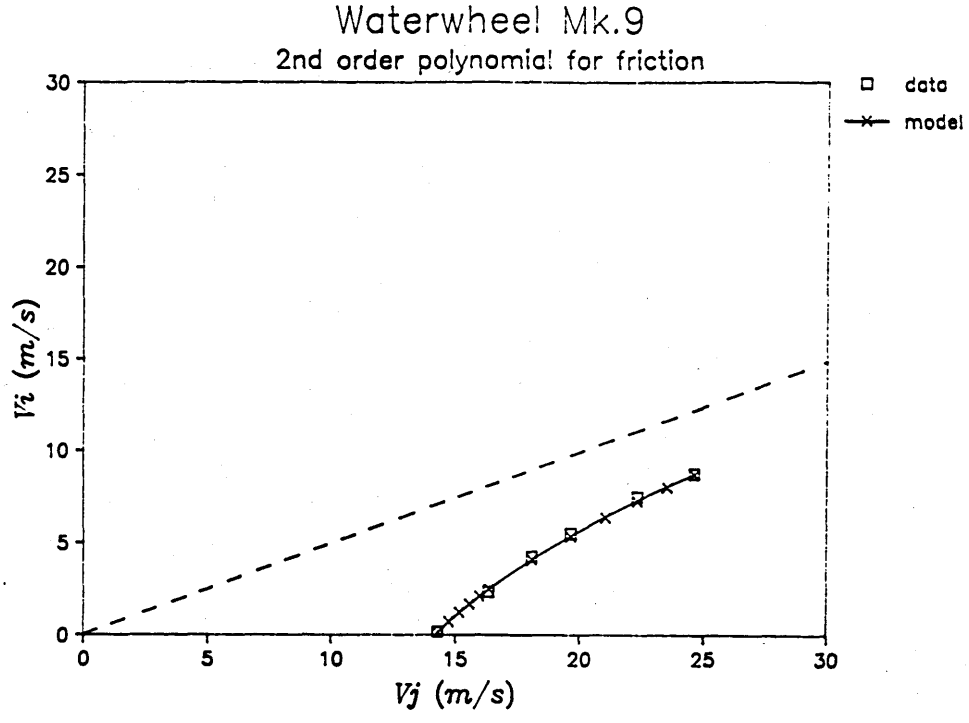

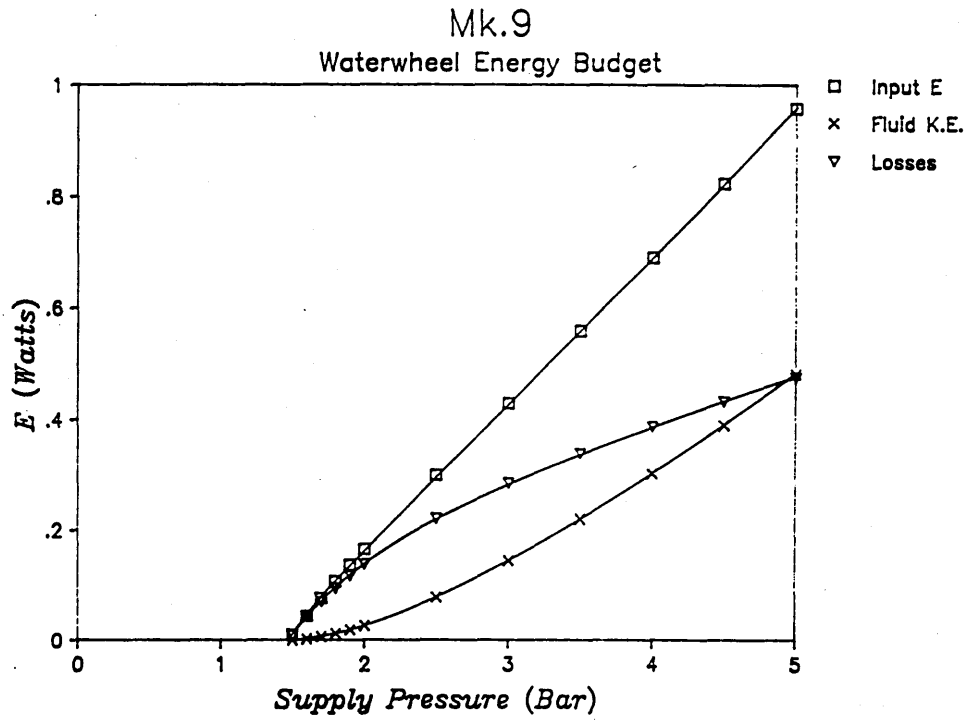

Figure 7.31 Rotational performance and energy expenditure for Waterwheel Mk.9 (with complex T)

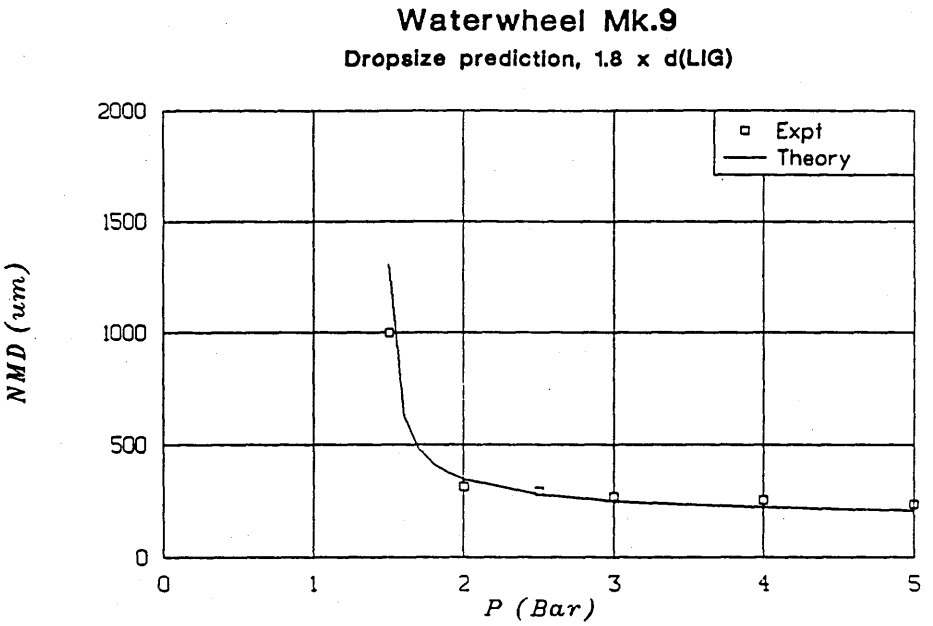

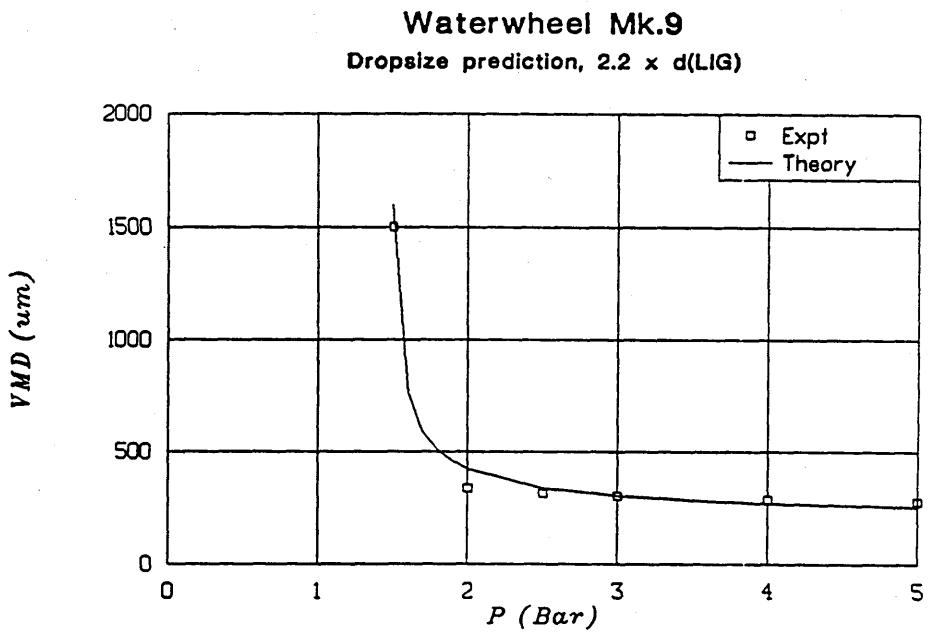

Figure 7.3m Prediction of dropsize for Waterwheel Mk.9

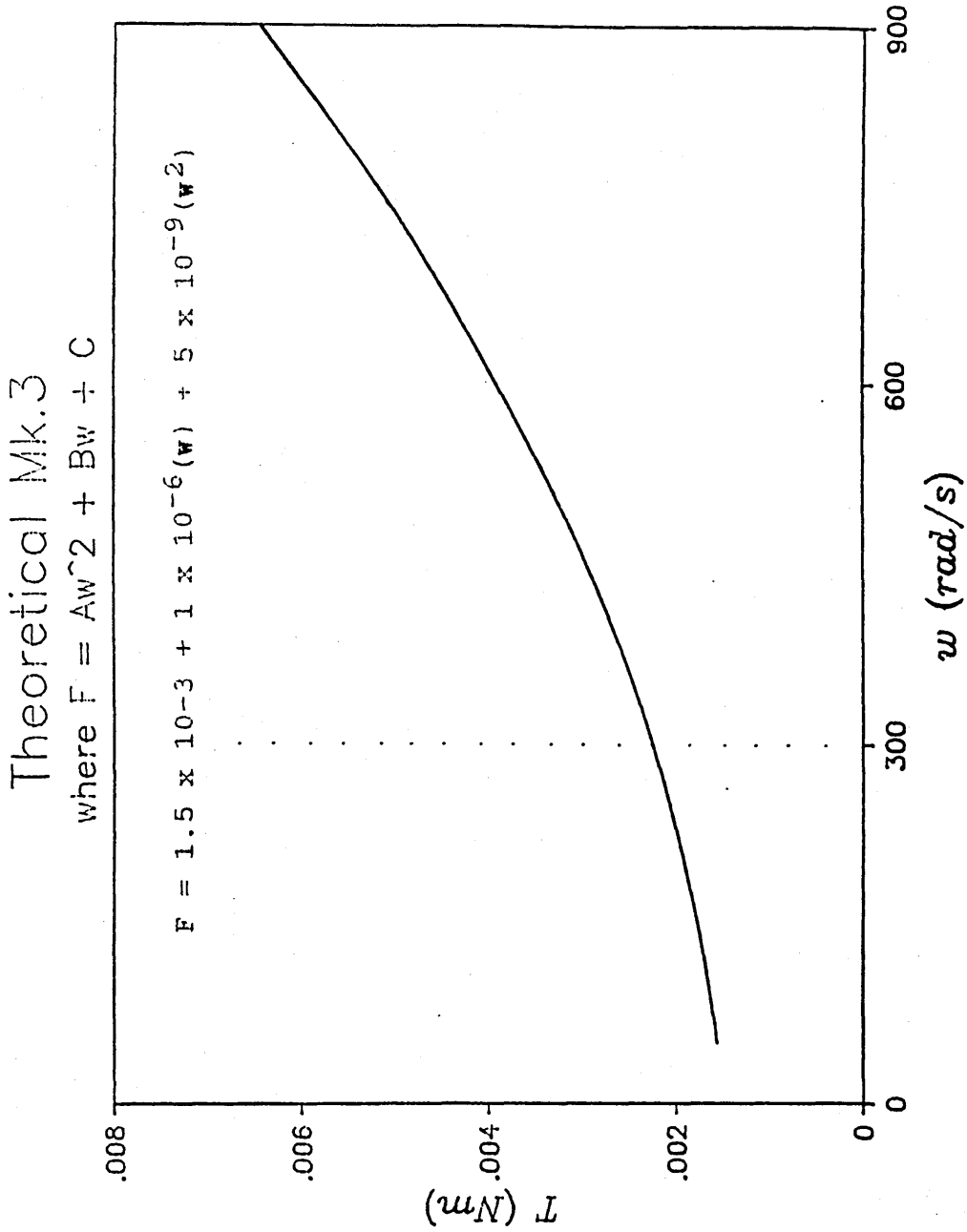

Figure 7.3o Complex relationship between total non-useful torque and rotational speed for Mk.3, lubricated plain bearing

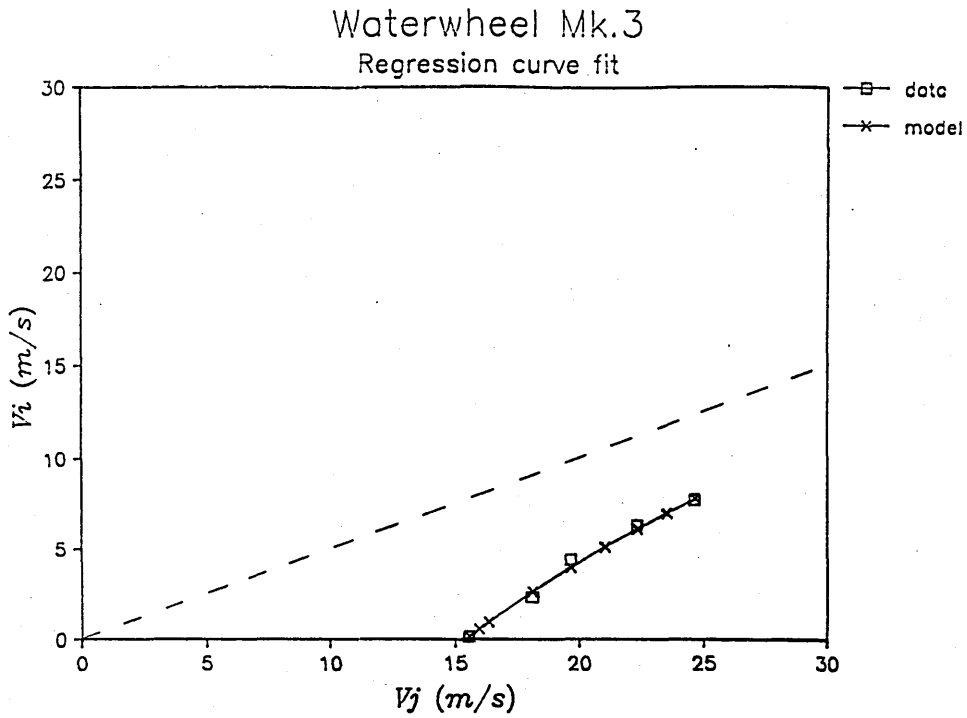

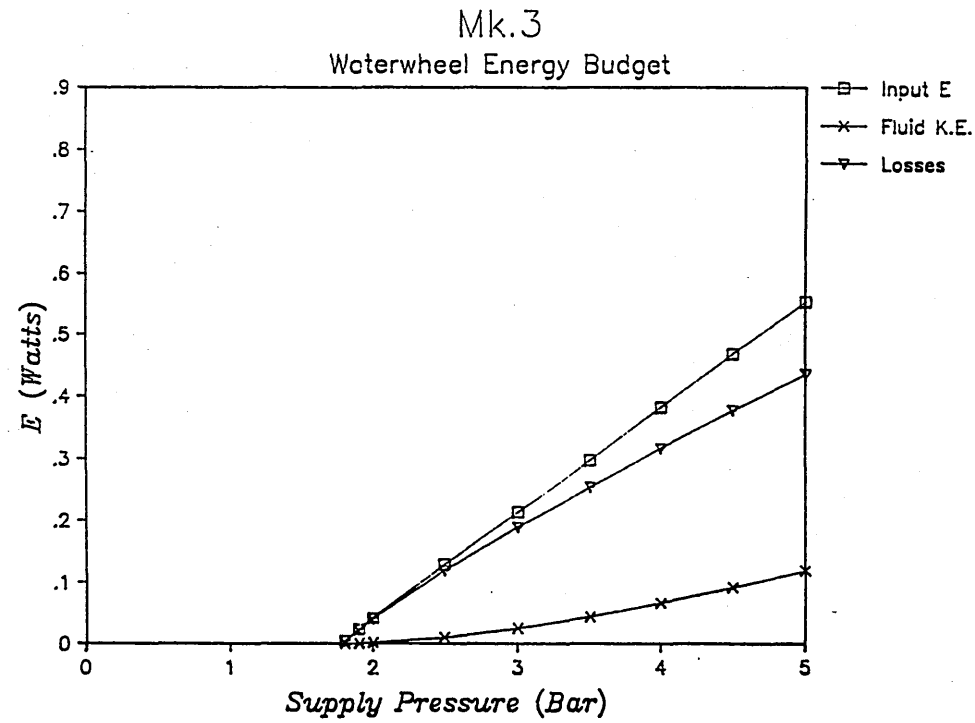

Figure 7.3p **Rotational performance and energy expenditure for Waterwheel Mk.3 (with complex T)**

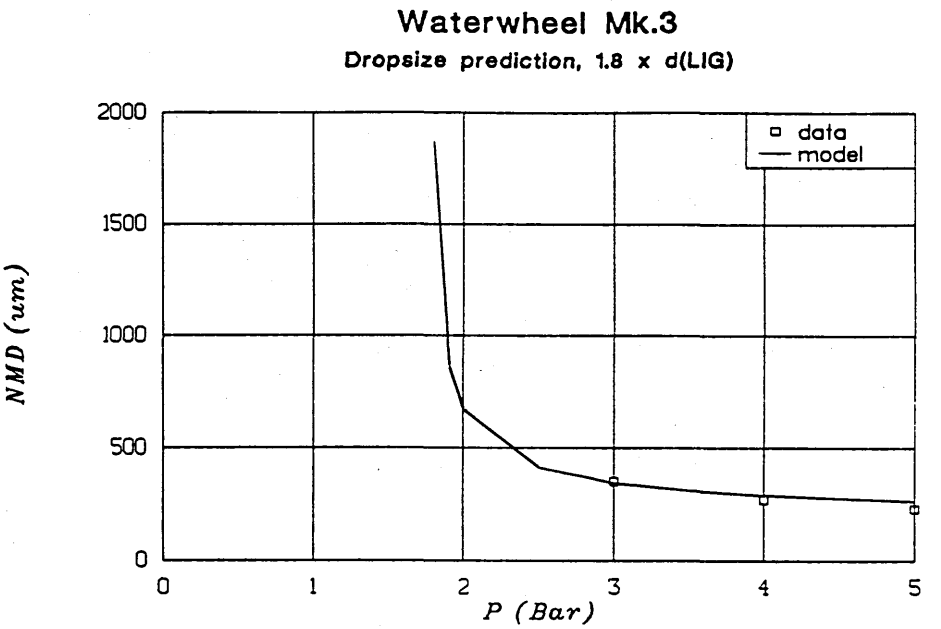

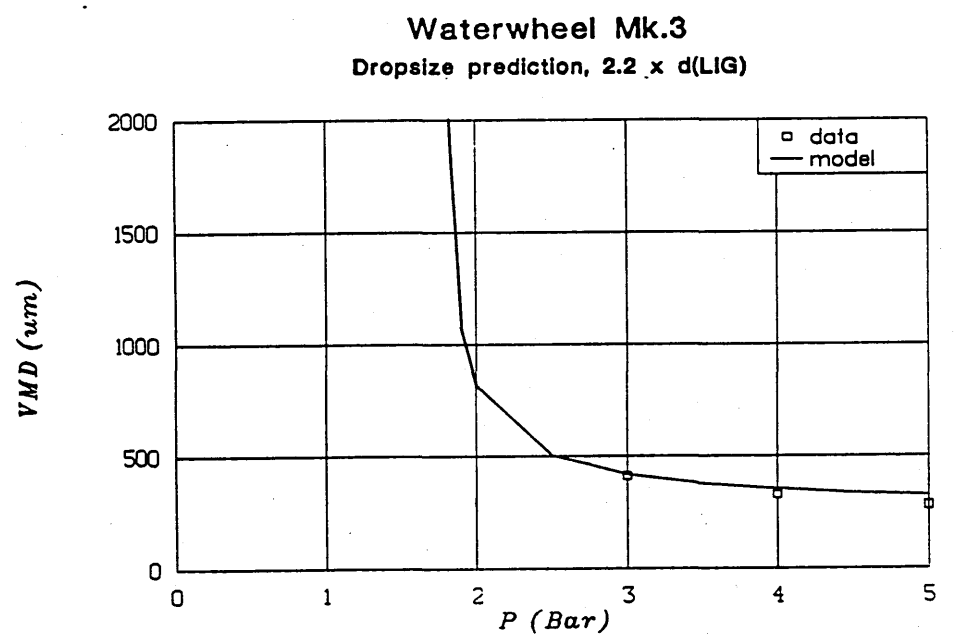

Figure 7.3q Prediction of dropsize for Waterwheel Mk.3

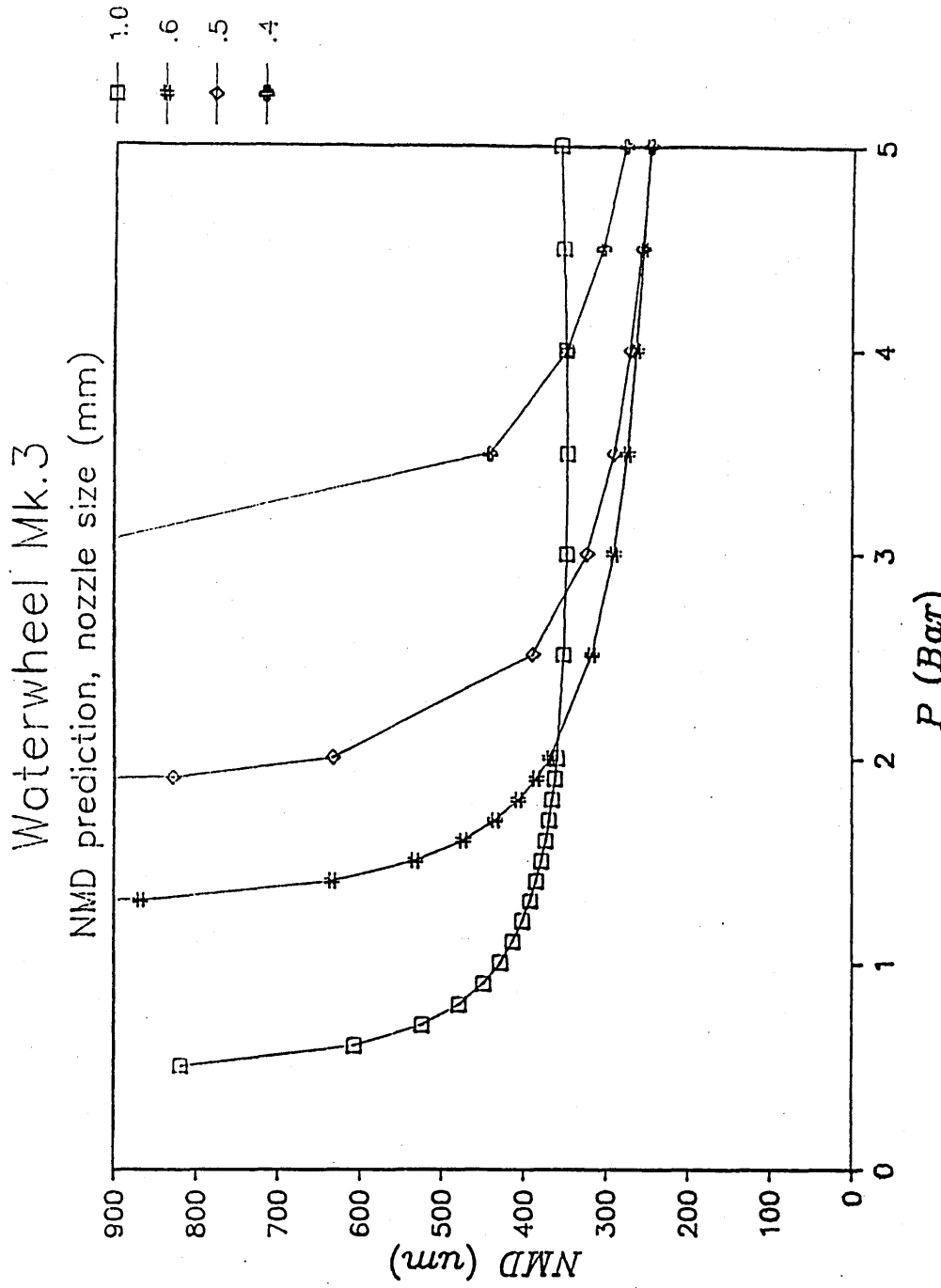

Figure 7.3r Demonstration of the complexity of the relationship between flowrate and dropsize.

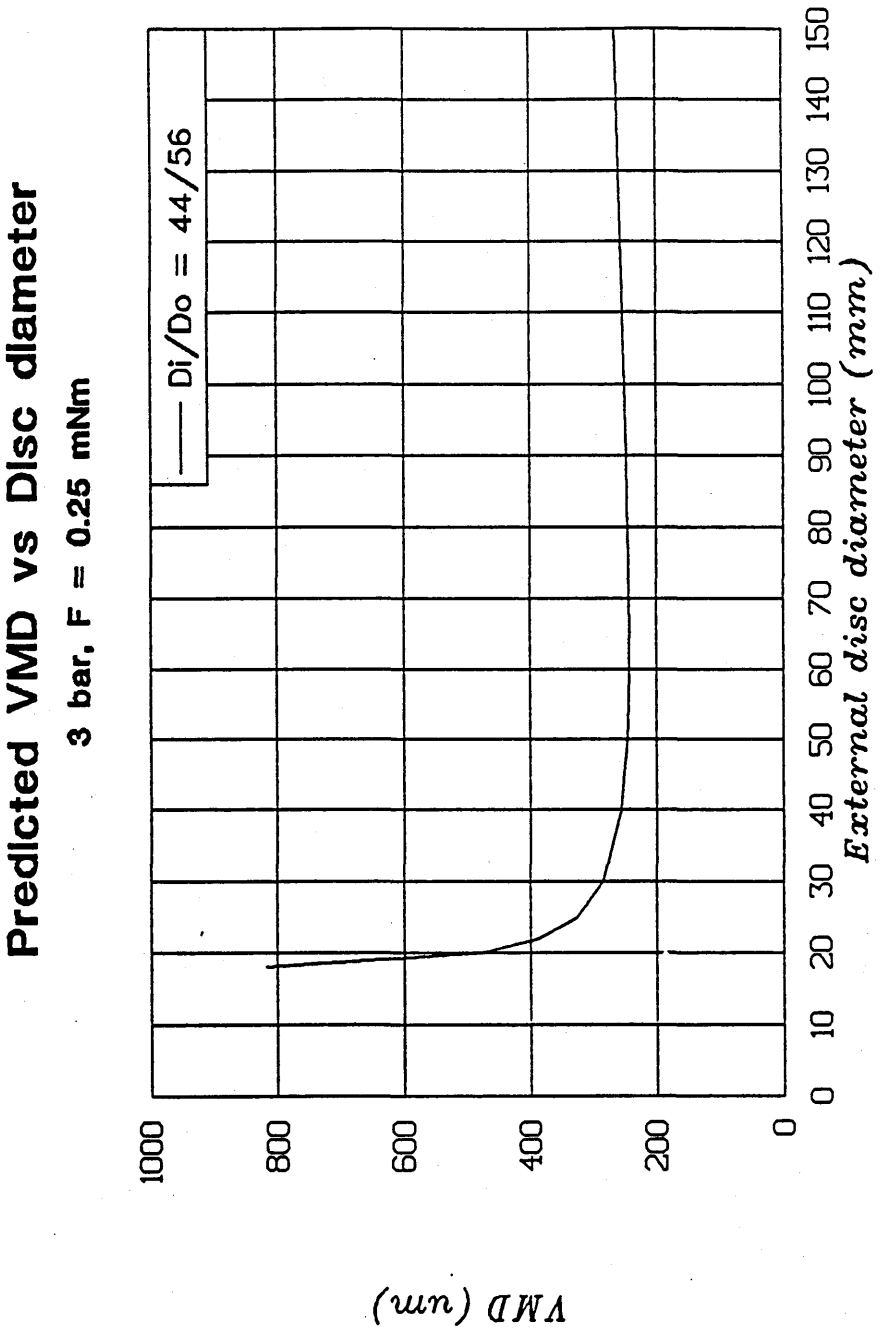

Figure 7.3s Predicted effect of size of atomiser on dropsize, showing optimum external diameter to be between 50mm and 70mm (WW Mk.7e configuration).

7.4 Estimated field performance

From dropsize data in Chapter 6, and from the model predictions of Chapter 7, it seems likely that a commercial version of the Waterwheel will be capable of producing a spray with an average dropsize around 200 to 300 µm, and is therefore suitable for the application of herbicides.

Assuming an intermediate value of 250µm as a typical value, according to the model, a total droplet velocity relative to air of around 10 ms^{-1} seems likely. The stop distance of a 250 µm droplet initially travelling horizontally at 10 ms^{-1} high above the ground is 56cm, or just under 60 cm.

A theoretical swath width assuming every droplet has constant size is therefore about 1.2m. In the literature for herbicide spinning discs, this value is commonly quoted for swath width.

In actual fact, there exists in most herbicide sprays produced by spinning discs, several drops larger than the average. A droplet spectra which may be described as narrow may be some droplets as large as 500µm, which have a stop distance of over 1m at 10ms^{-1}. These however are so few in number that they are not usually detected. Swath width measurable by staining of sensitive cards is generally less than 2m.

Figure 7.3a shows a typical swath pattern produced by Waterwheel Mk.6 held with the disc horizontal, moving at 1 ms-1, at a height of 1m above the ground. Water sensitive cards were placed in a linear array with 10cm spacings, to one side of the centre line over which the atomiser moved. One half of the illustrated deposit is simply a mirror image of the other. Peripheral fluid distribution had previously been checked to be even (Chapter 6).

The middle diagram shows how Peak Deposit and Coefficient of Variation of Deposit would vary if the swath was overlapped with different lane separations. If lane separation is 0.5m or less, the Coefficient of variation of deposit is very low at around 5%. With increasing lane separation, Coefficient of Variation increases, except at around 1.2m, where there is a minima of less than 15%. This therefore represents a an optimum lane separation for spraying operations. The lower diagram shows the form of the deposit produced using this lane separation.

Inorder to avoid contamination of spray on the legs of the operator, it is unlikely that the operating position of the Waterwheel will be with the disc horizontal. However, this should not make a great deal of difference to the basic form of the deposit, so long as disc inclination is towards the

direction of motion. Figure 7.2b shows that the form of the deposit with a disc inclined as much as 60°, is quite similar to that with the disc horizontal.

Figure 7.3c depicts a recommended method for spraying, with the lance held at about 45° to the ground in a forward direction or slightly to one side of the operator. If the height of the atomiser above the ground is kept at 25cm, a lance length of 70cm with a straight head should be sufficient for direct contamination with airborne spray to be avoided. For other methods, a longer length of lance may be required.

For a typical herbicide spraying program let us therefore assume the following parameters:

Average droplet size	=	250μm
Flowrate	=	240ml/min
Lane Separation	=	1.2m
Walking Speed	=	1m/s

Average application rate is therefore

$$\frac{240}{60 \times 1 \times 1.2} = 3.33 \quad ml/m^2$$

$$= 33.3 \quad \text{litres/hectare}$$

Volume of a single drop $= \pi/6 . (250 \times 10^{-6})^3$

$= 8.183 \times 10^{-12} \ m^3$

$$\text{Number of droplets} = \frac{3.333 \times 10^{-6}}{8.183 \times 10^{-12}}$$

$= 4 \times 10^5$ per m^2

or $= 40$ per cm^2

This is considered by the present author to be a sufficient to form a satisfactory deposit for most CDA herbicide applications.

272 A

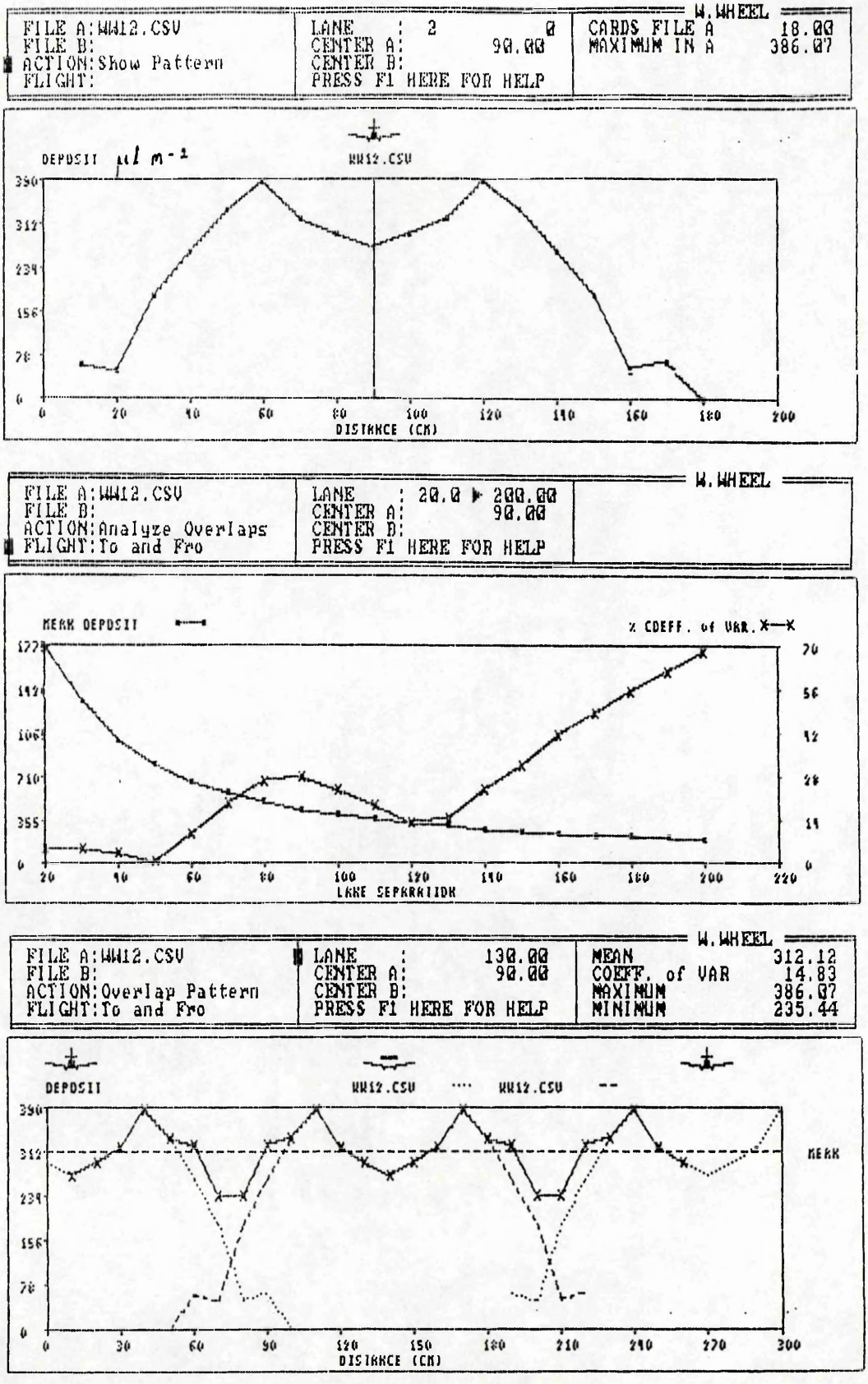

Figure 7.4a Swath pattern analysis for Waterwheel (Mk.6, 3 bar), with disc held horizontally

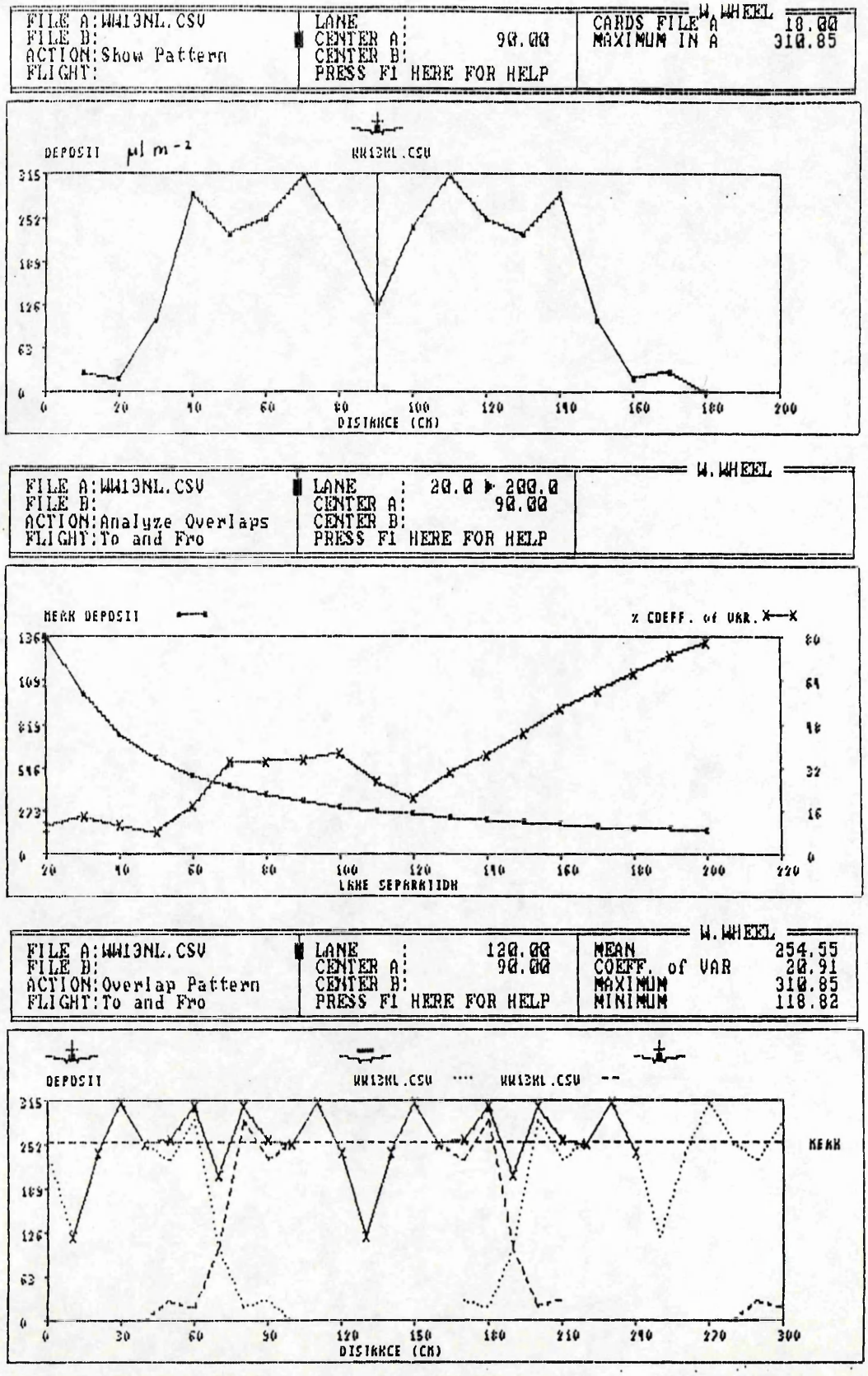

Figure 7.4b Swath pattern analysis for Waterwheel (Mk.6, 3 bar), with disc held at an angle of 60° towards direction of motion

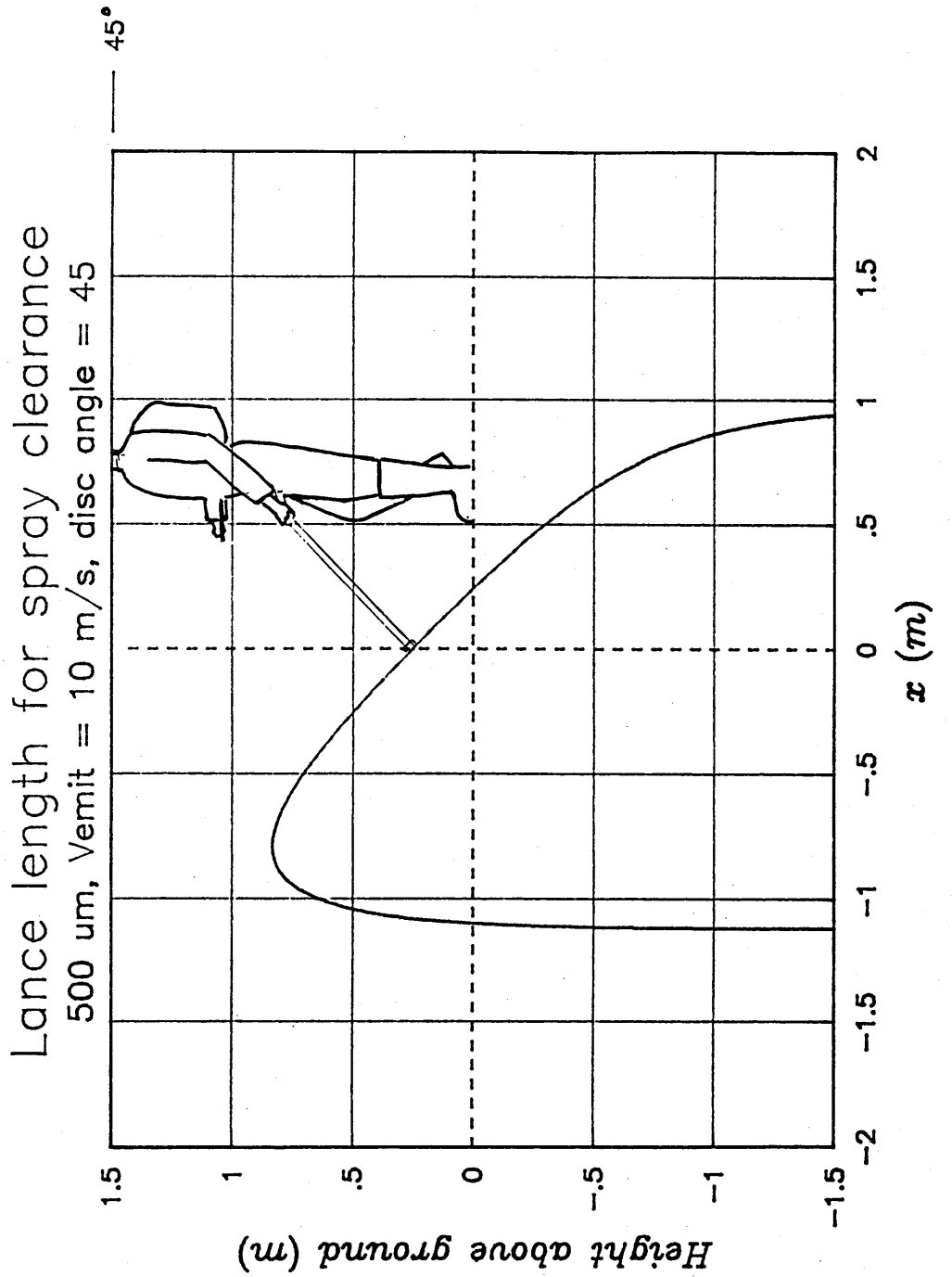

Figure 7.4c Indication of required lance length, from a consideration of trajectory of largest droplet .

Chapter Eight

CONCLUSION

This study has contributed to the field of pesticide application by providing an alternative rotary atomiser for Controlled Droplet Application of herbicides. The unit is driven by the spray liquid itself, and can be fitted to any standard spray lance.

Advantages are that it is inexpensive, has no electrical components to wear out, no requirement for special pumps, and will satisfy FEPA and COSHH regulations.

This may encourage the use of CDA for ground handheld application of herbicides, thus increasing the efficiency and environmental acceptability of the process.

A summary of the main findings of the study is as follows:

1) Work on early prototypes validated the concept of using an off-centre jet to drive a cup mounted upon an external bearing, at speeds sufficient to atomise the expelled liquid.

2) A prototype was then designed to be fitted to a standard spray lance. Tests showed that a bearing with low friction was required for satisfactory operation, and that lubricated dual miniature ball races were capable of providing this.

3) Dropsize was measured using laser dropsizing equipment. With modification of the design of grooves and issuing points on the atomising disc, a narrow droplet spectrum was produced with water, within a range suitable for herbicide CDA. Spray characteristics indicate less potential for spray drift, and lower water volumes compared to conventional application methods.

4) Above a critical supply pressure depending upon the friction of the bearing, dropsize was shown to be largely insensitive to supply pressure of the fluid, although spectral width of the spray tended to increase with increasing pressure. Dropsize insensitivity is regarded as a desirable characteristic with side lever operated knapsacks, due to the variation in supply pressure they produce. However, it is recommended that a constant pressure valve be used ahead of the atomiser, to ensure consistency in application rate.

5) Deposit pattern on the ground was assessed using sensitive papers and collectors. A fluid re-distribution system, in the form of weiring on the inner wall of the cup, was shown to be necessary to eliminate peripheral non-uniformity, arising from the off-centre feed. Although not strictly necessary for an even deposit arising from superimposed moving swaths, weirs were deemed necessary to ensure peripheral uniformity in dropsize, and therefore maintain the narrow overall droplet spectrum.

6) Tests carried out with various water based formulations, showed that acceptable droplet spectra could be produced. Formulations containing surfactant, however, required the use of an antifoaming agent.

7) Investigations of the behavior of fluid over rotating surfaces lead to the design of an atomising disc efficient in providing kinetic energy to the fluid. The annulus shaped disc had a special design of radial groove, which resisted slippage at high flowrates.

8) The action of the fluid drive system was found to be similar to a Pelton turbine, except that the jet is internal, and that there are no vanes. An expression was obtained for the input energy provided by the jet.

9) Equating input energy to fluid kinetic energy plus losses lead to an equation which could be solved to give the rotational speed of the atomiser.

10) Dropsize produced by the atomiser was predicted by assuming proportionality with undisturbed ligament radius, calculated from the radial velocity of the fluid, including an estimation of losses due to viscosity.

11) A simple model was formulated to predict the effect on performance of changing various design parameters such as inner wall cup radius, disc radius, tooth number, supply pressure, nozzle diameter, coefficient of discharge, and clearance from inner wall, fluid density, viscosity, and bearing friction characteristics.

12) Expenditure of energy and therefore efficiency can be predicted for any combination of the above. This is foreseen to be of particular use to manufacturers, interested in producing a commercial version of the Waterwheel.

Two conflicting areas of design have been highlighted and brought together by this study. Firstly there are the requirements for hydraulic efficiency of the turbine. For optimum efficiency, high flowrates and a large cup radius are required, inorder to provide sufficient torque to overcome bearing friction. However, there is a compromise in that low flowrates, and a small cup radius are preferable from an atomisational point of view.

Prototype Mk.7 is closest to the optimum configuration, if low bearing friction can be maitained with dust free lubricated miniature ballraces. However, if higher bearing friction has to be overcome, greater power input via increased flowrate is required, either by using a higher supply pressure, or by using a larger nozzle orifice diameter. To accomodate increased fluid layer thicknesses, a slightly larger cup may also be desirable. As regards optimum cup size for any future versions of the Waterwheel, the author recommends that the dimensions illustrated in drawing 11, Appendix I should be followed.

Chapter Nine

FUTURE WORK

Recommended future work can be split into two areas:-

i) further design optimisation with consideration of durability, reliability, and cost of mass production

ii) further development of the theory to predict dropsize

Based upon experience gained as a result of carrying out this work, the author suggests that the next prototype should be constructed with the following dimensions:

Internal diameter of cup	54mm
External diameter of atomising disc	70mm

The prototype should be tested with various types of bearing, although the following is recommended:

Dual miniature ballraces with :

External ballrace diameter	10mm
Bearing shaft diameter	4mm

An area of future work which the author foresees as being particularly useful, is a study of the friction generated by miniature bearings, with reference to how frictional torque may vary with factors such as rotational speed, lubrication and load. This may lead to a theoretical prediction which could be entered into the simple computer model for the Waterwheel (Chapter 7). This would negate the requirement to test each prototype with a large large number of different bearings.

The second area of recommended future work involves a refinement of the theory used to predict dropsize of the spray produced by the Waterwheel.

The present method simply relates dropsize $d_{(DROP)}$, by a simple constant breakup factor, to the final fluid layer thickness $d_{(LIG)}$, just prior to emmision at the tooth of the atomising disc. This is regarded by the author as a primary control effecting dropsize, and may be calculated by estimating the radial velocity of the fluid, including a consideration of viscous losses experienced by the fluid (Section 4.4).

It is recommended that additional experimental data should be obtained to support this theory. This could be achieved by construction of a series of different sized discs and

annulii, or alternatively by means of a sophisticated design of spinning groove; one in which both the length and the feed point may be varied to simulate a single groove on various annulii geometries.

It would also be desirable to find a successful technique of measuring radial fluid velocity directly, rather than simply measuring dropsize. This would most likely be achieved using a photographic method, and possibly a technique of introducing short pulses of dye or particles into the flow. Alternatively, width of fluid in the groove could be accurately measured, if constrast at the fluid groove boundary could be highlighted.

The "constant breakup factor" method provides a satisfactory prediction of dropsize if secondary effects affecting fluid emission from the tooth, and tertiary effects affecting ligament breakup can be ignored. Such secondary effects are at a minimum if ligaments are thick; ie rotational speeds are relatively low, and flowrates are relatively high, as is the case with the Waterwheel.

However, as flowrate is decreased, effects of surface tension at the tooth become more important. Also, as rotational speed increases, aerodynamic forces effecting disturbance of the ligament plays an increasingly more important role in determining dropsize. From this viewpoint, dropsizing in a vacuum may prove desirable.

If the secondary and tertiary controls were combined with the primary effect, a single model to predict dropsize of any liquid issuing from a spinning discs of any geometry, over a large range of flowrates, rotational speeds and for different liquid properties may be possible; if not, at least a useful target to aim for.

Chapter Ten

REFERENCES

Akesson, N.B.
Wilce, S.E.
Yates, W.E.
Bayer, D.E.
Increased efficiency and reduced drift losses from herbicide applications for weed control. International Conference for Tropical and Sub-Tropical Agriculture. ASAE pp 177-181 (1972).

Arnold, A.C.
(1) An evaluation of fourteen hand-held battery operated spinning disc sprayers. Tropical Pest Management 29 (2), pp 105-121, (1983).

Arnold, A.C.
(2) Power source for spinning disc sprayers and their economics. Tropical Pest Management, 31, (1985).

Ashton, F.M.
Movement of herbicides in soil with simulated furrow irrigation. Weeds vol 9 pp 612-619, (1961).

Bache, D.H.
Sayer, W.J.D.
Transport of Aerial Spray Parts I,II,and III. Agricultural Meteorology, 15, pp 257-271 (1975).

Bailey, R.J.
Phillips, M.
Harris, P.
Bradford, A.
The results of an investigation to determine the optimum drop size and volume of application for weed control with spinning disc applicators pp 995-1000, BCPC-Weeds, 1982.

Bals, E.J.
(1) The principles of and new developments in Ultra Low Volume Spraying. Proc. 5th BCPC Insecticide and Fungicide Conf.1, pp 189-193 (1969).

Bals, E.J.
(2) The reasons for CDA (Controlled Droplet Application). BCPC Conf.- Weeds. pp 659-666, (1978).

Bals, E.J.
(3) The principles of and new developments in ULV spraying: some reflections. Proc. BCPC Weeds, pp 1033-1037, (1982).

Bär, P
Uber die physikalischen Grundlagen der Zerstaubungs-Trock-nung. Doctoral dissertation, Karlsruhe Technical College, Germany (1935).

Barrentine, W.L.
Wooten, O.B.
Equipment for evaluating methods of applying pre-emergent herbicides. Weeds 15, pp 366-368 (1967).

Beer, F.P.
Johnstone, E.R.
Mechanics for Engineers
4th ed. Mc.Graw-Hill, (1987).

Bode, L.E.
Butler, B.J.
Pearson, S.L.
Bouse, L.F.
Characteristics of the Micromax Rotary Atomiser. Trans ASAE vol. 26 pp 999-1005, (1986).

Bode, L.E.
Butler, B.J.
Spray characteristics of rotary atomisers. Pesticide Formulations and Applicaton Systems: 2nd Conf. ASTM STP 795, pp 89-104, (1983)

Bode, L.E.
Butler, B.J.
Goering, C.E.
Spray drift and recovery as effected by spray thickener, nozzle type, and nozzle pressure. Trans ASAE Paper No. 75-1065 (1976).

Boize, L.M.
The atomisation characteristics of a spinning disc ULV applicator. J. agric. Eng. Res. vol 21, pp 87-99, (1976).

Boothroyd, G
Poli, C
Applied Engineering Mechanics
Statics and Dynamics
1st ed. Marcel Dekker, Inc. (1980).

Bouse, L.F.
Leerskov, R.E.
Drift comparisons of low expansion foams and conventional sprays. Weed Science. vol 21 (5) pp 405-409 (1973)

Bouse, L.F.
Carlton, J.B.
Merkle, M.G.
Spray recovery from nozzles designed to reduce drift. Weed Science, Vol 24, pp 361-365, (1976).

Brandemburg, B.C.
Raindrop^{TM} drift reduction spray nozzle ASAE, Paper No. 74-1595. (1974)

Buehring, N.W.
Roth, L.O.
Santelmann, P.W.
Plant response to herbicide spray dropsize and carrier volume. Trans ASAE vol 16 (4) pp 636-638 (1973).

Butler, B.J.
Akesson, N.B.
Yates, W.E.
Use of spray adjuvants to reduce spray drift. Trans. ASAE. 12, 2 pp 182-186 (1969)

Byass, J.B.
Lake, J.R.
Spray drift from a Tractor powered Field Sprayer. Pesticide Science, 8, pp 117-126, (1977)

Cameron A. — Basic Lubrication Theory 3rd ed. Ellis Horwood Ltd (1983)

Coffee, R.A. — Electrodynamic energy - a new approach to pesticide application. Proc. BCPC Conf. pp 777-789, (1979).

Combellack, J.H. — (1) Spot spraying with hand-held CDA equipment in Australia; a progress report on suitability of equipment and herbicides. BCPC No.22 pp 199-211, (1978).

Combellack, J.H. — (2) Herbicide application: a review of ground application techniques. Crop Protection 3 (1), pp 9-34, (1984).

Combellack, J.H. Matthews, G.A. — The influence of atomiser, pressure and formulation on the droplet spectra produced by high volume sprayers. Weed Research 21, pp 77-86 (1981a).

Cramer, H.E. Boyle, D.G. — The micrometeorology and physics of spray behavior. Pesticide Spray Technology Workshop, Emeryville, California (1973).

Crowther M.J. — Effect of Reynolds Number on the Formation of Droplets from Spinning Discs, MSc. Thesis, Cranfield Institute of Technology, (1986).

Dale, J.E. — The rope wick applicator - a new method of applying glyphosate. Proc. 31st Annual Meeting Southern Weed Science Society. p332. (1978)

Daugherty, R.L. Franzini, J.B. Finnemore, E.J. — Fluid Mechanics with Engineering Applications. 4th ed. Mc.Graw-Hill, (1989).

Davison, J.G. — The effect of growth substances on tomatoes. Ph.D thesis University of Nottingham. pp 200 (1961)

Deutschman A.D. Michels W.J. Wilson C.E. — Machine Design; Theory and Practice Macmillan, (1975)

Dombrowski, N. Fraser, R.P. — A photographic investigation into the disintergration of liquid sheets. Phil. Trans. Royal. Soc. London, Series A, 247, (924), pp 101-130 (1954).

Dombrowski, N Lloyd, T.L.	Atomisation of liquids by spinning cups The Chemical Engineering Journal vol 8 pp 63-81, (1974).
Douglas J.F. Gasiorek J.M. Swaffield J.A.	Fluid Mechanics 2nd ed. Pitman (1985)
Drummond, A.M.	Fluid Mechanics of drop formation with particular reference to spinning discs. Pesticide Accountancy Workshop, AFA-TN-13, National Research Council, Canada, pp 67-84, (1976).
Dumbauld, R.K. Rafferty,J.E. Cramer, H.E.	Dispersion deposition from aerial releases. 3rd symp. on Atmospheric turbulence, Diffusion and Air Quality pp 19-22 (1976)
Dumbauld, R.K.	Dispersion deposition from aerial spray releases. 3rd Symp. on Atmospheric Turbulence, Diffusion and Air Quality, pp 19-22, Am. Met. Soc.. 1976.
Eagle. D.J.	Hazard to adjoining crops from vapour drift of phenoxy herbicides applied to cereals. Aspects of Applied Biology 1 pp 33-39, (1982).
Eisenklam, P	On ligament formation from spinning discs and cups. Chem. Eng. Sci. vol 19 pp 693-694, (1964).
Elliott J.G. Wilson B.J.	The influence of weather on the efficiency and safety of pesticide application: The drift of herbicides BCPC Occasional Publication No.3 (1983).
Ford, R.E. Furmidge, C.G.L.	Formation of spray drops from viscous fluids. Pesticidal Formulations Research: American Chemical Society Advances in Chemistry Series, No. 68. (1969)
Fraser, R.P. Dombrowski, N. Routley, J.H.	The production of uniform liquid sheets from spinning cups. Chem. Eng. Sci. vol 18, pp 315-321, (1963)
Friedman, S.J. Marshall, W.R.	Centrifugal Disc Atomisation Section 13, Chemical Engineers Handbook 3rd Ed. by J.H. Perry. McGraw-Hill.

Frost, A.R.
Green, R.
Drop size spectra and spray distribution from a Micron Battleship disc Proc. BCPC-Weeds, pp 1059-1065, (1978).

Frost, A.R.
Rotary atomisation in the ligament formation mode. J. agric. Eng. Res. vol 26, pp 63-78, (1981).

Frost, A.R.
Lake, J.R.
The significance of drop velocity to the determination of dropsize distributions of sprays. J. Agric. Eng. Res. vol 26, pp 367-370, (1981).

Garnett, R.P.
A herbicide sprayer for small tropical farmers. Ph.D. Thesis, (unpublished), International Pesticide Application Centre, Silwood Park, (1983).

Goering, C.E.
Foster, R.A.
Bode, L.E.
Gebhardt, R.
Development of a shielded, spinning disc atomiser. Trans ASAE vol 15 (5) pp 814-817, (1973).

Goering, C.E.
Butler, B.J.
Paired field studies of herbicide drift. Trans ASAE, 18, pp 27-34. (1975)

Gorta, M.R.
A study of the atomisation characteristics of a spinning disc as determined by two laser based droplet analysers. MSc. Thesis, University of Reading, (1981).

Grodzinski, P.
Ingvestigations on shaft fillets. Engineering (London) vol. 152 p 321 (1941).

Harris, T.A.
Rolling Bearing Analysis John Wiley and Sons, (1966).

Haywood, J.D.
Combinations of foliar and soil applied herbicides for controlling hardwood brush. Down to Earth 36, (2), pp 14-15 (1980)

Hemphill, D.D.
Montgomery, M.L.
Response of vegetable crops to sub-lethal applications of 2,4-D. Weed Science, 29, pp 632-635, (1981)

Heywood, R.B.
Photoelasticity for Designers. Pergomon, N.Y. Chapter 11. (1969).

Hinze, J.O.
Milborn, H.
Atomisation of liquids by means of a rotating cup. Journal of Applied Mechanics, pp 145-153, (June,1950).

Jarmin, R.T.
Rotary atomisers. CIRU/Porton Down. Rep. No. 127.

Kamiya, T
Kayano, A.
On ligament type disintergration by a rotary disc atomiser. Kagaku Kogaku vol 34 (3) pp 55-60, (1970).

Kingham, H.G.
Fletcher, J.T.
The effects of MPCA and 2,3,6-TBA on glasshouse cucumbers. Weed Research, 3, pp 242-245, (1963).

Kinnersley, R.P.
Studies in fluid atomisation. MSc. Thesis (unpublished), Cranfield Institute of Technology, (1987).

Kirch, J.H.
The Microfoil Boom. Agrochem. Age, vol 11 (12) : pp 16-17 (1968).

Knollenberg, R.G.
(1) The optical array: an alternative to scattering or extinction for airborne particle size determination. Journal of Applied Meteorology, vol 9 (1) pp 86-103 (1970).

Knollenberg, R.G.
(2) The use of low power lasers in practical size spectrometry. Practical Appl. of low powered lasers (1976)

Lake, J.R.
Frost, A.R.
Green, R.
Measurements of drop size and spray distribution from a Micron Herbi disc. Proc. BCPC-Weeds, pp 399-405, (1976).

Last, A.J.
Parkin, C.S.
Systems for image analysis. Aspects of Applied Biology, AAB Symposium, Reading. (1987).

Marchant, J.A.
Dix, A.J.
The torque due to the liquid on a spinning disc atomiser. J. Agric. Engng Res. vol 33, pp 273-280, (1986).

Martin, J.A.
Fletcher, J.T.
The effects of sub-lethal doses of various herbicides on lettuce. Weed Research, 12, pp 268-271 (1972).

Matthews, G.A.
(1) CDA - Controlled Droplet Application PANS 23, vol 4, pp 387-394, (1977).

Matthews, G.A.	(2) New developments in pesticide application technology. Crop Protecton 1 (2) pp 131-145, (1982).
Maybank, J Yoshida, K Grover, R.	Droplet Size Spectra, Drift Potential and Ground deposition Pattern of herbicide sprays. Canadian Journal of Plant Science, 54, pp 541-546 (1974).
Merrington, A.C. Richardson, E.G.	Proc. Phys. Soc., vol 59, (1947).
Merritt, C.R.	The influence of application variables on the biological performance of foliage applied herbicides. Symp. on Spraying Systems for the 1980's, pp35-43, (1980).
Morel, M.	Applications d'herbicides par pulverisation centrifuge. Materials d'Application, Tecnoma, Epernay, pp 3-7, (1976).
Norster, E.R.	Drum atomisation studies. (unpublished) 76th meeting G.T.C.C. Combustion sub-committee, (1964). COA, Cranfield.
O'Connor, J.J. Boyd, J.	Standard Handbook of Lubrication Engineering, McGraw-Hill, (1968).
Oyama, Y Eguti, M Endou, T.	Studies on the atomisation of water droplets. Chem. Eng. Tokyo 17 269 (1953)
Palmgren, A	Ball and Roller Bearing Engineering 3rd Ed. SKF Industries/Burbank & Co., (1959)
Parkin, C.S. Wyatt, J. Wanner, R.	The measurement of drop spectra in agricultural sprays using a particle measuring systems optical array spectrometer. BCPC Monograph 24, pp 241-249, Croydon, (1980).
Peterson R.E.	Fatigue tests of small specimens. Proc. Am. Steel Soc. Treetment 18 p1041 (1930)
Peterson, R.E.	Stress concentration factors. Wiley-Interscience Pub. (1974).
Philipson, K	On the production of monodisperse particles with a spinning disc. Aerosol Science, vol 4 pp 51-57, (1973).

Prasad, R.
Cadogen, B.L.
Influence of small droplets on herbicide toxicity. Canadian Forestry Service, Forest Pest Management Institute pp 309-313, (1987).

Print, C.P.
Studies on a liquid driven spinning disc atomiser. MSc thesis (unpublished), Cranfield Institute of Technology, (1983).

Roberts, H.A.
Weed Control Handbook: Principles 7th Ed. BCPC/Blackwell, (1982).

Rogers, R.B.
The Windproof Sprayer. ASAE. Paper No. 84-1656, (1984).

Roth, L.O.
Tripp, G.W.
A roller brush atomiser. Trans. ASAE vol 16, pp 653-659, (1973).

Round, G.F.
Garg, V.K.
Fluid Mechanics, Chapter Ten, Turbomachines, Arnold, 1986

Rutland, D.F.
Jameson, G.J.
Droplet production by the disintergration of rotating liquid jets. Chemical Engineering Science. vol 25 pp 1301-1317, (1970).

Rutland, D.F.
Jameson, G.J.
Theoretical prediction of the sizes of drops formed in the breakup of liquid jets. Chemical Engineering Science. vol 25 pp 1689-1698, (1970).

Sanderson, R
The design of an air driven spinning disc atomiser. Ph.D. Thesis (unpublished), Cranfield Institute of Technology, (1982).

Scartett, B
Parkin, C.S.
Droplet production by controlled jet breakup. Chemical Engineering Journal, (1977).

Schweitzer, E.E.
2,4-D harms sugar beets. US Agricultural Research Service. Agricultural Research, 26, 13 (1978).

Smith, A.E.
Secoy, D.M.
Early chemical control of weeds in Europe. Weed Science 24, pp 594-597 (1976).

Smith, D.B.
Harris, F.D.
Butler, B.J.
Sheilded sprayer boom to reduce drift Trans. ASAE, pp 1136-1140 (1982)

Spillman, J.H. (1) Atomisers for the aerial application of herbicides-ideal and availiable. Crop Protection 1 (4), pp 473-482, (1982).

Spillman, J.H. (2) Rotary atomiser characteristics. COA, CIT, Cranfield.

Spillman, J.H. (3) Improvements required in spray formation to improve application technology. COA, CIT, Cranfield.

Stent, C.J. Electrostatic atomisation. Tropical Pest Management, vol 27 (2), pp 262-264, (1981).

Stewart, R.E.
Gratkowski, H. Aerial Application Equipment for Herbicidal Drift Reduction. USDA General Technical Report PNW-54 (1976)

Strutt, J.W.
(Lord Rayleigh) On the stability of jets.
Proc. London Mathematical Society, vol 10, pp 4-13, (1878).

Svensson, J.A. Growth and yeild of cultivated plants treated with herbicides: 3-TBA. Swedish Journal of Agricultural Research, 5, pp 235-243, (1975)

Tate, R.W.
Marshall, W.R. Atomisation by centrifugal pressure nozzles. Chemical Engineering progress 49, pp 226-234, (1953).

Taylor, W.A.
Merritt, C.R.
Drinkwater, J.A. An experimental, tractor mounted, very low volume uniform drop-size sprayer. Weed Research vol 16, pp 203-208 (1976).

Taylor, W.A. Controlled Droplet Application of Herbicides. WRO, Oxford.
Weed Research, pp 333-336.

Thomson, N.
Ley, A.J. The quantification of spray drop drift.
Proc. BCPC Conf. Weeds, pp 1039-1044, (1982).

Thornton, M.E.
Ayres, P. Review of herbicide application equipment developed at the weed research organisation U.K. Agricultural Research Council, WRO, Oxford, pp 124-130.

Turner, C.R.
Huntington, K.A. The use of water sensitive dye for the detection and assessment of small spray droplets. J. Agric. Engng. Res. 15 (4) pp 385-387 (1970)

Walton, W.H.
Prewitt, W.C.
The production of sprays and mists of uniform size by means of spinning disc type sprayers. Proc. of the Physical Society, Sec. B, Vol. 62, Part 6, pp 341-350, (1949)

Wentzell, J.M.
Particle size prediction from the spinning disc atomiser. Powder Metallurgy International vol 18, (1) pp 16-21, (1986)

Wilce, S.E.
Akesson, N.B.
Yates, W.E.
Drop size control and aircraft spray equipment. Agric. Aviation. 16(1) pp 7-16, (1974).

Wilcock, D.F
Booser, E.R.
Bearing Design and Application 1st ed. McGraw-Hill, (1957).

Won, Vann Y.
Self-propelled, floating, rotary liquid atomiser. US Patent, No. 4,582,255, date April 5, 1986.

Wooten, O.B.
McWhorter, C.G.
A device for sub-surface application of herbicides. Weeds 9, pp 36-41, (1961).

Wyse. D.C.
Habstritt, C.
A roller herbicide applicator. Proc. North Central Weed Control Conference 32, pp 144-145 (1977).

Yates, W.E.
Akesson, N.B.
Bayer, D.E.
(1) Effects of spray adjuvants on Drift Hazards. Trans ASAE, Paper No.74-1008 (1976)

Yates, W.E.
Akesson, N.B.
Bayer, D.E.
(2) Drift of glyphosate sprays applied with aerial and ground equipment. Weed Science, 26, pp 597-605 (1978)

Yates, W.E.
Akesson, N.B.
Monodisperse atomisation systems for Pesticide sprays. 1st Int. Conf. Liquid Atomisation and Spray Systems, Tokyo. pp 181-185, ICLASS (1978).

Yoshinori, K
Addie De
Ligament type disintergration of Non-Newtonian fluid in spinning disc atomisation. J.Non-Newtonian Fluid Mechanics, vol 10, pp 367-371, (1982).

Young, B.W.
A device for the controlled production and placement of individual droplets. Pesticide Formulations and Application Systems. vol 5, pp 13-22, (1986).

APPENDIX I

Design Drawings

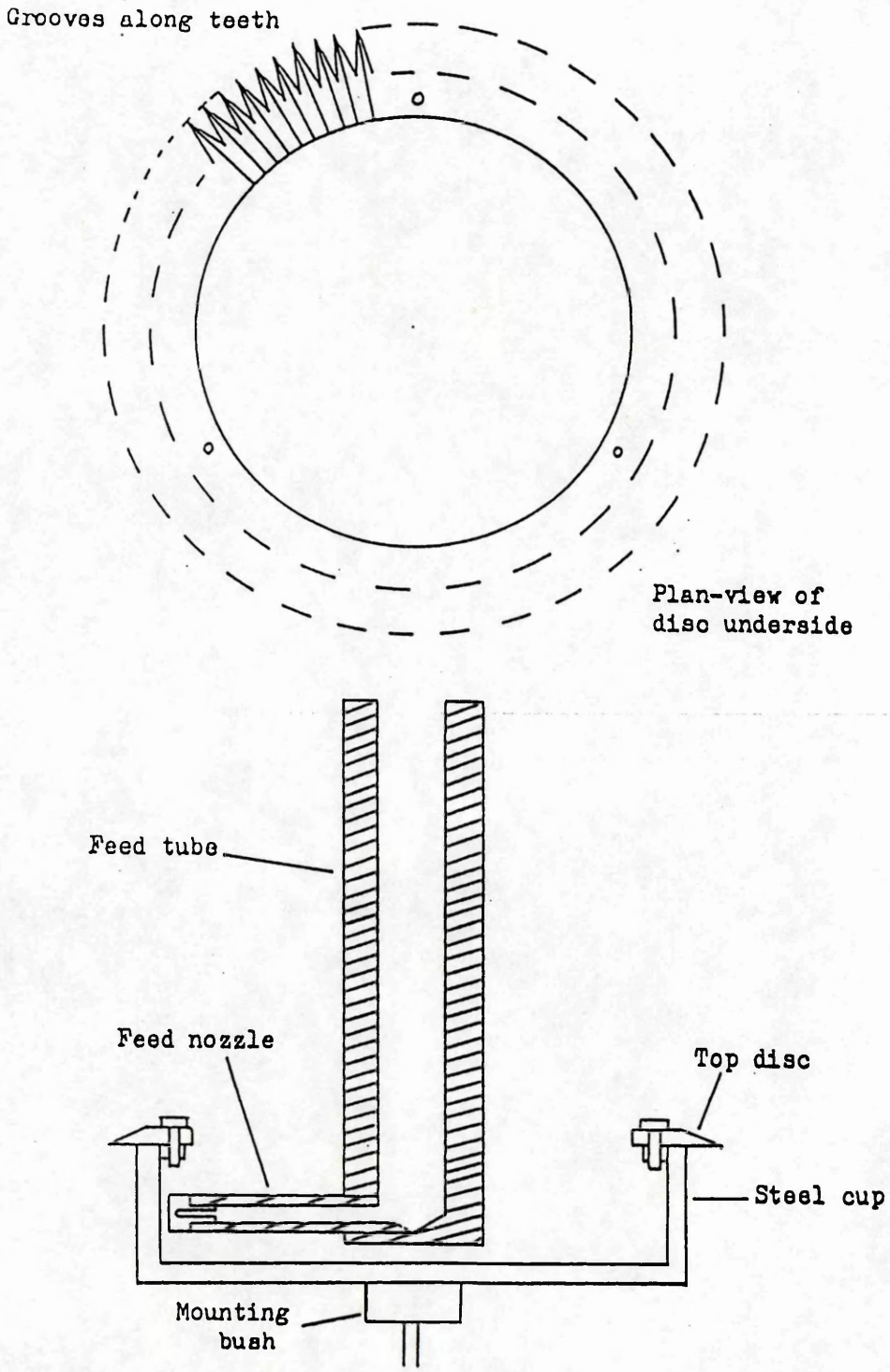

1 Waterwheel Mk.1 (from Kinnersley, 1987)

Schematic Diagram of the Cup of the MK 2 Atomiser

(Actual size)

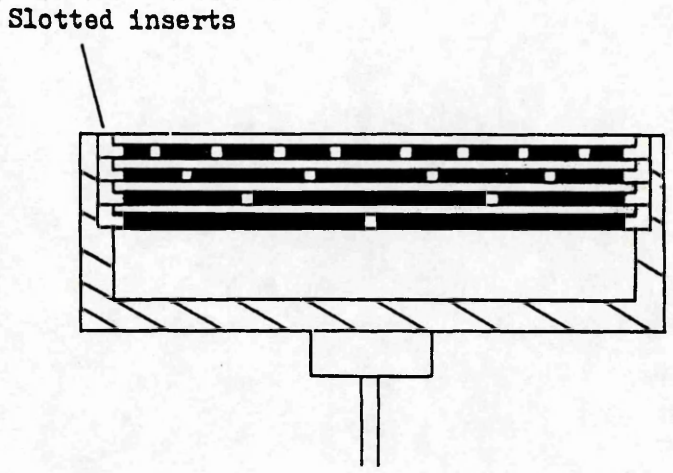

2 Waterwheel Mk.2 (from Kinnersley, 1987)

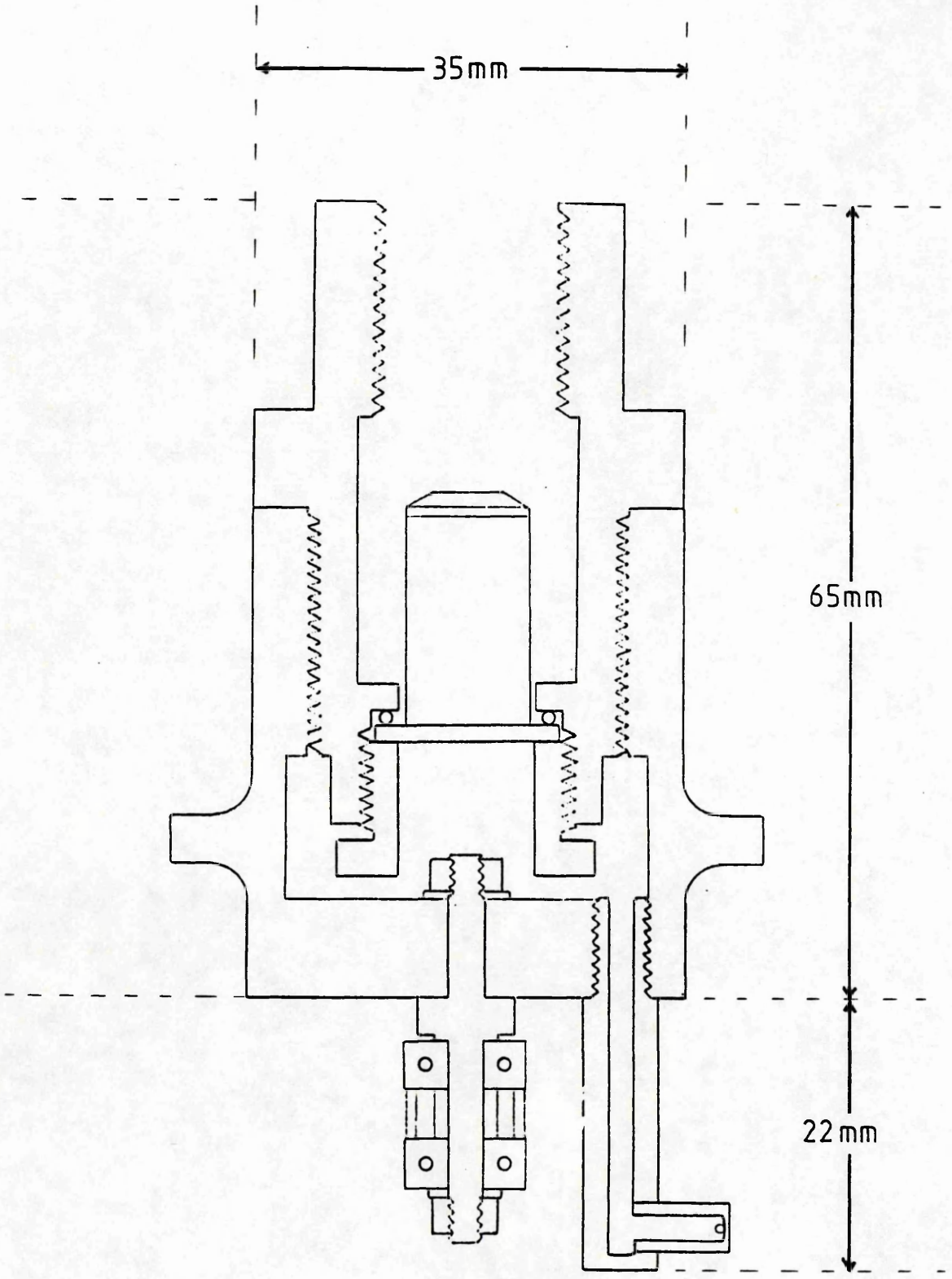

Drawing 3 Waterwheel Mk.5 filter and nozzle holder

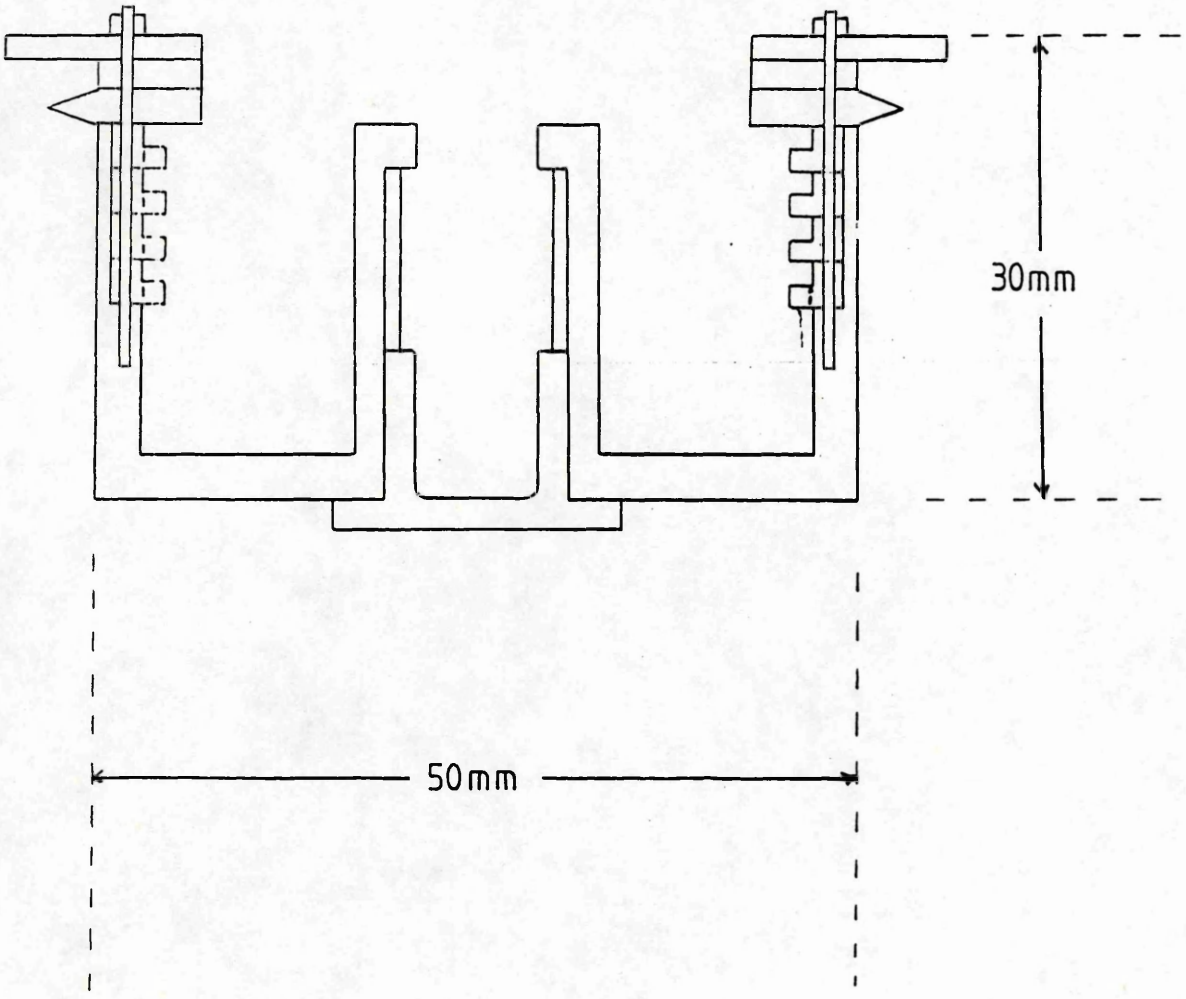

Drawing 4 Waterwheel Mk.5 cup

Waterwheel Mk.5 components list

1 drum
2 containing tube
3 two miniature ballraces
4 distance tube
5 shaft
6 lock nut
7 spring washer
8 dust cap
9 L shaped ring with 5 slots
10 L shaped ring with 10 slots
11 L shaped ring with 20 slots
12 L shaped ring with 40 slots
13 slots
14 liquid surface
15 grooved annulus plate
16 radial grooves
17 tooth point
18 space ring
19 guard ring
20 bolts (4)
21 advancing slope (45°)
22 following slope (vertical)
23 mounting tube
24 filter
25 seal
26 retainer
27 chamber
28 nozzle supply tube
29 nozzle
30 internal lock nut
31 washer

Alternative atomising disc

41 cylindrically channelled annulus plate
42 cylindrical holes
43 central face

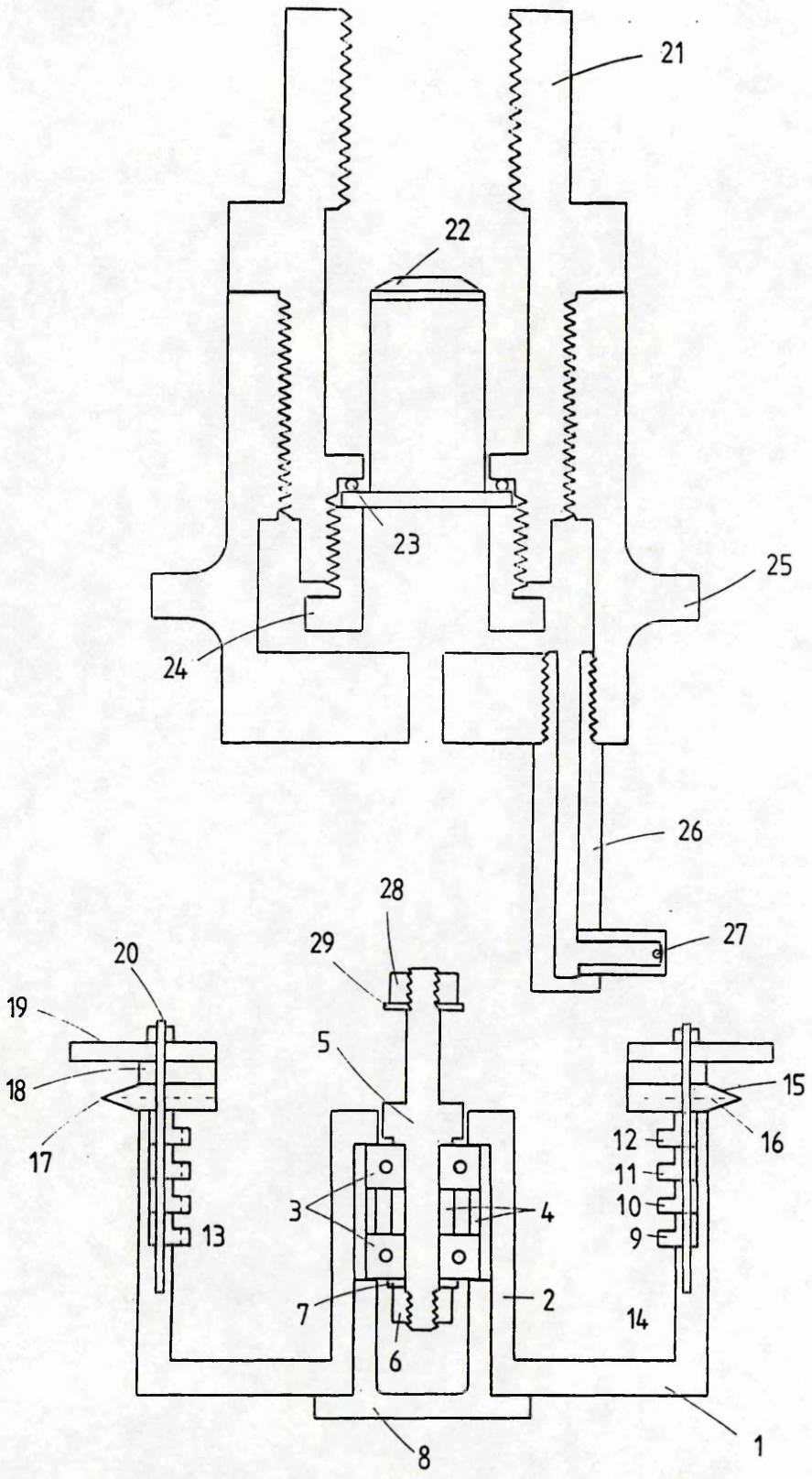

Drawing 5 Waterwheel Mk.5 numbered diagram

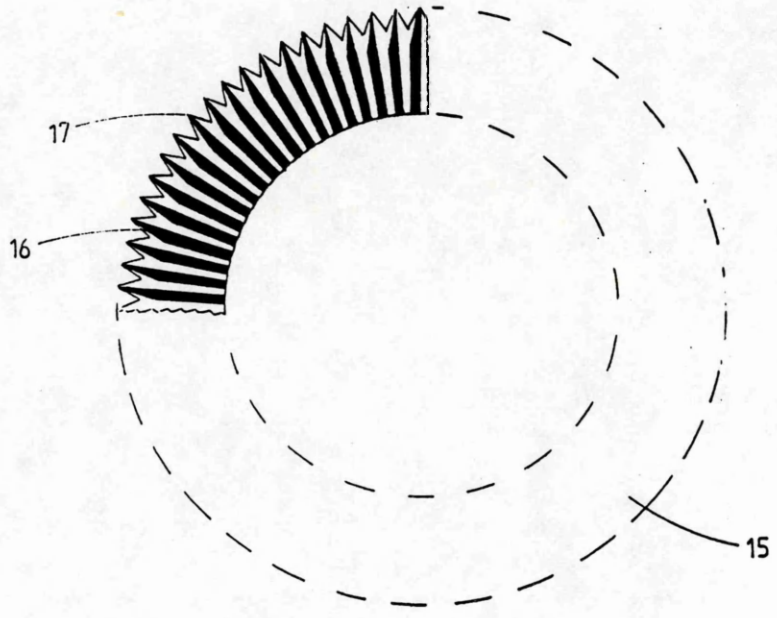

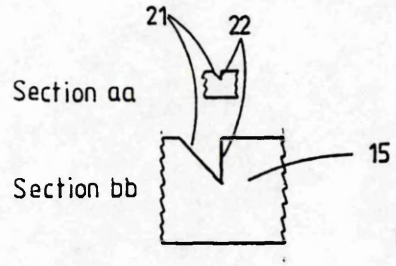

Figure 5.

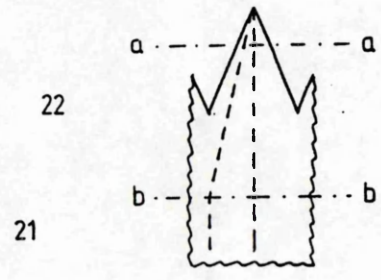

Drawing 6 Waterwheel Mk.5 disc details

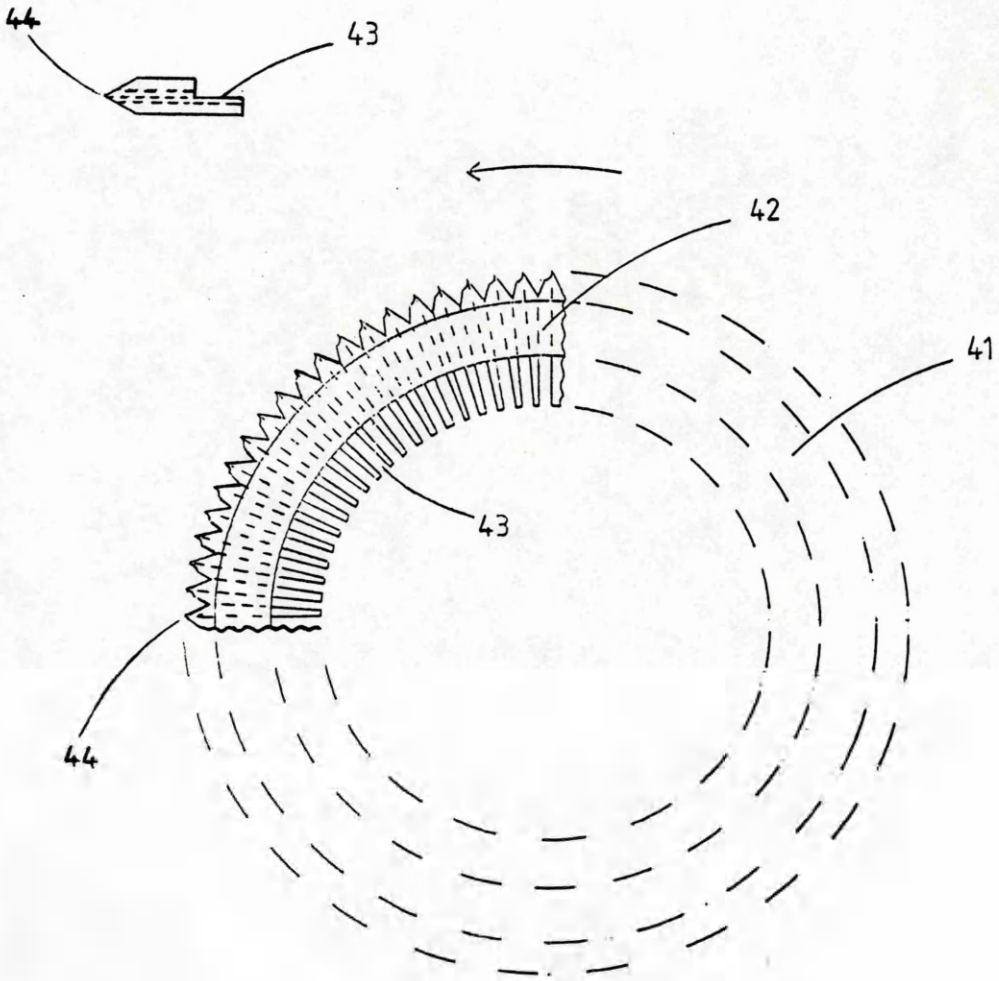

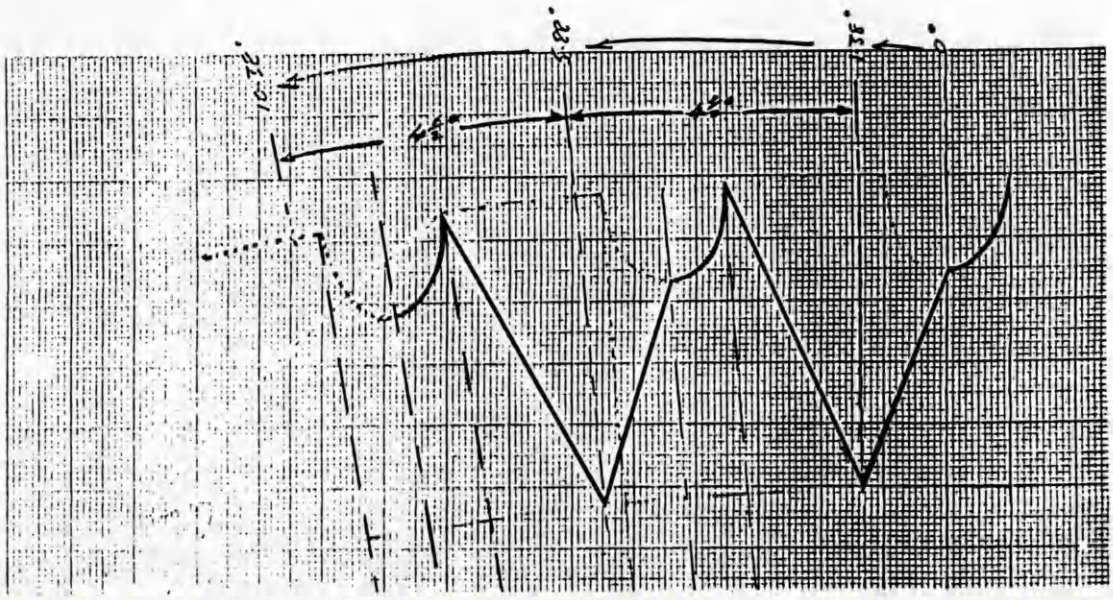

Drawing 7 Waterwheel Mk.6 cylindrically channelled disc

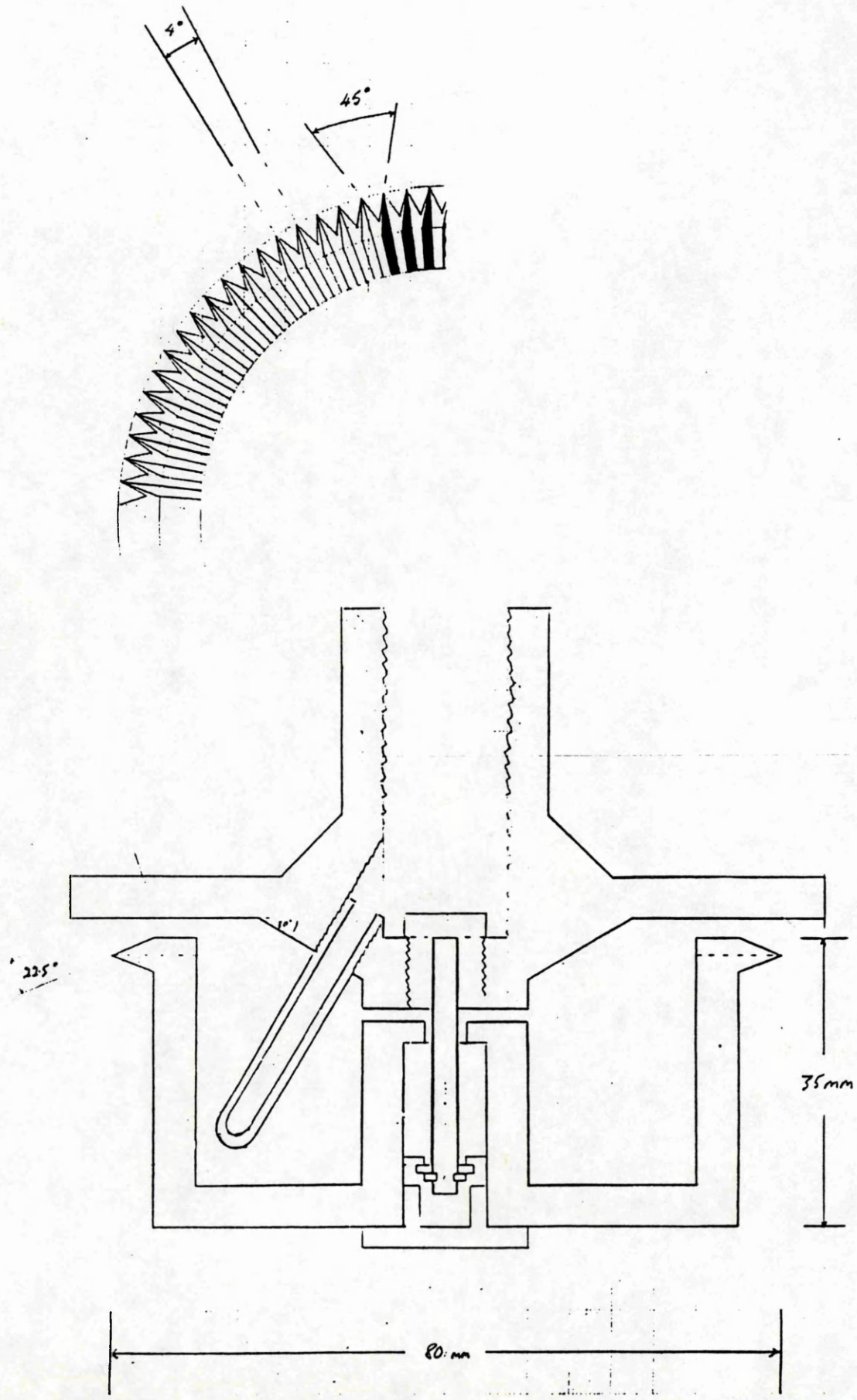

Drawing 8 Waterwheel Mk.9

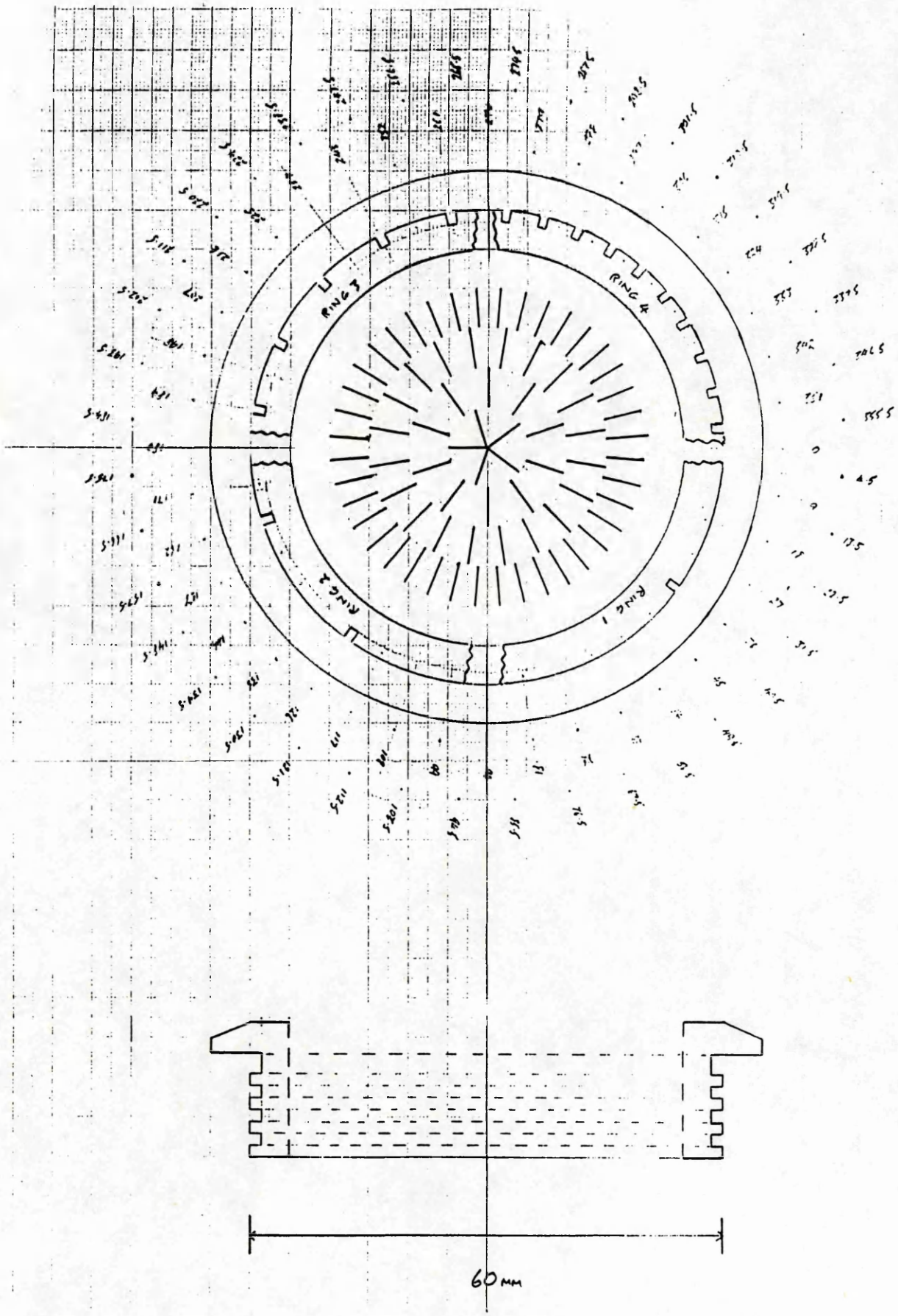

Drawing 9 Waterwheel Mk.9 fluid distribution system

Ring	4 (top)	3	2	1
Slots	40	20	10	5
Position (degrees) of slots clockwise from zero reference point	4.5			
		9.0		
	13.5			
			18.0	
	22.5			
		27.0		
	31.5			
				36.0
	40.5			
		45.0		
	49.5			
			54.0	
	58.5			
		63.0		
	67.5			
	76.5			
		81.0		
	85.5			
			90.0	
	94.5			
		99.0		
	103.5			
				108.0
	112.5			
		117.0		
	121.5			
			126.0	
	130.5			
		135.0		
	139.5			
	148.5			
		153.0		
	157.5			
			162.0	
	166.5			
		171.0		
	175.5			
				180.0
	184.5			
		189.0		
	193.5			
			198.0	
	202.5			
		207.0		
	211.5			
	220.5			
		225.0		
	229.5			
			234.0	
	238.5			
		243.0		
	247.5			
				252.0
	256.5			
		261.0		
	265.5			
			270.0	
	274.5			
		279.0		
	283.5			
	292.5			
		297.0		
	301.5			
			306.0	
	310.5			
		315.0		
	319.5			
				324.0
	328.5			
		333.0		
	337.5			
			342.0	
	346.5			
		351.0		
	355.5			

Drawing 10 Fluid distribution slot positions

Drawing 11 Provisional design for Waterwheel Mk.12

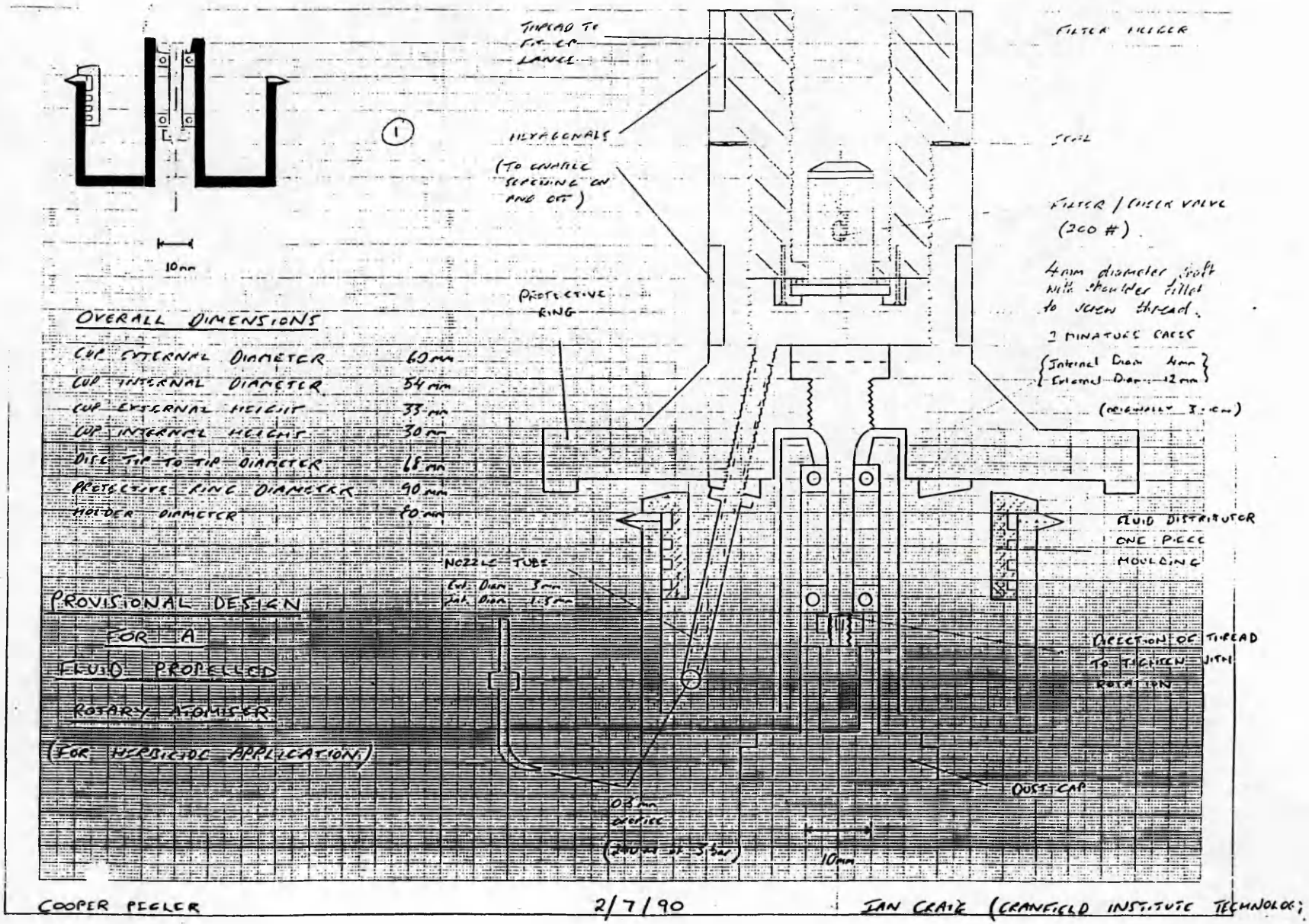

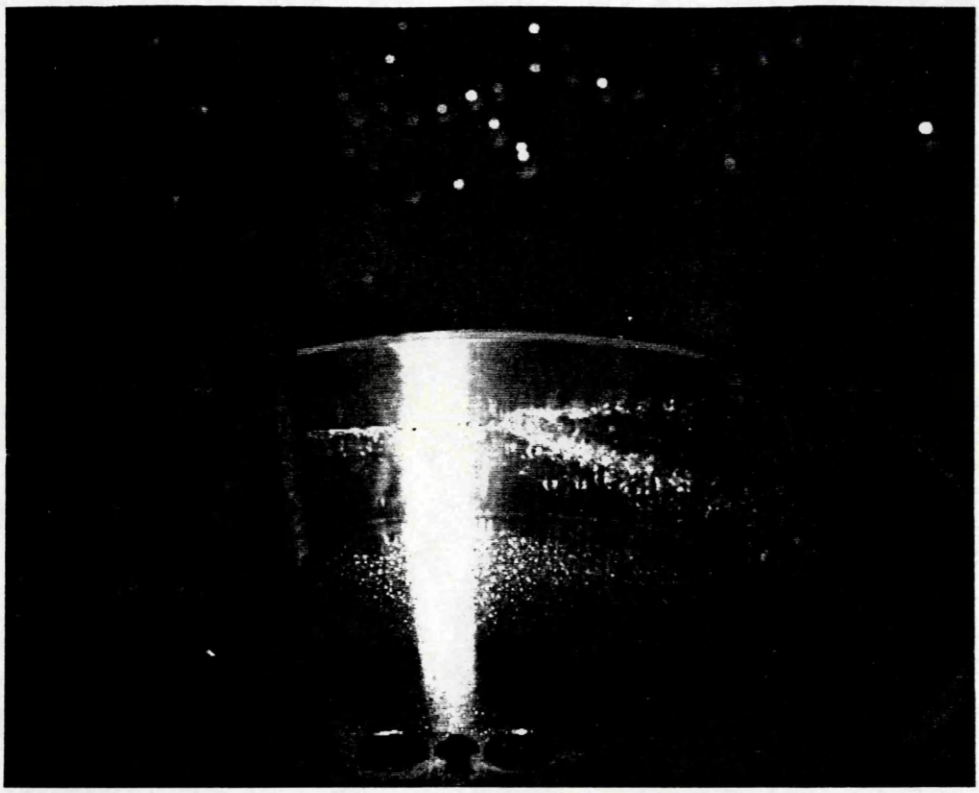

Plate 1 Impact of fluid jet onto inner wall of cup

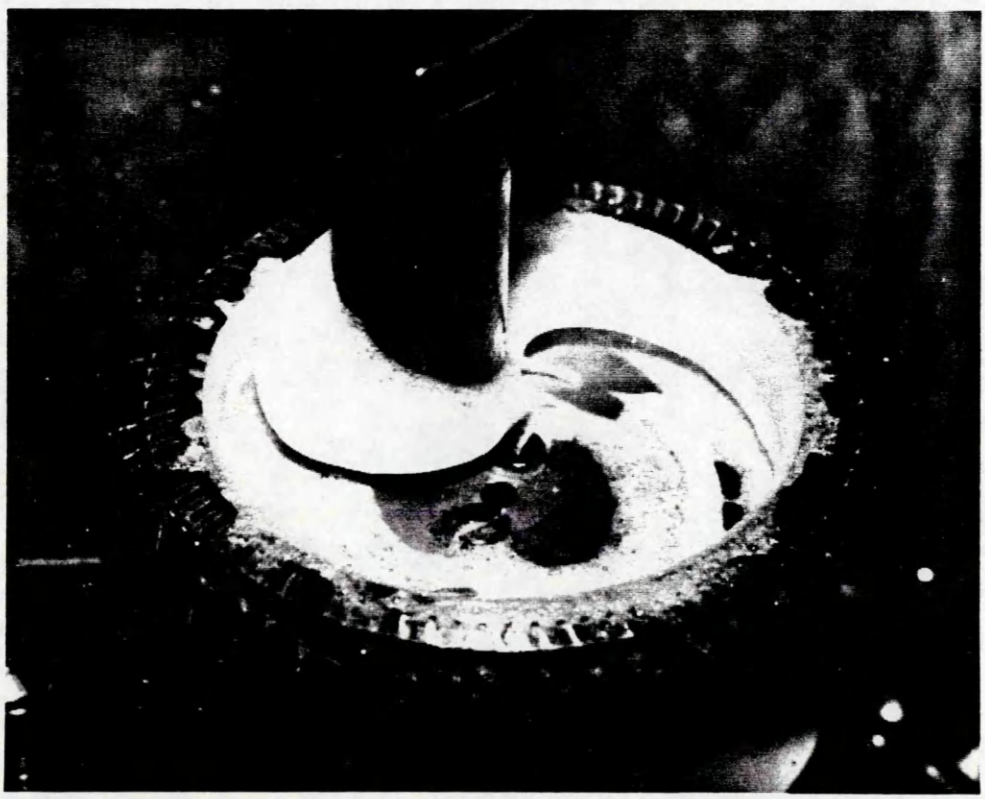

Plate 2 Problem of foaming with surfactant

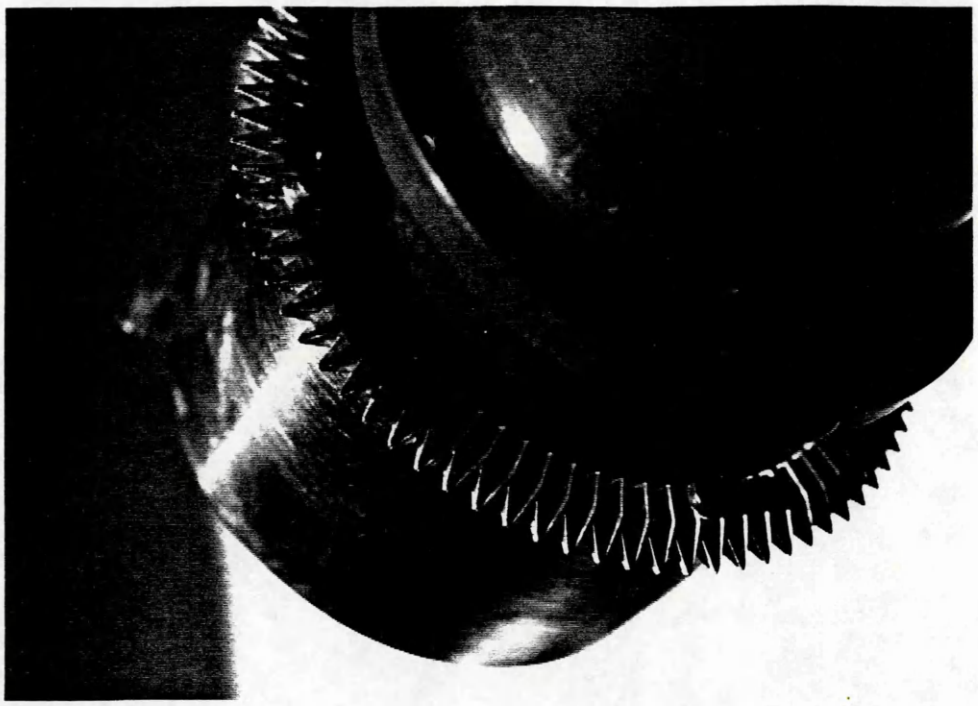

Plate 3 Waterwheel Mk.7 showing fine tooth detail

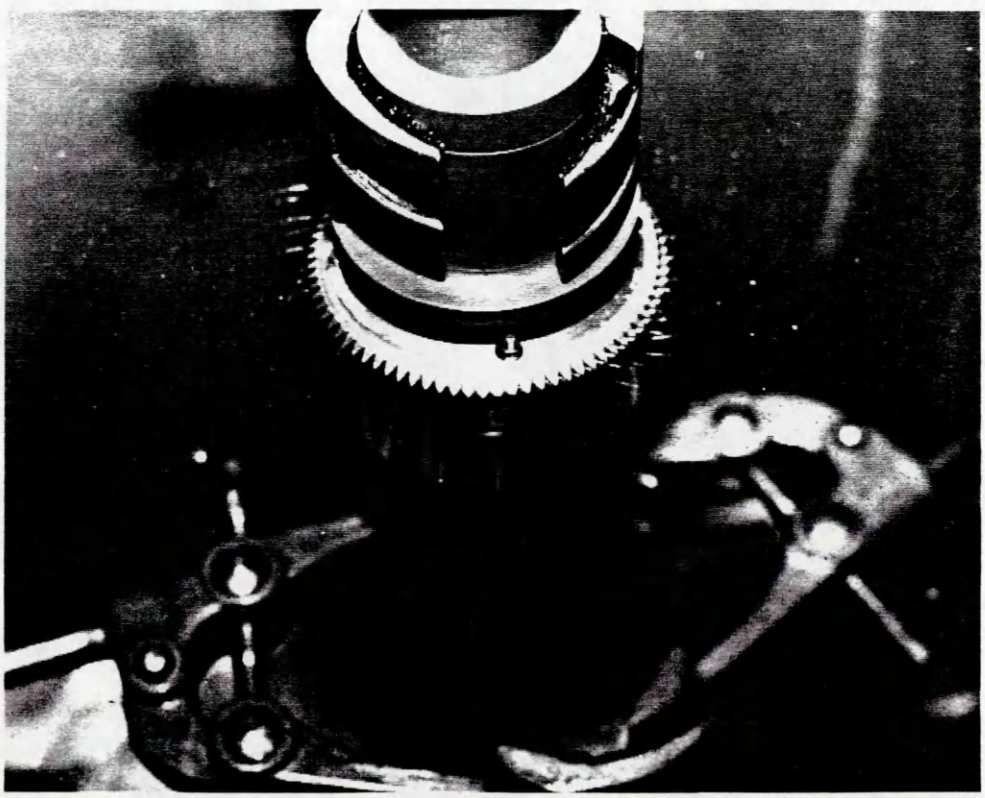

Plate 4 Waterwheel Mk.6 with cylindrically channelled disc spraying water.

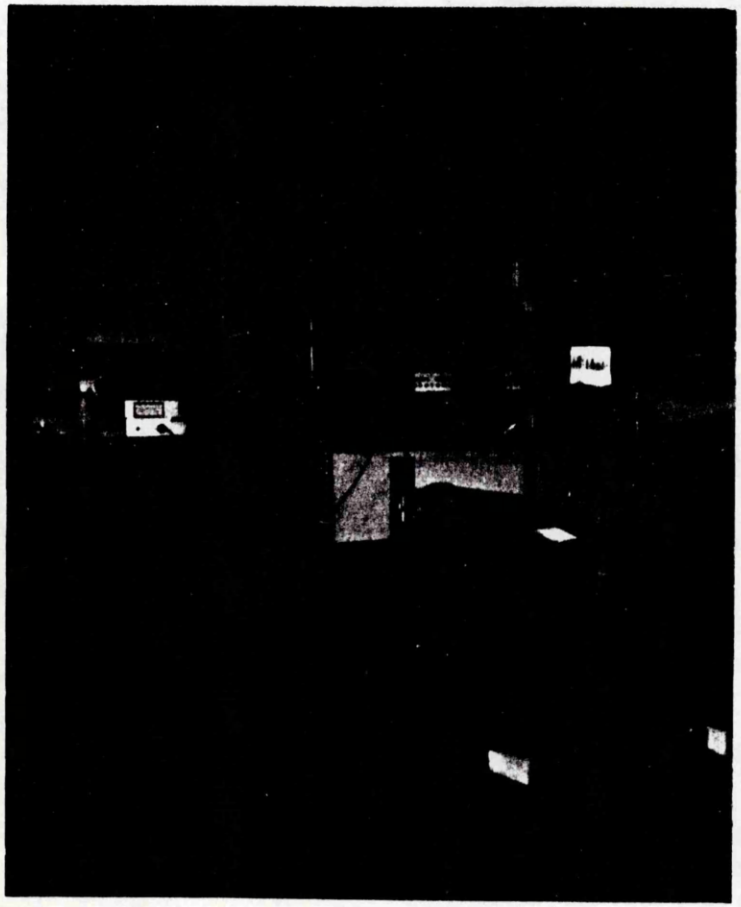

Plate 5 Spray test rig with dropsizing equipment

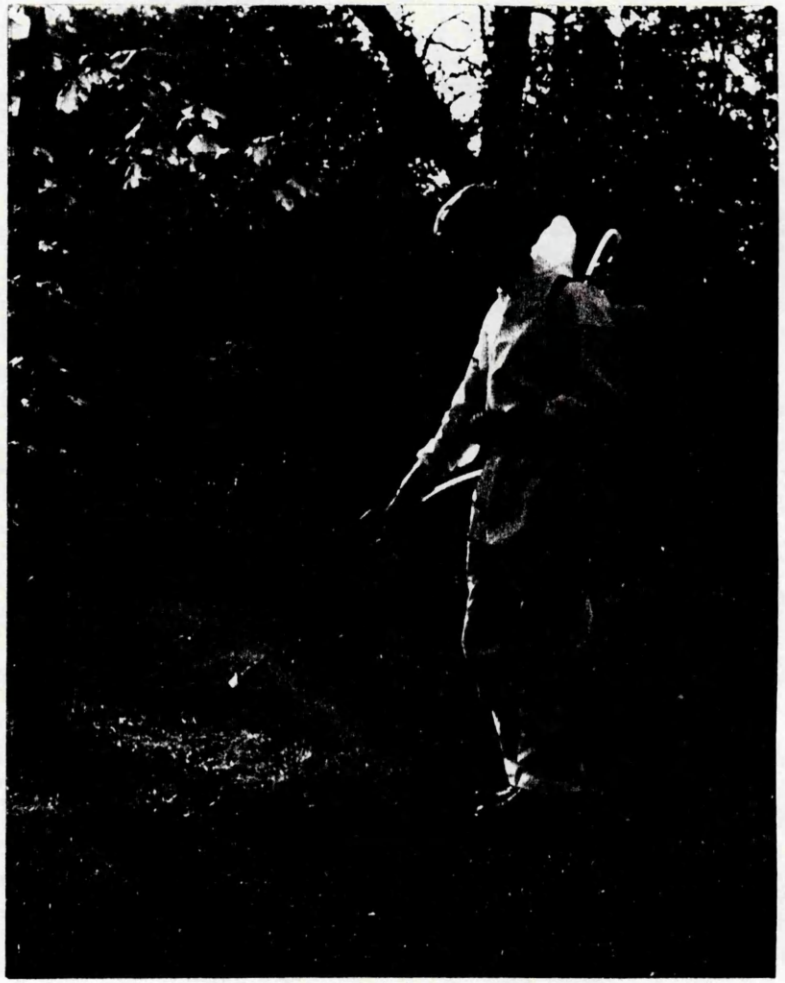

Plate 6 Waterwheel Mk.7 in action in the field